FLOW IN A TRANSVERSE SECTION OF ATHABASCA GLACIER, ALBERTA, CANADA

Thesis by

Charles Forest Raymond

In Partial Fulfillment of the Requirements

For the Degree of

Doctor of Philosophy

California Institute of Technology

Pasadena, California

1969

(Submitted May 22, 1969)

ACKNOWLEDGMENTS

I am especially indebted to Barclay Kamb for many helpful discussions concerning all aspects of the project. In particular his interest in the work and questioning of the results have provided a constant source of encouragement and stimulation.

Curtis Bauman, Sol Giles, Devere Smith, and James Westphal gave invaluable aid in the design and construction of essential field equipment. The success of the field operations was contributed to in large measure by Terry Bruns, Don Lashier, and Will Harrison, who provided dependable assistance in the field.

The Canadian Government graciously gave permission to work in Jasper Park and allowed the entry of field equipment into Canada. Special thanks go to Bill Ruddy and Chester Kongsrude of Snowmobile Tours, Ltd., who generously provided transport of equipment and supplies on the glacier.

I want to give special recognition to my wife Patricia whose camp-keeping skills were an indispensible contribution to the progress of the field work. I am also grateful for her cheerful help in the preparation of the manuscript.

During the period of this research I was supported by a National Science Foundation Graduate Fellowship. Research expenses were funded by the National Science Foundation.

ABSTRACT

Measurements of ice deformation at the surface and at depth in the Athabasca Glacier, Canada, reveal for the first time the pattern of flow in a nearly complete cross section of a valley glacier, and make it possible to test the applicability of experimental and theoretical concepts in the analysis of glacier flow. Tilting in nine boreholes (depth about 300 m, eight holes essentially to the bottom) was measured with a newly developed electrical inclinometer, which allows a great increase in the speed and accuracy with which borehole configurations can be determined, in comparison with earlier methods. The measurements define the distribution of the velocity vector and the strain-rate tensor over 70% of the area of the glacier cross section.

The main longitudinal component of flow has the following general features: (1) basal sliding velocity which exceeds 70% of the surface velocity over half of the width of the glacier, (2) marginal sliding velocity (not more than a few meters per year) much less than basal sliding velocity at the centerline (about 40 m yr^{-1}), (3) marginal shear strain rate near the valley walls two to three times larger than the basal shear strain rate near the centerline (0.1 yr^{-1}).

The observed longitudinal flow is significantly different from that expected from theoretical analysis of flow in cylindrical channels (Nye, 1965). The relative strength of marginal and basal shear strain rate is opposite to that expected from theory. In addition, the longitudinal flow velocity averaged over the glacier cross section (which determines the flux of ice transported) is larger by 11% than the

average flow velocity seen at the glacier surface, whereas it would be 2% smaller if the theoretical prediction were correct. These differences are caused to a large extent by the constant sliding velocity assumed in the theoretical analysis, which contrasts strongly with the actual distribution of sliding. The observed relation between marginal and basal sliding velocity is probably a general flow feature in valley glaciers, and may be caused by lateral variation of water pressure at the ice-rock contact. The observed pattern of longitudinal velocity over the section also shows in detail certain additional features incompatible with the theoretical treatment, even after the difference in boundary conditions (distribution of sliding velocity) is taken into account.

Longitudinal strain rate (a compression of about 0.02 yr^{-1} at the surface) decreases with depth, becoming nearly 0 at the bed in the center of the glacier. The depth variation cannot be explained completely by overall bending of the ice mass as a result of a longitudinal gradient in the curvature of the bed, and is at variance with existing theories, which require the longitudinal strain rate to be constant with depth.

Motion transverse to the longitudinal flow occurs in a roughly symmetric pattern of diverging marginward flow, with most of the lateral transport occurring at depth in a fashion reminiscent of extrusion flow. The observed lateral velocities averaged over depth (up to 1.9 m yr^{-1}) are compatible with the lateral flux required to maintain equilibrium of the marginal portions of the glacier surface under ablation (3.7 m yr^{-1}), and are driven by the convex transverse profile of the ice surface.

When the measured strain-rate field is analyzed on the basis of the standard assumption that the shear stress parallel to the glacier surface varies linearly with depth, the rheological behavior in the lower one-half to two-thirds of the glacier is found compatible with a power-type flow law with n = 5.3. However, the upper one-third to one-half of the glacier constitutes an anomalous zone in which this treatment gives physically unreasonable rheological behavior. In a new method of analysis, rheological parameters are chosen so as to minimize the fictitious body forces that appear as residuals in the equilibirum equations when evaluated for the measured strain-rate field. This new method requires no a priori assumptions about the stress distribution, although for simplicity in application, the mean stress is assumed constant longitudinally. This treatment shows that the anomalies in the near-surface zone are due to significant departures from linear dependence of shear stress on depth, and gives a flow-law exponent of n = 3.6, which is closer than n = 5.3 to values determined by laboratory experiments on ice.

TABLE OF CONTENTS

LIST OF TABLES

LIST OF FIGURES

CHAPTER I

INTRODUCTION

The mechanisms by which glaciers flow, and the resulting distribution of flow velocity within glaciers, are subjects that have received wide attention. In spite of recent progress in applying experimental results and theoretical calculations to the analysis of glacier flow, direct field observations of flow in glaciers have been restricted to the surface or to relatively confined and isolated regions in the interior. Early work on European valley glaciers, particularly the classic study of Mercanton (1916) on the Rhone Glacier, revealed the general pattern of velocity at the surface. Recent borehole experiments, of which the studies by Gerrard, Perutz and Roch (1952), Sharp (1953), Mathews (1959), Meier (1960), Shreve (1961), Savage and Paterson (1963), and Kamb and Shreve (1966) are examples, gave the general form of the depth distribution of ice velocity at isolated locations in a few glaciers.

Up to now, however, there has been no direct observation of the internal distribution of velocity across a complete section of a valley glacier. Thus, there has been no direct measurement of the total ice flux through any glacier cross section; the distribution of basal sliding velocity across a glacier and the effect of the valley sides on the flow have been objects of speculation subject to only indirect observational constraint. The primary goal of the present project is to fill this gap, and to bring to light features of the flow field of temperate valley glaciers that have not been recognized in

the earlier, less comprehensive measurements. At the same time, the measurements of flow velocity over a glacier cross section make it possible to test the recent theoretical calculations of Nye (1965), which predict velocity for rectilinear flow in cylindrical channels. A test of these calculations is a test of the adequacy of existing fundamental concepts as to the nature of glacier flow. Finally, from comprehensive measurements of internal flow velocity, the rheological properties of the flowing glacier ice can in principle be determined without many of the unverifiable assumptions about the stress and strain-rate field that were necessary in the earlier, more limited work.

A. Field Observations

A cross section of the Athabasca Glacier, Alberta, Canada, was chosen as a particularly suitable object for study. The geometry of the glacier in the reach of this cross section and the distribution of velocity at the glacier surface, as described by Paterson and Savage (1959), indicate that the velocity field should be typical of flow fields in valley glaciers having simple cylindrical channels, and should approximate the pattern of flow expected from the theory of Nye (1965).

A network of nine boreholes, eight of which penetrated the complete depth of the glacier (300 m), and a more extensive grid of surface markers, were placed in the chosen cross section during the summer of 1966. The change in position of the surface markers and

borehole profiles after approximately one year, as determined in 1967, gave the distribution of velocity and strain-rate components over about 70% of the total area of the section. Incomplete recovery of the borehole network in 1968 gave less extensive information, but provided significant data on the time variation of the velocity and strain-rate field.

Standard field techniques were used for the measurements. Surface markers were located by triangulation from points fixed on bed rock; borehole shapes were determined by inclinometer survey. A new type of inclinometer, which can be read remotely from the glacier surface, was developed and used for inclinometry of deformed boreholes. This new system represents a great improvement in efficiency and accuracy over earlier inclinometry methods.

B. Results

The distribution of ice flow velocity has an approximately symmetric pattern with the following general features: (1) a basal sliding velocity which exceeds 70% of the surface velocity across half of the width of the glacier; (2) a sliding velocity at the margins of not more than a few meters per year, very much less than the basal sliding velocity in the central part of the section of about 40 m yr^{-1}; (3) marginal shear strain rate near the valley walls two to three times greater than the basal shear strain rate at the valley bottom of about 0.1 yr^{-1}. The contrast between marginal and basal sliding velocity is probably characteristic of valley glaciers, and transverse

variation of water pressure at the glacier bed is suggested as the cause. The boundary condition of constant sliding velocity at the ice-rock contact assumed by Nye (1965) is not appropriate to the Athabasca cross section. In the theoretical distribution most appropriate to the geometry of the Athabasca Glacier, the relative strength of marginal and basal shear strain rate is opposite to that observed. As a result, the ratio between longitudinal velocity averaged over the area of the cross section and averaged over the glacier surface is not 0.98, as computed by Nye, but is instead 1.11. These differences are to a large degree due to the drastic difference in the boundary condition applied in the numerical calculations and the existing natural boundary condition. Closer scrutiny of the observed velocity distribution reveals the existence of more basic incompatibilities related to the non-rectilinear nature of the observed velocity field.

Motion transverse to the main longitudinal component of flow also takes place. The observed velocity normal to the glacier surface (on the average 3.5 m yr^{-1}) closely balances the observed ablation rate (about 3.7 m yr^{-1}). The distribution of the transverse motions is best described as a roughly symmetric pattern of diverging marginward flow. Observed lateral velocity averaged over the glacier thickness ranges up to 1.86 m yr^{-1}. Most of the lateral flow occurs at depth. It is shown that for the most part the observed marginward flow is compatible with the lateral flux required to maintain the marginal portions of the glacier surface in equilibrium. The elevation difference between the central part of the glacier and the

margins, about 7 m, is about the proper magnitude required to drive the observed motions. The symmetry of the pattern is disrupted by relatively large lateral velocities near the glacier centerline. This feature of the pattern is probably caused by deviations of the glacier bed from ideal cylindrical geometry.

Longitudinal strain rate (longitudinal gradient of flow velocity) varies significantly over the cross section, which is in marked contrast to the requirements of existing theories of glacier flow (Nye 1957, 1965). Maximum compression rate of about 0.02 yr^{-1} occurs at the surface in the central portion of the glacier; it decreases toward the glacier bed, and is zero at the bed in the central part of the channel.

Analysis of the measured strain-rate field for parameters in a power-type flow law was carried out by two methods: (1) a method similar to that used in past borehole experiments (e.g. Savage and Paterson, 1963; Kamb and Shreve, 1966), which assumes a linear variation of shear stress parallel to the surface, (2) a new method, which utilizes the gradients of strain-rate components, and for which the only assumption concerning the stress distribution is longitudinal independence of the mean stress. Analysis by the first method shows the existence of two zones within the glacier. In an anomalous near-surface zone extending to 1/3 to 1/2 of the glacier depth, the analysis fails to delineate acceptable rheological behavior. Deeper within the glacier, the analysis gives results compatible with a power-type flow law with $n = 5.3$. Analysis by the second method indicates that the

anomalous near surface zone is due to deviation of the shear stress from linear depth dependence. The second method, in which no direct assumptions concerning the shear stress are made, gives a power law with $n = 3.6$. The difference in the flow law parameters calculated by the two methods shows that deviations of the shear stress from strictly linear dependence are significant in the interpretation of deformation in boreholes. Calculated effective viscosity ranges from 6 to 20 bar yr in the volume covered by the strain-rate measurements.

C. Organization of the Material Presented

Chapter II describes the Athabasca Glacier, the study section, and the relation of the borehole array and surface strain-rate grid to the glacier geometry. In Chapter III field techniques are discussed. In the first section of Chapter IV coordinate systems and notation, which are used in the discussion of the data and the analysis of succeeding chapters, are introduced. In the remaining sections of Chapter IV the primary data are presented and discussed with respect to the information they give concerning the time variation of the velocity and strain-rate fields. Chapter V is devoted to a discussion of a new method by which all of the boreholes were analyzed as a unit to give a self-consistent velocity and strain-rate field over the complete borehole array. The distribution of velocity in the cross section is discussed in detail in Chapter VI. In Chapter VII a new approach to the problem of determining rheological parameters from an observed

strain-rate field of a medium deforming under the action of gravity is discussed and applied. The results are summarized and discussed in Chapter VIII.

For an understanding of the discussion of the primary scientific results, which is presented in Chapters VI and VII, Chapters II and IV provide adequate introduction. Chapters III and V will be of interest to those with specific interest in field techniques and methods of reducing borehole data to give velocity and strain-rate components.

CHAPTER II

THE FIELD EXPERIMENT

The Athabasca Glacier was chosen as being a particularly suitable glacier for this study. It has a simple geometry, as documented by excellent seismic results of Paterson and Savage (1963a). A network of triangulation stations around the perimeter of the glacier (Reid, 1961) and large scale (1:4800) topographic maps (Topographical Survey, 1962) provide an established framework for the precise location of points on the glacier surface. The accessibility of the glacier minimizes logistical problems.

First a general description of the glacier is presented. A more detailed discussion is given of the geometry of the study area and the arrangement of boreholes and surface markers.

A. The Athabasca Glacier

The Athabasca Glacier (52.2° N, 117.2° W) is located south of the main highway between Banff and Jasper in the Canadian Rockies of Alberta. It is one of several valley glaciers originating in the Columbia icefield, an ice cap of area 285 km^2 lying on the continental divide 90 km southeast of Jasper. Figure 1 gives a general view of the glacier and its relation to the surrounding terrain. From the edge of the icefield at an elevation of 2700 m, it descends, in a distance of 2 km, over a series of three gentle icefalls to an elevation of 2300 m. The terminus lies at an elevation of 1920 m. The section between the

lowest icefall and the terminus forms a tongue 3.8 km long with a nearly constant width of about 1.1 km. In this section the glacier channel has a northeasterly trend and is straight except for a slight bend 1 km above the terminus. Longitudinal surface slopes over most of this section range between 2^{o} and 6^{o}. One kilometer from the terminus the surface slope begins to increase progressively down glacier, reaching approximately 20^{o} at the terminus. Crevassing, other than marginal crevassing, is essentially non-existent. The margins are only sparsely crevassed. On the northwest side of the glacier the surface of the ice is debris-covered out to a distance of 300 m from the margin. The thickness of the debris is typically less than 10 cm except very close to the margin where it can be thicker. A weakly developed medial moraine is centered roughly 250 m out from the northwest margin. The zone of debris-covered ice on the southeast margin extends in 200 m from the margin. Because of the surface debris the ice margins can be only approximately identified.

Because of its accessibility, the Athabasca Glacier has received considerable attention from scientists. Of particular interest with respect to this project are those studies relating to the bed configuration and the geometry of the flow. A gravity survey (Kanesewich, 1963) and electrical resistivity studies (Keller and Frishknect, 1961) gave general information concerning bed topography. More detailed information was obtained in a seismic survey (Paterson, 1962; Patterson and Savage, 1963a). The longitudinal depth profile of the

glacier shows the glacier surface and bed to be roughly parallel, maintaining a center-line depth of approximately 315 m for a distance of 1.4 km below the lowest icefall. A progressive and relatively smooth decrease in depth prevails below this point except for some bed irregularities 1.4 km and 0.9 km above the terminus. Transverse profiles indicate that a relatively regular glacier cross section persists throughout the glacier tongue. Considerable information concerning surface ice velocity over the lower section of the glacier was obtained by Paterson and Savage (1963a). Their measurements show the pattern of flow at the surface to be simple, with the longitudinal surface velocity ranging from 75 m yr^{-1} just below the lowest icefall to 15 m yr^{-1} at the terminus. The surface longitudinal strain rate (longitudinal gradient of the surface velocity) has an average value of -0.015 yr^{-1} and ranges from -0.103 yr^{-1} near the base of the icefall to very slightly extending (+0.003 yr^{-1}).

Annual ablation averages 4 m of ice over the lower tongue. The average velocity normal to the surface closely approximates the average ablation rate indicating that the glacier surface is near equilibrium.

Temperature measurements (Paterson, personal communication) show that the glacier is at or close to the pressure melting point, except within about 10 m of the surface, where the ice is affected by the sub-freezing winter temperatures.

B. Field Site

In choosing a particular portion of the Athabasca Glacier for intensive deformation measurements, an effort was made to satisfy, as far as possible, those conditions which would allow a two-dimensional theoretical treatment, similar to that of Nye (1965), to be applied. The basic geometrical requirement for this type of theoretical treatment is that the glacier cross section be identical from point to point along the glacier, with surface slope constant in magnitude and direction; in other words, the ice body must have cylindrical geometry. Simple geometry is not sufficient to guarantee that the internal deformation will also be simple, since complex boundary stresses could result from variations in the nature of the glacier bed. Thus in choosing an appropriate transverse section of the glacier, attention was also given to the longitudinal variation of the surface strain rate as measured by Paterson and Savage (1963a). This gives an indication as to whether two-dimensional flow is in fact present. With these considerations in mind a section of the glacier centered 0.8 km below the icefall was chosen for study. (See figure 1 for location.)

Figure 2 shows the centerline longitudinal profile of the glacier over a reach that includes the study area. (Data based on Paterson, 1962.) The longitudinal component of slope of the surface and bed, and longitudinal strain rate are plotted. The location marked section A is the center of the region in which deformation measurements were made. Section A lies at an inflection point in the surface, at which

the surface slope is 4^{o}. The slope is constant to ± 10% over a length of 2 glacier depths (600 m) centered at section A. In this vicinity, the glacier at its centerline is thickening down stream with the divergence between the bed and surface being approximately 2^{o}. Figure 3 shows the transverse profile C of Paterson and Savage (1963a) with the transverse variation of the longitudinal component of surface slopes plotted. The width of the glacier here is 1250 m and the maximum depth 316 m. The longitudinal surface slope varies from 2.8^{o} to 4.1^{o} across the glacier. The distribution of surface slope can also be recognized in the topographic map (fig. 4). Although there are significant deviations of the geometry of this section of the glacier from ideal cylindrical geometry, the section approximates cylindrical geometry about as well as can ever be hoped for on a real glacier. As shown in figure 2, the longitudinal strain rate maintains a nearly constant value of $-0.02\ yr^{-1}$ over the same range in which the surface slope was acceptably constant. This gives some indication that the flow is two-dimensional.

C. Field Measurements

In the summer of 1966 an array of 9 boreholes and a more extensive grid of surface markers were established. Boreholes and surface markers were arranged in an approximately rectangular grid of longitudinal lines (henceforth referred to as lines and denoted by arabic numerals) and transverse sections (referred to as sections and denoted by capital letters) as shown in figure 4. Lines have

azimuth N 40° E. The spacing of the grid lines is 150 m or approximately half of the centerline depth, except near the margins where longitudinal lines are spaced 100 m apart. The boreholes are in three sections A, B, C of 5, 3, and 1 boreholes respectively. Each borehole is named according to its location in the grid. The relationship of these transverse sections to the region of constant centerline surface slope and longitudinal strain rate is shown in figure 2. Figure 3 shows the extent of coverage of the glacier cross section as determined by Paterson and Savage (1963a). It is assumed that all of the boreholes, except 4A, penetrated to bed rock, although the possibility some of them were stopped by debris imbedded in the ice several meters above the base cannot be discounted. Borehole 4A could not be continued below approximately 1/3 of the depth of the glacier because of debris in the ice. In a number of attempts to place boreholes in the marginal zones of debris covered ice, penetration below depths of about 20 m proved to be impractical for the same reason. The surface markers define three additional lines (6, 7, and 8) and three additional sections (D, E, and F). Stakes are also designated by their location in the grid. The locations of triangulation stations fixed on bedrock and from which surface markers and tops of boreholes were surveyed are shown in figure 4.

The choice of 150 m for the spacing of boreholes was arrived at as a compromise between the desire to resolve the essential features of the flow pattern and the goal of obtaining measurements over a large area. The main concern of these observations is not the

deformation field on the scale of individual crystals or local structural features, which would show unpredictable fluctuations in time and space. Of primary interest is the average deformation over volumes comparable to the cross section dimensions, which can be expected to relate directly to the cross section geometry, and to persist in time. For this purpose a spacing of 150 m was judged to give adequate resolution.

The configuration of the network of surface markers and boreholes at a specified time is determined by locating the surface markers and surface intersection of the boreholes by triangulation and tape measure and delineating the shape of the boreholes by making tilt measurements. For the purpose of achieving good statistics in the borehole data, tilt measurements were spaced as closely as time allowed. In deformed boreholes a spacing of 2 m was used.

Configuration determinations for the complete network were made for the initial state (summer 1966) and the deformed state after approximately one year (summer 1967). After two years (summer 1968), the locations of the tops of all the boreholes (except 1C) were determined by triangulation; tilt measurements in only two boreholes (3B, 2A) could be made. A history of borehole operations is given in table 1.

CHAPTER III

FIELD METHODS

The methods used for making surface and borehole measurements were for the most part similar to those which have been used in earlier borehole experiments. The description of techniques given in this chapter is thus brief. More detailed description of equipment and procedures is given in Appendix I. Some elaboration of the discussion is given when a procedure or piece of equipment is significantly different from that employed in the past. Emphasis is given to the performance of the methods in terms of efficiency, reliability, and the accuracy of the primary data which they give. An assessment of the errors in the data is particularly important, since the question of accuracy enters strongly into the possible interpretations of the velocity and deformation fields.

Surface measurements are first discussed. Some experiences gained in the use of a recent method of marking and recovering boreholes (Kamb and Shreve, 1966) and the results of a newly developed system for borehole inclinometry form discussions of particular interest in the section on borehole methods.

A. Surface Measurements

Standard techniques were used for the marking and location of points on the surface of the glacier. Markers were 2 cm by 2 cm soft wood stakes approximately 2 m in length. Stakes were driven into holes made with a SIPRE ice drill. Stakes for surface strain-

rate measurements were placed during the period of July and early August of 1966. The configuration of the stake network was determined by tape measurements in early September 1966 and again in July 1967. Absolute locations of selected markers and the tops of all of the boreholes were determined at approximately the same times by standard triangulation techniques.

Surveying was done with a Wild T2 theodolite, which can be read to 1" of arc. Multiple sightings indicate a standard sighting error of 3" and a maximum error of 8". Angles were turned from two stations on bedrock on the northwest margin of the glacier (fig. 4). The relative location of these stations is known to 2 cm. On the basis of the length of the lines of sight (324 to 1452 m), the angles of intersection (65° to 140°), and the sighting error, the standard error in horizontal position of the point sighted (the top of the stakes) is estimated to be 3 cm. Elevation of sighted points can be affected by refraction. To test for any systematic refraction effect, the difference between the two independent elevation determinations for a given stake was compared with the difference in the squared lengths of the corresponding lines of sight. It was concluded that any such systematic effect acting over the distances involved is much smaller than the observed differences. The maximum value of the magnitude of the difference between the two elevation determinations is 10 cm. A standard error of 3 cm for the vertical location of sighted points is indicated. An additional error enters when the location of the top of the stake is related to the element of ice, which the stake serves to

mark. This source of error is considered after a discussion of the tape measurements.

Relative positions of all stakes were determined by taping distances between them parallel to the surface. Distances to all neighboring stakes on grid lines (ca. 150 m) and grid diagonals (ca. 211 m) were measured with a 300 ft steel tape. Because of the large number of measurements involved, great care could not be taken to control accurately the number of suspension points and the tension in the tape. Nevertheless, repeatability of such distance measurements was within 8 cm.

Comparison of distances between stakes as determined by triangulation and taping shows that there is a systematic difference between the two methods. In making the comparison the differences were normalized to a common interval (150 m) and were corrected for the effects of surface deformation occurring between the time of taping and triangulation. In the survey of September 1966, the difference between the taped distances and the distances as determined by triangulation for 19 intervals had a mean of 23 cm and a standard deviation of 6 cm. The corresponding figures for the survey of July 1967, which are based on comparison of 13 intervals, are 18 cm and 17 cm. Such systematic differences could arise from an error in the base line distance between the bedrock triangulation stations, contraction of the tape with respect to its calibrated length from temperature effects, and deviation of the tape from a straight line path. The last of these possibilities is considered to be the dominant contributor. An average angular deviation of about 2^{o} from

a straight line path would produce such an effect.

The much larger standard deviation of the differences in 1967, as compared to 1966, was apparently caused by greater errors in identifying the stakes with points fixed in the ice. At the time of the tape and triangulation surveys of July 1967, many of the stakes were not tightly gripped by the ice and were tilted with respect to vertical as a result of enlargement of the hole by melting. Such was not the case in 1966. The resulting contribution to the differences comes from two sources: (1) the stake is moved in its hole by wind or melting between the time of sighting and the time at which the stake is visited to measure the displacement of the top of the stake caused by tilting; (2) different judgments were made at the time of taping and the time of triangulation as to the proper position of the stake in its enlarged hole. It is estimated that the second of these does not exceed 2 cm. Thus the first source must be largely responsible for the increase in standard deviation.

By using standard combinational formulae for variances the following standard errors are computed for the 1966 survey: 3 cm for absolute horizontal locations as determined by triangulation, 4 cm for relative locations on the surface as determined by triangulation and by taping suitably corrected for the systematic effect resulting from deviation of the tape from a straight path. For the 1967 survey the standard errors similarly calculated are 17 cm for absolute horizontal locations as determined by triangulation, 24 cm for the spacing parallel to the surface as determined by triangulation, and

7 cm for the spacing as determined by the corrected tape measurements. The greater accuracy of the spacing of stakes obtained by taping as compared to triangulation in 1967 is a consequence of the dominance of the first of the sources coming from loosening of the stakes. Such an error has direct effect on the triangulation results. It affects the tape results only indirectly through the uncertainty which is introduced in the value of the systematic correction to the taped distance.

In the determination of displacements over the interval between the surveys, account must be taken of possible drift of the stakes with respect to the ice. Stakes had to be reset several times between surveys because of ablation. This introduced errors resulting from uncertinaty in the original location of the stake in an enlarged hole, and lowering of the stake along a non-vertical line. The combined horizontal error from these sources is estimated to have a maximum value of 13 cm. There is considerable uncertainty in returning a loosened stake to its original elevation with respect to the surrounding ice because of two possibilities: the stake was not initially driven to the bottom of the hole in which it was set; once a stake has floated off the bottom, the hole may freeze closed. The errors resulting from such vertical drift cannot be evaluated, but they probably amount to less than 50 cm.

Consideration of the errors in absolute location of the markers in 1966 and 1967 and the errors from horizontal drift gives a standard error for horizontal displacement of approximately 20 cm. The

errors in relative location of points for 1966 and 1967 for tape measurements and the horizontal drift error give a standard error of 0.0007 for the extension of lines between the stakes.

Because of the unknown contribution of vertical drift, a standard error for vertical displacement cannot be estimated as above. A rough estimate of this error can, however, be gained by comparison of the vertical displacement as determined on two different markers at nearly the same location. There are only four locations where such comparison can be made. A standard error of about 35 cm is indicated.

B. Borehole Methods

The method of boring and recovering boreholes used on the Athabasca Glacier was essentially that developed and used by Kamb and Shreve (1966) on the Blue Glacier, Washington. Holes were bored with an electrically powered thermal drill ("hotpoint"). The thermal drills used for initial boring are cylindrically symmetric, so that penetration of the ice is along an essentially vertical line. A hole approximately 7 cm in diameter is produced. After initial boring of the hole, a stranded stainless steel aircraft cable, weighted at the bottom, is lowered down the hole to serve as a marker for later recovery of the borehole. Recovery is accomplished by use of a special thermal drill ("cable-following hotpoint") which is threaded onto the aircraft cable and is thus constrained to follow it, as long as it is held taut from the surface. The cable-following hotpoint also

produces a hole of approximately 7 cm diameter.

Recovery of the last few meters of boreholes (the length of the weight plus the distance it was lifted off the bottom of the original borehole) can not, in general, be accomplished. In the Athabasca Glacier holes this distance was 2 to 3 m. Weights were lifted off the bottom to avoid possible adverse effects of a strong shear zone on the weighted cable system. Such a zone could exist in the immediate vicinity of the bed.

This method can be expected to give more detailed information of the ice motion than is possible with holes cased with aluminum pipe. In addition it has considerable operational advantages over the older method of thermal boring, in which the borehole is cased by continually adding sections of pipe at the surface as the hotpoint penetrates the ice. A problem frequently encountered in the old method is that seizing of the borehole casing somewhere along its length prevents further penetration of the hotpoint (Meier, 1960). This is eliminated as a source of trouble in the new method. Since the power cable also serves as the only mechanical link between the surface and the hot point, the hot point can be rapidly lowered into or raised out of the hole, eliminating the necessity of 24 hour drilling and also facilitating replacement of hot points in the event of a failure. In addition a minimum of paraphernalia is involved. The time required for initial boring or recovery of a 300 m borehole varied from four to eight days. The employment of aircraft cable as a borehole marker also seems greatly to increase the probability of successful recovery of a borehole at a later time.

The problems of pipe buckling and breakage, and freezing within the pipe, are avoided.

The basic problems which arise with this method of borehole recovery are the danger of blocking a hole by tangling of the hotpoint suspension cable around the aircraft cable, and the possibility of not being able to follow the aircraft cable because of breakage. Breakage can occur when the rate of extension of the cable by ice deformation exceeds the rate at which the cable can relieve the resulting tension by pulling in additional cable from the surface. Both of these problems are particuarly accute in the Athabasca holes. Tangling presents a clear danger because of the great depth of the boreholes. The cold winters cool the upper 10 m of the ice to an extent which greatly inhibits the slipping of the aircraft cable through this zone.

In 1966 nine boreholes (accumulated length 2520 m) were marked with aircraft cables, for later recovery. All of these holes were completely recovered in 1967, except for the lowermost 100 m of one hole (hole 1C). The loss of the bottom of hole 1C was caused by cable tangling. No cables were broken by ice deformation, although considerable strain (up to 0.8% elongation) had accumulated in the cables over the year interval, as indicated by the relaxation of the cable as it was freed from the ice by the cable following hotpoint (fig. 5). In 1967 seven of the boreholes were marked with cables as before. However, in 1968 only two holes were successfully recovered. Four aircraft cables had been broken within 10 m of the surface and a fifth cable, while not broken, was damaged in a manner which prevented

passage of the cable-following hotpoint. The performance of this method is described and discussed in greater detail in Appendix I. Some modification is required in order to make it a completely reliable system.

If the aircraft cable were to migrate normal to itself, as would tend to happen if the cable were curved and under tension, the changing configuration of the cable would give an erroneous picture of the ice deformation. On re-entry into a borehole, after a 1 year interval, rates of hotpoint penetration significantly greater (up to six times) than the normal penetration rate in solid ice frequently occurred. This shows that the original borehole had, in part, remained open, and that the cable had not migrated significantly.

Tilts in initial and recovered boreholes were determined by inclinometer surveys. The originally drilled boreholes were checked for verticality by making tilt determinations every 15 to 20 m. The instrument used for these measurements was an optical inclinometer (Parson Survey Company), and is a proven instrument identical in mechanism to the inclinometers used previously on several glaciers for similar measurements (e.g. Savage and Paterson, 1963). The tilt survey of the deformed boreholes was done with a newly developed electrical inclinometer which can be read remotely from the surface. A detailed description of this instrument is given in Appendix I. (See also figures 6 and 7.) The rapidity and ease with which it can be used allow a much greater density of data to be taken than is possible with earlier methods. Measurements were taken at 2 m intervals, giving

approximately 150 tilt determinations for the deeper boreholes. Each such set of measurements can be made in about 5 hours. The substantial scatter in the tilt readings so obtained (figs. 11 and 12) indicates that a high density of data is essential for an adequate determination of the borehole configurations.

Tilt magnitude measurements for a deformed borehole fall in a band approximately 1^{o} in width. The root mean square deviations from a mean curve is typically 0.5^{o}, which is distinctly greater than the instrumental error of 0.1^{o}. The scatter is similar in initial and deformed boreholes after one or two years. This indicates that it probably is not a feature of the flow, but rather of the experimental technique. It is "noise" introduced by the way the boreholes are drilled, recovered, and measured. This is discussed further in Appendix II.

Because the spacing of measurements is much less than the scale of the depth variation of the general trend of tilting defined by the data, a tilt profile can be established through a smoothing procedure. The value of the tilt at a given depth can be established to within 0.07^{o} (standard error). The method of smoothing and the statistical analysis giving standard errors are discussed in Chapter IV and Appendix II.

The scatter in the azimuth of tilt is affected by two additional factors. One is that as the tilt magnitude becomes small the azimuth of tilt is undefined. This is responsible for the extremely large scatter in azimuth which occurs near the surface for several bore-

holes. The well defined band of 40^{o} width shown by all the boreholes in their deeper portions, as measured in 1967, is an expression of a possible $\pm 20^{o}$ error in azimuth caused by friction in the compass needle bearings. Modification of the inclinometer compass mechanism preceding the 1968 field season considerably reduced this effect, as is seen in the 1968 azimuth data for boreholes 2A and 3B, where the band width is approximately 10^{o} to 20^{o}. (See figure 12.)

CHAPTER IV

DATA

The displacement of surface markers and the change in shape of boreholes provide the basic data for the calculation of the internal distribution of velocity. For the purpose of discussion here and calculations in later chapters, coordinate systems and notation are first introduced. The data are then presented as they relate to surface velocities, surface strain rates and borehole configurations. Discussion concerning the spatial distribution of velocity and strain rate is brief. Where appropriate a more detailed qualitative discussion of particular features is given, in order to relate aspects of the quantitative consideration of flow quantites in Chapter VI and VII to features of the surface data. Quantitative consideration of the temporal variation of velocity and strain rate, in so far as is possible, is made in this chapter.

In addition to the velocity and strain-rate data, the measurements on surface markers give useful supplementary information on the present surface configuration and ablation rate. The computed elevations of surface markers corrected to the ice surface show that the elevation of the ice surface on September 9, 1966 was 3 m lower than the surface elevation as given by the topographic map (Topographic Survey, 1962). Surface slopes computed from the surface markers and the topographic map are in good agreement. Average ablation over the borehole array was about 3.7 m yr^{-1}.

A. Coordinate Systems and Notation

Several different coordinate systems were used in the reduction of the data. The following systems are defined.

(W,S,U) coordinate system is a system used by Paterson (1962). Coordinates, in this system, of all stations in the Athabasca triangulation network (Reid, 1961) were computed and tabulated by Paterson (1962). It is thus a convenient and useful frame of reference for determining absolute locations of surface markers. The x_2 or S axis is horizontal and has an azimuth of S 9.25° W; the x_1 or W axis is horizontal and normal to the x_2 axis in a westerly direction; x_3 or U axis is upward. Station 1 has a location of (2000.00 m, 2000.00 m) in the horizontal plane; the $x_3 = 0$ plane is at an elevation of 6000 ft.

(X,Y,Z) coordinate system has X axis horizontal in the direction of the average surface velocity (N 36.9° E), Y axis vertical downward, and Z axis horizontally across the glacier so as to make the system right handed. The origin is left unspecified and is chosen for convenience in the specific application. This system will be useful in the presentation and discussion of the inclinometry data, since the initial boreholes are parallel to the Y axis.

(x,y,z) coordinate system has z axis parallel to the Z axis. The x axis, instead of being horizontal as is the X axis, is taken parallel to the ice surface at the center of the borehole array, which has a slope 3.9°. The surface intersection on 8 September, 1966 of borehole 1A is taken as the origin. Essentially all of the analysis of

deformation was done in this coordinate system.

The (x',y',z') is a set of local systems defined for each point on the glacier surface. y' is taken normal to the local surface; x' is normal to y' with azimuth identical to the X and x axes, and z' is chosen to give a right-handed coordinate system. The origin is placed at the instantaneous ice surface. Surface strain-rate determinations from tape measurements are best considered in this system.

For discussions in which a specific coordinate system is not considered, coordinates (x_1,x_2,x_3) are used.

The following vector and tensor quantities are defined with respect to the system (x_1,x_2,x_3): the components u_i of velocity $\vec{v}$, the components $\dot{e}_{ij} = \frac{1}{2}(u_{i,j}+u_{j,i})$ of strain rate $\underset{\sim}{\dot{e}}$, the components $\dot{\omega}_{ij} = \frac{1}{2}(u_{i,j}- u_{j,i})$ of rotation rate $\underset{\sim}{\dot{\omega}}$, the components τ_{ij} of stress, the components g_i of the gravity field $\vec{g}$. If the position of the glacier surface along the x_2 axis is written as $x_2^s = x_2^s(x_1,x_2)$, then the x_1 (x_3) component of surface slope is defined to be $\alpha_1(x_1,x_3) = \partial x_2^s/\partial x_1$ $(\alpha_3(x_1,x_3) = \partial x_2^s/\partial x_3)$. It represents the tangent of the angle between the x_1 (x_3) axis and the intersection of the surface x_2^s with the x_2-x_1 $(x_3$-$x_2)$ plane. In practice, surface slope is calculated by a finite difference with Δx_1 (Δx_3) being approximately equal to the depth of the glacier, thus giving an average surface slope appropriate to the scale of the field experiment. If the trace of a borehole at time t is described parametrically by $x_1^b = x_1^b(x_2,t)$, $x_3^b = x_3^b(x_2,t)$ then the x_1 (x_3) component of tilt or

projected tilt is defined as $\gamma_1(x_2,t) = \partial x_1^b/\partial x_2$ ($\gamma_3(x_2,t) = \partial x_3^b/\partial x_2$). $\Gamma_1 = \tan^{-1} \gamma_{x_1}$ ($\Gamma_3 = \tan^{-1} \gamma_{x_3}$) represents the angle between the x_2 axis and the trace of the borehole when viewed along the x_3 (x_1) axis.

The above quantities are denoted in a specific coordinate system of interest by replacing the numeral subscript with the corresponding axis variable; for example, if the (x_1,x_2,x_3) coordinates are identified with the (x',y',z') system, then the above quantities are denoted $u_{x'}$, $e_{x'x'}$, $\omega_{x'x'}$, $\tau_{x'x'}$, $\alpha_{x'}$, $\gamma_{x'}$, etc. For convenience, the components of velocity with respect to the systems (x,y,z) and (x',y',z') are written (u,v,w) and (u',v',w') rather than with the subscript notation.

B. Surface Velocities

The locations of surface markers on the glacier were computed from the triangulation measurements using plane trigonometry. Initial locations of surface markers in (W,S,U) and (x,y,z) coordinates are given in table 2. Magnitude and direction of the average velocity of markers, and the interval over which the average was taken are given in table 3.

Areal Distribution

Velocity averaged from September 1966 to July 1967, and normalized to one year, ranges from 31 m yr^{-1} to 54 m yr^{-1} over the area where theodolite measurements were made. The azimuths of

the velocity vectors average about N 36.9° E and deviate from this quantity by less than 2°. Direction of average surface slope is approximately N 40° E.

Transverse variation of longitudinal velocity u at sections A, B, and C is shown in figure 8. The centerline of flow, as defined by the maximum (in a transverse profile) of the longitudinal component of velocity, falls approximately 1/2 way between borehole lines 1 and 2. In section A the transverse velocity profile can be extended essentially to the northwest margin on the basis of tape measurements. These measurements indicate that the longitudinal velocity at stake 8A is 11 m yr^{-1}. Extrapolation of the velocity profile indicates that near the margin a zone of decreased velocity gradient must exist if there is not to be negative (up glacier) velocity at the margin. Similar extrapolation at the southeast margin leads to the same conclusion. On both sides of the glacier the marginal sliding velocity can be no greater than a few meters per year.

The y component of velocity v ranges from -2.6 m yr^{-1} to -5.6 m yr^{-1}. The range is a result of transverse variation in longitudinal surface slope and ablation rate. On the southeast side of the glacier v is generally larger because of a lower longitudinal surface slope and a higher ablation rate when compared to the northwest side. The average normal velocity v' of 3.5 m yr^{-1} closely balances the average ablation rate of approximately 3.7 m yr^{-1}.

Time Variation

At three locations (holes 1B, 3A, and 5A) the longitudinal component of velocity over two different time intervals (9/8/66 to 7/13/67 and 9/8/66 to 7/28/67) can be compared. In these locations the average longitudinal component of velocity was respectively 1.19 m yr^{-1}, 1.06 m yr^{-1}, and 1.22 m yr^{-1} greater during the second time interval as compared with the first. The standard error for the above quantities is 0.35 m yr^{-1}. The average velocity during the latter two weeks of July 1967 was 50 ± 15% greater than the corresponding average over the interval 9/8/66 to 7/13/67. Average velocity over the interval 9/8/66 to 7/28/67 was 2 to 3% greater than during the interval 9/8/66 to 7/13/67. Such temporal velocity variations have been observed on several glaciers. The variation reported here is similar in magnitude to weekly variations reported by Paterson (1964) for the Athabasca Glacier. The consistency of the velocity difference for three locations indicates that to an approximation better than the accuracy of the present velocity measurements, the process causing the velocity variation leaves the surface deformation rates locally unchanged.

The velocities averaged over the interval 9/8/66 to 7/28/67 can be compared with those for the interval 7/28/67 to 7/28/68. The differences between the two time averages, when suitably corrected for effects resulting from longitudinal strain rate (table 4), have an average value of 3.56 m yr^{-1}. This corresponds to a decrease in annual velocity of approximately 8%. The spread in the differences

(maximum difference minus minimum difference) is 1.38 m yr^{-1}, which is distinctly less than the average of 3.56 m yr^{-1}. Thus, as was the case with the short term velocity variation observed in July 1967, the above annual velocity variation has tended to affect the glacier surface in a more or less rigid manner. Some systematic differences between the surface deformation pattern over the two intervals can, however, be discerned. The decrease in the surface velocity toward the glacier margins was greater than near the center line; the decrease at section B was slightly greater than at section A. The second effect is less pronounced than the first, so that points along the same longitudinal line are affected more or less equally, in comparison with points lying on different lines.

Observations on several glaciers (Elliston, 1963; Paterson, 1964) indicate that fluctuations in surface velocity are correlated with variations in discharge of streams originiating at the glacier terminus and in the surrounding terrain. If the abundance of melt or rainwater implied by high stream flow significantly increased the pressure in the basal hydraulic system of a glacier, as has been observed to occur (Mathews, 1964), an increase in sliding velocity could be expected on the basis of existing theories of basal sliding (Weertman, 1964; Lliboutry, 1968). The velocity variations reported here are compatible with such an interpretation. The lower average velocity over the period July 1967 to July 1968 as compared to the previous years average could be a result of weaker or less frequent episodes of high sliding velocity during the late spring and early summer of

1968 than was the case in 1967. Early summer of 1968 was unusually cool in contrast to the unusually warm summer of 1967. Ablation rates in July 1968 were less than half of the rate for July 1967 of 4 cm of ice per day. In July of 1968 snow on the valley walls was less abundant than during the previous July. These are all indications that there could have been a considerable difference in the amount of water available to the sub-glacier hydraulic system.

C. Surface Strain Rates

Surface strain-rate components at the center of most of the squares formed by the grid lines were computed from taped distances by the method of Nye (1959). The standard error given by this treatment corresponds closely with that which could be expected on the basis of the independent assessment of the accuracy of the tape measurements discussed in Chapter III. For some squares and rectangles in the outlying parts of the surface strain-rate net only one diagonal had been taped. For these quadrilaterals a determinant procedure based on analysis of triangles was used. The accuracy of the results are essentially the same as for those squares where both diagonals were measured. Values for the surface strain rates are tabulated in table 5. Minimum principal strain rates range from $-0.123\ yr^{-1}$ to $-0.015\ yr^{-1}$. Maximum principal strain rates range from $-0.002\ yr^{-1}$ to $0.166\ yr^{-1}$.

Areal Distribution

The distribution of surface strain rate shows the basic features which one would expect in the ablation region of a valley glacier. The planes of maximum compression are symmetric with respect to a centerline of flow and convex downstream. The changing orientation of the principal strain rates and a progressive increase in strain level with distance from the centerline is a reflection of the marginal shear.

The distribution of the components of surface strain rate is shown in figure 9. In any idealized picture of flow in a symmetric channel, the strain-rate components $\dot{e}_{x'x'}$ and $\dot{e}_{z'z'}$ would be symmetric and the component $\dot{e}_{x'z'}$ antisymmetric across the centerline of flow. The observed distributions show definite deviation from these symmetry conditions, which shows that the slight asymmetry of the channel (fig. 3) and surface (fig. 4) exert observable influence on the pattern of flow. Shear strain rate $|\dot{e}_{x'z'}|$ averaged over the area of the grid squares attains maximum values of 0.10 to 0.15 yr^{-1} on the northwest margin of the glacier. In the area of the borehole array, $|\dot{e}_{x'z'}|$ is less than 0.05 yr^{-1}; $\dot{e}_{x'x'}$ has values ranging from -0.023 to -0.016 yr^{-1}; $\dot{e}_{z'z'}$ has values ranging from -0.002 to +0.005 yr^{-1}.

Marginal crevasses, where they occur within the surface strain-rate net, are perpendicular to directions of maximum extension, as expected (Meier, 1960). Marginal crevasses seem to exist only where the principal extension rate exceeds a value of about

0.1 yr^{-1}, so that marginal crevassing is limited to the area of the glacier outside lines 6 and 7. Although the borehole array covers a large portion of the width of the glacier, none of the boreholes are in the zones of strong marginal shearing.

Time Variation

Tape measurements were not made in the 1968 field season, so that strain-rate calculations as extensive and accurate as those obtained for the 1966-1967 interval cannot be made for the 1967-1968 interval. The triangulation survey does, however, provide some information over a limited area, which allows a comparison of the surface strain rates for the two years. (See table 6.) Since the marginal portions of the glacier showed a velocity decrease greater than did the centerline, an increase in the magnitude of the marginal shear $|\partial u/\partial z|$ is indicated. The largest increase in shear-rate magnitude occurred close to the centerline with the increase between lines 2 and 1 (0.009 yr^{-1}) and 1 and 3 (0.006 yr^{-1}) being greater than that between lines 4 and 2 (0. yr^{-1}) and 3 and 5 (0.001 yr^{-1}). The approximate summetry of the effect suggests that it may be of some general significance. The marginal accuracy of the measurements (standard error 0.003 yr^{-1}) and the limited areal coverage, however, would render any such interpretation rather speculative.

D. Borehole Tilting

Tilt data, taken in the originally bored holes, are given in figure 10, with the exception of borehole 4A, for which no initial tilts were measured. The initial tilts were measured at 15 to 20 m intervals with a Parsons Survey Co. optical inclinometer. When plotted on a polar diagram, as in figure 10, the initial tilts are seen to be randomly distributed about vertical, as would be expected because of the cylindrical symmetry of the hotpoint used for boring the holes. The root-mean-square deviation from vertical of the component of tilt in a vertical plane is 0.25°.

Tilt data for boreholes after approximately one year's deformation are given in figures 11 and 12. In most of the holes, the tilt magnitudes are less than 2° down to a depth of 200 m, below which a relatively rapid and progressive increase with depth is observed. At the bottom of the boreholes, observed tilt magnitudes are typically about 6°, which corresponds to an engineering strain rate of approximately $0.1\ yr^{-1}$. This is less than the shearing rate near the margins of 0.2 to $0.3\ yr^{-1}$ as revealed by the surface strain-rate measurements. Tilts significantly greater than this occur only in two boreholes (3B, 5A) and are restricted to the bottom 10 to 15 m of the hole. The largest tilt measured after one year's deformation was 16°.

In all of the boreholes the azimuth of tilt below 150 m is closely aligned with the direction of the average surface velocity (fig. 12). Most boreholes show directions of tilt in their near surface portions distinctly different from that of the average surface velocity, the

direction of local surface velocity, or the direction of local surface slope (table 7).

Components of tilt

Components of tilt Γ_X and Γ_Z for the deformed boreholes are given in figures 13 and 14. To facilitate comparison of the different boreholes, the data have been normalized to a one year interval; points plotted represent the measured value divided by the time interval between completion of the original borehole and the inclinometry survey of the deformed hole. The signs of the tilts correspond to the sense of the shear strain rate ($e_{x'y'}$ or $e_{y'z'}$) implied by the tilting. Thus a longitudinal tilt Γ_X is positive when it represents an up-glacier tilt. Most of the longitudinal tilts are negative indicating the predominance of down-glacier tilting as would be expected; a transverse tilt Γ_Z is positive when the tilting is toward the negative z axis.

The longitudinal tilt profiles are similar to the tilt-magnitude profiles of figure 11, since the direction of tilt tended to be aligned with the down-glacier direction. The alignment is not perfect, however, hence definite tilting in the transverse plane does occur, as is clearly shown in figure 14. The largest transverse tilt observed after one year's deformation was only slightly in excess of 1^{o}.

Smoothing of tilt profiles

For some of the subsequent analysis and for efficiency in presenting results, it was found desirable to use smoothed tilt data. The

curves drawn in figures 11, 12, 13 and 14 are smooth curves selected to represent the data. In smoothing the tilt data there are two choices. The tilt magnitudes and tilt azimuths can be independently smoothed, or alternatively the two components of projected tilt can be independently smoothed. Each of these approaches has certain advantages and disadvantages.

The main advantage of the first approach is that any systematic error in the azimuth of tilt can be eliminated. Such a systematic error could arise from a tendency of the inclinometer to rotate preferentially in one sense as it is lowered down the hole, thus producing an asymmetry in the error caused by friction in the compass needle. This source of error is easily eliminated in the deeper portions of the holes by taking the center of the well-defined band into which the azimuth readings fall, rather than taking the median. A further factor is that any error in an azimuth determination always has the effect of diminishing the measured component of tilt in the correct plane of tilt. This is a second order effect, but nevertheless, for a 20^{o} error in azimuth, it amounts to 7%, and is thus a systematic effect, which can be minimized by eliminating the noise in the azimuth determinations before computing the projected tilt profiles. The main problem which can arise in this procedure is that the condition of tilts symmetrically distributed about the vertical is not well displayed in terms of tilt magnitudes and azimuth of tilt considered independently. Such a situation is approached near the surface in several boreholes (1B, 2A, 2B) where the tilt magnitude becomes small. If such a situation occurs, where the tilt magnitudes are large, inde-

pendent smoothing of the tilt magnitude and azimuth can lead to totally anomalous results.

If the second approach, that of smoothing the projected tilts, is pursued, the above geometrical problems are avoided. Any systematic errors resulting from the asymmetric nature of the noise in the azimuth and the width of the noise band would, however, be difficult to eliminate.

The method finally adopted was to use both approaches. First the tilt magnitudes and azimuths were smoothed independently as shown by the solid line curves (figs. 11 and 12). Smoothed longitudinal and transverse tilt profiles were then computed and plotted on the same plot as the tilt components computed from the unsmoothed quantities. These curves were then adjusted in places where the geometrical problems described above gave unacceptable results. The resulting curves shown in figures 13 and 14 are the smoothed curves which are used in subsequent calculations.

General features of borehole tilting

Longitudinal tilting is caused by interaction of several of the components of strain rate and rotation rate when considered in the coordinate system (x',y',z'). This is a result of the fact that the boreholes were not parallel to the coordinate axis. The instantaneous longitudinal tilting rate is given by the formula

$$\frac{D\gamma_{x'}}{Dt} = (\dot{e}_{x'y'} + \dot{\omega}_{x'y'}) + \gamma_{x'}(\dot{e}_{x'x'} - \dot{e}_{y'y'}) + \gamma_{z'}(\dot{e}_{x'z'} + \dot{\omega}_{x'z'}) - \gamma_{x'}^2(\dot{e}_{x'y'} - \dot{\omega}_{x'y'}) + \gamma_{x'}\gamma_{z'}(\dot{e}_{y'z'} - \dot{\omega}_{y'z'}) \qquad (1)$$

which follows from general formulae derived by Shreve and Sharp (unpublished). Since the boreholes deviate less than 4^{o} from being parallel to y', so that $\gamma_{x'}$ and $\gamma_{z'}$ are small with respect to 1, and if $\omega_{x'y'}$ is presumed to be small, then the major contribution is produced by the shear strain rate parallel to the surface $e_{x'y'}$. For this discussion, the contributions from the other components of strain rate can be neglected, so that $e_{x'y'}$ is proportional to the tilting rate $D\gamma_{x'}/Dt$. Further, since the surface slope, the tilts, and the curvature in the borehole are small,

$$\frac{D\gamma_{x'}}{Dt} = \frac{\partial\gamma_{x'}}{\partial t} + v_y \frac{\partial\gamma_{x'}}{\partial y} \approx \frac{\partial\gamma_{x'}}{\partial t} \propto \Gamma_X ,$$

where Γ_X is the tilt one year after emplacement of the initially vertical borehole. In addition it is assumed that the shear stress parallel to the surface, $\tau_{x'y'}$, varies linearly with depth. This is an assumption which has been made in the interpretation of all previous borehole experiments. On this basis the plots of longitudinal tilting rate versus depth in figures 13 represent the stress-strain-rate relationship for ice, and define an effective viscosity $\eta = \tau_{x'y'}/2e_{x'y'} \propto Y/\Gamma_X$. For example, a linear fluid would plot as a straight line. In a nonlinear material, such as ice, the effective viscosity depends on the components of strain rate; deviation of the plot from linearity together with knowledge of the strain-rate components gives information about the form of the dependence. It is worthwhile discussing the longitudinal tilts under these simplifications because it provides an intuitive framework in which the original

data can be discussed and related to the derived quantities to be considered later.

Longitudinal tilts for borehole 3A show the features which would be generally expected for a strain-rate softening material such as ice. Consider the smoothed profile (fig. 13f). The tilting rate at the surface is zero since $\tau_{x'y'}$ is zero and thus $e_{x'y'}$ is zero there. The apparent finite slope of the curve at the surface indicates that the effective viscosity is finite, as would be expected if the other strain-rate components were not zero. The progressive increase in tilt magnitude accompanied by a monotonic decrease in the slope magnitude of the profile is what would be expected as a result of the lowering of the effective viscosity as the shear strain rate increases with depth. Although all of the boreholes conform in a general manner to the pattern of borehole 3A, a number of deviations from it occur.

Several boreholes, most notably holes 1B and 2B, show non-zero tilting rates at the surface (figs. 13b and e). Such an effect was also observed in the boreholes 314 and 322 of Savage and Paterson (1963) which were initially in this region of the glacier. As shown by Savage and Paterson, such non-zero tilting can be understood as an effect of a rotation rate $\omega_{x'y'}$ acting at the surface of the glacier. In Chapter VI-B quantitative comparison for all the boreholes shows that the rotation rates implied by the surface tilting rates agree with what would be expected on the basis of the distribution of longitudinal velocity and surface curvature.

A striking feature displayed by most tilt profiles (1A, 1C, 2B, 3B, 5A) is a rather extensive depth range (typically 100 to 250 m)

over which the slope of the tilt profile remains nearly constant (fig. 13). In several cases (1A, 2B) the tilt profiles actually show a slight concavity toward the depth axis. These features indicate that other depth-dependent strain-rate components, in addition to the shear strain rate, influence the effective viscosity to a significant degree.

Most boreholes, especially holes 1B and 3B, have tilt profiles which are essentially vertical over a significant depth range (up to 100 m). When allowance for the rotation discussed above is made, this would indicate that a very high effective viscosity exists close to the surface. Such high viscosity is unexpected because of the non-zero surface strain rates.

These features are considered in Chapter VII, where it is shown that to some extent they can be understood on the basis that effective viscosity is determined by the second strain-rate invariant. It is also shown that the shear stress must deviate from strictly linear dependence.

The profile of borehole 2A shows a remarkable break in the trend of increasing tilt rate with depth. Over the lowermost 40 m the tilting rate remains essentially constant, rather than showing the strong progressive increase usually observed. This anomaly reflects a pronounced deviation from the normally-assumed linear variation of shear stress with depth. It is an example of a zone of relatively low basal shear stress at the bed, as though the bed were abnormally smooth near the bottom of borehole 2A.

The distribution of transverse tilt rate with depth is not so easily discussed as it lacks any significant structure in individual

boreholes. Correlation of trends from borehole to borehole, however, presents an interesting picture. This is better discussed in terms of the integrated tilt profiles discussed below. Non-zero transverse tilting at the surface is larger than could be expected from a surface rotation rate $\omega_{y'z'}$ as calculated from the distribution of longitudinal velocity u' and the transverse variation of longitudinal surface slope (Chapter VI-B and D).

Time variation of borehole deformation.

In the two boreholes (2A, 3B) which were recovered in the third summer's field work, comparison of tilts after one and two years' deformation is possible. In this comparison several distinct influences can be expected to produce a temporal variation in the tilting-rate distribution in a given borehole. First, the most obvious of these is a time variation of the boundary stresses, resulting in a corresponding time dependence of the internal deformation rates. Second, as the borehole location changes during flow, an apparent time variation will be observed if there are strain-rate gradients in the direction of its motion. Third, in a homogeneous strain-rate and rotation-rate field, constant in time, the apparent rotation rate of a line segment depends on its orientation. Thus even in these uniform circumstances, as finite tilting accumulates, an apparent time variation in the tilting rate is to be expected. These effects on the longitudinal tilting rate can be investigated quantitatively by differentiating equation (1) with respect to time. In the case where $\gamma_{x'}$ and $\gamma_{z'}$

are small and the strain rates are small, the term $(\dot{e}_{x'y'} - \dot{\omega}_{x'y'}) = \partial u'/\partial y'$ dominates, as noted before. In this approximation the differentiation yields:

$$\frac{D}{Dt}\left(\frac{\partial \gamma_{x'}}{\partial t}\right) \cong \frac{\partial}{\partial t}\frac{\partial u'}{\partial y'} + u' \frac{\partial}{\partial x'}\left(\frac{\partial \gamma_{x'}}{\partial t}\right) \qquad (2a)$$

The first right-hand-side term corresponds to a real time variation of the deformation rates or the first effect cited above. The second term is a result of the advection of the borehole or the second effect. An advection term $w'(\partial/\partial z')(\partial \gamma_{x'}/\partial t)$ can be neglected since w' is very closely zero. The third effect cited above proves to be negligible in this approximation. $(D/Dt)(\partial \gamma_{x'}/\partial t)$ can be evaluated by considering the tilting rates for the two successive year intervals for holes 2A and 3B. $u'(\partial/\partial x)(\partial \gamma_{x'}/\partial t)$ can be estimated for 2A and 3B by assuming a linear variation of tilting rate between the pairs 2A and 2B, and 3A and 3B respectively. Thus the difference in the time-average value of $\partial u'/\partial y'$ for the two-year intervals can be evaluated. If there were no time variation of the strain rates, the 1968 normalized tilt profiles for 2A and 3B should be displaced from the 1967 normalized profiles by an amount approximately 1/6 of the spacing of the 1967 pairs 2A and 2B, and 3A and 3B respectively. A factor of 1/3 arises from the fact that the annual displacement is approximately 1/3 of the spacing of the borehole pairs. An additional factor of 1/2 arises because the 1968 profiles normalized to 1 year are considered rather than the difference between the 1968 and 1967 tilts. 2A of 1968 would be displaced toward 2B and 3B would be displaced away from 3A as a

result of the sense of the motion. The approximation $\gamma_{x'} \cong \gamma_X + \alpha_X$, gives explicit formulae for $(\partial/\partial t)(\partial u'/\partial y')$ in terms of the tilts measured in 1966, 1967, and 1968:

$$\frac{\partial}{\partial t}\left(\frac{\partial u'}{\partial y'}\right)^{2A} \cong 2\left(\frac{1}{2}\gamma_X{}^{2A}(68) - \frac{5}{6}\gamma_X{}^{2A}(67) - \frac{1}{6}\gamma_X{}^{2B}(67)\right) \text{ yr}^{-2}$$

(2b)

$$\frac{\partial}{\partial t}\left(\frac{\partial u'}{\partial y'}\right)^{3A} \cong 2\left(\frac{1}{2}\gamma_X{}^{3B}(68) - \frac{7}{6}\gamma_X{}^{3B}(67) + \frac{1}{6}\gamma_X{}^{3A}(67)\right) \text{ yr}^{-2}.$$

($\gamma_X(66) = 0$, hence it does not explicitly appear in these equations.) In figure 15the normalized 1967 tilt profiles are plotted as dashed lines and the normalized 1968 profile is shown as a solid line. For both cases the pattern is not as simple as that which would be expected for time dependence of $\partial u'/\partial y'$, thus indicating either that there was a real but small difference in the average value of $\partial u'/\partial y'$, that the assumption of linear variation with x of tilting rate is not valid, or that the experimental errors are obscuring the pattern.

Evaluation of the change in the time average values of $\partial u'/\partial y'$ between the two years by formulae (2b) gives values which, over most of the depth of both boreholes are negative. This is apparent from figure 15 which shows the 1968 curve being generally displaced to the left of the position expected if the strain rate did not vary in time. Over most of the depth range the calculated values correspond to time-rate-of-change of engineering strain rate of -0.002 yr^{-2} to -0.008 yr^{-2} (table 8). On the basis of the accuracy to which the tilt profiles are determined, a standard error of ± 0.002 yr^{-2} could be expected. Thus it seems unlikely that the effect is purely a result of measure-

ment errors. In the lower 1/4 of the boreholes, the indicated rate of change in $\partial u/\partial y$ ranges from zero to strongly positive ($0.03\ yr^{-2}$) very close to the bottom of hole 3B. The values calculated at these depths are, however, highly suspect, since the assumption of linear x-variation of tilting rate could break down close to the glacier bed. It is quite possible, if not probable, that the rates of change of $\partial u/\partial y$ calculated from equation (2b) are a result of local variations in the spatial distribution of the strain-rate field rather than an actual temporal variation. On the other hand, the negative values of $(\partial/\partial t)(\partial u/\partial y)$, which persist over considerable depths where a linear variation of tilting rate could be expected to be more reliable, and which are consistent in the two boreholes, probably indicate a real but small time variation of the strain-rate field. Since $\partial u'/\partial y'$ is negative at all depths (except possibly near the surface), the negative difference corresponds to an increase in $|\partial u'/\partial y'|$. The average value of the difference in $\partial u/\partial y$ over the whole depth of both boreholes is approximately $-0.002\ yr^{-1}$. This corresponds to an increase in the magnitude of differential velocity with respect to the surface of approximately $0.5\ m\ yr^{-1}$ from the first year interval to the second.

The sense of the change in borehole deformation from 66-67 to 67-68 is the same as that observed for the surface strain rates measured in the central portion of the glacier, which also showed stronger marginal shear rate in the second year interval as compared to the first. It is noteworthy that on the area of the cross section where this change is best determined, the sense of the time variation of the velocity gradients $\partial u/\partial y$ and $\partial u/\partial z$ is such as to produce greater

differential velocity between the glacier bed and the center portion of the surface for the second year interval. Thus acting alone it would produce a difference in the surface velocities between the two years opposite to the observed decrease. Thus the decrease in the observed surface velocities must be caused by a decrease in the glacier sliding velocity. This has been partially counteracted by an increase in the deformation rates.

A change in deformation rates could be expected even if the sliding velocity decreased uniformly over the bed. A redistribution of stress in the glacier is required in order that the same flux can be transported under the changed sliding condition. The redistributed stress would act to bring the glacier surface into a new equilibrium configuration. This phenomenon is of particular significance with respect to the theory of kinematic wave propagation (Nye, 1960).

E. Differential Displacement in Boreholes

Integration of γ_X and γ_Z gives the difference in X and Z coordinates of a point on a borehole at depth Y and the coordinates of the surface intersection of the borehole (Y = 0):

$$\Delta X(Y,t) = \int_o^Y \gamma_X(Y',t)\, dY'$$

$$\Delta Z(Y,t) = \int_o^Y \gamma_Z(Y',t)\, dY' \quad . \tag{3}$$

The accuracy of ΔX and ΔZ thus calculated can be determined from

the analysis of the tilt measurements as discussed in detail in Appendix II. For the initial boreholes a standard error of 30 cm is calculated for ΔX and ΔZ at a depth of 300 m. The standard errors of ΔX and ΔZ at a depth of 300 m in deformed boreholes are calculated to be 20 and 27 cm respectively. The standard errors have values of zero at the surface and increase approximately as the square root of depth.

The borehole configurations for the smoothed tilts, normalized to one year's deformation, are shown in figures 16 and 17. Boreholes lying on the same longitudinal line are plotted against the same origin. Initial borehole configurations are all identical and are represented by the Y scale. The deformed borehole configuration plotted then represents the differential displacement with respect to the surface as a result of ice deformation over the period of one year. Longitudinal differential displacements at the bottoms of those boreholes which penetrate to the glacier bed range from 5.7 to 13.7 m. Transverse differential displacements up to 3.2 m in magnitude occurred.

Longitudinal differential displacements

One notable feature of the differential longitudinal displacements is that for all of the boreholes reaching bedrock the differential displacement is a relatively small percentage of the surface displacement. The largest contribution to surface motion from differential displace-

ment was observed in borehole 5A (33%). For all other holes the differential displacement lies between 12 and 22%, thus a large part of the surface velocity is produced either by sliding or by concentrated deformation in a thin basal zone no more than a few meters thick.

Another important feature of the differential longitudinal displacements (fig. 16) is the systematic relationship between the differential displacement of boreholes in section B when compared with the borehole on the same line in section A. In the three cases where this comparison can be made (lines 3, 1, 2), the differential displacement of the section A boreholes becomes with increasing depth progressively greater than the corresponding displacement in the section B boreholes, as is indicated by the divergence of the three pairs of curves. This demonstrates a variation with depth of the longitudinal strain rate. Since section B lies down-glacier from section A, the sense of the variation is increased extension at depth relative to the surface. When borehole 1C is compared with borehole 1A a similar relationship of relative extension at depth is seen to exist. Savage and Paterson (1963) showed from indirect measurements that the longitudinal strain rate could not be expected to be constant with depth over a large portion of the Athabasca Glacier. The observations presented here directly confirm Savage and Paterson's prediction of relative extension at depth for this portion of the glacier. These observations are significantly at variance with existing theoretical treatments of glacier flow, which require the longitudinal strain rate to be constant with depth. Possible causes of the observed

behavior are discussed in Chapter VI-C.

Transverse differential displacements

The presence of substantial transverse differential displacements is shown in figure 17. The importance of the transverse displacements is demonstrated by the following observations. The transverse displacement near the bottom of boreholes can be as much as 30% of the corresponding longitudinal displacement as is the case in borehole 1A. For the boreholes which show significant transverse differential displacement at depth, the near surface transverse displacements exceed the corresponding longitudinal displacements to a depth typically of about 100 m. In the case of borehole 3B this is the case to a depth of 184 m.

There is a systematic spatial distribution of the differential transverse displacements (fig. 17). Neglecting for the moment the profiles for 1A and 1C, there is a general pattern of divergence of the profiles away from the centerline of flow. Profiles of boreholes near the centerline (1B, 2A, 2B) are essentially vertical; profiles of boreholes to the left of the centerline on the plot (3A, 3B, 5A which lie toward the southeastern margin of the glacier with respect to the centerline) show marginward differential displacement increasing in magnitude with depth, and are thus inclined to the right. The strength of the effect is stronger with increasing distance from the centerline. On the other side of the centerline boreholes corresponding to 3A, 3B, and 5A are largely lacking. However, the differential transverse displacements shown by borehole 4A give

some evidence for the symmetry of the effect. In Chapter VI-D it is shown that such a systematic pattern of transverse displacement can be generally expected in the ablation region of a valley glacier.

The relatively large differential transverse displacements shown by boreholes 1A and 1C are clearly anomalous in that both holes lie close to the centerline of flow, where transverse velocity would be expected from symmetry considerations to be small over the whole depth of the glacier. These anomalous effects must be related to peculiarities of the local flow situation and can not represent a general feature of flow in a valley glacier.

The existence of significant, depth-dependent transverse displacements is particularly noteworthy in light of the assumption of plane strain made in almost all theoretical discussions of glacier flow and analyses of borehole deformations.

CHAPTER V

CALCULATION OF THE INTERNAL DISTRIBUTION OF VELOCITY AND STRAIN RATE

Present boring methods produce holes which are initially vertical rather than normal to the glacier surface. This complicates the interpretation of borehole tilting in terms of the flow quantities which are of primary interest. First a brief discussion of methods of interpretation of borehole data used in previous experiments is given. Then an iterative procedure by which self consistent velocities and strain rates can be calculated from the data from a borehole array is described. The steps in the procedure are related to the earlier methods where possible. The distribution of velocity and strain rate as calculated by the new method are presented and the accuracy considered. All calculations are carried out in the (x,y,z) system.

A. Method of Calculation

In previous borehole experiments the interpretation of borehole tilting in terms of strain-rate components has been done by various methods, all of which involve a number of assumptions. The most general treatment to date is that of Shreve and Sharp (unpublished). The following formulae can be derived from their treatment:

$$\frac{D\gamma_x}{Dt} = \frac{\partial u}{\partial y} + \gamma_x\left(\frac{\partial u}{\partial x} - \frac{\partial v}{\partial y}\right) + \gamma_z \frac{\partial u}{\partial z} - \gamma_x\left(\gamma_x \frac{\partial v}{\partial x} + \gamma_z \frac{\partial v}{\partial z}\right)$$

$$\frac{D\gamma_z}{Dt} = \frac{\partial w}{\partial y} + \gamma_z\left(\frac{\partial w}{\partial z} - \frac{\partial v}{\partial y}\right) + \gamma_x \frac{\partial w}{\partial x} - \gamma_z\left(\gamma_x \frac{\partial v}{\partial z} + \gamma_z \frac{\partial v}{\partial x}\right) \qquad (1)$$

where the components of tilt $\gamma_x(y,t)$ and $\gamma_z(y,t)$ are defined as in Chapter IV-A, and $D/Dt = (\partial/\partial t) + v(\partial/\partial y)$. The components of tilting rate depend in a complex manner on all nine velocity gradients, and the orientation of the borehole trace. Clearly all nine velocity gradients cannot be determined from the distribution of instantaneous tilt and tilting rate in a single borehole without further relationships. One such relationship which can be expected to hold is the condition of incompressibility.

$$\frac{\partial u}{\partial x} + \frac{\partial v}{\partial y} + \frac{\partial w}{\partial z} = 0 \qquad (2)$$

This is still not sufficient, so that assumptions concerning some of the velocity gradients must be made.

In the first quantitative borehole experiment (Gerrard, Perutz, and Roch, 1952) all contributions to the tilting rate $\partial\gamma_x/\partial t$ were neglected except $\partial u/\partial y$, so that $\partial u/\partial y \cong \partial\gamma_x/\partial t$. This approximation would hold exactly in the case of homogeneous simple shear parallel to the surface or in the case $\gamma_x = \gamma_z = 0$. Nye's (1957) analysis of the same data took into account the presence of longitudinal strain rate $\partial u/\partial x$ assumed to be equal to the surface value over the whole depth of the glacier. Assumption of plane strain and incompressibility give $\partial v/\partial y = -\partial u/\partial x$, thus in this case

$$\frac{\partial u}{\partial y} \cong \frac{\partial \gamma_x}{\partial t} - 2\gamma_x \frac{\partial u}{\partial x}$$

other contributions being neglected. Savage and Paterson (1963) showed how the assumption that the surface value of $\partial u/\partial x$ applies

to the whole depth can be improved upon by estimating the value of $\partial v/\partial y$ averaged over the depth of the glacier from surface measurements, knowledge of the basal sliding velocity, and the slope of the bed with respect to the surface. In previous borehole experiments transverse tilting was either not observed, or was considered to be negligible.

Instead of analyzing a single borehole on the basis of equations (1) and extra assumptions, as has been necessary in the past, it is appropriate to analyze all of the borehole data at once, with the possibility of eliminating many of these assumptions. This possibility was one of the motivations for the three-borehole experiment on the Blue Glacier (Kamb and Shreve, 1966) and for the coordinated borehole array of the present experiment. The feasibility of this is readily apparent in relation to equations (1) and (2). If the gradients of the components of velocity in directions parallel to the surface (i.e., $\partial u/\partial x$, $\partial u/\partial z$, $\partial v/\partial x$, $\partial v/\partial z$, $\partial w/\partial x$, $\partial w/\partial z$) were known, then by use of these formulae $\partial u/\partial y$, $\partial w/\partial y$, and $\partial v/\partial y$ can be calculated. The problem then is to estimate, insofar as is possible, the velocity gradients parallel to the surface at each of the boreholes, by comparison of the displacements in adjacent boreholes.

In the reduction of the Athabasca borehole data the basic approach has been that implied by the above discussion. However, the calculations were made by using the differential displacement profiles rather than the tilt profiles themselves, in a manner somewhat similar to a method used by Savage and Paterson (1963). The motivation for this is that it leads to a method which is easily visualized

geometrically in terms of displacements, and which is readily adapted to computation on a digital computer. First the method used to calculate the components of velocity along a single borehole is described, and its relationship with the formula presented above is discusssd. The technique by which all of the boreholes were considered simultaneously in order to calculate self-consistent velocity and strain-rate fields throughout the borehole array is then described.

Analysis of a single borehole

The problem of how to determine the depth distribution of u and w from the initial and final coordinates is now considered. It is assumed that the distribution of v and the x and z gradients of u, v, and w are known. Let $x_i(y)$, $z_i(y)$ represent the initial x and z coordinates of a borehole at depth y, and $x_f(y)$, $z_f(y)$ represent the coordinates after a time interval Δt. In this present discussion only the longitudinal component of velocity is discussed. Exactly the same considerations apply to the transverse component. Since the y component of velocity v is in general non zero a specified element of ice initially at depth y_i lies at a different depth y_f on the borehole after the time interval Δt. The difference in depth $\Delta y = y_f - y_i$ is determined by the distribution of v and the time interval Δt. The path of the element in the x, y plane is some curve joining $x_i(y_i)$ and $x_f(y_f)$ as shown in figure 18. The average longitudinal velocity of the element over the interval Δt is $(x_f(y_f) - x_i(y_i))/\Delta t$.

The calculation of the average velocity of the element and its assignment to a specific point in space are made as follows. Define

$$u^*(y) = \frac{1}{\Delta t}\left(x_f(y + \tfrac{1}{2}\Delta y) - x_i(y - \tfrac{1}{2}\Delta y)\right) \tag{3}$$

and

$$\begin{aligned} x^*(y) &= \tfrac{1}{2}\left(x_f(y) + x_i(y)\right) \\ z^*(y) &= \tfrac{1}{2}\left(z_f(y) + z_i(y)\right) . \end{aligned} \tag{4}$$

In order to calculate $u^*(y)$, Δy can be approximately evaluated by

$$\Delta y \simeq v\left(x^*(y), y, z^*(y)\right)\Delta t . \tag{5}$$

Intuitively it could be expected that the velocity u at some point roughly halfway between the initial and final locations of an ice element would be equal to the average velocity of the ice element. It is thus suggested that the quantity $u^*(y)$, which is the average velocity of the borehole element for which y_i and y_f are equal distance above and below depth y, gives to some approximation the velocity u at a point of depth y, which is halfway between the initial and final boreholes as given by $x^*(y)$ and $z^*(y)$. The derivative of $u^*(y)$ with respect to y is approximately equal to the directional derivative of u parallel to the curve defined by $x^*(y)$ and $z^*(y)$. In order to interpret $u^*(y)$ in terms of the velocity field the following approximate formulae are used:

$$u^*(y) \cong u\left(x^*(y), y, z^*(y)\right) \tag{6}$$

$$\begin{aligned} \frac{du^*(y)}{dy} \cong{}& \frac{\partial u}{\partial y}\left(x^*(y), y, z^*(y)\right) + \gamma_x^*(y)\frac{\partial u}{\partial x}\left(x^*(y), y, z^*(y)\right) \\ &+ \gamma_z^*(y)\frac{\partial u}{\partial z}\left(x^*(y), y, z^*(y)\right) . \end{aligned} \tag{7}$$

In fact, if the velocity field is assumed independent of time, it can be shown that

$$\Delta y = v\left(x^*(y), y, z^*(y)\right) \Delta t\left(1 + O[(\dot{e}\Delta t)^2] + O[\vec{v}\Delta t \cdot \vec{\nabla}\dot{e}\Delta t]\right)$$

$$u^*(y) = u\left(x^*(y), y, z^*(y)\right)\left(1 + O[(\dot{e}\Delta t)^2] + O[\vec{v}\Delta t \cdot \vec{\nabla}\dot{e}\Delta t]\right)$$

$$\frac{du^*(y)}{dy} - \gamma_x^*(y)\frac{\partial u}{\partial x}\left(x^*(y), y, z^*(y)\right) - \gamma_z^*(y)\frac{\partial u}{\partial z}\left(x^*(y), y, z^*(y)\right) \tag{8}$$

$$= \frac{\partial u}{\partial y}\left(x^*(y), y, z^*(y)\right)\left(1 + O[(\dot{e}\Delta t)^2] + O[\vec{v}\Delta t \cdot \vec{\nabla}\dot{e}\Delta t]\right),$$

where $\dot{e}$ and $\vec{\nabla}\dot{e}$ represent the components of strain rate and their gradients at the curve $x^*(y), z^*(y)$.

In the event the strain-rate field is homogeneous the error introduced by using the approximate formulae (5), (6), and (7) goes as the square of accumulated strain experienced by an element of ice which traverses the space between the initial and final borehole locations. Further, in practice it can be expected that strain-rate gradients will be small compared to the general strain-rate level. Thus when accumulated strain in the interval Δt is small, as is the case with the deformation over the period of one year in the Athabasca boreholes, the approximation implied by equations (5), (6), and (7) can be expected to be a good one. After proceeding upon the basis of this approximation to a final calculation of the velocity field, strain rates and strain-rate gradients, it is possible to test the validity of the approximation quantitatively. Explicit formulae have been derived for the correction terms with contributions from derivations of

velocity higher than second order being neglected. Because of their length they will not be included here. They indicate, however, that the error associated with the approximation is negligibly small (less than 0.1%). Other sources of error are considerably larger than this as will be discussed.

To summarize, u can be calculated along the curve defined by equations (4) by use of equations (5), (3), and (6) from the initial and final borehole coordinates and the y component of velocity v. $\partial u/\partial y$ can be calculated along the curve from equation (7) if $\partial u/\partial x$ and $\partial u/\partial z$ are known.

Differentiation with respect to y of equations (3) and (5) shows that in the limit $\Delta t \rightarrow 0$ they are equivalent to the first of equations (1). In the limit $\Delta t \rightarrow 0$, note that

$$x_f(y) = x^*(y) = x_i(y) = x(y,t_i)$$

$$z_f(y) = z^*(y) = z_i(y) = z(y,t_i) \qquad (9)$$

$$\frac{\Delta y}{\Delta t} = \frac{y_f - y_i}{\Delta t} = v\Big(x(y,t_i),y,z(y,t_i)\Big) \quad .$$

In this limit differentiation of equation (3) gives

$$\frac{du^*}{dy} = \frac{D\gamma_x}{Dt} + \gamma_x\left[\frac{\partial v}{\partial y} + \gamma_x\frac{\partial v}{\partial x} + \gamma_z\frac{\partial v}{\partial z}\right] \quad , \qquad (10)$$

and differentiation of equation (6) gives

$$\frac{du^*}{dy} = \frac{\partial u}{\partial y} + \gamma_x\frac{\partial u}{\partial x} + \gamma_z\frac{\partial u}{\partial z} \quad . \qquad (11)$$

Setting the left sides of equations (10) and (11) equal gives the first of

equations (1).

For the purpose of practical application of these formulae, it is desirable that they be used in a different form. The first reason is that application of these equations requires the use of both borehole coordinates and tilt components. In the iterative computer calculation ultimately used, this would require either an unnecessarily large storage block, or a repeated calculation of tilt from borehole coordinates. Secondly, it is desirable to have the quantities known on a line of constant x and z, so that when interpolation between boreholes is made, the interpolation formulae are independent of depth. For these reasons the procedure is modified as follows. Let $y_s(x,z)$ be a datum surface, which represents the surface of the glacier at a specific time (in this case 9/8/66). u can be calculated on the y-coordinate line through the surface intersection of the original borehole from its value on the curve $x^*(y)$, $z^*(y)$, given by equation (3), by applying a suitable correction to take account of the x and z gradients of u. To first order in x^* and z^*,

$$u\left(x_i(y_s),y,z_i(y_s)\right) = u^*(y) - \frac{\partial u}{\partial x}\left(x_i(y_s),y,z_i(y_s)\right)\left[x^*(y)-x_i(y_s)\right] - \frac{\partial u}{\partial z}\left(x_i(y_s),y,z_i(y_s)\right)\left[z^*(y)-z_i(y_s)\right] \quad (12)$$

Equation (12) involves no further approximation if $\partial u/\partial x$ and $\partial u/\partial z$ are independent of x and z. Since the lengths over which the correction is made are small ($x^* < 25$ m, $z^* < 1.5$ m) and the quantities $\partial^2 u/\partial x^2$, $\partial^2 u/\partial x \partial z$, $\partial^2 u/\partial z^2$ and higher derivatives are small, no significant error is introduced. Explicit evaluation of the contribu-

tion from second derivatives of u substantiates this.

Equation (5) could also be similarly modified so that Δy can be calculated from $v\left(x_i(y_s), y, z_i(y_s)\right)$. In these calculations, however, $\partial v/\partial x$ and $\partial v/\partial z$ have been taken to be zero, which gives $v\left(x^*(y), y, z^*(y)\right) = v\left(x_i(y_s), y, z_i(y_s)\right)$. This additional assumption turns out to be of negligible consequence because of the actual smallness of these gradients and the indirect way in which v enters in the formulae for u and $\partial u/\partial y$. Equations (3), (4), (5), and (12), and the same considerations applied to the transverse component of velocity, give

$$
\begin{aligned}
u(y) = \frac{1}{\Delta t}\left[x_f\left(y + \tfrac{1}{2}v(y)\Delta t\right) - x_i\left(y - \tfrac{1}{2}v(y)\Delta t\right)\right] \\
- \frac{\partial u(y)}{\partial x}\left[x^*(y) - x_i(y_s)\right] - \frac{\partial u(y)}{\partial z}\left[z^*(y) - z_i(y_s)\right] \\
w(y) = \frac{1}{\Delta t}\left[z_f\left(y + \tfrac{1}{2}v(y)\Delta t\right) - z_i\left(y - \tfrac{1}{2}v(y)\Delta t\right)\right] \\
- \frac{\partial w(y)}{\partial x}\left[x^*(y) - x_i(y_s)\right] - \frac{\partial w(y)}{\partial z}\left[z^*(y) - z_i(y_s)\right]
\end{aligned}
\qquad (13a)
$$

For notational compactness u(y) denotes $u\left(x_i(y_s), y, z_i(y_s)\right)$, $\partial u(y)/\partial y$ denotes $\partial u/\partial x\left(x_i(y_s), y, z_i(y_s)\right)$, etc. Since in equations (13a) all quantities either depend only on y or on their values along a line parallel to the y coordinate axis, calculation from them of $\partial u/\partial y$ and $\partial w/\partial y$ can be directly made.

Equations (13a), which are the basic equations for the analysis of the displacements in a single borehole for longitudinal velocity, can be used as they stand. It is, however, desirable to partition the equations into contributions from the surface displacements of the

borehole at depth. At any time t, the borehole coordinates can be described by the location of the intersection of the borehole with a datum plane of constant y and the x and z coordinates relative to that point. Thus

$$x(y,t) = x(y_s,t) + \Delta x(y,t)$$

$$z(y,t) = z(y_s,t) + \Delta z(y,t)$$

where the plane $y = y_s$, which passes through the intersection of the original borehole with the datum glacier surface, has been chosen as the datum plane (fig. 18). Let

$$D_x = x_f(y_s) - x_i(y_s) \quad , \quad D_z = z_f(y_s) - z_i(y_s)$$

represent the borehole displacement on the datum plane during the time interval Δt (fig. 18) and define the surface longitudinal velocity to be

$$u_s = \frac{1}{\Delta t} D_x - \frac{1}{2} \frac{\partial u(y_s)}{\partial x} D_x - \frac{1}{2} \frac{\partial u(y_s)}{\partial z} D_z + \frac{v(y_s)}{2} \left(\gamma_{x_f}(y_s) + \gamma_{x_i}(y_s) \right)$$

$$w_s = \frac{1}{\Delta t} D_z - \frac{1}{2} \frac{\partial w(y_s)}{\partial x} D_x - \frac{1}{2} \frac{\partial w(y_s)}{\partial z} D_z + \frac{v(y_s)}{2} \left(\gamma_{z_f}(y_s) + \gamma_{z_i}(y_s) \right). \tag{13b}$$

Note that with these definitions u_s and w_s are approximately equal to $u(y_s)$ and $w(y_s)$ as defined by equation (13a). The correspondence is exact when the surface segment of the borehole lacks curvature, which in practice is the case. Equation (13a) can now be written as

$$u(y) = u_s + u_d(y)$$
$$w(y) = w_s + w_d(y) \qquad (13c)$$

thus defining differential velocities $u_d(y)$ and $w_d(y)$. The quantities u_s and w_s can be determined unambiguously in terms of the quantities measured at the surface by triangulation and taping. $u_d(y)$ and $w_d(y)$ are quantities that can be determined from knowledge of the distributions of v, $\partial u/\partial x$, $\partial u/\partial z$, $\partial w/\partial x$, and $\partial w/\partial z$ over the depth of the borehole.

Although this approach is more complicated than the direct application of equations (13a), it has the advantage that it is possible to tie the derivates with respect to x and z of u and w directly to these quantities measured at the surface, i.e.,

$$\frac{\partial u_\alpha(y)}{\partial x_\beta} = \frac{\partial u_\alpha(y_s)}{\partial x_\beta} + \frac{\partial u_{d\alpha}(y)}{\partial x_\beta} \qquad (13d)$$

where α and β assume values of 1 or 3. There is no constraint to use surface strain rates calculated only from the velocities at the top of boreholes, and the triangulation and taped distances from a wider network of stakes can be used to give more accurate values at the surface for these derivatives.

An additional advantage of this approach is that it can be readily adapted to take care of the probable situation that surface displacements measured by triangulation and differential displacements measured by inclinometry were determined over different time intervals. If the deformation rates and thus the differential velocities with respect

to the surface are independent of time, as actually seems to be the case to a good approximation, as was discussed in Chapter IV, the differential velocities can be calculated on any convenient time interval.

Analysis of a borehole array

The problem of how to analyze the data for the whole borehole array simultaneously is now considered. The aim is to compute a self-consistent velocity and strain-rate field, the gradients of velocity necessary for the application of equations (13) (or equations (1)) being obtained by comparison of adjacent boreholes. The following iteration procedure, schematically illustrated in figure 19, is used. First, depth distributions of $\partial u/\partial x$, $\partial u/\partial z$, $\partial w/\partial x$, and $\partial w/\partial z$ at each of the boreholes are assumed. As an initial approximation these quantities are chosen to be equal to their surface values at the location of the specific borehole to which they referred (i.e., $\partial u_d(y)/\partial x = 0$, $\partial u_d(y)/\partial z = 0$, etc.). By use of incompressibility (equation (2)) $\partial v/\partial y$ is thus determined; integration over y and knowledge of the surface values of v determine $v(y)$ over the whole depth of the glacier at the borehole:

$$v(y) = v(y_s) + \int_{y_s}^{y} \frac{\partial v(y')}{\partial y} \, dy' \quad . \tag{14}$$

Now all quantities necessary to the application of equations (13) are known, and u_d and w_d can be calculated. By fitting appropriate interpolating functions to u_d and w_d at any depth y, $\partial u_d/\partial x$,

$\partial u_d/\partial z$, $\partial w_d/\partial x$, and $\partial w_d/\partial z$ can be computed and combined with the surface values to give $\partial u/\partial x$, $\partial u/\partial z$, etc. at that depth. The cycle is repeated until no change in the velocity field occurs by further repetition.

The choice of method for interpolating u_d and w_d must be made with particular care. One possible method is to fit a determinate polynomial to the value of the quantity to be interpolated (u_d or w_d at a specific depth y) at the nine boreholes. An appropriate polynomial for the arrangement of the boreholes (fig. 4) is

$$u_\beta = C_0^{(\beta)}(y) + C_1^{(\beta)}(y)x + C_2^{(\beta)}(y)xz + C_3^{(\beta)}(y)z + \frac{1}{2} C_4^{(\beta)}(y)xz^2$$

$$+ \frac{1}{2} C_5^{(\beta)}(y)z^2 + \frac{1}{6} C_6^{(\beta)}(y)z^3 + \frac{1}{2} C_7^{(\beta)}(y)x^2 + \frac{1}{24} C_8^{(\beta)}(y)z^4 .$$

For $x = z = 0$ the five boreholes of section A allow the calculation of derivatives with respect to z of order up to 4 thus determining C_0, C_3, C_5, C_6, and C_8; the pairs of boreholes of flow lines 2, 1, and 3 allow the calculation of $\partial u_\beta/\partial x$ and its derivatives with respect to z up to second order giving C_1, C_2, and C_4; from the single hole of section C, $\partial^2 u_\beta/\partial x^2$ can be calculated. Such a determinate polynomial is the least restrictive interpolating function which can be computed from the available data, and in this sense involves the fewest assumptions concerning the nature of the velocity field, and thus seems a desirable way to proceed. The problems which can arise in the fitting of determinate polynomials are, however, well known, so that one must proceed with caution.

Because the distributions of u_d have a smooth variation, with

consistent trends at all depths in the region of the boreholes, the determinate polynomial is a reasonable interpolating function for this component of velocity. It is desirable, however, to constrain $\partial u_d/\partial x$ at boreholes 5A and 4A, where no direct measurement of this quantity has been made. The reason for this constraint is that the extrapolation of $\partial u_d/\partial x$ to these locations under the use of equation (14) is very sensitive to small shifts in $\partial u_d/\partial x$ on the longitudinal lines 2, 1, and 3, and thus is untrustworthy. Such a constraint is accomplished by adding terms $\frac{1}{6} k_1 xz^3$ and $\frac{1}{24} k_2 xz^4$ to the polynomial. Thus

$$u_d(x,y,z) = C_0(y) + C_1(y)x + C_2(y)xz + C_3(z) + \frac{1}{2} C_4 xz^2 + \frac{1}{2} C_5 z^2 + \frac{1}{6} C_6(y)z^3 + \frac{1}{2} C_7(y)x^2 + \frac{1}{24} C_8(y)z^4 + \frac{1}{6} k_1(y)xz^3 + \frac{1}{2} k_2(y)xz^4 \qquad (15)$$

The eleven coefficients C_0 to C_8, k_1 and k_2 are determined by the value of u_d at the nine boreholes and the two constraints on $\partial u_d/\partial x$. The actual constraint, which is applied, is to require that $\partial u_d/\partial x$ be zero at all depths in the boreholes 4A and 5A, thus the calculations are made for these boreholes under the assumption that the surface values of $\partial u/\partial x$ apply to the whole depth of the glacier at these locations.

The results of this method of interpolation on u_d at depths of 0, 100, 200, and 300 m are shown in figure 20. The main point to be noted is that the determinate polynomial, constrained as described above, produces a satisfactory interpolating function for u_d (fig. 20a). The danger of greatly amplifying small fluctuations in the data by the

fitting of determinate polynomials does not manifest itself here. Further the constraints placed on $\partial u_d/\partial x$ at boreholes 5A and 4A are reasonably compatible with the pattern of this quantity at boreholes 2A, 1A, and 3A (fig. 20b).

In the case of w_d the problem of interpolation is considerably more complicated. A consistent trend in w_d across the borehole array, such as is the case with u_d, is lacking (fig. 21). The pattern of diverging marginward transverse flow would produce a consistent picture amenable to interpolation at section A except that it is seriously disrupted by the anomalous transverse velocities in borehole 1A. The sawtooth nature of the pattern indicates that any interpolation undertaken is subject to considerable uncertainty. The use of a determinate polynomial, as is done in the case of u_d, tends to accentuate the sawtooth nature of the distribution of w_d. For this reason this method was considered undesirable. Instead simple difference formulae for the evaluation of derivatives of w_d are employed. Where possible central differences are taken. The evaluation of the derivatives of w_d is then accomplished by fitting local curves (parabolas and straight lines) rather than fitting a curve applicable to the whole array. This can be expressed in a simple way analytically because the boreholes are in an approximately square grid of spacing 150 meters. All the formulae are expressible in terms of the differences in w_d between adjacent boreholes. With the notation $(M,N) = [w_d^M - w_d^N]/150$ and the definitions $K_1 = (1B,1A)$, $K_2 = (2B,1B)$, $K_3 = (2A,1A)$, $K_4 = (2B,2A)$, $K_5 = (1B,3B)$, $K_6 = (1A,3A)$, $K_7 = (3B,3A)$, $K_8 = (3A,5A)$, $K_9 = (1A,1C)$, and $K_{10} = (4A,2A)$, the

formulae for the derivatives are then as follows:

	$(\partial w_d/\partial x) =$	$(\partial w_d/\partial z) =$
1A	$(K_1+K_9)/2$	$(K_3+K_6)/2$
1B	$(3K_1-K_9)/2$	$(K_2+K_5)/2$
1C	$(3K_9-K_1)/2$	0
2A	K_4	$(K_{10}+K_3)/2$
2B	K_4	0
3A	K_7	$(K_6+K_8)/2$
3B	K_7	0
4A	0	0
5A	0	0

(16)

At boreholes 4A and 5A, where no direct information on $\partial w_d/\partial x$ is available, $\partial w_d/\partial x$ is set equal to zero. At boreholes 1C, 2B, 3B, 4A, and 5A, where marginward extrapolation of w_d must be completely hypothetical, $\partial w_d/\partial z$ is set equal to zero. The results of these procedures for calculating the derivatives of w_d with respect to x and z at depths of 0, 100, 200, and 300 m are shown in figure 21.

A basic problem is encountered in the application of these methods of interpolation of u_d and w_d as a result of the fact that all of the boreholes are not of the same depth. As y increases to a value greater than the depth of a borehole the number of points available for interpolation is reduced by one. Simply reducing the order of the interpolation formulae would introduce unwanted discontinuities in the depth profiles of the x and z gradients of u and w at the

depths of the bottoms of the boreholes. The alternative is to do some sort of extrapolation, thus providing for a smooth transition. In making an extrapolation by examination of the trends above the bottom of a borehole not only can unwanted discontinuities be avoided, but also the accuracy of the interpolation can be maintained in some range below the bottom of the borehole. Since most of the boreholes are very closely the same depth, the interval over which such extrapolation has to be made for them is small compared to the length of the boreholes and the depth scale over which significant variations in the borehole tilt components occur. For the three boreholes 5A, 1C, and 4A this is not the case, and extrapolation would have to be made over depths of approximately 50, 100, and 200 m respectively. One method of extrapolation might be to extrapolate all of the borehole profiles to the depth of the deepest borehole. Another possibility would be to extrapolate an appropriate coefficient in the determinate polynomial in the case of u_d, or in the appropriate difference in the case of w_d, to depths below the bottom of a borehole on the basis of the results of the calculations at shallower depths.

The method of extrapolation which is used relies mainly on the second of the above approaches, although direct extrapolation of boreholes is also used. The method is as follows. First the profile of borehole 4A is extrapolated to 200 m (see fig. 20a). The extrapolated profile is taken similar to that of 5A in order to enforce approximate symmetry. Also the profile of 1A is extrapolated several meters to a depth equal to that of hole 1B. Then starting from the surface, interpolation is done using all nine points down to the depth of the

bottom of the extrapolated borehole 4A. At this point C_8 of formula (15) and K_{10} of (16) are extrapolated to the depth of the deepest hole. At depths below 200 m, by placing the extrapolated value of C_8 in formula (15), the other coefficients can be determined from the values of u_d in the remaining boreholes and the constraints on $\partial u_d/\partial x$ at the locations of boreholes 4A and 5A. The remaining quantities of equation (16) are straightforwardly calculated from the values of w_d in the remaining boreholes. On reaching the limit of available data in borehole 1C at 210 m, C_7 and K_9 are extrapolated with a resultant reduction in the number of coefficients to be determined in equations (15) and (16) at greater depth. This is continued until the bottom of the deepest borehole is reached. The coefficients C_n and K_n are extrapolated in order of decreasing subscript value as the bottoms of boreholes 4A, 1C, 5A, 3A, 3B, 2A, and 2B are sequentially reached. The equality of depth between hole 1B and the extrapolated hole 1A eliminates the necessity of extrapolating C_1.

Extrapolation of a coefficient C_n or K_n is done by passing a parabola through the last (deepest $y = y_\ell$) calculated value with a slope there equal to that of the least square line through the deepest point and points 20 and 40 m above, and with a curvature equal to that of the least square parabola through the deepest point and points 20, 40, 60, and 80 m above. Thus

$$
\begin{aligned}
C(y) &= a(y^2 - y_\ell^2) + b(y - y_\ell) + c \\
a &= [2C(y_\ell) - C(y_\ell - 20) - 2C(y_\ell - 40) - C(y_\ell - 60) + 2C(y_\ell - 80)]/140 \\
b &= [C(y_\ell) - C(y_\ell - 40)]/40 \\
c &= C(y_\ell)
\end{aligned}
\qquad (17)
$$

The reason for extrapolating borehole 1A to a depth equal to that of borehole 1B is simply a matter of convenience in programming for calculation on a digital computer.

The mechanics of the extrapolation procedure do not require that the profile of borehole 4A be extrapolated. If borehole 4A is not extrapolated and the coefficients C_1 to C_8 are extrapolated in the order and manner described above, the resulting interpolating functions for u_d at depths greater than that of the bottom of the unextrapolated borehole 4A are unreasonable. The reason for this is that in the top 100 m, where u_d is closely zero in all of the boreholes, the value calculated for C_8 is thus essentially zero over the whole depth range. Consequently, at depths greater than 100 m, as the much stronger differential motion in borehole 5A begins to manifest itself, progressively larger values of C_6 (the coefficient of the z^3 term) are calculated, thus producing interpolating functions which tend to be antisymmetric and which actually predict positive u_d beneath the bottom of borehole 4A. This is clearly unacceptable; extrapolation of the profile of borehole 4A to a depth (200 m) is sufficient to establish a trend in C_8 leading to an approximately symmetric pattern in the interpolating functions at all depths. Another way of avoiding the difficulty, without making an arbitrary extrapolation of borehole 4A, is to interchange the order of extrapolation of C_6 and C_8. This causes C_6 to be constrained to values essentially zero over the whole depth. The strong differential velocity u_d at 5A contributes to C_8. The results of these two alternative approaches are essen-

tially identical except for an expected slight difference in the value of $\partial u/\partial z$ at borehole 2A. The interpolating curves shown in figure 20a are those resulting from the extrapolation of borehole 4A. All succeeding results are also calculated on this basis.

The iterative cycle (fig. 19) was programmed for computation on the IBM 7094, the basic formulae for step 1 being equation (14), for step 2 being equations (13), and for step 3 being equations (15), (16), and (17). Calculations were carried out on the smoothed borehole profiles (figs. 16 and 17) at five-meter intervals. The continuous curves of the smoothed profiles were represented in the computer by coordinate values spaced at five-meter intervals. Coordinates at intervening depths were computed by interpolation. For convergence it was required that at all points the change in any component of velocity be less than 1 cm yr^{-1}. This condition was met after four traverses of the cycle. Execution time in the 7094 was 50 seconds.

B. Results of the Calculations

A feature of the computed velocity field is that the value for the y component of velocity v predicted at the glacier bed is not in complete agreement with what would be expected on the basis of the requirement that the velocity normal to the bed be zero. This comparison is made in table 9 (column 5). For this reason the com-

puter program was also run with a variation in step 1 which constrains v to have a value consistent with the normal velocity requirement at the bed. This was done by calculating v in the normal manner by equation (14), and then modifying it as follows

$$v_m(y) = v(y) - \left(v(y_b) - v_b\right) \frac{(y - y_s)^2}{(y_b - y_s)^2}$$

where y_b is the depth of the bed and v_b is the required value of v there. In this way the distribution of $\partial v/\partial y = -(\partial u/\partial x) - (\partial w/\partial z)$ as calculated from the interpolating functions determines the shape of the depth profile of v. It is adjusted in order to achieve the proper value at the bed. The square of the ratio $(y - y_s)/(y_b - y_s)$ was used in order to concentrate the correction to v at the deeper levels of the boreholes. The difference between the results for u, w, and their derivatives computed by the modified and unmodified versions of step 1 are negligible compared with the measurement errors of the surface displacements and differential displacements upon which they depend. Only the values of v are significantly different. The modified solution is no longer consistent with the condition of incompressibility. The degree to which incompressibility is violated gives an indication of the uncertainty in the evaluation of $\partial u_d/\partial x$ and $\partial w_d/\partial z$ as is discussed in part C of this chapter.

In the discussion of the distribution of velocity below and in Chapter VI, the results of the modified calculation are used, since the resulting v is expected to be more accurate. Since a similar modification of $\partial u/\partial x$ and $\partial w/\partial z$ cannot be unambiguously made,

the unmodified solution, which is internally consistent and satisfies incompressibility, is used in the detailed calculations concerning the distribution of strain rate made in Chapter VII.

Internal distribution of velocity

The distributions of u and w with depth, which were calculated at each borehole, are not presented, since they are similar to the longitudinal and transverse differential displacement profiles of figures 16 and 17. Contour diagrams of u on sections A and B are shown in figure 22. These diagrams better illustrate the relationship of the velocity u between the various holes, and give a picture of the areal distribution of observed longitudinal velocity in the cross sections. The contours were drawn through the points calculated to have the appropriate velocity at the locations of the boreholes. They were not constrained by the actual interpolation on u_d used in the calculation, but were simply drawn in the spaces between boreholes so that they looked reasonable. (They also define another set of possible interpolating functions for u_d, similar but not identical to the set actually used. This again illustrates the basic uncertainty in the interpolation.) Marginward extension of the diagrams beyond the limits of the borehole array was made on the basis of the results of the surface survey. For comparison a contour diagram for a theoretical distribution of longitudinal velocity, as calculated by Nye (1965), is also included (fig. 23).

w and v are presented in the flow diagrams of figure 23. An arrow represents the vector $v\hat{y} + w\hat{z}$ evaluated at the origin of

the arrow. The arrows thus illustrate the pattern of flow normal to the longitudinal direction. Arrows were also plotted at points in the speces between boreholes. w and v were each interpolated by drawing smooth curves through the calculated values at the boreholes. The smooth curves for v are shown in figure 24.

Distribution of longitudinal strain rate

A contour diagram of $\partial u/\partial x$ (fig. 25) gives the areal distribution of longitudinal strain rate on a section half way between sections A and B, where this quantity is best determined. The depth distributions of $\partial u/\partial x$ in this intermediate section at lines 3, 1, and 2 are also presented (fig. 26).

Depth distribution of strain rate at borehole sites

The distribution with depth of the tensor components of strain rate for each borehole is presented in graphical form in figure 27. The strain rates are straightforwardly calculated from the velocity gradients computed in the iterative calculation described above, except for the lack of computed values of $\partial v/\partial x$ and $\partial v/\partial z$. Because of the indirect manner in which v enters into the calculation of u and w and the actual smallness of these derivatives, the assumption that $\partial v/\partial x = \partial v/=z = 0$ has no significant effect on the values calculated for u, w, and their derivatives with respect to y. Since that assumption leads to considerable simplification in the calculations, it was adopted. These quantities, however, enter directly into the tensor strain-rate components. In order to evaluate $\partial v/\partial x$ and

$\partial v/\partial z$, several methods present themselves, the most obvious of which is to interpolate at given depths y on the values of v calculated at the borehole locations. As must be clear from the discussion of interpolating procedures of the previous section, this can be a tedious and uncertain process. It is noted, however, that the calculated values of v at the boreholes indicate that $\partial v/\partial x$ and $\partial v/\partial z$ are approximately independent of depth. This interesting and perhaps somewhat unexpected observation is discussed in Chapter VI-D and illustrated in figure 25 and table 9. In view of this it is suggested that $\partial v/\partial x$ and $\partial v/\partial z$ need only be evaluated at the surface. To evaluate these quantities, instead of interpolating on the values of v as determined by triangulation, which are subject to relatively large measurement error, $\partial v/\partial x$ and $\partial v/\partial z$ at the top of each borehole were chosen on the basis that the shear strain rate parallel to the local glacier surface is zero (i.e., $e_{x'y'} = e_{y'z'} = 0$). The remaining components of strain rate in the primed coordinate system ($e_{x'x'}, e_{z'z'}, e_{x'z'}, e_{y'y'}$) are known from the surface strain-rate measurements and the condition of incompressibility. Thus $e_{xy} = \frac{1}{2}(\partial u/\partial y + \partial v/\partial x)$ and $e_{yz} = \frac{1}{2}(\partial w/\partial y + \partial v/\partial z)$ can be calculated at the surface from the usual rule for transformation of tensor components under a coordinate transformation. If the transformation from the (x,y,z) to the (x',y',z') system is described by $x'_i = a_{ij}x_j$ and the components of strain rate with respect to the primed system are denoted as $\dot{e}'_{ij}$, then

$$\frac{\partial v(y_s)}{\partial x} = -\frac{\partial u(y_s)}{\partial y} + 2a_{i1}a_{j2}\dot{e}'_{ij}$$

$$\frac{\partial v(y_s)}{\partial z} = -\frac{\partial w(y_s)}{\partial y} + 2a_{i2}a_{j3}\dot{e}'_{ij} \qquad (18)$$

Taking at each borehole $\partial v(y)/\partial x \cong \partial v(y_s)/\partial x$ and $\partial v(y)/\partial z \cong \partial v(y_s)/\partial z$ all nine velocity gradients are known over the complete depth and the tensor strain rates can be calculated.

C. Accuracy of the Calculated Components of Velocity and Strain Rate

The accuracy of the calculated components of velocity u and w can be estimated from equations (13a) with the use of the statistical quantities already computed for the borehole coordinates, and estimates of the accuracy of $\partial u/\partial x$, $\partial u/\partial z$, $\partial w/\partial x$, $\partial w/\partial z$, and v. This is done simply by using the rules for calculating the variances of sums and products. From the differentiated form of equations (13a) standard errors for $\partial u/\partial y$ and $\partial w/\partial y$ can be estimated in a similar manner. As was the case in the computation of u and w, the estimation of the errors is a circular process. Since, however, the contributions to errors in u and w from errors in v and in the x and z gradients of velocity are of the nature of small corrections to the primary contributions coming directly from the error in the borehole coordinates, the estimate of error for u and w and their y derivative is only weakly dependent on the errors in these quantities. Thus the standard error in u and w can be estimated

using liberal estimates for the standard error for these secondary quantities. In this way the standard errors for u and w will be slightly overestimated. After thus evaluating the errors in u and w, standard errors for $\partial u/\partial x$, $\partial u/\partial z$, $\partial w/\partial x$, $\partial w/\partial z$, and v can be calculated and checked against the original estimates. Following this plan, standard errors $\sigma_u(y)$, $\sigma_w(y)$, $\sigma_{\partial u/\partial y}$, $\sigma_{\partial w/\partial y}$, are calculated assuming $\sigma_{\partial u/\partial x} = \sigma_{\partial u/\partial z} = \sigma_{\partial w/\partial x} = \sigma_{\partial w/\partial z} = 0.004\ \text{yr}^{-1}$, and $\sigma_v = 0.5\ \text{m yr}^{-1}$. In addition, values of $|\partial u/\partial x| = 0.02\ \text{yr}^{-1}$, $|\partial u/\partial z| = 0.16\ \text{yr}^{-1}$, $|\partial w/\partial x| = 0.02\ \text{yr}^{-1}$, $|\partial w/\partial z| = 0.01\ \text{yr}^{-1}$, and $v = 4\ \text{m yr}^{-1}$ were taken to apply at all depths. $\frac{1}{2}\left(x_f(y)+x_i(y)\right)/2 = 25$ m, $\frac{1}{2}\left(z_f(y)+z_i(y)\right) = 1.5$ m, $\frac{1}{2}\left(\gamma_{x_f}(y)+\gamma_{x_i}(y)\right) = 0.10$, $\frac{1}{2}\left(\gamma_{z_f}(y)+\gamma_{z_i}(y)\right) = 0.02$, $\frac{1}{2}\frac{\partial}{\partial y}\left(\gamma_{x_f}(y)-\gamma_{x_i}(y)\right) = 0.0016\ \text{m}^{-1}$, and $\frac{1}{2}\frac{\partial}{\partial y}\left(\gamma_{z_f}(y)-\gamma_{z_i}(y)\right) = 0.0006\ \text{m}^{-1}$ are also taken to apply at all depths. Then utilizing the standard errors computed for the surface intersection, the integrated tilts, the local tilt, and the slope of the tilt profile in Chapter III and Appendix II, the following formulae are obtained:

$$\sigma_u^2(y) = (0.22)^2 + (0.0217)^2\ (y/m)\ m^2\ yr^{-2}$$

$$\sigma_w^2(y) = (0.22)^2 + (0.0235)^2\ (y/m)\ m^2 yr^{-2}$$

$$\sigma_{\partial u/\partial y} = 0.0019\ \text{yr}^{-1}$$

$$\sigma_{\partial w/\partial y} = 0.0020\ \text{yr}^{-1}$$

Even though maximum estimates of the above secondary quantities were applied uniformly at all depths, the depth-independent part of

the estimates for σ_u^2 and σ_w^2 are almost completely dominated by the standard error of 0.20 m estimated for the location of the surface intersection of the borehole. In this calculation the depth dependences in σ_u^2 and σ_w^2 come entirely from the standard errors in differential longitudinal displacement ($0.0217\sqrt{y}$) and transverse displacement ($0.235\sqrt{y}$). The greatest contribution to the standard error in $\partial u/\partial y$ and $\partial w/\partial y$ is, as expected, the error in the components of tilting rate (0.0015 yr^{-1} and 0.0019 yr^{-1} respectively).

The accuracy of $\dot{e}_{xy}$ and $\dot{e}_{yz}$ depends on the accuracy of $\partial v/\partial x$ and $\partial v/\partial z$, as well as on that of $\partial u/\partial y$ and $\partial w/\partial y$. In calculating $\dot{e}_{xy}$ and $\dot{e}_{yz}$ it was assumed that $\partial v/\partial x$ and $\partial v/\partial z$ were constant over the full depth of the glacier, and had values required by the calculated values of $\partial u/\partial y$ and $\partial w/\partial y$ at the surface under the condition that $\dot{e}_{x'y'} = \dot{e}_{y'z'} = 0$ at the surface. Thus, unless the ice is strongly anisotropic at the surface, the errors in $\partial v/\partial x$ and $\partial v/\partial z$ will be identical in magnitude and opposite in size to the errors in $\partial u/\partial y$ and $\partial w/\partial y$, so that in the calculation of $\dot{e}_{xy}$ and $\dot{e}_{yz}$ the errors cancel. However, at such a depth that the calculated values of $\partial u/\partial y$ and $\partial w/\partial y$ are relatively independent of the values calculated at the surface, no such cancellation can be expected and the errors can add. Such a depth would be between 50 and 100 m. If the error in $\partial u/\partial y$ and $\partial w/\partial y$ at the surface is taken to be twice the normal value of 0.002 yr^{-1}, as suggested in Appendix II because of edge effects in the definition of the data smoothing curves, then at depths greater than 50 to 100 m one could expect a standard error in the strain rates $\dot{e}_{xy}$ and $\dot{e}_{yz}$ of 0.0023 yr^{-1} as long as $\partial v/\partial x$ and

$\partial v/\partial z$ are in fact independent of depth. This last condition is valid to within $\pm 0.003\ yr^{-1}$ as indicated by observations shown in table 9 (column 6) and figure 24. Including this in the calculation gives a standard error of about $0.003\ yr^{-1}$ for $\dot{e}_{xy}$ and $\dot{e}_{xz}$.

The error in the x and z gradients of u and w is now considered. There are two basic sources of uncertainty in these quantities. The first is the uncertainty in the values of u and w at the borehole locations. The second is the uncertainty involved in the interpolation used to estimate the gradients. The first source is open to direct quantitative evaluation. The second cannot be directly evaluated.

The contribution from the first source can be roughly estimated by considering the effects on the calculated gradients in u_d and w_d in terms of simple differences. If there are adjacent boreholes on either side of a borehole at which a velocity gradient is to be evaluated, then the gradient is determined approximately by a central difference. The error in the evaluation of the difference is approximately $\sigma_{\partial u_\alpha/\partial x_\beta} \approx \sigma_{u_\alpha}\sqrt{2}/300$, which gives

$$\sigma_{\partial u_d/\partial x}(y) = \sigma_{\partial u_d/\partial z}(y) = 0.0018(y/300\,m)^{1/2}\ yr^{-1}$$

and

$$\sigma_{\partial w_d/\partial x}(y) = \sigma_{\partial w_d/\partial z}(y) = 0.0019(y/300\,m)^{1/2}\ yr^{-1}$$

If there are not boreholes on both sides but only on one side, then the gradient must be approximated by a non-central difference. The experimental error in evaluating such a difference will be approxi-

mately twice as large as those cited above. To make a more accurate assessment of the effect of small variations in u_d and w_d at each of the boreholes on the calculated gradients of u_d and w_d requires use of equations (15) and (16). In view of the inability to evaluate directly the contribution from interpolation error, such refinement is not worthwhile. The above estimates for the error in the gradients of differential velocity and the estimates for the surface strain-rate components give

$$\sigma^2_{\dot{e}_{xz}}(y) = (0.0001)^2 + \left(\frac{k}{\sqrt{2}}\right)^2 \left(\frac{y}{300\,m}\right) \text{ yr}^{-2}$$

$$\sigma^2_{\dot{e}_{xx}}(y) = \sigma^2_{\dot{e}_{zz}}(y) = (0.001)^2 + (k^2)\left(\frac{y}{300m}\right) \text{ yr}^{-2}$$

where $0.002 \leq k \leq 0.004$ depending on to what extent the borehole is surrounded by other boreholes.

Although the interpolation error cannot be directly estimated, some idea of the average error in the sum $(\partial u/\partial x + \partial w/\partial z)$ can be obtained from constraints placed on $\partial v/\partial y$ by v determined at the surface by triangulation, v at the glacier bed as required by the condition that the velocity normal to the bed be zero, and the condition of incompressibility. As is shown in table 9 (column 5) the value of $\partial v/\partial y$ computed from $(\partial u/\partial x + \partial w/\partial z)$ and integrated over the depth of the glacier is not in agreement with the above conditions. The disparity is on the average about 1 m yr^{-1}. Errors in estimating v at the glacier bed on the basis of the normal velocity conditions (y_b of table 9) and in the measurement of v at the glacier surface (v_s of table 9) must also contribute to the differences. If, however, it

is assumed that the sole source of the difference comes from errors in $(\partial u/\partial x + \partial w/\partial z) = - \partial v/\partial y$ an upper limit of 0.003 yr^{-1} can be placed on the error in this quantity averaged over the depth of the glacier. This value is consistent with the estimates of $\sigma_{\dot{e}_{xx}}$ and $\sigma_{\dot{e}_{zz}}$ calculated with interpolation error neglected, which suggests that the additional interpolation error is not large.

In Chapter III a standard error of 0.35 m yr^{-1} was estimated for v at the surface. The bed slope with respect to the x and z axis is known to an accuracy of about 0.5^{o} which indicates that v at the glacier bed is determined to within 0.5 m yr^{-1}. Since the distribution of v was constrained at both the surface and the bed, the uncertainty in the intervening space should not greatly exceed 0.5 m yr^{-1}.

The estimated errors of the various flow parameters are summarized in table 10.

CHAPTER VI

INTERNAL DEFORMATION: INTERPRETATION AND COMPARISON WITH EXISTING THEORIES

The distributions of velocity and strain rate, as calculated and presented in Chapter IV, are the first direct observations which give a coherent picture of internal deformation over a significant portion of a complete valley glacier cross section. In this chapter significant features of the pattern of flow are described and interpreted. In particular an attempt is made to distinguish those features which could be expected to be typically exhibited by flow of valley glaciers from those which result from influences peculiar to the cross section studied.

The main features of the distribution of longitudinal velocity are: high sliding velocity over the central portion of the glacier, low sliding velocity at the margins, stronger shear strain rate near the margins than at the base of the glacier in its central portion, and contours of constant velocity, which are approximately semicircular and have shapes significantly different from the cross section boundary shape. Transverse variation of water pressure at the glacier bed is suggested as a possible cause of the greater sliding velocity in the center of the glacier as compared to the margins. The observed pattern of flow is considerably different from that calculated by Nye (1965) for a cross section of similar geometry. The distribution of longitudinal strain rate shows that the deformation field is not completely two-dimensional.

The observed pattern of lateral flow is discussed and shown

to be compatible with the lateral flow which is necessary to maintain equilibrium of the surface at the margins of the glacier. The elevation differences associated with the curved transverse surface profile are sufficient to drive the flow.

A. Distribution of Longitudinal Velocity

The important features of the distribution of u are illustrated in figure 22. The manner in which the diagram was constructed is discussed in Chapter V.

Sliding Velocity

One of the most striking features shown in figure 22 is the generally high basal sliding velocity, which persists across most of the width of the glacier in both sections A and B. This fact was anticipated in Chapter III-E, where the differential displacements in the boreholes were compared to their surface displacements. The contribution of basal sliding velocity to surface velocity at the centerline of sections A and B was 81 and 87% respectively. The dominance of the contribution of basal sliding velocity to the surface velocity at a given longitudinal line is only slightly decreased toward the margins. This is supported directly by the fact that the basal sliding velocity is still 70% of the total surface velocity at the location of borehole 5A and indirectly by the additional constraints placed on the velocity contours outside of the borehole array by the surface measurements. A zone of particularly high sliding velocity is centered around line 2 in both sections A and B.

In contrast to the high basal sliding velocity, which persists

over most of the width of sections A and B, is the relatively small marginal sliding velocity at the surface on both sides of the glacier (Chapter IV-A). On the northwest margin the ice velocity is very close to zero. On the southeast side the velocity at marker 7A is about 60% of the centerline velocity. Although direct measurements do not extend to the margin, simple extrapolation indicated that the marginal velocity must certainly be less than a few meters per year (fig. 8).

The large transverse gradients in the sliding velocity implied by the high basal velocity and low marginal velocity are particularly significant.

Shear strain rate and shear stress at the bed

A significant manifestation of the relative strength of the basal and marginal sliding velocities is that the marginal shear strain rate ($\partial u/\partial z$ near the valley sides) is greater than the basal shear strain rate ($\partial u/\partial y$ at the valley bottom). This fact is easily noted by observing the relative spacing of the velocity contours in figure 22a. It indicates that the glacier is being supported to a greater extent by "friction" at its margins as compared with "friction" along its base.

A very important consequence of this condition is that the basal shear stress at the centerline, calculated by use of the shape factor appropriate to the glacier cross section, will be over estimated, since such a calculation only gives the average shear stress along the ice-rock contact. Setting the shear stress τ_{xy} at the centerline to be equal to the average shear stress at the ice-rock contact gives

$$\tau_{xy} = f \rho g_x H$$

where f is given by the area A of the cross section divided by the product of the length of the ice-rock interface P times the maximum depth H. For the Athabasca cross section f is 0.58. A more appropriate shape factor f based on the observed strain rates seems to be about 0.5, as discussed in Chapter VII. This is a value which would be estimated, if the calcuation of f were made on the basis of the shape of the roughly semicircular velocity contours rather than the shape of the channel cross section.

Possible causes of sliding velocity behavior

The persistence of a basal velocity amounting to 70 to 90% of the surface velocity across most of the glacier width probably represents a contribution to the overall glacier motion much greater than is typical. Previous borehole experiments indicate that although basal sliding is highly variable, it contributes on the average about 50% to the total surface velocity (Kamb, 1964). Even though the observed high basal sliding velocities appear to be anomalous, the observation that the basal sliding velocities are greater than the marginal sliding may be typical of the pattern of flow in valley glaciers. From the observations in one glacier cross section, which are presented here, certainly no conclusive statements can be made. However, the fact that the effect is manifested on both sides of the glacier, that the transverse gradients in sliding velocity are much greater than the longitudinal gradients, and that the variation in sliding velocity

is apparently monotonic with distance away from the centerline of flow except for the slight perturbations at line 2 suggest that the distribution is of general significance, rather than being the result of random perturbing influences. Additional evidence that basal sliding may typically exceed marginal sliding in valley glaciers comes from surface measurements on several glaciers, which show that marginal sliding velocities are generally considerably less than 50% of the centerline surface velocity, a fact pointed out to the author by B. Kamb (personal communication). Specific examples are given by Meier (1960, p. 26, fig. 24) for the Castleguard sector of the Saskatchewan Glacier, where marginal velocity is less than 20% of the centerline surface velocity for four transverse profiles spaced roughly 0.4 km apart along the glacier. Other examples are Blue Glacier (Meier et al., unpublished), Rhone Glacier (Mercanton, 1916, map no. 3) and Austerdalsbreen (Glen and Lewis, 1961).

It is not unreasonable to expect that in the event basal sliding significantly exceeds marginal sliding, the shear strain rate (and thus shear stress) near the margin will exceed the shear strain rate (and shear stress) at the valley bottom, as is the case in the Athabasca sections. This should be the case at least if the half width of the glacier cross section does not greatly exceed the depth.

If these effects are indeed typical of the flow of valley glaciers, there must be something to be learned from them about the sliding process and conditions beneath the glacier which affect it. Since there is relatively lower sliding velocity at a location of relatively higher stress, the cause must be transverse variations in the param-

eters which affect the sliding velocity vs. stress relation, rather than the internal distribution of stress which which would occur if such parameters exhibited no lateral variation. The two parameters which theoretical considerations indicate are fundamental in determining the sliding response to an applied stress are macrotopography or roughness of the bed and the difference between the average normal stress at the ice interface and the pressure in any water existing between the ice and rock (Weertman, 1964; Liboutry, 1968). High roughness and high pressure difference will impede the sliding.

The effect can possibly be understood on the basis of the lateral variation of the water pressure at the bed. If the normal stress at the ice interface is assumed to be equal to the lithostatic overburden pressure, then the pertinent difference in pressure can be represented as

$$\Delta p(\delta, z) = \rho_w g_y \delta - (\rho_w - \rho_i) g_y H(z)$$

where z represents the location in the section, $H(z)$ the depth there, and δ the level of the water (see fig. 29). It is assumed further that there are no z pressure gradients in the water layer. ρ_w and ρ_i represent the density of the water and the density of ice. Starting from the deepest part of the section (which is taken to be $z = 0$) the pressure difference Δp increases toward the margin and reaches a maximum at the point z_δ, where the ice-bed rock contact intersects the water surface. Beyond that point it decreases to zero at the glacier margin. By examining $r(\delta) = \Delta p(\delta, z_\delta)/\Delta p(\delta, 0)$, which is plotted as a function of water level δ in figure 30, it is seen that

the value of the pressure difference at z_δ can be considerably larger than the value at the centerline when the water level is high (i.e., as δ approaches 0.1 H). In this event, in a typical glacier cross section the region of maximum Δp would be very close to the margin, and its retarding effect could possibly produce a smaller marginal sliding velocity than that occurring at the center line. The effect thus produced would be approximately the same on both sides of the glacier, and would show the largest gradients in the sliding velocity where the valley sides are steep.

That sufficiently high water levels actually exist in valley glaciers is not known. Monitoring of the water level in the Athabasca glacier boreholes has shown that during the summer, water pressure in hydraulic systems deep within the glacier is sufficient to maintain water levels at heights less than 40 m below the surface. Although these pressures do not necessarily reflect the pressure at the glacier bed, they give indication that high water pressure at the glacier bed is not an unreasonable expectation. Whether existing water stands could produce sufficient amplitude in the lateral variation of Δp to produce the effect cannot be tested, since glacier sliding theory is not yet developed to the point where the effects of water pressure can be quantitatively assessed. However, the large short-period variations in surface velocity observed on this and other glaciers, which are correlated with variations in stream discharge at the glacier snout and thus presumably with variations in the pressure distribution in the subglacial hydraulic system, indicate that water pressure can have a strong effect on glacier sliding. This supports the plausibility

of the hypothesis.

Several features of the distribution of sliding velocity are, however, incompatible with this hypothesis. The gradient in sliding velocity between lines 3 and 5, which is well documented at section A, seems to be much greater than would be expected there on this basis, since the transverse slope of the bed is small. At a corresponding location on the other side of the section there is a maximum in the sliding velocity and a low gradient. These features indicate that variations in the other parameter (bed roughness) must also at least contribute to, if not dominate, the distribution of sliding velocity. A systematic difference in roughness between deeper and shallower parts of the bed could conceivably arise through glacial abrasion.

Flux through the cross section

A parameter of hydrological interest is the ratio of the average value of u over the cross section to the average value of u over the width at the surface, that is $\langle u \rangle_A / \langle u \rangle_s$. Calculation of $\langle u \rangle_A$ from figure 22a gives the value of 40.5 m yr^{-1}; a value of 36.5 m yr^{-1} is calculated for $\langle u \rangle_s$. Thus $\langle u \rangle_A$ equals $1.11 \langle u \rangle_s$. At least in this case calculations of the ice flux based on the assumption that the mean velocity u in the cross section is equal to the mean surface velocity will not be grossly incorrect. The value of u averaged over depth at the centerline, $\langle u \rangle_H$ has a value of 49.7 m yr^{-1}. This is considerably greater than the average of u over the cross section; $\langle u \rangle_A / \langle u \rangle_H$ is 0.82. The geometrical average $\langle u \rangle_G = \sqrt{\langle u \rangle_H \langle u \rangle_s}$, which has a value of 42.6 m yr^{-1}; gives a better approximation to $\langle u \rangle_A$ than

either $\langle u \rangle_H$ or $\langle u \rangle_s$ considered singly.

Total ice flux through section A is computed to be 1.09×10^7 $m^3\ yr^{-1}$.

Width ratio of velocity contours

Another significant feature of the distribution of longitudinal velocity represented in figure 22 is found by considering the width ratio of the velocity contours. The width ratio R is half the distance between the surface intersections of a contour divided by the maximum depth of that contour. The width ratio systematically decreases as one considers contours of increasing velocity. The important fact to be noted here is that the width ratio passes from values greater than one to values less than one, as is shown in table 11. The significance of this becomes apparent below when the observed distribution of u is compared to the theoretical distributions computed by Nye (1965).

Comparison with solutions of Nye

Nye (1965) computed numerical solutions to the problem of steady rectilinear flow of an isotropic material obeying a power law (n = 3) in cylindrical channels of various cross sections. He considered only symmetric cross sections, with sliding velocity independent of location in the section, although these conditions are not essential to his numerical method. The fundamental assumptions on which the numerical treatment is based are that of rectilinear flow (in which $u = u(y,z)$ and $v = w = 0$) and homogeneity of the

rheological properties. Nye's solution for a parabolic channel of width ratio 2 is shown in figure 23. Such a channel approximates quite well the actual cross sections A and B of the Athabasca Glacier, except for the protrusion on the southeast valley wall. The solution has been scaled to cover approximately the observed range of velocities.

Nye's solution shows features which contrast strongly with the observed pattern of u. Clearly the drastic difference in the boundary condition assumed by Nye and the boundary condition appropriate to the Athabasca sections contributes very strongly to this difference. The most obvious incompatibility between the theoretical and observed distributions is that the relative strength of marginal to basal shear is opposite for the two distributions. A difference in the quantity $\langle u \rangle_A / \langle u \rangle_s$ also exists. Nye pointed out that for many of his solutions the ratio was close to one. For the parabolic channel of width ratio 2 his result was 0.980, which is distinctly smaller than the observed value of 1.11. These differences could probably be rectified by applying a more realistic velocity boundary condition in the theoretical treatment.

A more basic incompatibility can be discerned when the width ratios of the observed contours are considered. By considering the solution to the flow problem for boundaries having the shape of the observed velocity contours, the problem in terms of geometry and boundary conditions becomes exactly that considered by Nye. Consider section A, where the velocity contours are nearly symmetric.

Nye enunciated some principles based on symmetry which related the solution in a channel of width ratio R to the solution in a channel of width ratio $1/R$ for certain classes of boundary shapes. These are particularly simple for a boundary with $R = 1$, which has symmetry such that there is nothing which distinguishes the planes $z = 0$ and $y = 0$. This is the case when the boundary has reflection symmetry about the y axis and about the lines at $\pm 45^{o}$ from the y axis. In this event clearly all velocity contours interior to the boundary must have width ratios equal to 1. Since the contour for $u = 46$ m yr^{-1} has width ratio 1, all contours interior to this one should have the same ratio 1. Table 11 show that this is not the case for the observed velocities. This indicates that the flow is influenced observably by either the longitudinal strain rate $\partial u/\partial x$, by gradients in v and w, by longitudinal stress gradients, or by inhomogeneity in the rheological properties of the ice.

B. Interpretation of Surface Values of $\partial u/\partial y$ and $\partial w/\partial y$

If the ice is isotropic, the shear strain rate components $\dot{e}_{x'y'}$ and $\dot{e}_{y'z'}$ must be zero at the glacier surface, since $\tau_{x'y'}$ and $\tau_{y'z'}$ are zero there. Thus, under the assumption of isotropy, non-zero $\partial u'/\partial y'$ and $\partial w'/\partial y'$ must be a result of rotation acting at the surface (see Chapter IV-D). This hypothesis is nowtested quantitatively.

If $\partial u'/\partial y'$ and $\partial w'/\partial y'$ are caused by rotation, then there must be gradients in the y' component of velocity v', such that $\partial v'/\partial x' = - \partial u'/\partial y'$ and $\partial v'/\partial z' = -\partial w'/\partial y'$. These conditions give

$$\dot{e}_{x'y'} = \dot{e}_{y'z'} = 0$$

$$\dot{\omega}_{x'y'} = \frac{\partial u'}{\partial y'} = -\frac{\partial v'}{\partial x'}$$

$$\dot{\omega}_{y'z'} = -\frac{\partial w'}{\partial y'} = \frac{\partial v'}{\partial z'}$$

$\partial u'/\partial y'$ and $\partial w'/\partial y'$ can be calculated from $\partial u/\partial y$ and $\partial w/\partial y$ as given by borehole tilting, knowledge of the surface strain rate components, and standard transformation procedures. In fact the differences between the quantities in the primed and unprimed system are much smaller than the measurement errors because the difference in axis orientations is so small. (This can be seen in figure 28, where the values of $\dot{e}_{xy}$ and $\dot{e}_{yz}$ attain values very close to zero at the surface even though the exact condition is $\dot{e}_{x'y'} = \dot{e}_{y'z'} = 0$.)

Independent estimates of $\dot{\omega}_{x'y'}$ and $\dot{\omega}_{y'z'}$ can be made in two other ways. First this can be done by appropriate direct differencing of v' as determined by triangulation measurements to get $\partial v'/\partial x'$ and $\partial v'/\partial z'$. A second approach is to use the distribution of u' as determined by triangulation and estimate $\partial v'/\partial x'$ and $\partial v'/\partial z'$ from the surface slope gradients by using the following formulae:

$$\frac{\partial v'}{\partial x'} = u' \frac{\partial \alpha_{x'}}{\partial x'}$$

$$\frac{\partial v'}{\partial z'} = u' \frac{\partial \alpha_{z'}}{\partial x'} = u' \frac{\partial \alpha_{x'}}{\partial z'}$$

These follow simply from (1) the requirement that a borehole element

near the surface and initially normal to the surface must remain normal to the surface, and (2) the assumption that the surface is in equilibrium. The surface slope at points of interest was computed from the topographic map (Topographic Survey, 1962) by averaging over a centered length of approximately one glacier depth. Slope gradients were similarly calculated from the difference in slope over an interval of one glacier depth centered on the point of interest.

Comparisons of the three independent estimates of $\dot{\omega}_{x'y'}$ and $\dot{\omega}_{y'z'}$ are given in table 12. In the table, values of $\dot{\omega}_{x'y'}$ and $\dot{\omega}_{y'z'}$ as determined by triangulation survey are given only in the cases where central differences could be used. For the most part $\dot{\omega}_{x'y'}$ is small, and there is agreement between the three independent estimates within the tolerance allowed by the measurement errors. In the case of $\dot{\omega}_{y'z'}$ where the values are small there is agreement as was the case for $\omega_{x'y'}$. For those cases where $\dot{\omega}_{y'z'}$ estimated from the boreholes takes on values considerably different from zero the agreement between the independent estimates is not complete. In general the estimates from borehole tilting give the largest rotation rate, from triangulation an intermediate value, and from the surface slope the smallest value. The latter two estimates agree to within the measurement errors. The first two estimates are also compatible. The consistent difference in magnitude of the effect between the various estimates of $\dot{\omega}_{y'z'}$ seems to be more than a matter of chance. The consistently smaller rotation rates computed from the surface configuration suggest that the surface (represented by the 1962 topographic map) may not be in equilibrium with the present regime of flow, and

that if this regime persisted, the surface would ultimately develop stronger gradients in the transverse variation of longitudinal slope. There is a difference in scale between the first estimate (r) and the other two estimates (t and s). Rotation estimated from the surface tilting of the borehole represents an average over an interval in z of less than 50 m, whereas the other two estimates represent averages over an interval in z of approximately 300 m. (The agreement between the first and second estimates is improved in the cases of boreholes 3B and 4A if one considers the value of $\partial w/\partial y$ at a depth of 50 m. For 3B $\partial w'/\partial y' = -0.008$/yr; for 4A $\partial w'/\partial y' = +0.005$/yr. The comparison is unaffected by this procedure at the other boreholes.) It is not clear why such a difference in scale should lead to consistently different results.

C. Distribution of Longitudinal Strain Rate

All existing theories of glacier flow require the longitudinal strain rate $\partial u/\partial x$ to be either zero or constant over the glacier thickness. In the Athabasca Glacier cross sections, the distribution is far from being constant. Figure 26, which is a contour diagram of $\partial u/\partial x$ half way between sections A and B, where this quantity is best determined by the data, shows a rather complex distribution. A significant feature of the distribution is that there is a general tendency for the compression rate $(-\partial u/\partial x)$ to decrease toward the glacier bed.

The compression rate decreases with depth at all three lines

(1, 2, and 3), where depth information is available (fig. 27). In all three cases the trend with depth is approximately linear. Such a linear variation with depth could be produced by uniform bending about the z-axis. Approximately uniform bending would probably occur if there were a downstream change in longitudinal curvature of the bed, accompanied by a similar change of curvature of the flow lines, as illustrated in figure 31. The bending rate is given by $\partial\dot{\omega}_{x'y'}/\partial x'$. Several estimates of bending rate can be made by differencing the various estimates of $\dot{\omega}_{x'y'}$ at the glacier surface, which were made in the previous section. As was the case in estimating the values of $\dot{\omega}_{x'y'}$ and $\dot{\omega}_{y'z'}$, there is considerable dependence of the result on the method by which it is calculated. For the case for which $\dot{\omega}_{x'y'}$ was estimated from the distribution of surface slope, $\partial\omega_{x'y'}/\partial x'$ becomes approximately $u'(\partial^2\alpha_{x'}/\partial x'^2)$, which shows the explicit dependence on the curvature gradient. This relation can be applied at the glacier bed as given by Paterson (1962), as well as at the surface.

At a given location on the glacier surface a uniform bending rate acting there should produce over the depth of the glacier H a total difference in the longitudinal strain rate

$$\Delta\left(\frac{\partial u}{\partial x}\right)\cong\Delta\left(\frac{\partial u'}{\partial x'}\right) = +\frac{\partial\omega_{x'y'}}{\partial x'}H$$

In table 13 the observed difference in $\partial u/\partial x$ at flow lines 1, 2, and 3 is compared with expected values from bending based on the various estimates of bending rate. The values are in general too small to

completely account for the observed difference in $\partial u/\partial x$. At line 1 the estimates based on the values of v determined by triangulation and the curvature gradient of the bed at the glacier centerline are compatible with the observed $\Delta(\partial u/\partial x)$. There is, however, considerable uncertainty in each of these quantities, so the agreement does not necessarily substantiate that bending can account completely for the observed $\Delta(\partial u/\partial x)$. It does seem probable, however, that bending does contribute at line 1. This may also be the case at line 2. There seems to be no evidence that bending contributes at line 3.

A transverse variation of $\partial u/\partial x$ could also be produced by uniform bending about the y axis. The traverse variation of $\partial u/\partial x$ across the glacier is incompatible with such an interpretation. In addition, since the glacier channel is straight, there is no apparent reason such bending should occur.

The areal distribution of $\partial u/\partial x$ on the cross section is not compatible with a uniform bending rate affecting the whole section, since $\partial u/\partial x$ is not a linear function of y and z. This fact is of general significance since linearity of $\partial u/\partial x$ is a general requirement for the strain-rate field to be independent of x (Appendix III). Thus the distribution of $\partial u/\partial x$ illustrates the three-dimensional character of the deformation field and the corresponding equilibrium problem. The rather complex distribution of $\partial u/\partial x$ is probably a result of a number of factors such as those acting to maintain equilibrium of the glacier surface, the bending effects cited above, and constraints placed on the longitudinal variation of u at the glacier

bed by the parameters which determine the slip velocity.

D. Distribution of Components of Velocity w and v

Several observational facts suggest that a transverse component of velocity w commonly exists in valley glaciers in the ablation region (Sharp, 1960). Direct measurements of surface velocity near the margins of the Saskatchewan Glacier (Meier, 1960) showed the existence of a strong marginward component of velocity. The fact that striations on recently exposed sides of glaciated valleys show a tendency to run up the valley walls indicates that marginward flow often exists at depth. The presence of large, crested lateral moraines on many glaciers suggests that some process for the concentration of debris has acted. General marginward flow could achieve such concentration. The typically convex transverse surface profile of valley glaciers in the ablation region must tend to drive marginward flow.

There are obvious considerations based on equilibrium of the glacier surface and the viscous incompressibility of ice which show why a transverse component of velocity directed toward the margin should exist in the ablation region of a valley glacier. Some of these are briefly discussed by Nielsen (1955). After describing the observed pattern of transverse flow in the Athabasca sections these considerations are discussed in some detail. The distribution of the transverse component of velocity w and the normal component v are illustrated in figure 24, which was constructed as discussed

in Chapter IV.

General description

The distribution of w gives striking confirmation of the existence of marginward flow. Note that most of the lateral transport occurs at depth. This feature is particularly noteworthy in that it brings to mind the hypothesis of extrusion flow as put forward by Demorest (1943). The pattern is symmetrical, except for the relatively large transverse velocity at borehole 1A, which is unexpected because of the close proximity of hole 1A to the center of the channel. The magnitude of the transverse motions is not negligible when compared to the differential longitudinal component of velocity. The contribution of gradients in w to the overall strain-rate level is considerable. It exceeds the contribution of the longitudinal strain rate $\partial u/\partial x$ over considerable depths in several of the boreholes (figs. 28).

The presence of a component of velocity v at the glacier surface is required in order to maintain the elevation of the surface. Since the longitudinal slope of the glacier bed with respect to the x axis and the longitudinal sliding velocity are in general nonzero, the condition that the velocity be normal to the bed gives vectors which are not parallel to the cross section perimeter.

A surprising feature of the distribution of v is that the difference between v at the glacier bed and at the surface is independent of location (see table 9, column 6). The significance of this is that variations in v at the glacier bed are manifested strongly at

the surface with relatively little damping. This is well illustrated for the case of transverse variation of v in figure 25.

Cause of lateral flow

For the purpose of getting deeper insight into the pattern of transverse flow, some conditions on the average of w over the depth of the glacier H(z) at a given location z in the transverse section x, i.e.

$$\langle w \rangle_{H(z)} = \frac{1}{H(z)} \int_0^{H(z)} w(x,y,z)\, dy$$

can be derived. The main tool is the condition of incompressibility, which in integral form requires that

$$A' \langle \frac{\partial u}{\partial x} \rangle_{A'} = \iint_{A'} \frac{\partial u}{\partial x}\, dy\, dz = \int_{C'} \vec{v} \cdot \vec{n}'\, d\ell \qquad (1)$$

where A' is any subarea of the cross section with boundary C'. $\vec{n}'$ is the outward pointing unit normal to C'. Using the notation shown in figure 29, equation (1) can be applied to the area A(z) to give $\langle w \rangle_{H(z)}$ when the surface and basal values of v and w together with the transverse slope of the glacier surface and bed are known. For simplicity a cylindrical geometry, with planar upper surface (y = 0) and with the generators of the glacier bed parallel to the x axis is considered. In this case $\vec{v} \cdot \vec{n}' = 0$ on the bed, and equation (1) becomes

$$A(z) \langle \frac{\partial u}{\partial x} \rangle_{A(z)} = H(z) \langle w \rangle_{H(z)} + \int_z^{W_+} v_s(z)\, dz \qquad (2a)$$

where $v_s(z)$ is the value of v along the surface.

An immediate consequence of incompressibility is that in a cylindrical channel the condition that $\langle w \rangle_{H(z)} = 0$ requires an unreasonable velocity distribution. This is shown by assuming

$\langle w \rangle_{H(z)} = 0$ and observing what happens as $z \to W_+$, where $H(z) \to 0$. For $z \cong W_+$ equation (2a) gives

$$\langle \frac{\partial u}{\partial x} \rangle_{A(z)} \cong \frac{v_s(W_+)(W_+ - z)}{A(z)}$$

Note that $\lim_{z \to W_+} \frac{A(z)}{(W_+ - z)} = 0$. Consequently, if there is non-zero ablation at $z = W_+$, then in order to maintain the elevation of the surface, $\partial u/\partial x$ must be infinite there. Under the stricter assumption that $w = 0$ everywhere, the source of this problem is clearly illustrated by direct integration of the differential form of incompressibility to get

$$\langle \frac{\partial u}{\partial x} \rangle_{H(z)} = \frac{1}{H(z)} \int_0^{H(z)} \frac{\partial u(x,y,z)}{\partial x} dy = - \frac{v_s(z)}{H(z)}$$

Since the longitudinal strain rate has less depth over which to act near the glacier margin where $H(z)$ becomes small, the average value of $\partial u/\partial x$ over that reduced depth must be correspondingly larger. In a typical cross section the distribution of $\partial u/\partial x$ and the accompanying u required to produce finite v_s near the edge would have the unacceptable feature of extreme gradients in the marginal shear rate $\partial u/\partial z$. Thus in the case of cylindrical channels, w or more generally $\langle w \rangle_{H(z)}$ cannot be everywhere zero in the ablation (or accumulation) region.

An important consequence of equation (2a) concerning the relative magnitude of $\partial w/\partial z$ and $\partial u/\partial x$ can be derived. First note that equation (2a) when applied to the whole glacier cross section, of area $A = A(W_-)$, gives the average value of $\partial u/\partial x$ over the com-

plete section $(\partial u/\partial x)_A$, which is required to supply the necessary flux through the surface to counteract ablation.

$$\left\langle \frac{\partial u}{\partial x} \right\rangle_A = \frac{1}{A} \int_{W_-}^{W_+} v_s(z)\, dz$$

Differentiation of equation (2a) gives

$$\frac{d\langle w \rangle_{H(z)}}{dz} = -\frac{\alpha_T(z)}{H(z)} \langle w \rangle_{H(z)} - \frac{1}{H(z)} \int_{W_-}^{W_+} v_s(z)\, dz \left\{ \frac{-v_s(z)}{\int_{W_-}^{W_+} v_s(z)\, dz} + \frac{H(z)}{A} \frac{\left\langle \frac{\partial u}{\partial z} \right\rangle_{H(z)}}{\left\langle \frac{\partial u}{\partial x} \right\rangle_A} \right\} \tag{2b}$$

where $\alpha_T(z) = dH(z)/dz$ and is the transverse slope of the bed with respect to the surface. The value of $\frac{d}{dz}\langle w \rangle_{H(z)}$ is related to $\left\langle \frac{\partial u}{\partial z} \right\rangle_{H(z)}$ through the equation

$$\frac{d}{dz}\langle w \rangle_{H(z)} = \left\langle \frac{\partial w}{\partial z} \right\rangle_{H(z)} + \frac{\alpha_T(z)\left(w_b(z) - \langle w \rangle_{H(z)}\right)}{H(z)} \tag{2c}$$

where $w_b(z)$ is the transverse sliding velocity at the glacier bed. At $z = 0$, where $\alpha_T = 0$, equations (2b) and (2c) give

$$\left\langle \frac{\partial w}{\partial z} \right\rangle_{H(0)} = -\left\langle \frac{\partial u}{\partial x} \right\rangle_{H(0)} \left\{ 1 - \frac{A}{HW} \frac{W v_s(0)}{\int_{W_-}^{W_+} v_s(z)\, dz} \frac{\left\langle \frac{\partial u}{\partial x} \right\rangle_A}{\left\langle \frac{\partial u}{\partial x} \right\rangle_H} \right\} \tag{3}$$

Thus if the value of v_s at the centerline is equal to its average value over the surface and if $\partial u/\partial x$ averaged over the centerline depth equals the average over the cross section area, then

$$\left\langle \frac{\partial w}{\partial z} \right\rangle_{H(0)} = - \left\langle \frac{\partial u}{\partial x} \right\rangle_{H(0)} \left[1 - \frac{A}{HW} \right]$$

For any reasonable cross section $\frac{A}{HW} < 1$, so it can be concluded that for the ablation region where $\langle \partial u/\partial x \rangle_A < 0$ the average value of $\partial w/\partial z$ over the depth of the glacier at the centerline is extensile. For a parabolic cross section, simple geometry shows $A/WH = 2/3$, which gives

$$\left\langle \frac{\partial w}{\partial z} \right\rangle_{H(0)} = - \frac{1}{3} \left\langle \frac{\partial u}{\partial x} \right\rangle_{H(0)}$$

Thus in a typical glacier cross section $\partial w/\partial z$ is not necessarily negligible compared to $\partial u/\partial x$ even at the centerline. This suggests that the hypothesis of plane strain at the centerline of a glacier in the ablation region may lead to errors of the same order incurred by neglecting the longitudinal strain rate. In this regard it is important to note that the magnitude of this effect does not depend simply on W/H, but depends on the channel shape.

To investigate the size of the transverse motions equation (2a) can be used under the simplifying assumptions that v_s is constant across the section, and that $\partial u/\partial x$ is constant over the area of the section. In a particular instance where these assumptions do not hold the details of the distribution of $\langle w \rangle_{H(z)}$ may not be correctly predicted. If, however, v_s is taken equal to its average over the surface and $\partial u/\partial x$ equal to its average over the cross section area, then good estimates of the size of the transverse motions can be obtained. The first of these assumptions is approximately true on

the Athabasca Glacier, and should hold on other glaciers, since ablation rate is largely determined by elevation, a parameter independent of location on a transverse section. Although, as the discussion of the previous section indicates, the distribution of longitudinal strain rate can be far from constant, this assumption is adopted for these estimates. In the case that $\partial u/\partial x$ decreases toward the margins, as observed on the Athabasca Glacier, the assumption of constancy will lead to an underestimation of the required marginward flow. With these assumptions

$$\frac{\partial u}{\partial x} = \left\langle \frac{\partial u}{\partial x} \right\rangle_A = \frac{W}{A} v_s$$

and

$$\langle w \rangle_{H(z)} = - \frac{v_s W}{H(z)} \left(\frac{W_+}{W} - \frac{z}{W} - \frac{A(z)}{A} \right) \tag{4}$$

The distribution of $\langle w \rangle_{H(z)}$ as defined by equation (4) is illustrated in figure 36 for the class of symmetric boundary shapes which can be described by

$$H(z) = H \left[1 - \left(\frac{|z|}{W_+} \right)^{\beta} \right]^{1/\alpha}$$

The types of boundaries which can be so described are extensive. For example, parabolic cross sections are described by $\alpha = 1$, $\beta = 2$; elliptic cross sections are described by $\alpha = 2$, $\beta = 2$. As α becomes large the cross section approaches a rectangular cross section. In the case that $\alpha = 1$

$$\langle w \rangle_{H(z)} = - \frac{v_s}{\beta} \frac{W_+}{H} \left(\frac{z}{W_+} \right) \tag{5}$$

that is, $\langle w \rangle_{H(z)}$ is a linear function of z with

$$\frac{d\langle w \rangle_{H(z)}}{dz} = -\frac{v_s}{\beta H} = -\frac{v_s W}{A}\frac{1}{\beta+1} = -\frac{1}{\beta+2}\frac{\partial u}{\partial x}$$

(Note, however, that when $\alpha_T(z) \neq 0$, $d\langle w \rangle_{H(z)}/dz$ cannot be related to $\langle \partial w/\partial z \rangle_{H(z)}$ without knowledge of the transverse basal sliding velocity w_b as shown by equation (2c)). When $\alpha > 1$ for a given β, the valley walls are steeper, with infinite slope at the margin, and the valley bottom is flatter. The average transverse motions are then, as expected, less than required for $\alpha = 1$. Since the walls are vertical at the margin, $\langle w \rangle_{H(z)}$ goes to zero as z approaches W_+ or W_-. Channels with $\alpha < 1$, for which the slope at the margin is zero, could not be expected to maintain equilibrium there, and clearly do not represent a situation actually occurring in nature.

For the case of a parabolic cross section of width ratio 2 (i.e., $W_+/H = 2$)

$$\langle w \rangle_{H(z)} = -v_s\left(\frac{z}{W_+}\right)$$

Thus it can be concluded that in typical glacier cross sections, transverse velocities on the order of the surface ablation rate must be expected. The motion will in general be toward the nearest margin. The strength of the transverse motions, in the sense of an average over depth, will be greatest near or at the margins.

Another variable of interest is the total transverse transport

$$q_z(z) = H(z)\langle w\rangle_{H(z)} = \int_0^{H(z)} w(x,y,z)\, dy$$

It can be shown under the assumptions leading to equation (4), that $q_z = 0$ at the margins, and that it has extreme values at the points on the cross section where $H(z)$ is equal to A/W, which is just the average depth of the section. The distribution of q_z is shown in figure 32.

Interpretation of observed lateral flux

Some of the features of the observed transverse flow in the Athabasca Glacier can be compared to predictions based on the assumption of cylindrical geometry. To predict the value of $\langle \partial w/\partial z\rangle_{H(z)}$ at the centerline equation (3) can be used. Evaluation of $\langle \partial u/\partial x\rangle_A$ and $\langle \partial u/\partial x\rangle_{H(0)}$ from figure 26 shows that $\langle \partial u/\partial x\rangle_{H(0)} \cong \langle \partial u/\partial x\rangle_A \cong -0.012\ \mathrm{yr}^{-1}$. From the measured surface velocities $v_s(0)$ is $-3.3\ \mathrm{m\ yr}^{-1}$ and the average of $v_s(z)$ over the surface is $-3.8\ \mathrm{m\ yr}^{-1}$. With these quantities and $A/HW = 0.68$, equation (3) gives

$$\left\langle \frac{\partial w}{\partial z}\right\rangle_{H(0)} = -0.41 \left\langle \frac{\partial u}{\partial x}\right\rangle_{H(0)} = 0.005\ \mathrm{yr}^{-1}$$

which is to be compared with the observed values of $+0.005\ \mathrm{yr}^{-1}$ at borehole 1A and $+0.003\ \mathrm{yr}^{-1}$ at borehole 1B. Values of $\langle w\rangle_{H(z)}$ at the various flow lines can be calculated by use of equation (5) with $\beta = 2$ and $W_+/H = 2$ corresponding to a parabolic channel of width ratio 2. (Recall that the validity of (5) depends on the additional assumptions that v_s and $\partial u/\partial x = (W/A)v_s$ are constant.) These

are compared to the observed values in table 14. The observed values in the table corresponds to the average of the values for the A and B boreholes of a given longitudinal line, except at line 5 where the value of borehole 5A was taken. In general the agreement is good except at line 1 where larger displacements are observed than would be expected on the basis of these assumptions.

The very large transverse displacements observed at boreholes 1A ($\langle w \rangle_{H(z)} = -0.97$ m yr^{-1}) and 1C are clearly incompatible with an interpretation in terms of a symmetric cylindrical channel acted on by a uniform longitudinal strain rate. These effects must be the result of some asymmetry in the bed configuration and the distribution of longitudinal strain rate. Between lines 1 and 3 there is a rather sharp change in the longitudinal slope of the glacier bed as indicated by the differences in borehole depths at sections A and B. At line 2 the longitudinal slope of the bed with respect to the x-axis is about $+2.0^{o}$; at line 1 it is about $+1.2^{o}$; at line 3 it is about -1.0^{o}. Positive sign means the bed is more steeply inclined than the x-axis, so that where the x-axis parallels the surface slope the glacier is thickening down stream. Thus the glacier is flowing over what can be described as a diverging ramp. This causes a considerable lateral gradient in the component of velocity v as shown in figure 24, and would tend to produce a rotation at line 1 of the same sense as the observed $\partial w/\partial y$ in borehole 1A. Thus the large values of $\partial w/\partial y$ would be expected on this basis. What is apparently a greater anomaly is the fact that the transverse flux is toward line 3. The effect of the non-cylindrical nature of the bed just described would

tend to produce a flux toward line 2, in order to maintain the glacier surface level laterally. This is opposite in direction to the observed flux. Thus the condition of incompressibility would require that $\partial u/\partial x$ between holes 1A and 3A be relatively extensile compared to $\partial u/\partial x$ between holes 2A and 1A. In fact there is some evidence for this as is shown in figure 26. Half way between sections A and B the average of $\partial u/\partial x$ over depth at line 2 is $-0.0016\ yr^{-1}$ and at flow line 3 is $-0.0012\ yr^{-1}$.

In order to make a more precise quantitative interpretation of the observed average transverse displacements it is necessary to start with equation (1) and proceed without making the various assumptions which were made in the derivation of formulae (2) to (5). This requires detailed knowledge of the glacier geometry and the distribution of longitudinal strain rate in the cross section of interest. Although rather extensive and reliable data on the glacier geometry are available, there is a considerable area of the ice-rock contact over which the sliding velocity is high, but where knowledge of the divergence of the bed with respect to the surface is lacking. Thus $\vec{v} \cdot \vec{n}'$ cannot be evaluated over a large portion of the bed. In figure 26 a distribution of $\partial u/\partial x$ for the complete glacier cross section (A-B) is presented. However, over a significant portion of this cross section near the margins considerable extrapolation is involved. For these reasons it is difficult to make exact quantitative comparison on the basis of equation (1) applied to areas A' which extend into the marginal regions of the cross section. In addition, even in that part of the section where direct measurements were made, the

uncertainty in $\partial u/\partial x$ is sufficiently large to cause errors in $\langle w \rangle_{H(z)}$ of the same size as those produced by neglecting the longitudinal divergence of the surface and the bed.

Some idea of the uncertainty involved is obtained by noting that $\langle \partial u/\partial x \rangle_A$ equals -0.012/year as computed from figure 26. Under the assumption of cylindrical geometry a value of $-0.017\ yr^{-1}$ would be required to produce the observed flux through the glacier surface. This difference would indicate an error in the evaluation of $\langle \partial u/\partial x \rangle_A$; the difference could also be made up by a velocity into a section of $0.9\ m\ yr^{-1}$ averaged over the length of the ice-rock contact. In the center of the section, the flux across the bed profile is mainly out of the section as shown in figure 24. Thus it would be required that there be significant flux into the section in the marginal portions. This is actually to be expected since the glacier is becoming narrower in the reach of this section.

These considerations indicate that the good agreement in table 14 is somewhat fortuitous. The assumption that $\partial u/\partial x$ is constant on the section and equal to $\frac{1}{A}\int v_s(z)\,dz = -0.017\ yr^{-1}$ and the assumption of cylindrical channel shape, which are inherent in equation (5) have lead to errors which have to some extent cancelled each other. Nevertheless the comparison indicates that the observed transverse motions are compatible with those necessary to maintain the elevation of the glacier surface as required by the viscous incompressibility of ice.

Transverse surface elevation differences

The details of the transverse flow pattern involving the actual depth distribution of w, and the specific transverse profile, which the glacier surface must assume in order to produce the requisite driving stresses, is a difficult non-linear boundary value problem, which will not be considered here. It is possible, however, to make a simple order of magnitude estimate of the elevation difference between the central and marginal parts of the glacier surface, which would be required, in order to drive the observed transverse flux.

Consider the problem, illustrated in figure 33, of a rectangular region of depth H and width W, which is occupied by a viscous material of viscosity η. At the top of the slab a sinusoidally varying normal stress is applied,

$$\tau_{yy} = -N \cos hz$$

where N is positive and $h = 2\pi/W$. The shear-stress τ_{xy} is taken to be zero. On the other boundaries of the region it is required that the velocity normal to the boundary and the shear stress parallel to the boundary be zero.

This problem is different from the one of interest. Most obvious is the difference in boundary shape. The boundary condition that the shear stress parallel to the boundaries be zero is, however, more reasonable than might at first be expected. The actual profiles of w show in general small values of $\partial w/\partial y$ (and $\dot{e}_{yz}$) at the bottom of the boreholes, thus indicating that τ_{yz} is small (less than 0.05 bar). Also since the sliding velocities u_b are high (40 m yr^{-1})

it could be expected that a value of τ_{yz} much smaller than τ_{xy} would be sufficient to produce the relatively small transverse sliding velocities (3 m yr^{-1} maximum). The boundary condition applied at $y = 0$ on the slab is also different than the actual boundary condition of interest. In the case of a real glacier the natural boundary condition is that the actual glacier surface, presumably convex upward, is a stress-free surface. This condition is approximated by taking the surface of the slab to be the mean elevation of the true glacier surface. The normal stress on the slab surface is given by the weight of the overlying material between the slab surface and the actual glacier surface, thus

$$N = \rho g_y \Delta H$$

In general, the required surface configuration will not be sinusoidal. It can be expected, however, that the actual elevation difference between the center and margins will not be strongly dependent on the shape of the surface profile. The assumption that the material can be described as a homogeneous Newtonian fluid is a considerable simplification. The effective viscosity at depth can be expected to be less than that near the surface, as a result of the large strain rate associated with the longitudinal flow. An appropriate average viscosity is taken.

The goal is to relate the maximum transverse flux to the normal stress amplitude N (and thus the glacier surface profile) by solving the equations of equilibrium. The details of the solution are

discussed in Appendix IV. The velocity solution is of the form

$$v(y,z) = \phi(hy)\, h \cos hz$$
$$w(y,z) = -\frac{d\phi(hy)}{dy} \sin hz \qquad (6)$$

The average transverse velocity at any location z is given by

$$\langle w \rangle_H = \frac{1}{H}\int_0^H w(y,z)\, dy = \frac{\sin hz}{H}\phi(0)$$

since $\phi(hH) = 0$ as required by the condition that $v(H,z) = 0$. Solution of the equilibrium problem shows that

$$N = 2\eta h^2 \phi(0) Q(\ell)$$

where

$$Q(\ell) = \frac{e^{2\ell} + 4\ell - e^{-2\ell}}{e^{2\ell} - 2 + e^{-2\ell}}$$

and $\ell = 2\pi H/W$. Thus N is related to the maximum transverse flux $q_z)_{max}$, which equals $H\langle w \rangle_H$ evaluated at $hz = \pm \pi/2$ $(z = \pm W/4)$, by

$$N = 2\eta h^2 q_z)_{max} = 8\pi^2 \eta \frac{q_z)_{max}}{W^2} Q$$

If the maximum transverse flux is equal to that observed at borehole 5A (an average of 1.8 m yr^{-1} over a depth of 260 meters), with $W = 1.2$ km, $H = 300$ m, and an appropriate average viscosity (10 bar-yr is a reasonable viscosity, as shown in Chapter VII), the required normal stress amplitude is 0.36 bar. This corresponds to an elevation difference between the center and margin of 7.8 m.

The actual elevation differences are 7.6 m for the southeast side and 6.1 m for the northwest side. The height of the existing "central hump" on the Athabasca Glacier thus seems to be sufficiently high to drive the observed transverse flow.

Depth distribution of the transverse flow

By considering the form of $\phi(hy)$ in equations (6) the depth distribution of the lateral flow of the approximate problem with rectangular boundaries can be compared to the observed depth distribution of w. The solution for $\phi(hy)$ is given in Appendix IV. ϕ and $d\phi/dy$ are plotted in figure 34. The $d\phi/dy$ curve corresponds to the depth distribution of w. The shape of the $d\phi/dy$ curve is similar to the observed distribution of transverse displacements (see figure 17). In the approximate problem the value of $w\,(d\phi/dy)$ at the bed is 2.5 times greater than the value at the surface; thus, as is the case with the observed distribution, most of the marginward transport occurs at depth.

Both the observed and the approximately calculated patterns of flow represent a kind of extrusion flow or "pressure controlled" flow as envisioned by Demorest (1943). Although such flow has been discredited as a mechanism for the longitudinal component of flow, it can be expected to represent the normal pattern of transverse flow associated with a convex transverse surface profile. (In the length of a valley glacier above the firn limit, where the surface profile would be concave, transverse intrusion flow could be expected to occur.) The problem of how the upper layers of ice

can be equilibrated when they are resting on a stratum of faster moving ice, which was overlooked by Demorest, does not arise because of the lateral confinement imposed by the valley walls. The "tub" visualized by Demorest, which he explicitly removed when he applied his ideas to the main transport, is still in place in the transverse flow problem.

Depth dependence in the gradients of v

The observation that the gradients in v are relatively independent of depth is worthy of consideration. In particular notice the transverse variation of v (fig. 25). $\partial v/\partial z$ has significant values at the glacier bed which are related to the transverse variation of the bed slope and the sliding velocity at the bed. For example, the average value at the bed of $\partial v/\partial z$ between boreholes 3A and 2A is $+0.007\ yr^{-1}$. It is surprising that $\partial v/\partial z$ should have a value just as large at the surface, where triangulation measurements show the same average to be $0.008\ yr^{-1}$. The relatively small scale variations in v imposed at the glacier bed would be expected to be damped over the thickness of the glacier and thus produce weaker variations at the glacier surface.

To get a feeling for the amount of damping to be expected, consider a viscous slab of thickness H. The top surface of the slab is taken to be stress free. On the bottom surface it is required that the shear stress be zero and that the velocity normal to the surface have a sinusoidal variation of wave length λ. It can be shown (Appendix IV) that the ratio R of the amplitude of the

normal velocity response at the top of the slab to the amplitude of the applied normal velocity at the base is given by

$$R(\ell) = \frac{e^{\ell} 2(\ell+1) + e^{-\ell} 2\ell}{e^{2\ell} + 4\ell + e^{-2\ell}}$$

where $\ell = 2\pi H/\lambda$. An appropriate wave length for the observed transverse variation of v is about 2H, or 600 meters (fig. 25). This corresponds to $\ell = \pi$ which gives a value of the ratio R of 0.35. Since the observed amplitude is essentially undiminished between the bed and the surface, the distribution of v must be viewed as anomalous. Possibly factors, other than the boundary condition at the glacier bed, which affect the distribution of v could act to produce this effect.

Although the perturbations in v at the bed are not damped out, it is interesting to note that the topographic features at the glacier bed which produce the variations in v are in fact subdued at the glacier surface. The smaller values of $\partial v/\partial z$ estimated at the surface on the basis of the surface topography, as compared with the directly measured values, are an indication of this fact. (See table 12.) At the bed the difference in longitudinal slope between boreholes 3A and 2A is 3.0° but at the surface the difference is 1.0°. This agrees with the expected damping. This fact emphasizes the anomalous nature of the distribution of v.

CHAPTER VII

ANALYSIS OF STRAIN-RATE FIELD FOR RHEOLOGICAL PROPERTIES

In Chapter VI it was established that the deformation field is not two-dimensional and that there are a number of features which complicate the general pattern of flow. It can thus be expected that the distribution of the stresses is complex and cannot be determined by simple static equilibrium considerations. Thus the task of determining in situ rheological parameters for the flowing ice is a considerable challenge.

The general problem of how to analyze the motions of a flowing medium to determine rheological parameters is considered. A method of analysis based on general assumptions concerning the rheology of the material, but which requires no assumptions concerning the distribution of stess, is developed. The problems of applying it to the present data are discussed.

The analysis shows that to some approximation the distribution of shear stress across the width of the glacier is linear with depth; thus a method of analysis similar to that used in past borehole experiments can be applied to all of the present boreholes. A more general analysis shows, however, that there is significiant deviation of the shear stress from strictly linear depth dependence.

A. Restrictions on the Material

Before discussing the analysis of the strain-rate field, some assumptions concerning the response of ice to an applied stress are outlined below.

The basic assumption is that ice behaves as an isotropic incompressible fluid with a response which is independent of hydrostatic pressure. Under these assumptions the most general relationship giving strain rate in terms of the stresses is

$$\dot{e}_{ij} = B(I'_2, I'_3)\tau'_{ij} + C(I'_2, I'_3)(\tau'_{ik}\tau'_{kj} - \frac{2}{3} I'_2 \delta_{ij}) \qquad (1)$$

(Glen, 1958), where $p = -\frac{1}{3}\tau_{ii}$ is the mean compressive stress, $\tau'_{ij} = \tau_{ij} + p$ are the stress deviators, and I'_2 and I'_3 are the second and third invariants of the tensor τ'_{ij}. Since the strain-rate response to stress is assumed to be independent of mean stress, only the stress deviators appear.

The assumption that ice behaves as a fluid, that is, that the stresses are determined only by the strain rates and do not depend on the strain history, or correspondingly that the strain rates depend only on the presently applied stress and not on the loading history, can be expected to be approximately valid in practical application to flow of glaciers, since over the greater part of the volume of most glaciers the stress acting on a given element of ice varies only very slowly in time. Also there is the implicit assumption that under constant load a steady state non-zero strain rate is reached after a sufficiently long time interval.

There is experimental evidence that hydrostatic pressure does not markedly affect the response of ice to stress (Rigsby, 1957). It is also clear that under a constant applied stress, the density of any material cannot indefinitely change at a constant rate, so that in terms of fluid behavior the incompressibility of ice is a requirement.

The assumption of isotropy can, however, be questioned. Extensive measurements of crystal orientation in samples of glacier ice (Rigsby, 1953; Kamb, 1959) demonstrate that preferred orientations of the cyrstals almost always exists. Because of the very strong plastic anisotropy of ice single crystals (Nakaya, 1958), it can therefore be expected that glacier ice will in general exhibit anisotropic mechanical behavior. The strength of such anisotropy has not as yet been quantitatively investigated. There is no evidence that typical glacier ice is strongly anisotropic in its mechanical properties.

Even with these simplifying assumptions the "flow law" expressed by equation (1) is complex. The additional assumptions $C(I_2', I_3') = 0$ and $B(I_2', I_3') = B(I_2')$ are made. The verification of these assumptions requires combined load experiments which test the response under complex applied stress. Very few experiments of this type have been done. Glen (1958), in discussing some experiments of Steinemann, has shown that, although there is some reason to doubt these two assumptions, a flow law of the form

$$\dot{e}_{ij} = B(I_2')\tau'_{ij}$$

is approximately valid. Until more extensive experimental information is available the complex analysis with the more general flow law of equation (1) is not justified. The simplified flow law is the flow law considered by Nye (e.g., 1957, 1965) in his theoretical analyses of various problems in glacier flow. To conform to his notation, let $\tau^2 = I_2' = \frac{1}{2}\tau'_{ij}\tau'_{ij}$ and $\dot{\epsilon}^2 = \frac{1}{2}\dot{e}_{ij}\dot{e}_{ij}$ be the second invariants of the stress-deviator and strain-rate tensors. Then

$$\dot{e}_{ij} = f(\tau)\tau'_{ij}$$

which can be written

$$\tau'_{ij} = 2\eta(\dot{\epsilon})\dot{e}_{ij} \qquad (2)$$

Such a material can be thought of as a viscous fluid in which the "effective viscosity" is determined by the overall strain-rate level as expressed in the value of $\dot{\epsilon}$.

B. Methods of Analysis

In laboratory experiments direct determination of rheological parameters can be made by applying a known stress and observing the resulting response. Glen (1955) has shown experimentally that the quasi-viscous response of initially isotropic polycrystallic ice to uniaxial compression can be represented as a power-type flow law

$$\dot{e} = B'\sigma^n$$

where n is a constant and B' depends on temperature. σ and $\dot{e}$

here represent the applied compressive stress and the resulting compression rate. Depending on how the experiments are interpreted, Glen infers a value for n of 3.2 or 4.2. In terms of the generalized flow law of equation (2) Glen's results can be expressed as

$$\eta(\dot{\epsilon}) = B\dot{\epsilon}^{-\alpha} \tag{3}$$

where

$$\alpha = 1 - \frac{1}{n} \quad \text{and} \quad B = \frac{1}{2}B'^{-\frac{1}{n}}$$

In field experiments, the experimenter has no control of the stresses. Thus to make a direct comparison of measured deformations to the stresses producing them, he must either independently measure the stress field or make assumptions concerning it. The direct measurement of stresses in flowing medium presents many difficult problems and is not practical.

Analysis based on linear depth-variation of shear stress

Rheological interpretations of the deformation measured in all past borehole experiments have by necessity been based on assumptions concerning the distribution of stress. Nye (1951, 1957) has shown that for a glacier of constant thickness and surface slope, in which the strain-rate field is of phase-strain type and has no longitudinal dependence, the stress field is statically determined. In this case the shear stress $\tau_{x'y'}$ is linear with depth:

$$\tau_{x'y'} = \bar{\rho} g_{x'} y'$$

where $\bar{\rho}$ is the average density between $y' = 0$ (the surface) and depth y'. Nye (1952) suggested that the effects of the valley sides can be approximately accounted for by inclusion of a shape factor $f = A/PH$ as follows:

$$\tau_{x'y'} = f\bar{\rho}g_{x'}y' \tag{4}$$

(A, P, and H are the area, length of the ice-rock contact, and centerline depth of the cross section as shown in figure 28.)

Analyses of previous borehole experiments (e.g. Nye, 1957; Paterson and Savage, 1963; Kamb and Shreve, 1966) have been carried out on the basis of a shear stress given by equation (4). The analysis can be carried out in several ways. One can estimate η at a depth y' from equations (2) and (4):

$$\eta = f\frac{\bar{\rho}g_{x'}y'}{2\dot{e}_{x'y'}}$$

If the logarithm of η thus calculated is plotted against the log of the observed $\dot{\epsilon}$ (based on direct measurements or suitable assumptions) for a large number of depths y', then linearity of the resulting array, with slope between 0 and -1, would confirm the applicability of the power law. The slope of the curve would determine α. (α must lie between 0 and 1 for n between 1 and ∞.)

The results of borehole experiments analyzed as above have in general given remarkable confirmation of Glen's experimentally determined flow law, and show that a power flow law with n between 3 and 5 is a good approximation to the gross rheological behavior

of glacier ice. They also give indirect evidence of the soundness (to some approximation) of the assumptions made by Nye in his early analyses (1951, 1957). Some irregularities were, however, observed.

Nye (1965) has shown, in his calculations of rectilinear flow in cylindrical channels with constant sliding velocity over the bed, that the shear stress is only approximately linear with depth. The present observations, as discussed in Chapter VI, show that, in the Athabasca sections, the strain-rate field is not independent of x, and that plane strain does not prevail even at the centerline. Thus it is possible that the shear stress deviates to some degree from linear depth dependence. In addition, the estimation of the shear stress at the bottom of the glacier based on a shape factor correction would give a value which is too large if the correction is based on the channel shape. For these reasons it is desirable to seek a method of analysis not requiring the assumption of equation (4) for the shear stress. The specific goals of such an analysis are either to calculate the shear stress distribution so that the above method, but with the modified stress distribution, can be applied, or to develop a new method in which the stress distribution is not explicitly used.

Analysis based on strain-rate gradients

If a flow law of the form of equation (2) is assumed, the distribution of effective viscosity η can be investigated in any volume where the deformation field is known, by using the equations of

equilibrium and a minimum of assumptions on the stress distribution. The equations of equilibrium are

$$\tau_{ij,j} + \rho g_i = 0$$

In this case the body force is gravity $\rho \vec{g}$, where ρ is the local density. Combined with equation (2), these become

$$(2\eta \dot{e}_{ij})_{,j} - p_{,i} + \rho g_i = 0 \tag{5a}$$

The basic idea of the method of analysis proposed here is well illustrated by considering equations (5a) for the case of rectilinear flow of a linear incompressible fluid of constant density in a cylindrical channel with a planar upper surface $y = 0$. In this case, the equations of equilibrium reduce to

$$\eta \nabla^2 u + \rho g_x = 0$$

$$p = \rho g_y y \tag{5b}$$

If the curvatures of the velocity field ($\nabla^2 u$) can be measured, then the viscosity can be evaluated.

When the effective viscosity η is a function of $\dot{\epsilon}$, η will not be independent of location, and equations (5a) are more complicated. Under the assumption that ice density is homogeneous, they become, in terms of the (x,y,z) coordinates,

$$2\dot{e}_{xx}\frac{\partial \eta}{\partial x} + 2\dot{e}_{xy}\frac{\partial \eta}{\partial y} + 2\dot{e}_{xz}\frac{\partial \eta}{\partial z} + \eta\nabla^2 u - \frac{\partial p'}{\partial x} + \frac{\partial y_s}{\partial x}\rho g_y + \rho g_x = 0$$

$$2\dot{e}_{xy}\frac{\partial \eta}{\partial x} + 2\dot{e}_{yy}\frac{\partial \eta}{\partial y} + 2\dot{e}_{yz}\frac{\partial \eta}{\partial z} + \eta\nabla^2 v - \frac{\partial p'}{\partial y} = 0 \qquad (6)$$

$$2\dot{e}_{xz}\frac{\partial \eta}{\partial x} + 2\dot{e}_{yz}\frac{\partial \eta}{\partial y} + 2\dot{e}_{zz}\frac{\partial \eta}{\partial z} + \eta\nabla^2 w - \frac{\partial p'}{\partial z} + \frac{\partial y_s}{\partial z}\rho g_y = 0$$

where $p'(x,y,z) = p(x,y,z) - \rho g_y(y - y_s(x,z)) - p_a$ is the difference between the mean compressive stress, $p(x,y,z)$ and the "overburden pressure," defined by the body force integrated from the surface plus atmospheric pressure p_a. Since the surface is stress free, except for a normal stress equal to the atmospheric pressure, certain conditions on η and p in terms of the velocity field and its derivatives must hold. Namely

$$\tau_{x'y'} = 2\eta\dot{e}_{x'y'} = 0$$

$$\tau_{y'z'} = 2\eta\dot{e}_{y'z'} = 0 \qquad (7a)$$

and

$$\tau_{y'y'} + p_a = 2\eta\dot{e}_{y'y'} - p' = 0 \qquad (7b)$$

for $y = y_s(x,z)$. Equations (6) are linear partial differential equations to be solved for η and p' with the boundary conditions given by equations (7).

To gain some insight into the problems involved in the solution of equations (6), it is useful to consider again the special case where the material has a planar top surface $y = 0$ and the flow field

is rectilinear, but now it is not assumed that η is independent of location. With $p' = 0$ the second and third equations are trivially satisfied. The first equation becomes

$$\frac{\partial u}{\partial y}\frac{\partial \eta}{\partial y} + \frac{\partial u}{\partial z}\frac{\partial \eta}{\partial z} + \eta\nabla^2 u + \rho g_x = 0 \ . \qquad (8a)$$

The second of equations (7a) and equation (7b) are also trivially satisfied. The remaining boundary condition at $y = 0$ is

$$\eta \frac{\partial u}{\partial y} = 0 \ . \qquad (8b)$$

(8a) is a first order partial differential equation with a single independent variable η to be determined. In general a single characteristic curve passes through each point (Hill, 1950, p. 345). The direction of the characteristic is given by

$$\frac{dy}{dz} = \frac{\partial u}{\partial y} \Big/ \frac{\partial u}{\partial z}$$

Thus the characteristic curves are parallel to the gradient of u. On a contour diagram of u the curves would run normal to the contours. Thus, the first derivative of u in a direction normal to a characteristic is zero, which shows that the shear strain rate and consequently the shear stress across a cylindrical surface parallel to a characteristic and the x-axis are zero. Another fact to be noted is that when $\partial u/\partial y = \partial u/\partial z = 0$ a curve of any direction dy/dz will have the above properties and thus more than one characteristic can pass through such a point. In figure 35 the characteristics are drawn for a hypothetical distribution of u.

Characteristics have two basic properties. The first is that specifying the dependent variable (in this case η) along a characteristic will in general not enable one to determine the solution elsewhere. The second is that the dependent variable cannot be arbitrarily specified along a characteristic, in fact specifying its value at one point on the characteristic determines the value at all other points on the characteristic . These two properties can be expressed analytically by transforming equation (8a) to local coordinates (t,n), where

$$\hat{t} = \frac{-\vec{\nabla} u}{|\vec{\nabla} u|} \quad , \quad \hat{n} = \hat{x} \times \hat{t}$$

Such a coordinate system at a given point has axis $\hat{t}$ parallel to the characteristic curve and axis $\hat{n}$ parallel to the u contour at that point. The characteristics are curves of constant n; the u contours are curves of constant t. The system is an orthogonal curvilinear coordinate system and defined by transformation functions

$$t = t(y,z)$$

$$n = n(y,z)$$

In these coordinates equation (8a) can be written

$$h_t \frac{\partial}{\partial t}(\eta h_t \frac{\partial u}{\partial t}) - \frac{h_t}{h_n} \frac{\partial h_n}{\partial t}(\eta h_t \frac{\partial u}{\partial t}) = -\rho g_x \qquad (9)$$

where the fact that $\partial u/\partial n = 0$ has been used.

$$h_t^2 = \left(\frac{\partial t}{\partial y}\right)^2 + \left(\frac{\partial t}{\partial z}\right)^2 \quad \text{and} \quad h_n^2 = \left(\frac{\partial n}{\partial y}\right)^2 + \left(\frac{\partial n}{\partial z}\right)^2$$

are the scale moduli of the coordinate axes t and n.

Values of η at points not lying on a characteristic can not be calculated from values of η specified on that characteristic. This means that equations (8) do not represent a well posed boundary value problem, since the boundary condition is applied on a characteristic. Nevertheless a unique solution can be obtained if there is only one point in the cross section where $\partial u/\partial y = \partial u/\partial z = 0$. In a real glacier cross section it is reasonable to expect that there is only one such point and that it lies at the surface. In this case, every point in the cross section is joined to the point where $\partial u/\partial y = \partial u/\partial z = 0$ by a characteristic (fig. 35). If a condition on η is applied at this point, then equation (9) defines a solution satisfying equilibrium (8a) at all points. A suitable condition is: $\eta h_t \frac{\partial u}{\partial t} = 0$ at the point where $\partial u/\partial y = \partial u/\partial z = 0$. This is equivalent to requiring that the shear stress be zero, where the shear strain rate is zero. With this condition equation (8b) is also satisfied.

There is a very simple physical explanation for the above conclusion. Since there is no shear stress parallel to a characteristic curve, gross equilibrium of a pie shaped segment of the cross section bounded by two characteristics (n_1 and n_2) and a velocity contour (t) must be accomplished by application of a shear stress across the velocity contour (see figure 35). If the distance along the velocity contour (t) between n_1 and n_2 is $\ell\ (n_1, n_2, t)$ and $A(n_1, n_2, t)$ is the included area, then the average shear stress is

$$\tau = \rho g_x A(n_1, n_2, t)/\ell(n_1, n_2, t)$$

τ can be identified with the quantity $\eta h_t \frac{\partial u}{\partial t}$.

Thus in the case of rectilinear flow the distribution of velocity u and equations (6) and (7) (or equivalently equations (8)) uniquely determine the distribution of the quantity $\tau = \eta h_t \frac{\partial u}{\partial t}$ and thus the distribution of η. The analysis can be carried out without any assumptions concerning the distribution of stress. This result is easily generalized to the case for which the ice density is not homogeneous.

The same arguments apply for the slightly more general velocity distribution where the strain-rate components are independent of x, but a constant longitudinal strain rate is allowed to act. The most general form of such a velocity field is given in Appendix III. The glacier surface is required to be cylindrical with generators parallel to the x axis. The boundary condition (7b) then requires that $\partial p'/\partial x = 0$. The first equilibrium equation reduces to (8a). Since there are no longitudinal stress gradients and the surfaces across which the shear stress is zero are cylindrical surfaces with generators parallel to the x axis, equation (8a) uniquely determines τ and η in the same way through equation (9). Since, however, there must be non-zero components of velocity v and w, as required by incompressibility, the second and third equilibrium equations will not be automatically satisfied. In general there are hypothetical distributions of v and w which satisfy the requirement of incompressibility and any boundary conditions over the glacier surface and bed compatible with incompressibility, but which

do not satisfy the second and third of equations (6). Thus, a solution of (6) with boundary conditions (7) will not exist for an arbitrary distribution of velocity with x-independent strain rates. If for an observed x-independent field, the second and third equilibrium equations were not satisfied with the viscosity distribution uniquely determined by the first, this could be taken to indicate that the flow law given by equation (2) is incompatible with the observed motions. In making such an interpretation one would of course have to give due consideration to the errors of observation.

In the analysis of more complex distributions of velocity, the questions of existence and uniqueness also arise. The question of compatibility, which arose in the discussion above, can be expected generally to exist simply because there are two unknowns and three equations to satisfy; thus a solution to equations (6) may not exist for a specified distribution of velocity. Also, by virtue of the assumed isotropy of the ice, the shear strain rate parallel to the glacier surface vanishes at the surface; thus the coefficient of the derivative of η normal to the surface, in equation (6), vanishes, so that this derivative becomes indeterminate at the surface. As was the case for x-independent flow fields, equations (6) and (7) do not constitute a well-posed boundary-value problem. Whether a solution is nonetheless unique, as in the case of x-independent flow, is, however, a question that has remained unanswered.

For the purpose of practical application of these ideas, however, these mathematical difficulties are not significant. Although for an observed distribution of velocity equations (6) may be incom-

patible or the solution to (6) with conditions (7) may not have a unique solution, a valid approach is to seek the best solution consistent with a specific model of the flow law. In view of the uncertainty in any observational data, this would indeed seem to be the most reasonable way of proceeding.

Approximate solution based on minimizations of residual body sources

Instead of attempting to solve equations (6), approximate solutions are sought by the following method. η and p' are parameterized in terms of specific models of the functional dependence of these quantities on x, y, z, that is

$$\eta = \eta(x,y,z;\ell_1,\ldots,\ell_m)$$

$$p' = p'(x,y,z;\ell_{m+1},\ldots,\ell_n)$$

For example one possible model is to let η and p' be represented by three-dimensional polynomials. η can also be parameterized directly in terms of the second strain-rate invariant $\dot{\epsilon}^2$,

$$\eta = \eta(\dot{\epsilon}^2;\ell_1,\ldots,\ell_m)$$

In equations (6) $\partial\eta/\partial x_i = (\partial\eta/\partial\dot{\epsilon}^2)(\partial\dot{\epsilon}^2/\partial x_i)$. η probably has a relatively simple function dependence on $\dot{\epsilon}$. The actual spatial distribution of η can, however, be very complex. Thus proceeding in this manner has the advantage that a model capable of giving the actual distribution will require fewer parameters, and parameters in a flow law given by equation (2) can be directly evaluated.

In general, with specific choices of the n parameters ℓ_k the equations of equilibrium (6) will not be satisfied at a given point x,y,z; that is, there will be residuals r_x, r_y, r_z, to the three equations. One can think of the residuals as defining a body force field $\vec{r} = \vec{r}(x,y,z;\ell_1,\ldots,\ell_n)$. Fictitious forces $-\vec{r}$ would be required in order to produce equilibrium with the specific choice of parameters. Also the boundary conditions given by equations (7) will not be satisfied. There will be residuals s_x, s_y, s_z defining a distribution of surface traction $\underline{s} = \underline{s}(y_s(x,z);\ell_1,\ldots,\ell_n)$. It is proposed to choose the parameters of a given model such that the residual forces are minimized in the sense that

$$F^2(\ell_1,\ldots,\ell_n) \equiv \iiint_V \vec{r}\cdot\vec{r}\,dv + \iint_S \vec{s}\cdot\vec{s}\,da \qquad (10a)$$

is required to be a minimum. The conditions

$$\frac{\partial F^2}{\partial \ell_k} = 0 \quad k = 1,\ldots,n$$

give n equations for the n parameters $\ell_1,\ldots,\ell_n$.

In the actual application of this technique to field data it is advantageous to consider equation (10a) in a discrete form, so that the equilibrium equations can be considered at selected points where the strain rates and their gradients are best determined. Thus

$$F'^2(\ell_1,\ldots,\ell_n) = \sum_{n=1}^{N} \vec{r}\cdot\vec{r} + \sum_{m=1}^{N} \vec{s}\cdot\vec{s} \qquad (10b)$$

is minimized. The sums are over N distinct points (x,y,z) in the interior

and M distinct points $y_s(x,z)$ on the surface. The value of F'^2 or the root mean square residual force $\sum = \sqrt{F'^2/(N+M)}$ is a measure of the fit to the data.

In this discrete form the minimization of F'^2 is identical to the usual least squares problem. Consideration of equations (6) and (7) at the selected points gives $3(N+M)$ conditional equations to determine the n unknown parameters. When $3(N+M) > n$ the n conditions on $\partial F'^2/\partial \ell_k$ give n normal equations which determine the parameters $\ell_1,\ldots,\ell_n$.

If η and p' are linear functions of the parameters, then the conditional equations will be linear. The usual theorems on least square procedures apply. The normal equations will be linear and will define a unique solution for the parameters $\ell_1,\ldots,\ell_n$.

In order to examine models, where η does not depend linearly on the parameters, a successive approximation procedure for the case when $\eta = \eta(\dot{\epsilon}^2;\ell_1,\ldots,\ell_m)$ is developed. For a given choice of the ℓ_n the equations of equilibrium give

$$\frac{\partial \eta}{\partial \dot{\epsilon}^2}(\dot{\epsilon}^2;\ell_1,\ldots,\ell_m)\mu_i + \eta(\dot{\epsilon}^2;\ell_1,\ldots,\ell_m)\kappa_i - \frac{\partial p'}{\partial x_i}(x,y,z,\ell_{m+1},\ldots,\ell_n) + f_i = r_i \qquad (11)$$

where $\mu_i = 2\dot{e}_{ij}\dot{\epsilon}^2_{,j}$, $\kappa_i = \nabla^2 u_i$, $f_x = \rho\left(g_x + \frac{\partial y_s}{\partial x}\right)$, $f_z = \rho\left(g_z + \frac{\partial y_s}{\partial z}\right)$, and $f_y = 0$. If incremental changes $\delta\ell_k$ in the ℓ_k are made, there will be a corresponding variation δr_i in r_i which is given to first order in the $\delta\ell_k$ by

$$\delta r_i = \sum_{j=1}^{m} \left(\frac{\partial \eta}{\partial \ell_j \partial \dot{\epsilon}^2} \mu_i + \frac{\partial \eta}{\partial \ell_j} \kappa_i \right) \delta \ell_j + \sum_{j=m+1}^{n} \frac{\partial p'}{\partial \ell_j \partial x_i} \delta \ell_j$$

Similarly the boundary conditions are

$$2\eta(\dot{\epsilon}^2; \ell_1, \ldots, \ell_m) \dot{e}_{x'y'} = s_{x'}$$

$$2\eta(\dot{\epsilon}^2; \ell_1, \ldots, \ell_m) \dot{e}_{y'z'} = s_{z'}$$

$$2\eta(\dot{\epsilon}^2; \ell_1, \ldots, \ell_m) \dot{e}_{y'y'} - p'(x,y,z; \ell_{m+1}, \ldots, \ell_n) = s_{y'}$$

Incremental changes in $\underline{s}$ in terms of the $\delta \ell_k$ are given by

$$\delta s_{x'} = 2\dot{e}_{x'y'} \sum_{j=1}^{M} \frac{\partial \eta}{\partial \ell_j} \delta \ell_j$$

$$\delta s_{z'} = 2\dot{e}_{y'z'} \sum_{j=1}^{M} \frac{\partial \eta}{\partial \ell_j} \delta \ell_j$$

$$\delta s_{y'} = 2\dot{e}_{y'y'} \sum_{j=1}^{M} \frac{\partial \eta}{\partial \ell_j} \delta \ell_j - \sum_{j=m+1}^{N} \frac{\partial p'}{\partial \ell_j} \delta \ell_j$$

By choosing $\delta \ell_k$ so as to minimize

$$F'^2 = \sum_{n=1}^{N} (\vec{r} + \delta\vec{r}) \cdot (\vec{r} + \delta\vec{r}) + \sum_{m=1}^{M} (\vec{s} + \delta\vec{s}) \cdot (\vec{s} + \delta\vec{s})$$

conditional equations

$$A_{ij}(\ell_k) \delta \ell_j - b_i(\ell_k) = r'_i \tag{12}$$

are obtained. A_{ij} is a $3(N+M) \times n$ matrix, b_i is a $3(N+M)$ com-

ponent vector. The equations are ordered as follows: N x-equilibrium equations, N y-equilibrium equations, N z-equilibrium equations, M x' boundary conditions, M z' boundary conditions, and M y' boundary conditions. The $A_{ij}(\ell_k)$ and $b_i(\ell_k)$ are then given by:

for $i = 1,\ldots,N$

$$r'_x = r_x + \delta r_x$$

$$b_i = -f_x - \mu_x \frac{\partial \eta}{\partial \dot{\epsilon}^2}(\dot{\epsilon}^2;\ell_1,\ldots,\ell_m) - \kappa_x \eta(\dot{\epsilon}^2;\ell_1,\ldots,\ell_m) + \frac{\partial p'}{\partial x}(x,y,z;\ell_{m+1},\ldots,\ell_n) \tag{12a}$$

$$A_{ij} = \begin{cases} \mu_x \dfrac{\partial \eta}{\partial \ell_j \partial \dot{\epsilon}^2} + \kappa_x \dfrac{\partial \eta}{\partial \ell_j} & j = 1,\ldots,m \\ -\dfrac{\partial p'}{\partial \ell_j \partial x} & j = m+1,\ldots,n \end{cases}$$

for $i = N+1,\ldots,2N$ equation (12b) and for $i = 2N+1,\ldots,3N$ equation (12c), let $x \to y$ and $x \to z$ in the above equations;

for $i = 3N+1,\ldots,3N+M$

$$r'_i = s_{x'} + \delta s_{x'}$$

$$b_i = -2\dot{e}_{x'y'}\eta$$

$$A_{ij} = \begin{cases} 2\dot{e}_{x'y'} \dfrac{\partial \eta}{\partial \ell_j} & j = 1,\ldots,m \\ 0 & j = m+1,\ldots,n \end{cases} \tag{12d}$$

for $i = 3N+M+1,\ldots,3N+2M$ equations (12e), let $x' \rightarrow z'$;

and for $i = 3N+2M+1,\ 3N+3M$

$$r_i' = s_{y'} + \delta s_{y'}$$

$$b_i = -2\dot{e}_{y'y'}\eta + p' \tag{12f}$$

$$A_{ij} = \begin{cases} 2\dot{e}_{y'y'}\dfrac{\partial \eta}{\partial \ell_j} & j = 1,\ldots,m \\ -p' & j = m+1,\ldots,n \end{cases}$$

The desired minimization is accomplished by solving the normal equations

$$\mathcal{A}_{ij}\delta\ell_j = \mathcal{B}_i \tag{13}$$

where

$$\mathcal{A}_{ij} = A_{ki}A_{kj}$$

$$\mathcal{B}_i = A_{ki}b_k$$

The normal equations give a unique solution for $\delta\ell_1,\ldots,\delta\ell_n$. The original estimates of the parameters ℓ_n are then corrected to $\ell_k + \delta\ell_k$. The procedure is repeated until no further change in the ℓ_k is computed.

If η and p' depend linearly on their respective sets of parameters then the successive approximation procedure converges in one step. The resulting solution is unique. If η (or p') is not

a linear function of its parameters, then in general several correction steps must be taken. Further, in this case it may be possible that the quantity F'^2 given by equation (10) has local minima and maxima. For this reason in the application of this technique with non-linear models it is advisable to test whether the converged values of the ℓ_k correspond to a minimum and whether there are other minima in the domain of acceptable ℓ_k. The first test can be accomplished by keeping track of F'^2 in the successive steps and noticing whether each step reduces F'^2. The second test can be made by seeing whether different starting values of the parameters lead to the same converged solution.

A troublesome feature of the above method of minimizing residual body forces was discovered when it was applied to the strain-rate field calculated from the unsmoothed tilt data. The results gave viscosities much smaller than expected, and residuals approximately equal to the body force. Intuition provides the following explanations for this behavior. The noise in the tilt data gives local fluctuations in the calculated strain-rate components. If the mechanical properties of the material are homogeneous, as is implicitly assumed by the use of equation (2), and if the parameters of the flow law (2) are such as to give non-zero viscosity, then there must also be local fluctuations in the stress gradients, which in general cannot be equilibrated by the applied forces unless there is a fortuitous cancellation of the contributions of noise from different boreholes. If local strain-rate gradients are much larger than the

gradient of the overall trend, then, in order that the local stress gradients are not overwhelmingly large compared to the body force density, the flow law parameters will be chosen so that the viscosity is smaller than required by the overall gradient and the acting body force. Thus the estimates of flow law parameters are biased by the existence of noise. The effect of noise can be simply analyzed for the case of rectilinear flow of a linear fluid described by equation (5b) by considering hypothetical data. The analysis shows that as the noise amplitude in the measured values of $\nabla^2 u$ becomes very large as compared to the real value, the estimated viscosity goes to zero and the residual body force is equal to the acting body force. As the noise amplitude becomes small compared to the actual value, the biasing effect goes to zero. This was one of the more compelling reasons for representing the tilt data by smooth curves. Use of the smoothed data in the above analysis involves the implicit assumption that the scatter in the tilt data comes from experimentally introduced noise and does not represent real features of the flow. This is a reasonable assumption (Appendix II-B).

C. Application to the Athabasca Data

The above techniques are now applied to the strain-rate field derived from the smoothed data. First, arguments are presented which show that shear stress parallel to the surface will be approximately linear with depth across the width of the glacier. Because of

this an analysis based on linear variation of shear stress is presented. Second, the technique of using strain-rate gradients, and minimizing residual body forces is applied. In the analysis it is assumed that ice density is independent of position and has a value of 0.90 gm/cm^3.

Linear shear stress analysis

One possible way of proceeding with the analysis is to calculate the distribution of shear stress τ through equation (9). This procedure would be valid only if the longitudinal strain rate $\partial u/\partial x$ were constant throughout the volume of this part of the glacier, the strain rates were independent of x, and the glacier surface were cylindrical with generators parallel to x. Even though there are complexities in the actual distributions of flow variables and surface slope, which clearly violate these requirements, the distribution of shear stress thus derived should be approximately correct. Realizing the approximation involved, a precise calculation is not made. Since the u velocity contours are approximately semicircular (fig. 22), the (t,n) coordinates can be associated with the standard polar coordinates (r,θ), where $y = r\cos\theta$ and $z = r\sin\theta$. In this case $h_t^2 = (\partial r/\partial y)^2 + (\partial r/\partial z)^2 = 1$ and $h_n^2 = 1/r^2$. Equation (9) becomes

$$\frac{\partial \tau}{\partial r} + \frac{\tau}{r} = -\rho g_x$$

with the condition $\tau = 0$ at $r = 0$. The solution is

$$\tau = -\frac{1}{2}\rho g_x r \qquad (14)$$

This is, of course, a result established long ago by Nye (1952) for rectilinear flow in a cylindrical semi-circular channel. It shows that, under the assumption of x-independence, the shear stress τ_{xy} can be expected to be approximately linear with depth across the width of the glacier, that is

$$\tau_{xy} = \tau \cos\theta = -\frac{1}{2}\rho g_x y$$

The analysis of all of the boreholes can be made by one of the previously used methods. Here $\log \eta$, where $\eta = \tau_{xy}/2\dot{e}_{xy}$, is plotted against $\log \dot{\epsilon}$.

The above formulae are written with respect to the (x,y,z) system, which is the system with x parallel to the glacier surface at the centerline. The longitudinal slope at the centerline is 3.9^{o}. Since the glacier surface is not a cylindrical surface, there is some ambiguity in choosing the best coordinate system. For example a system with the x_1 axis parallel to the surface slope averaged over the area of the complete borehole array could be more appropriate. Such an average surface slope is about 3.4^{o}. Another possibility is that each borehole be analyzed on the basis of the local surface slope, as computed from averages over areas with dimensions equal to the depth of the borehole.

Approximation of the velocity contours with concentric semi-circles involves the implicit assumption that the shear strain rate

$\dot{e}_{xy} = \frac{1}{2}(\partial u/\partial y)$ goes to zero on a horizontal line $y = \text{const}$. The actual free surface condition is $\tau_{x'y'} = 0$ at $y = y_s(x,z)$, thus it is most reasonable to measure the increase in shear stress in terms of depth below the actual local surface.

The above formulae generalized to a coordinate system $(\bar{x},\bar{y},\bar{z})$ where $\bar{z}$ is parallel to z, but $\bar{x}$ has a plunge different from x by an angle $\delta_{\bar{x}}$, become

$$\tau_{\bar{x}\bar{y}} = -\frac{1}{2}\rho g_{\bar{x}}(\bar{y} - \bar{y}_s(\bar{x},\bar{z}))$$

$$\dot{e}_{\bar{x}\bar{y}} = \dot{e}_{xy}\cos 2\delta_{\bar{x}} + \frac{1}{2}(e_{yy} - e_{xx}) \sin 2\delta_{\bar{x}} \qquad (15)$$

$$\eta = \tau_{\bar{x}\bar{y}}/2\dot{e}_{\bar{x}\bar{y}}$$

$\delta_{\bar{x}}$ is positive if $\bar{x}$ corresponds to a steeper slope than x. Figure 36 shows the results of this analysis when applied in the set of coordinate systems with $\bar{x}$ parallel to the local surface at each borehole location ($\delta_x = -1.1^\circ$ to $+0.1^\circ$). Results for the (x,y,z) system ($\delta_x = 0$) and for the coordinate system with $\bar{x}$ parallel to the average surface slope ($\delta_x = -0.5^\circ$) are almost identical to the results presented in figure 36.

The curves $\log\eta$ vs. $\log\dot{\epsilon}$ for the different boreholes show certain similarities in all three coordinate systems. An approximately linear portion of the curve corresponds to the lowermost 50 to 100 m of the borehole. The depth corresponding to the open circle plotted in figure 36 and above which the linear trend does not persist is given in table 15, column 4. The termination of the

linear trends in boreholes 1A and 2B by dips in the curves is associated with a depth range where the shear strain rate vs. depth profile is convex away from the depth axis, and the ratio $(\bar{y}-\bar{y}_s)/\dot{e}_{\bar{x}\bar{y}}$ does not decrease with increasing depth as fast as it would in the case of a more typical depth variation of shear strain rate. The steep portions of the curves exhibited by all boreholes correspond to those depth ranges where the second strain-rate invariant is relatively independent of depth, but the ratio $(\bar{y}-\bar{y}_s)/\dot{e}_{\bar{x}\bar{y}}$ decreases markedly with depth. The onset of this behavior occurs at greater depth in the section B boreholes than in the section A holes. The near vertical portions of the curves for boreholes relatively distant from the centerline (4A, 5A) are to the right (higher strain rate) of the corresponding portions of the curves for boreholes close to the centerline (1A, 1B). This systematic distribution is a reflection of the difference in shear strain rate $\dot{e}_{\bar{x}\bar{z}}$ at the different boreholes. $\dot{\epsilon}$ shows a minimum in all the boreholes at depths ranging from 75 to 165 m. These depths are tabulated in table 15, column 3. Since the ratio $(\bar{y}-\bar{y}_s)/\dot{e}_{\bar{x}\bar{y}}$ is monotonic in this depth range, the curves $\log \eta$ vs. $\log \dot{\epsilon}$ are double valued. At depths shallower than that of the minimum in $\dot{\epsilon}$ the curves have large positive slopes.

The curves for none of the boreholes can be unambiguously interpreted in terms of a power-type flow law. Such a flow law would require the curves to be linear. The double valued nature of the curves clearly indicates that they do not represent any flow law represented by equation (2) which can be applied uniformly at all

depths, even with a form other than a power law. In addition, if the material were homogeneous, the large negative slope exhibited by all the curves over significant depth ranges would imply an unacceptable inverse relationship between stress and strain rate; in other words an increased stress would result in a diminished strain rate. These features indicate that over a considerable depth range in the boreholes the analysis is not giving a valid picture of rheological properties. Either there is a significant inhomogeneity in the rheological properties of the ice, or a rheological behavior different than is describable by equation (2), or a failing of the assumption of the linear depth variation of shear stress, or a large effect of measurement errors.

In order to evaluate the effect of errors of observation, the relative error in η is of interest. As calculated on the basis of the assumption of linear variation of the shear stress, it is

$$\frac{\delta\eta}{\eta} = \frac{\dot{e}_{\bar{x}\bar{y}}}{(\bar{y}-\bar{y}_s)}\,\delta\left(\frac{(\bar{y}-\bar{y}_s)}{\dot{e}_{\bar{x}\bar{y}}}\right) = -\frac{\delta\dot{e}_{\bar{x}\bar{y}}}{\dot{e}_{\bar{x}\bar{y}}} \qquad (16)$$

The depth at which $\dot{e}_{\bar{x}\bar{y}}$ exceeds the estimated error in $\dot{e}_{\bar{x}\bar{y}}$ ranges from 30 to 100 m for the various boreholes. This means that in the near surface parts of the boreholes a relative error exceeding 100% in the estimated viscosity η is possible. This corresponds to an error in log η of about ± 0.5. This can be compared to the error at the depths where the linear trend in the log η vs. log $\dot{\epsilon}$ curves are broken. There the relative error in η is about 10%, which corresponds to an error in log η of about $\pm$ 0.05. Thus the

anomalous steep slope and double valuedness of the curves might be a result of a strong manifestation of observational errors as the glacier surface is approached. At first sight it would seem strange that observational uncertainty could act consistently to overestimate the viscosity near the surface. However, this could occur as follows. Since $\dot{\epsilon}$ is relatively independent of depth, the condition required to give a meaningful plot interpretable in terms of equation (2) is that η also be independent of depth. This would be the case if the dependence of $\dot{e}_{\overline{x}\overline{y}}$ on depth were linear. It is easily seen that if the curve $\dot{e}_{\overline{x}\overline{y}}$ vs. $\overline{y}$ is concave away from the $\overline{y}$ axis the computed viscosity must increase upward. The smoothed curves which represent the longitudinal tilt data may be biased to be concave near the surface because of the overall concave nature of the tilt profiles, the large depth range over which the smoothing averages were taken, and edge effects associated with the lack of data above the surface.

Examination of the longitudinal tilt data (fig. 13) shows, however, that positive evidence for a concave part of some of the borehole tilt profiles exists near the surface. This is particularly evident in the boreholes of section B, where tilting rate remains essentially constant down to depths of 100 m. This means that shear strain rate remains zero over a considerable depth range near the surface. The stronger manifestation at section B is a reflection of the decrease with depth of the compression rate (fig. 27). Depths above which the smoothing curves for a borehole could be altered

within the constraints of the data in order to produce a significantly different result are tabulated in table 15, column 2 and plotted as solid circles in figure 36. The parts of the log η vs. log $\dot{\epsilon}$ curves corresponding to depths shallower than these depths do not necessarily represent real effects. In all of the boreholes except 1C, 2A, and 3A the strong upswing of the log η vs. log $\dot{\epsilon}$ curves begins at significantly greater depths. Thus the effect is not caused solely by measurement errors.

The short segment of large positive slope shown by the log η vs. log $\dot{\epsilon}$ curve for the deepest part of borehole 2A is a definite anomaly not attributable to observational error. It is correlated with the unusual depth dependence of the observed longitudinal tilting rate in the lowermost 40 m of the borehole (fig. 13d).

The dips in the curves of boreholes 1A and 2B are associated with definite convex parts of the longitudinal tilt profiles (fig. 13a and e). Adjustments of the depth distribution of $\dot{\epsilon}$ within limits set by the estimated error can not eliminate these features.

The curve for borehole 1C plotted in figure 36 gives good examples of apparent anomalies probably resulting entirely from the possible large relative error in the estimated viscosity and slight fluctuations in the depth dependence of $\dot{e}_{xy}$ not demanded by the data. The sharp dip in the curve is correlated with a slightly convex portion of the longitudinal tilt profile between depths at approximately 60 and 130 m (fig. 13c). The upward swing at shallower depths correlates with the concave part of the profile above 60 m. These

features are not required by the data.

Although there are features of the $\log \eta$ vs. $\log \dot{\epsilon}$ curves of figure 36 which indicate that the assumptions of the analysis must in part fail, the approximately linear curves shown by the deeper portions of each of the boreholes and the linear trend defined by the combined data from all of the boreholes can be interpreted in terms of a power law, $\eta(\dot{\epsilon}) = B\dot{\epsilon}^{-\alpha}$. The slopes $(-\alpha)$ of the linear parts of the curves are closely the same in all three of the coordinate systems in which the computations were made. The intercept (B) or position of the curve along the $\log \eta$ axis does, however, depend on the specific coordinate system. The best agreement between the curves for different boreholes is achieved when the plots are made with respect to the coordinate systems defined by the local surface slope (fig. 36). Apparently the surface slope averaged over an area with dimensions approximately equal to the borehole depth better defines the shear stress at the bottom of a borehole than the average value over the larger area of the complete borehole array.

Flow law parameters α and B were computed from the general trend defined by all of the data and the linear parts of the individual borehole curves (fig. 36). The results are given in table 16. There is a considerable range in α for the individual boreholes, as could be anticipated in view of the distinctly different tilt profile shapes which were measured in the different boreholes. Large values of B, which correspond to the value of η at $\dot{\epsilon} = 1\ \mathrm{yr}^{-1}$, are associated with small values of α (and vice versa) as a result of the fact that the linear trends for all boreholes converge at a

strain rate $\dot{\epsilon} = 0.05\ \mathrm{yr}^{-1}$. Extension of the linear trends to $\dot{\epsilon} = 1\ \mathrm{yr}^{-1}$ gives values of B depending systematically on the slope. In order to make comparisons which are valid in the range of the observed strain rate, the flow law is normalized such that

$$\eta = B^{*}\left(\frac{\dot{\epsilon}}{\dot{\epsilon}_{o}}\right)^{-\alpha}$$

with $\dot{\epsilon}_{o} = 0.05\ \mathrm{yr}^{-1}$. Thus $B^{*} = B(0.05\ \mathrm{yr}^{-1})^{-\alpha}$. With this normalization, values of B^{*} lie between 9 and 10 bar yr. α and B^{*} are plotted in figure 37.

The question arises whether the spread in the values of α represents a real effect or is simply a result of measurement errors. The errors in $\dot{e}_{\overline{x}\overline{y}}$ and $\dot{\epsilon}$ at a given depth are not independent. In addition the errors in either of these quantities at different depths are not independent because of the smoothing operation which was applied to the data from which they are derived. Thus the estimation of the accuracy of α is not straightforward. If the shear stress is accurately linear with depth, the slope of the log η vs. log $\dot{\epsilon}$ curve can be written explicitly as

$$\alpha = -\frac{d \log \eta}{d \log \dot{\epsilon}} = -\left(\frac{1}{\dot{e}_{\overline{x}\overline{y}}}\frac{\partial \dot{e}_{\overline{x}\overline{y}}}{\partial \overline{y}} \Big/ \frac{1}{\dot{\epsilon}}\frac{\partial \dot{\epsilon}}{\partial \overline{y}}\right)\left(\frac{\dot{e}_{\overline{x}\overline{y}}}{\overline{y}-\overline{y}_{s}} \Big/ \frac{\partial \dot{e}_{\overline{x}\overline{y}}}{\partial \overline{y}} - 1\right) \quad (17)$$

Since in the deeper parts of the boreholes, where the log η vs. log $\dot{\epsilon}$ plots are approximately linear, the shear strain rate $\dot{e}_{\overline{x}\overline{y}}$ is the largest contribution to $\dot{\epsilon}$ (fig. 28), the ratio $\frac{1}{\dot{e}_{\overline{x}\overline{y}}}\frac{\partial \dot{e}_{\overline{x}\overline{y}}}{\partial \overline{y}} \Big/ \frac{1}{\dot{\epsilon}}\frac{\partial \dot{\epsilon}}{\partial y}$ is approximately one; thus

$$\frac{\delta\alpha}{1-\alpha} = \frac{1}{\dot{e}_{\bar{x}\bar{y}}} \frac{\partial \dot{e}_{\bar{x}\bar{y}}}{\partial \bar{y}} \delta\left(\dot{e}_{\bar{x}\bar{y}} / \frac{\partial \dot{e}_{\bar{x}\bar{y}}}{\partial \bar{y}}\right) = \kappa \qquad (18)$$

This corresponds to a relative error in the power law exponent $n = \frac{1}{1-\alpha}$ of κ. By using the estimates of standard error for the smoothed values of $\dot{e}_{\bar{x}\bar{y}}$ ($0.003\ yr^{-1}$) and $\partial \dot{e}_{\bar{x}\bar{y}}/\partial \bar{y}$ ($0.0002\ yr^{-1}m^{-1}$), which amount to respective errors of about 10% and 40% at the depths under consideration, and by assuming these errors to be independent, a value of 0.41 is calculated for κ. This gives a relative error in n of 41%. Such an estimate applies to the slope ($-\alpha$) at a single point on the curve. In those boreholes (e.g. 2B) where the depth range corresponding to the linear segment of the curve is short compared to the length of the average used in the smoothing of the data (100 m), the estimate directly applies. If the linear segment corresponds to depth ranges approaching 100 m (e.g. boreholes 3A, 3B), then equation (18) with $\kappa = 0.4$ overestimates the standard error. By using the standard error in the average of $\partial \dot{e}_{\bar{x}\bar{y}}/\partial \bar{y}$ over a 100 m depth interval, which is estimated to be $\sqrt{2}\ \sigma_{\dot{e}_{\bar{x}\bar{y}}}/100$ and which corresponds to a 10% relative error, a factor κ of 0.14 in equation (18) or a 14% error in n is calculated to be more appropriate in these cases.

Although the observational uncertainty is large, the spread in the slopes ($-\alpha$) of the linear parts of the log η vs. log $\dot{\epsilon}$ curves for the different boreholes is too great to be attributed entirely to measurement errors.

If linearity of shear stress and a shape factor of 1/2 are

applicable, the accuracy of B^* is determined mainly by the accuracy to which surface slope is known. Surface slope is known to within 5%. Thus the scatter in B^*, which is about $\pm 5\%$, is not significant. Because of the large errors in α there is, however, considerable uncertainty in B (up to 30%).

The values of the parameters α and B, as given by a straight line fit by eye to the general trend of all of the boreholes, are 0.81 and 0.85 bar $yr^{1+\alpha}$ respectively. The accuracy of these determinations can be estimated by considering the scatter in the values computed from the individual boreholes. Use of the standard formula for the standard error of the mean gives approximate standard errors for α and A of 0.05 and 0.17 bar $yr^{1+\alpha}$ respectively.

Method of minimization of residual body forces

The above analysis, based on a linear depth-dependence of shear stress, only approximately takes into account the distribution of u over the cross section, and completely neglects the x dependence of the strain-rate field. The u contours show a systematic pattern that differs slightly but definitely from the concentric semicircular pattern for which the shear stress would be exactly a linear function of y. Also, the actual strain-rate field is x dependent. In order to include these features in the analysis for rheological parameters, and hopefully to clarify some of the anomalies arising in the linear shear-stress treatment, the technique of minimizing residual body forces is used.

Of the three equilibrium equations (6) the x-equilibrium equation can be considered of dominant importance. The longitudinal flow occurs in direct response to a body force, whereas the flow normal to the main component of flow represents relatively small adjustments imposed by the longitudinal flow. Thus consideration of the x-equilibrium equation provides the basic information for the evaluation of viscosity. The remaining two equilibrium equations provide information on the distribution of p', which allows evaluation of $\partial p'/\partial x$, and can be viewed as providing a correction to the distribution of viscosity calculated from x-equilibrium under an assumed distribution of p'. Because of the indirect way in which v is evaluated from the borehole data, and because of the distribution of w in the cross section (fig. 21) evaluation of $\nabla^2 v$ and $\nabla^2 w$ is very imprecise. For this reason the second and third equilibrium equations have not been considered in the analysis. This eliminates the possibility of relating the mean stress directly to the data and requires assumptions concerning this quantity to be made.

Boundary conditions (7a) are exactly satisfied as long as η at the surface is finite, and thus they do not provide additional information in the minimization of the residuals. They need not be considered.

Note that with the above considerations only equations (12a) (x equilibrium) and (12f) (normal boundary condition) are included in the set of conditional equations to be analyzed. $\mu_x = 2[\dot{e}_{xx} \frac{\partial \dot{\epsilon}^2}{\partial x} +$

$e_{xy} \frac{\partial \dot{\epsilon}^2}{\partial y} + e_{xz} \frac{\partial \dot{\epsilon}^2}{\partial z}]$ and $\kappa_x = \nabla^2 u$ were calculated along the boreholes at 5 m intervals.

The x and z gradients in $\dot{\epsilon}^2$ at a given depth were calculated using first and second differences in the computed values of $\dot{\epsilon}^2$ at the borehole sites at that depth. By adopting the notation $(M,N) = [\dot{\epsilon}^2)_M - \dot{\epsilon}^2)_N]/150$ and defining the differences

$$K_1 = (1B,1A)\ ,\quad K_2 = (2B,1B)\ ,\quad K_3 = (2A,1A)\ ,$$
$$K_4 = (2B,2A)\ ,\quad K_5 = (1B,3B)\ ,\quad K_6 = (1A,3A)\ ,$$
$$K_7 = (3B,3A)\ ,\quad K_8 = (3A,5A)\ ,\quad K_9 = (1A,1C)\ ,$$
$$K_{10} = (4A,2A)\ ,$$

the explicit formulae used for evaluation of the gradients can be expressed as follows:

	$\frac{\partial \dot{\epsilon}^2}{\partial x}$	$\frac{\partial \dot{\epsilon}^2}{\partial z}$
1A	$(K_1 + K_9)/2$	$(K_3 + K_6)/2$
1B	$(3K_1 - K_9)/2$	$(K_2 + K_5)/2$
1C	$(3K_9 - K_1)/2$	$(K_3 + K_6)/2$
2A	$(K_4 + K_9)/2$	$(K_{10} + K_3)/2$
2B	$(3K_4 - K_9)/2$	$(3K_2 - K_5)/2$
3A	$(K_7 + K_9)/2$	$(K_6 + K_8)/2$
3B	$(3K_7 - K_9)/2$	$(3K_5 - K_2)/2$
4A	0	$(3K_{10} - K_3)/2$
5A	0	$(3K_8 - K_6)/2$

$\partial \dot{\epsilon}^2/\partial x$ is set zero at boreholes 4A and 5A, where it cannot be

directly evaluated. $\partial^2 u/\partial x^2$ and $\partial^2 u/\partial z^2$ were computed from the interpolating functions on differential longitudinal velocity, u_d, which were used in the iterative calculation of the velocity field discussed in Chapter V-A, and values at the surface given by the surface measurements.

The x and z gradients of $\dot{\epsilon}^2$ and the curvatures $\partial^2 u/\partial x^2$ and $\partial^2 u/\partial z^2$ are subject to uncertainty as a result of possible interpolation errors similar to those which were considered in the evaluation of the x and z velocity gradients (Chapter V-C). Since, in this case, second derivatives are involved, the uncertainty from this source is even greater. This is particularly true for $\partial^2 u_d/\partial x^2$ at all boreholes except in borehole 1A above 200 m. The interpolating function for u_d contains the implicit assumption that $\partial u_d/\partial x$ is independent of x and z as determined by an appropriate difference between u_d in holes 1B, 1A, and 1C. Below the bottom of hole 1C (200 m) extrapolation is involved. Interpolation errors can also enter strongly in the evaluation of $\partial^2 u_d/\partial z^2$ at borehole 2A below 100 m and boreholes 3B, 2B, and 5A, because these holes lie on the lateral margins of the array.

The y gradient in $\dot{\epsilon}^2$ was calculated from the first difference of $\dot{\epsilon}^2$ between depths spaced 5 m apart. $\partial^2 u/\partial y^2$ at depth y was computed from the second difference in u using the point at depth y and points 5 m above and below.

In the calculations the surface slope averaged over one borehole depth is used to evaluate $\partial y_s/\partial x$.

In choosing a possible model for p' two facts are to be noted.

First is that the surface strain rates are relatively independent of x (x gradients in the surface strain rates are less than 0.2×10^{-4} m^{-1} yr^{-1} in the area spanned by the borehole array, as compared to the typical values of 0.5×10^{-3} m^{-1} yr^{-1} of $\partial \dot{e}_{xy}/\partial y$ in the deeper parts of the boreholes.) In view of the normal stress boundary condition, this indicates that p' is to a first approximation independent of x at the surface. (If the flow law derived from all of the borehole data and a linear shear stress depth distribution applies at the glacier surface, then $\partial p/\partial x$ is less than 10% of the acting body force ρg_x.) Second is that since the y-equilibrium equation is not considered, the depth variation of p' cannot be directly related to the data. For these reasons it is assumed that p' is independent of position. By making this assumption, the effects of the longitudinal gradients in mean stress on the flow are neglected. The longitudinal forces associated with the gradient in τ'_{xx} are still included, however.

The minimization of residuals can be carried out over any set of points chosen from the points spaced at 5 m intervals along the boreholes, where K_x and C_x were calculated. Results for the parameters α and B of a power law derived from the following sets of points are tabulated in table 17: (1) the complete depth range of single boreholes, (2) all boreholes taken together over the complete depth range, (3) the depth range which corresponds to the linear portions of figures 36 of single boreholes, and (4) all such depth ranges considered together. Single borehole analyses were not carried out for boreholes 1C and 4A, because of their relatively

small depths and small ranges in $\dot{\epsilon}$. The root-mean-square residual body forces are also tabulated in units of the body force acting parallel to the local surface slope. Values of this quantity are typically between 0.3 and 0.4 times the acting body force, except in the case of the analysis of the restricted depth ranges of single boreholes, in which case it can be considerably smaller. With the viscosity distributions implied by the above flow laws, the root-mean-square residual forces, which would occur as a result of measurement errors, are estimated to be 15 to 20%. This estimate does not include the effect of interpolation errors, which cannot be quantitatively evaluated.

Errors for the calculated parameters can be estimated by a standard procedure for least squares analysis. The errors thus estimated ($0.02 \leq \sigma_\alpha \leq 0.11$, and $0.05 \leq \sigma_B \leq 0.36$) cannot, however, be interpreted to be standard errors because they were calculated from the smoothed tilt profiles and thus must underestimate the standard error. The accuracy of the parameters is more likely to be similar to that implied by the larger standard errors estimated for the corresponding results obtained in the linear shear stress analysis, since the results of both methods are constrained by the same data.

As is the case with the results based on the linear depth-variation of shear stress, the flow law parameters derived from different boreholes show a considerable range, with boreholes 3B and 2B lying at one end of the range (large α, small B) and boreholes 1B and 2A at the other (small α, large B).

Depth dependence of shear stress

The near surface behavior of the log η vs. log $\dot{\epsilon}$ curves (fig. 36) has two possible explanations. First is that the shear stress deviates from a linear depth dependence. Second is that a flow law given by equation (2) does not apply because the material is not homogeneous or the effective viscosity is not determined only by the second strain rate invariant. In order to distinguish between these possibilities the residual body force fields for the pertinent distributions of viscosity are shown in figure 38.

The dotted curves of figure 38 give the distribution of residual body force versus depth at each of the boreholes calculated by using equation (6) with p' constant and the viscosity distribution given by equations (15) with $\bar{x}$ parallel to the local surface slope. The residuals thus calculated attain values much larger than the actual acting body force as the surface is approached. This is a result of the very large near-surface viscosities and the attendant viscosity gradients which result from application of equation (15). The residuals tend to become negative near the surface, because the viscosities predicted by equations (15) are much greater for section B than for section A at equivalent depths, so that $\partial\eta/\partial x$ is large and positive and the contributions to equilibrium of $\partial\tau'_{xx}/\partial x = 2\frac{\partial}{\partial x}\eta e_{xx}$ are consistently negative. The contribution from $\partial\tau_{xz}/\partial z = 2\frac{\partial}{\partial z}\eta e_{xz}$ can be positive or negative depending on the relationship of η in adjacent holes in the same section. The greater viscosity at equivalent depth in hole 1B as compared to hole 2B causes this contribution to be positive at 2B. With this viscosity distribution $\partial\tau_{xy}/\partial y = 2\frac{\partial}{\partial y}\eta e_{xy}$ is $\frac{1}{2}\rho g_x$

and does not contribute to the excessively large residuals.

The distribution of residuals indicates that the viscosity derived from equation (15) does not give a reasonable representation of the existing viscosity distribution near the surface. Thus the sharp rise of the curves (fig. 36) cannot be caused completely by a real increase in viscosity near the surface, but must indicate that the shear stress deviates to some extent from a linear depth dependence. There is no compelling reason to conclude that rheological inhomogeneity exists or that a flow law of form given by equation (2) is inapplicable. The depth distribution of shear strain rate near the surface, of which the sharp upturn in the $\log \eta$ vs. $\log \dot{\epsilon}$ plots is a manifestation, is caused by a shear stress $|\tau_{xy}|$ which increases with depth less rapidly than predicted by equation (15). The acting body force then must be equilibrated by the other stress gradients $\partial\tau_{xx}/\partial x$, $\partial\tau_{xz}/\partial z$, or $\partial p/\partial x$.

The dashed and the solid curves in figure 38 give the depth distribution of residual body force at each borehole calculated from equation (11) with p' constant by using respectively the flow law determined from the linear part of the $\log \eta$ vs. $\log \epsilon$ curve for that borehole (fig. 36) and the flow law derived by the minimization of residual body forces over the complete depth of that borehole. In either case the boreholes for which there is definite evidence for a strong upturn in the $\log \eta$ vs. $\log \epsilon$ plot (1A, 1B, 2B, 3B, 5A) have distributions of residual body force showing a strong decrease with depth. The negative gradient terminates at a depth corresponding roughly to the depth that marks the onset of the anomalous near-

surface behavior. In order that the small gradient in τ_{xy}, which is given by the concave distribution of $\dot{e}_{xy}$ and the nearly constant value of $\dot{\epsilon}$, be equilibrated, it is necessary that the other stress gradients entering in the x-equilibrium equation have appropriate depth dependences to compensate for the changing value of $\partial\tau_{xy}/\partial y$. The gradient in the residuals indicates that this is not the case for $\partial\tau'_{xx}/\partial x$ and $\partial\tau_{xz}/\partial z$. Thus there is no evident cause for the non-linearity of the depth distribution of τ_{xy}, which seems to be required by the observed depth distribution of shear strain rate.

The calculations of the residual force field do not take into account any longitudinal gradient in the mean stress. (It was assumed $\partial p/\partial x = 0$.) It is thus possible that the non-linear depth dependence in τ_{xy} is caused by a depth-dependent longitudinal gradient in mean stress that cannot be ascertained with the existing data. The longitudinal gradient in mean stress can, however, be calculated at the surface through equation (7b). It is possible at least to test whether such gradients reduce the residual forces at the surface. If a power law with α and B equal to any of the sets of parameters listed in tables 16 and 17 applies uniformly at the surface, then the mean stress gradients are less than 10% of ρg_x. The mean stress is more compressive down glacier, which gives a gradient of the proper sign to reduce the residual forces, but the size of the gradients is too small to reduce the residuals to a level compatible with equilibrium. (At the surface the strain rates and their gradients are known to an accuracy sufficient to determine the residual forces to within 0.2 in

body force units.) Thus it seems unlikely that a depth dependent gradient in mean stress, calculated on the basis of homogeneous power-law properties, can account for the residuals at depth.

A possible, though highly speculative, solution to this apparent dilemma is that near the surface the effective viscosity corresponding to equivalent $\dot{\epsilon}$ is higher at section B than at section A as if the ice were longitudinally inhomogeneous. At the surface this would give more negative values for the contributions of $\partial\tau'_{xx}/\partial x$ and $\partial p/\partial x$ to equilibrium and reduce the positive residuals. Since $|\dot{e}_{xx}|$ decreases with depth, $\partial\tau'_{xx}/\partial x$ would become more positive with depth and would contribute to eliminating the negative gradient in the residual forces. A power law with a value of the parameter B 20% greater at section B than at section A and equivalent values of α at both sections would give contributions from $\partial\tau'_{xx}/\partial x$ and $\partial p/\partial x$ large enough to eliminate the residual forces at the surface.

A clear instance of deviation of shear stress from linear dependence occurs in the lowermost 40 m of borehole 2A (fig. 13d). This demonstrates graphically the effect that local differences in the properties of the glacier bed can have on the flow, and is particularly significant with respect to the present discussion. Since flow law parameters are determined to a large extent by deformation in the lowermost parts of boreholes, where strain rates are high and show significant variation, the effects of such fluctuations in bed properties can strongly influence the results of an analysis for rheological parameters.

Comparison of the two methods

In figure 38 the displacement of the solid curves from the dashed curves toward the axis of zero residual body force shows that the degree of disequilibrium corresponding to the least-squares flow law is less than for the flow law derived from the linear shear-stress treatment. A displacement independent of depth indicates an adjustment of parameter B resulting from depth-independent contributions from $\partial\tau_{xz}/\partial z$ in addition to that included in equation (15), and from $\partial\tau'_{xx}/\partial x$. Such contributions do not imply any deviation of τ_{xy} from linear dependence, but only a change in the proportionality factor. A systematic difference in the gradients of the two curves indicates that changing the parameters results in a depth-dependent redistribution of stress. A change in the flow-law parameter α is thus involved. The adjustment of the parametrs can be seen by comparison of tables 16 and 17.

For explicit comparison, the results of the linear shear stress treatments and the least square analyses, which were restricted to the depth ranges corresponding to the linear portions of the $\log \eta$ vs. $\log \dot{\epsilon}$ curves (fig. 36), are plotted in figure 37. These comparisons are more meaningful than comparisons made with the least squares analyses applied to the complete depth of boreholes, because the possible effects of different weighting of the different depth ranges of the boreholes do not enter. The differences between the results of the two methods show that the effects of the deviation of the velocity contours from a concentric semi-

circular pattern and the observed x dependence of the strain-rate field have a significant influence in the calculation of flow law parameters.

If the point for hole 2B, which was calculated from a particularly short depth interval (20 m) and small range in $\dot{\epsilon}$ (0.029 to 0.032 yr^{-1}) and which is therefore subject to considerable uncertainty, is neglected, the range in α for the least squares analyses (0.61 to 0.83) is significantly less than for the linear shear stress analyses (0.56 to 0.98). Thus it seems reasonable that the spread in α, as determined on the basis of linear shear stress, is caused by a deviation from such linearity, and that the least squares procedure is successful in correcting for such deviations. The remaining spread in α can be attributed to the uncertainty in the measurements and calculation of gradients. The range in $B^* = B(\dot{\epsilon}_o)^{-\alpha}$ from the least squares treatment (6.0 to 15.2 bar) is increased with respect to the range for the linear shear stress results (9.0 to 10.0 bar). The greater range in B^* is caused to some extent by the fact that the comparison is made at $\dot{\epsilon}_o = 0.05\ yr^{-1}$ which was chosen specifically to minimize the spread in B^* as given by the linear shear stress results. Nevertheless the spread in B^* from the two methods cannot be equalized by reasonable adjustment of $\dot{\epsilon}_o$. The spread in B^* probably comes from failure of the explicit assumption that the longitudinal gradient of mean stress is zero, and the implicit assumptions involved in the calculation of the strain-rate components and their gradients by a specific interpolation procedure.

Results

For the purpose of defining a "best" flow law on the basis of the Athabasca borehole data, the results derived from combined analysis of all of the boreholes can be considered to be most significant. If the spread in the results for individual boreholes is caused by the limitations of the accuracy and extent of the data, then it could be expected that such influences would tend to cancel in the combined analysis including all of the boreholes. If the spread represents existing inhomogeneity in the ice, then the combined analysis defines a flow law describing, in some sense, the average properties of the ice.

The results for the power law parameters B and α, which were calculated from the general trend defined by figure 36, the least-squares analysis applied to the complete depth of all of the boreholes, and the least-squares analysis restricted to the lower parts of the boreholes, are plotted in figure 39 as points a, b, and c respectively. For comparison several other sets of parameters, as determined by laboratory experiments and field data of other investigators, are also plotted. Included are the flow laws determined experimentally by Glen (1955) for polycrystalline ice at $-0.02^{\circ}C$ (points 1 and 2), the experimental results of Butkovich and Landauer (1958) as extrapolated to $0^{\circ}C$ by Paterson and Savage (1963b) (point 3), the results from the analysis of the closure of several tunnels by Nye (1953) (point 4), and a result from recent borehole measurements on the Blue Glacier (Kamb and Shreve, unpublished) (point 5).

The result based on the linear shear-stress analysis and the Blue Glacier result, which was calculated by a similar method, are in very close agreement. The agreement between the present results and those determined on the Blue Glacier is particularly significant because of the difference between the deformation rates in the two field studies. The present results represent strain rate $\dot{\epsilon}$ between 0.02 and 0.10 yr^{-1}; the Blue Glacier determination was based on measured strain rates between 0.1 and 0.6 yr^{-1}. The identical values of $\alpha = 0.81$ ($n = 5.3$) for the two experiments are slightly larger than the value of $\alpha = 0.76$ ($n = 4.2$) which represents the largest of the values obtained by laboratory measurements.

The least-squares analyses give values of α which fall in the range spanned by the experimental values reported here. The values of B are, however, displaced relative to the experimental values in a sense which corresponds to relatively higher viscosity. Presumably the least-squares analysis (points b and c) should be more reliable than the point based on the assumption of a linear shear stress variation (point a), since, in so far as is possible, account is taken of the stress gradients $\partial\tau'_{xx}/\partial x$ and $\partial\tau_{xz}/\partial z$.

CHAPTER VIII

CONCLUSIONS AND RECOMMENDATIONS

The results of this field study call into question a number of concepts concerning glacier flow. The calculations of Nye (1965), which are the most comprehensive and rigorous to date, fail to a significant degree to predict the distribution of longitudinal velocity observed on the Athabasca Glacier (Chapter VI-A).

The failure was shown to be caused in large measure by the difference in the boundary conditions as assumed in the theoretical analysis and as actually exists in the cross section under observation. This demonstrates the importance of the boundary condition applied to the bed in theoretical predictive calculations such as Nye's (1965), and the need for greater understanding of the phenomenon of glacier sliding. The observed contrast between basal sliding in the central portion of the channel and marginal sliding is of significance in hydrological applications of glacier flow theory and provides information about the sliding process. The generality of such a contrast should be directly examined further by making marginal sliding measurements in conjunction with borehole experiments which determine basal slip velocity. The hypothesis that such an effect results from a lateral variation in basal water pressure needs to be tested directly by monitoring of water pressure in boreholes and measurements of the distribution of bed roughness across glacier channels.

The observed distribution of velocity also differs from the theory of Nye (1965) in a manner which is not accountable in terms

of the boundary condition used in the calculation. Nye (1965) made his calculations under the assumption that the flow field is rectilinear and has no longitudinal dependence, and that the material is homogeneous. Both of the conditions of the flow field are violated to some extent in the cross section of the Athabasca Glacier (Chapter VI-C and D). It is also possible that the material is not rheologically homogeneous. The specific source of the disparity between the observations and theory remains unidentified, and is a question which needs further consideration.

A two-dimensional calculation similar to Nye's (1965), but allowing a more general non-rectilinear velocity field with x-independent strain-rate components (Appendix III) and carried out with a more realistic boundary condition, would be an important extension of Nye's work. Such a calculation could be of use in isolating any effects of the longitudinal dependence of the strain rate or rheological inhomogeneity of the ice from effects caused by the non-rectilinear nature of the flow.

The distribution of $\dot{e}_{xx}$ in the cross section (Chapter VI-C) indicates that the strain-rate field is not longitudinally independent. The importance of longitudinal stress gradients, where significant gradients in surface and bed slope exist, has been recognized (Robin, 1967). The distribution of longitudinal strain rate observed here and the implied longitudinal gradients in the strain-rate and stress fields may indicate that longitudinal stress gradients play a role in glacier flow in the ablation region of valley glaciers even when the surface and bed slopes are relatively uniform.

It has long been recognized (Nye, 1951, 1957) that longitudinal compression is a response to ablation through which a glacier maintains its thickness. Lateral flow, as observed in the Athabasca Glacier cross section (Chapter VI-D), is an essential feature of this response which has been largely overlooked. Lateral flow velocities of the same order of magnitude as the normal velocity at the glacier surface, and lateral extension ($\dot{e}_{zz}$) in the central portion of the glacier of the same order of magnitude as the longitudinal compression rate ($-\dot{e}_{xx}$) can in general be expected. The convex transverse surface profiles typical of the ablation region of valley glaciers exist in order to supply the driving stresses for the required transverse flow.

The observed decrease in longitudinal compression rate ($-\dot{e}_{xx}$) with depth and the existence of transverse extension ($\dot{e}_{zz}$) at the centerline are particularly significant in that they cast doubt on the applicability of the theory of Nye (1957), which requires that $\dot{e}_{xx}$ is independent of depth and that $\dot{e}_{zz}$ is zero.

All previous analyses of borehole deformation have been made under the assumption that shear stress parallel to the surface is linear with depth. The present data indicate that significant variation of the shear stress from linear depth dependence exists (Chapter VII-C), although the specific cause of such a deviation has not been identified.

A challenge for further study is to understand the mechanism of stress redistribution, which is responsible for the anomalously

slow increase in the magnitude of shear strain rate with depth near the surface. The slower increase in shear strain rate with depth at section B as compared to section A, the smaller width ratio of velocity of contours at section B as compared to section A, and the marked decrease of longitudinal compression rate with depth are interrelated features of the flow field which need explanation and probably provide clues to the specific mechanism of stress redistribution.

The new methods of analysis (Chapter VII-B) are valuable tools in the analysis of glacier flow, since they require only general assumptions concerning the rheology of ice and no assumptions about the distributions of stress. The full potential of these methods could not be realized even with the extensive measurements of the present project, largely because of the uncertainty in determining gradients of flow quantities by interpolation between boreholes. Spacing of the boreholes closer than $\frac{1}{2}$ of the glacier depth and a more extensive borehole array would provide significant improvement. The efficiency of the present techniques of boring and inclinometry (Chapter III-B) and the reliability of borehole recovery achievable by use of aircraft cables as borehole markers (Appendix I-B), now make such extensive and detailed measurements possible. The method developed for the interpretation of tilt data from borehole arrays in terms of velocity and strain-rate components (Chapter V-A) provides a framework within which data from borehole arrays more extensive than the present one can be reduced to give the flow quantities needed for the new methods of rheological analysis.

For gaining further understanding of the distribution of stress and velocity in glaciers, the experience of this research emphasizes the importance of concentrated and detailed deformation measurements, giving complete strain-rate information, as opposed to scattered glacier-wide measurements.

APPENDIX I

DESCRIPTION AND EVALUATION OF EQUIPMENT AND PROCEDURES

A. Equipment and Field Procedures

Thermal drills

The two types of thermal drills ("hotpoints") used, a standard boring hotpoint for making the original holes and a cable-following hotpoint for borehole recovery, were both designed by R. Shreve. These hotpoints were found to be highly reliable. Both types are of similar construction. Flat resistance wire of total resistance 19.6 ohms is wound around a cylindrical copper core, one end of which forms the nose or melting surface of the hotpoint. The standard boring hotpoint has almost perfect cylindrical symmetry. The cable-following model has a 1/8" hole through a lip projecting from the hotpoint nose. The cable to be followed is threaded through this hole.

The hotpoints are designed for a maximum amperage of 11 amps when the instrument is in ice water. Actual operating amperage on the Athabasca glacier operation was typically between 9 and 10 amps. At this amperage, a hole 6 to 7 cm in diameter is produced with a penetration rate of 6 to 7 m/hour. The standard boring hotpoint was used on the end of a seven-foot section of standard 1 1/4" galvanized steel pipe which provided weight to improve efficiency and served as a guide to keep the initial borehole straight. The cable-following hotpoint was mounted on a brass tube three feet in overall length. The tube was in three sections, so that sections could be

removed in order to make a shorter assembly in the event that sharp corners in the deformed borehole were encountered.

Power cables

For most of the boring operations, electrical cable with four stranded copper conductors (18 AWG) was used. Two conductors were used in parallel, giving a circuit resistance of 6.5 ohms per 1000'. Electrical connection to the hotpoint was made with banana-type plugs. 100 per cent reliability is obtained without the difficult problem of providing for water-tightness, which is required when single-unit plugs, such as Cannon connectors, are used. Four-conductor Cannon plugs potted with silicon rubber were used for all connections at the surface.

The power cable also served as the mechanical link between the hotpoint and the surface. The cable strength of 150 lbs. is considered marginal for this purpose. The considerable advantage of having only one cable down the hole, however, was found to outweigh the risk involved. To make mechanical connection of the cable to the hotpoint, the cable was bound back on itself to form a loop. The loop was reinforced with a cable thimble and secured to a sleeve on the top of the hotpoint assembly by passing a bar through it.

Power cables of various lengths (300', 500', 950', 1000') were employed. The shortest cable appropriate to boring at a given depth was used whenever possible in order to reduce line loss and thus make maximum use of available power. Provision was also made for joining two cables. Electrical and mechanical connections were

accomplished in a manner similar to that for connecting to the hotpoint.

The four-conductor cables just discussed were found to have a tendency to twist when under tension. This could be expected from the manner of their construction, in which the four conductors are gently twisted into helices around one another. This tendency is particularly strong in new cables. This effect is of no consequence in the initial boring of holes, but in the process of cable following, it causes a great danger of irretrievably tangling the power cable around the aircraft cable being followed. In 1967 this caused a great deal of loss in field time, and contributed to the loss of a hotpoint and the lower 100 meters of hole 1C. In 1968, two-conductor shielded coaxial cable was tried. This cable has a cylindrically symmetric construction, with a single center conductor insulated from a double braided outer shield, which provides the second conducting path. A thin polyvinyl chloride sheath is laid over the braided shield and forms an insulating outer cover. Experience with this cable on the Athabasca glacier indicates that this type of cable greatly reduced the problem of cable tangling. In addition, for applications where only two conductors are required, this type of construction is very efficient in that an equivalent line resistance can be obtained with a cable smaller in diameter and lighter in weight.

Power supply

Electrical power was supplied by two 3000 watt portable generators. At the altitude of the Athabasca field site, the maximum

output of the generators was actually between 2300 and 2400 watts.

Power supply to the hotpoint was controlled by a SCR control circuit based on the time constant of an RC circuit with variable resistance. This control system was designed by J. Westphal. Each control unit contained a 250-volt a.c. voltmeter and a 10-amp RF ammeter for direct monitoring of the generator output voltage and current to the hotpoint.

The hotpoint was almost always run at full power. Sometimes circumstances arose such that for brief periods the hotpoint may not have been submerged in ice water and thus had to be run at reduced power in order to avoid a burnout. One such circumstance arose from the fact that the surface ice in this area of the Athabasca glacier is below freezing, and the holes thus tend to freeze up rapidly at the surface. The period of one night is typically sufficiently long that in the morning the hotpoint cannot be directly lowered without first enlarging the hole. If the water level has dropped, this must be done at low power.

Heater bars

The danger of trapping a hotpoint in a borehole as a result of the borehole closing near the surface during a long period of boring was also a great problem. With only the power input resulting from power cable dissipation, some difficulty in retrieving a hotpoint could be expected after only four hours. In order to avoid the inconvenience and time loss involved in raising the hotpoint every three or four hours for the purpose of enlarging the hole near the surface, heater bars

were used to provide power input in the near-surface section of the borehole. The heater bars were operated at the same time boring was proceeding at the bottom of the hole, thus allowing long periods of continuous operation. Heater bars used were commercially constructed, 2 feet long, 1 1/2" x 3/16" in cross section, with a resistance of 27 ohms. Three such bars were used in series at 115 volts, dissipating 160 watts.

Drilling stand and aircraft cable assembly

A wooden box (15 1/2" x 16" x 12") mounted on four wooden legs (2" x 2") set into the ice was centered over each borehole and served as a stand for drilling purposes and storage of aircraft cable over the winter. During the drilling operation, a spool was mounted between two of the legs of the stand in a manner such that power cable could be easily wound on and off by means of a hand crank. Cable passed from the spool over a sheave mounted on the top of the box, through a hole in the top of the box, and then down the borehole to the hotpoint. The sheave was coupled to a revolution counter. The change in depth corresponding to one revolution could be calibrated, and was approximately one meter (1.063 m).

A small drum (6" diameter, 6" long) was mounted in the interior of the wooden box to serve as storage for the aircraft cable over the winter. The end of the aircraft cable in the borehole was wound on one side of this drum. On the other side, a band of adjustable tension with both ends secured to the wooden box and passing around the drum served as a friction brake. For wintering over, all

holes in the wooden box were blocked to prevent packing of snow around the mechanism.

Cable used for marking most of the boreholes was 1/16" diameter, 7 x 7 construction stainless steel aircraft cable with a strength of 480 lbs. and an elongation at breaking of approximately 1%. In one hole (hole 2A), a cable of similar construction but 3/32" diameter was used. A steel weight was attached at the lower end of the aircraft cable. The dimensions of the weight (1 11/16" diameter, 3' long) are just slightly larger than those of the inclinometer. This weight serves two purposes. First, it carries the cable down the hole. Second, it fixes the cable at the lower end, so that the borehole can be enlarged in the event that the aircraft cable is free in the hole, but the hole is too small to allow passage of the inclinometer. This is necessary because, in order to follow the cable with a cable-following hotpoint, the aircraft cable must be kept under tension.

Inclinometers

Two types of inclinometer were used on the Athabasca glacier. Inclinometry of the initial boreholes was done with an optical-type instrument loaned by Parsons Survey Company. These instruments are proven instruments and have been used in most of the borehole experiments done to date. The instrument works by recording the positions of a pendulum bob and compass needle on a photographic disc. The main disadvantage of this method is that after each measurement the inclinometer must be raised to the surface and loaded with a new photographic disc. The time spent in loading and the

amount of winding involved in lowering into a deep hole make this method very time consuming.

In order to be able to obtain a higher density of data than would be obtainable with such optical inclinometers, a more efficient instrument was designed and built and was used in the deformed boreholes. The new type of inclinometer has an electric output and can be read remotely from the surface, so that complete logging of a hole can be accomplished with only one lowering of the instrument. The basic method employed is similar to that in the optical inclinometers. The position of a pendulum bob and compass needle are determined by the electrical output of solar cells mounted in a manner such that the area of illumination by a light source of fixed intensity changes with changing orientation. The light source is powered and controlled from the surface, and is monitored in the instrument by a separate solar cell not affected by any displacement of the pendulum or compass. The method of illumination measurement is temperature dependent, since the efficiency of the solar cells depends on temperature. Hence the instrument as designed would not be satisfactory for general applications in a temperature-changing environment, unless the temperature dependence of the standard solar cell were exactly matched to that of the other cells in the instrument. However, in the nearly isothermal environment of a water-filled borehole, the temperature dependence presents no problem. The total temperature variation over a depth of 300 meters is about 0.2°C.

Figure 6 illustrates the geometry of the instrument and the manner in which it works. Below the light source is the pendulum

unit. A square pendulum bob is suspended from four chains. Beneath the weight are four silicon solar cells mounted normal to the sides of the pendulum weight in such a manner that approximately 50% of the area of each cell is shaded from the light source at zero inclination. Cells on opposite sides of the pendulum weight are connected back to back as shown in figure 6. The output of each cell pair is then approximately zero at zero inclination, and changes as one of the cells becomes more covered and the other less covered, as the instrument is tilted. The output from cell pairs gives the components of tilt along the two perpendicular axes x and y which are fixed with respect to the instrument body. Maximum possible inclination is determined by the length of the suspension chains. Pendulums of different maximum amplitude can be interchanged in the instrument.

The compass assembly is mounted above the light. A magnet is mounted on a shaft that turns in jewel bearings. A card rigidly attached to this shaft has a spiral shaped aperature cut in it, so that the area of illumination on a solar cell above the card depends on the relative azimuthal orientation of the card and the inclinometer case. Selenium solar cells were used, because they were available in a shape suitable to this application. Two such cells are read independently.

For a complete determination of instrument orientation, five current measurements are made. With the system used, current output ranges from 0 to 10 μA. The output is read on an API tautband meter capable of 0.2% reproducibility. The forms of the output versus orientation curves are given in figure 7 for the compass and

and for the 10° pendulum used for almost all of the measurements. Because the output for a single cell registering the orientation of the compass card must be continuous and give the same value on a rotation of 360°, the output from a single cell cannot give an unambiguous result. Thus it was found necessary to have two compass readout cells, A_1 and A_2. The output of a single cell gives a pair of possible orientations. The two pairs, from the two cells, are compared, and the orientation which is common to both pairs is chosen as the correct one. It determines the azimuth of the x and y axes of the pendulum unit with respect to magnetic north. The x and y outputs of the pendulum unit can be simply combined to give tilt magnitude and direction of tilt provided that the pendulum is suspended in such a manner that the bob does not twist as it is displaced, so that the x output does not change upon tilting in the y direction and visa versa. This requires that the suspension chains be parallel and of equal length. It is rather easy to achieve this to a degree which limits difference in tilt magnitude as computed only from the x and y output as compared with the actual value to less than 1%. Twisting of the pendulum would require calibration along many directions of tilt or essentially a complete two-dimensional calibration. Such calibration was done only once, in order to verify that the effects of twisting were negligible.

Because of the five independent current measurements required for an orientation determination, a stepping relay was placed in the instrument. Activation of the relay from the surface causes successive instrument components to be connected to the output

channel. The individual measurements are thus made in sequence. With this feature, a four-conductor cable provided a sufficient number of independent conductors.

The complete inclinometer assembly was placed in a water-proof outer case sealed with O-rings. The cable used with the inclinometer contained four "copper weld" conductors (number 18AGU), and was manufactured by Vector Cable Company, originally for use in heat flow measurements. The cable was connected electrically to the instrument with a four-prong Cannon plug. This plug was also isolated from the water in the borehole by O-ring seals.

In actual operation, the instrument is calibrated before and after each use, because of the possibility of drift resulting from changes in light intensity and the efficiency of the cells. In the case of the pendulum unit, the calibrations before and after always agreed to within 1% of the maximum amplitude of the pendulum, and this value is taken as the accuracy of the tilt magnitude determination achieved in the borehole measurements. Systematic error in the tilt magnitude calibration was evaluated and eliminated by rotating the instrument 180° and recalibrating. Experience over the period of one field season and two months of cold room experiments indicates that the pendulum unit output is stable over a period of four months at the 1% level. In the case of the compass unit, an error of ±20° in azimuth was possible because of friction in the compass bearings. For the third summer's field work, the instrument was modified by attaching a vibrator to the case, near the compass shaft. The vibrator (an eccentric cam powered by an electric motor) was activated during

the operation of the relay switch. This greatly improved the operation of the compass system.

B. Experiences in Borehole Recovery

The experiences with the method of using aircraft cables as markers for borehole recovery provide some useful information concerning the reliability of the method and possible modifications.

For most of the boreholes, a one-year interval produced an average elongation of about 1% and maximum local elongations of about 2%. Thus some sliding of the cable through the ice was necessary in order to avoid breakage. This can occur by a regelation mechanism in ice at the pressure melting point. Presumably in ice which is significantly below the pressure melting point, such slippage could not occur. Thus recognition of a surface layer of ice definitely below the pressure melting point presented a clear danger to the success of this technique.

No cables broke over the 1966-67 winter. But all cables were under considerable tension after wintering over, as shown by the fact that additional cable was pulled into the holes as the holes were redrilled (fig. 5). The curves of figure 5 represent the combined effect of (1) the release of strain in the part of the cable which is being freed from the ice as the cable-following hotpoint penetrates, and (2) release of strain in that part not yet freed, but nevertheless undergoing relaxation because of the changing tension boundary condition at its upper end as the hotpoint penetrates.

For all of the cables, the total elongation of the cables is definitely less than the borehole elongation, by 2.1 m on the average. This indicates that either, in spite of the cold surface ice, cable was pulled in from the surface, or the weights at the bottom of the holes were pulled up the holes before they became securely gripped by the ice. That the first is possible is suggested by the fact that the local borehole elongation of about 2%, typical of the tops of all the boreholes, would have broken all the cables if some readjustment had not taken place in the surface ice. The second is possible since in two boreholes (3B, 4A), after a one-year period, the weights were still free. Although this was not the case with any other boreholes, it indicates the possibility that the weights in the other holes could have remained free for at least part of the year. In addition, the weights were encountered in reboring in 1967 on the average 1.8 m higher than would have been expected from a consideration of ice surface elevations and the strain rates. This indicates that nearly all of the accommodation was accomplished by lifting of the weights up the hole, rather than by pulling cable in from the surface.

The typical experience in recovering a borehole is that for the first several meters, no cable is pulled into the hole. After boring to between 5 and 15 m, cable starts to be pulled in very rapidly, with as much as 1.2 m being pulled in in 5 m of further boring. After this episode of rapid pulling in, the rate becomes greatly reduced, to about 0.2 m per 100 m bored. This slow rate persists typically until 80 m depth. Thereafter a rather steady rate of approximately 0.5 m per 100 m bored persists. These features are illustrated in figure 5.

The apparently relaxed state of the aircraft cable, which was always observed very close to the surface, is believed to result from local melting around the cable as a result of absorbtion of radiation penetrating the ice. The extremely rapid rate at which cable is pulled in as the hotpoint penetrates below the cold surface layer cannot be attributed to local relief of elongation in the cable. The total amount of cable pulled in during the near-surface episode (about 1 m) and the breaking elongation (1%) indicate that essentially instantaneous relaxation is occurring over a length of at least 100 m. This demonstrates the large contrast in the facility of the cable to creep through the cold surface ice and the more temperate ice beneath. For all the boreholes showing an initial phase of rapid cable pull-in, the average elongation remaining in the aircraft cable after completion of the episode was roughly the same value of about 0.3 to 0.4%. This would seem to indicate that in temperate ice of a thickness of 300 m elongations greater than 0.4% would not be expected even at the very highest strain rates observed in glacial flow as long as the cable is free to be pulled in from the surface. Since 0.4% is safely below the breaking elongation of 1%, the 1/16" diameter cable used should be adequate in situations where the ice is at the pressure melting point throughout.

Although no cables were broken over the winter 1966-67, average elongation of the cables up to 0.8% had accumulated, indicating that the system was operating with very little margin of safety. The 3/32" diameter cable which was placed in hole 2A showed a behavior considerably different from that of the 1/16" cables (see

fig. 5). The absence of an initial phase of rapid pull-in may indicate that because of its greater tension under an equivalent strain, this cable was able to pull through the surface ice. Thus using a heavier cable may be one way in which the problem created by cold surface ice could be attacked.

Over the winter of 1967-68, four of seven cables left for later recovery were broken by ice deformation. The tops of the cables were left coiled on the ice surface. They were not set up in the manner which they had been the previous winter, because it was desired to leave no equipment on the glacier surface. Also it was felt at the time this decision was made, in the summer of 1967, that cable had not been pulled in from the surface during the 1966-67 winter. Conditions at the lower end of the cables were also different for the two winters. For the winter of 1966-67, the weights were initially free. However, in the summer of 1967, most of the weights could not be melted free, so that for the entire period between recovery in 1967 and 1968, the weights acted to fix the lower end of the cables with respect to the ice. These differences in end conditions are no doubt the cause of the large percentage of cable breakages over the winter of 1967-68.

The two boreholes successfully recovered (2A, 3B) showed average elongations very close to 1% and apparently just barely survived. Both of these holes are unusual in that hole 3B had a weight which was successfully freed in 1967, and hole 2A was the hole which had the stronger cable. In the case of hole 2A, however, it is known from a mark made in 1967 that no significant amount of cable was pulled in from the surface over the winter. It is thus

believed that the survival of this cable is not a result of its greater strength, but is more likely related to the value of the average strain rate parallel to the hole, which is smaller in this hole than in holes where cables were broken. This is probably also the case for the cable in borehole 5A. (Although the cable for borehole 5A was not broken, it was not successfully recovered because a frayed spot on the cable prevented lowering of the cable-following hotpoint.)

All of the cables which failed were broken within 7 m of the surface, which is no doubt the result of the combined effects of the firm gripping of the cable by the cold ice and the high local strain rate producing a 2% elongation of the borehole. Although little cable was pulled into the boreholes during the winter of 1966-67, it is possible that the proximity of a free end of the cable at the surface was the major factor which allowed the minor near-surface adjustments necessary to prevent breakage in the cold surface layer to take place. Whether or not having fixed the cables so they could have been easily pulled in from the surface would have been sufficient to prevent the breakages which occurred over the 1967-68 winter cannot, however, be definitely resolved.

From these experiences, it would seem that in temperate ice this system of marking boreholes can be expected to work consistently without modification. Even though there was a very good recovery percentage for 1966-67, the system was operating with a small margin of safety, which depended on the accident of the weights remaining free, a condition which an experimenter cannot hope to control. Thus it seems that before this system is used again on a glacier where cold

surface ice can have an appreciable effect, some modification should be made. The basic approaches which might be considered are: (1) to use cables of a construction such that the breaking elongation exceeds any elongation which would be expected in the process of deformation; (2) to increase the strength to drag ratio, by either providing the cable with a smooth surface which cannot be grabbed by the ice, or by increasing its diameter; (3) to guarantee a free end condition at the lower end of the cable by having a weak mechanical link, or by providing a means whereby extra cable could be stored within and pulled out of the weight.

APPENDIX II

"NOISE" IN BOREHOLE TILT MEASUREMENTS

The scatter ("noise") in the borehole tilt measurements requires discussion in order to specify the accuracy with which the experimental parameters of interest are determined. The quantities of interest here are the values of the local tilt, the local slope of the tilt profile, and the borehole coordinates with respect to the surface of the initial and deformed boreholes. One would also like to isolate the source or sources of the noise. An additional question of importance is whether the scatter is caused by the flow of the glacier, or whether it is purely a consequence of the experimental technique.

A. Errors in Experimental Quantities

The accuracy with which the data determine the general trend of tilt with depth, as represented by the chosen smoothing curves can be made without specific reference to the source of the scatter in the data, by a purely statistical analysis requiring only general assumptions concerning the nature of any contributing source of noise.

Consider the deviations $\zeta(Y)$ and $\xi(Y)$ of $\Gamma_X(Y)$ and $\Gamma_Z(Y)$ from any two arbitrary smooth curves. Noting that Γ_X and Γ_Z and thus ζ and ξ are determined at only discrete points Y_k spaced ΔY (2 m) apart, the notation can be simplified by denoting $\zeta(Y_k)$ and $\xi(Y_k)$ by ζ_k and ξ_k, respectively. Let distributions $f_N(\zeta_{k_1}, \xi_{k_1}; \ldots; \zeta_{k_N}, \xi_{k_N})$ give the probability of measuring specific values for the 2N random variables ζ_{k_1} to ζ_{k_N} and ξ_{k_1} to ξ_{k_N}. Although specific knowledge of

the probability distributions f_N is not available, they are introduced for the purpose of making definitions and clarifying the nature of the assumptions which must be made.

For notational efficiency, let η represent either the random variable ζ or ξ. In the usual manner, the first moment of the random variable η is given by

$$\mu_\eta(Y_k) = E[\eta_k] = \int_{-\infty}^{\infty} \eta_k f_1(\zeta_k, \xi_k) d\zeta_k d\xi_k, \tag{1}$$

and the statistical autocorrelation function is defined by

$$R_\eta(Y_k, Y_{k'}) = E[\eta_k, \eta_{k'}] = \int_{-\infty}^{\infty} \eta_k \eta_{k'} f_2(\zeta_k, \xi_k; \zeta_{k'}, \xi_{k'}) d\zeta_k d\xi_k d\zeta_{k'} d\xi_{k'} \tag{2}$$

Note that $R_\eta(Y_k, Y_{k'}) = R_\eta(Y_{k'}, Y_k)$. In addition $R_\eta(Y_k, Y_k)$ is the non-central second moment of the random variable η_k. The variance of η_k is

$$\sigma_\eta^2(Y_k) = R_\eta(Y_k, Y_k) - \mu_\eta^2(Y_k) \tag{3}$$

The normalized statistical autocorrelation function is defined to be

$$\rho_\eta(Y_k, Y_{k'}) = \frac{R_\eta(Y_k, Y_{k'}) - \mu_\eta(Y_k)\mu_\eta(Y_{k'})}{\sigma_\eta(Y_k)\sigma_\eta(Y_{k'})} \tag{4}$$

These statistical functions can be used to estimate the accuracy with which the data determine the smoothing curves for Γ_X and Γ_Z and the quantities of interest derived from them. Consider the curves defined by

$$\eta_k^* = \eta^*(Y_k) = \frac{1}{N^*+1} \sum_{n=-\frac{N^*}{2}}^{\frac{N^*}{2}} \eta(Y_k + n\Delta Y) = \frac{1}{N^*+1} \sum_{n=-\frac{N^*}{2}}^{\frac{N^*}{2}} \eta_{k+n} \tag{5}$$

where ΔY is the spacing between consecutive tilt measurements and N^* is even and less than the total number of tilt measurements N in a given borehole. $\eta^*(Y)$ thus defined is a running average with each point having unit weight.

The actual smoothing curves were not determined by a running average as above, but were drawn by hand with the averaging done by eye. An analysis applied to the curves η^* should, however, give an idea of the uncertainty in the choice of the hand-drawn smoothing curves if N^* is chosen equal to the number of points effectively used in the visual average. An appropriate N^* would seem to be the number of points in a depth interval of approximately 100 m ($N^* = 50$). This is consistent with the elimination of any fluctuations of wave length less than 100 m, as was done in the smoothing. In addition, the average given by equation (5) implicitly requires that there be $N^*/2$ data points on both sides of the point k which is under consideration. In the upper and lowermost parts of the boreholes, this is not the case. Thus there are edge effects, and as a result, the smoothing curve cannot be as precisely located near the surface and bed. Such edge effects are neglected in the following analysis. To approximately account for edge effects, the error in tilting rate at the surface and at the bottom of the boreholes can be taken to be twice the value derived in the analysis below.

The formulae giving the first moments and variances of the random variables

$$\eta^*(Y_k), \qquad S^*(Y_k) = \frac{d\eta^*(Y_k)}{dY},$$

and

$$I^*(Y) = \int_o^{Y_k} \eta^*(Y)dY \cong \Delta Y \sum_{n=1}^{k-1} \eta^*(Y_k)$$

n be derived. They are

$$\mu_{\eta^*}(Y_k) = E[\eta_k^*] = \frac{1}{N^*+1} \sum_{n=\frac{-N^*}{2}}^{\frac{N^*}{2}} \mu_\eta(Y_{k+n}) \tag{6a}$$

$$\sigma_{\eta^*}(Y_k) = E[(\eta_k^* - N_{\eta^*}(Y_k))^2]$$

$$= \frac{1}{(N^*+1)^2} \sum_{n=\frac{-N^*}{2}}^{\frac{N^*}{2}} \sum_{n'=\frac{-N^*}{2}}^{\frac{N^*}{2}} R_\eta(Y_{k+n}, Y_{k+n'}) - \mu_{\eta^*}^2(Y_k) \tag{6b}$$

$$\mu_{S^*}(Y_k) = E[S_k^*] = \frac{1}{N^*\Delta Y} \left(\mu_\eta\left(Y_k + \frac{N^*}{2}\right) - \mu_\eta\left(Y_k - \frac{N^*}{2}\right)\right. \tag{7a}$$

$$\sigma_{S^*}^2(Y_k) = E[(S_k^* - \mu_{S^*}(Y_k))^2]$$

$$= \frac{1}{N^*\Delta Y} \left\{\sigma_\eta^2\left(Y_k + \frac{N^*}{2}\right) + \sigma_\eta^2\left(Y_k - \frac{N^*}{2}\right)\right. \tag{7b}$$

$$\left. -2\left[R_\eta\left(Y_k + \frac{N^*}{2}, Y_k - \frac{N^*}{2}\right) + \mu_\eta\left(Y_k + \frac{N^*}{2}\right)\mu_\eta\left(Y_k - \frac{N^*}{2}\right)\right]\right\}$$

$$\mu_{I^*}(Y_k) = E[I_k^*] = \frac{\Delta Y}{N^*+1} \sum_{m=1}^{k-1} \sum_{n=\frac{-N^*}{2}}^{\frac{N^*}{2}} \mu_\eta(Y_{m+n}) \tag{8a}$$

$$\sigma_{I^*}(Y_k) = E[(I_k^* - \mu_{I^*}(Y_k))^2]$$

$$= \frac{(\Delta Y)^2}{(N^*+1)^2} \sum_{m=1}^{k-1} \sum_{m'=1}^{k-1} \sum_{n=\frac{-N^*}{2}}^{\frac{N^*}{2}} \sum_{n'=\frac{-N^*}{2}}^{\frac{N^*}{2}} R_\eta(Y_{m+n}, Y_{m'+n'}) - \mu_{I^*}^2(Y_k) \tag{8b}$$

As these formulae stand, however, they are useless in that the necessary statistical quantities such as the moments and correlation functions cannot be determined. These quantities could be estimated from the outcomes of a large number of identical experiments in which a number of boreholes would be placed in the same identical location by exactly the same technique and surveyed with the same instrument after identical intervals of time. Since the only quantities essential to the application of formulae (6), (7), and (8) are $\mu_\eta(Y_k)$ and $R_\eta(Y_k, Y_{k'})$, only these would have to be estimated. Note that the usual estimators for $\mu_\eta(Y_k)$ and $R_\eta(Y_k, Y_{k'})$ are

$$\mu_\eta(Y_k) = \frac{1}{M} \sum_{\alpha=1}^{M} \eta_\alpha(Y_k)$$

$$R_\eta(Y_k, Y_{k'}) = \frac{1}{M} \sum_{\alpha=1}^{M} \eta_\alpha(Y_k)\eta_\alpha(Y_{k'}) \tag{9a}$$

where M is the number of experiments performed and $\eta_\alpha(Y_k)$ is the outcome of the α^{th} experiment at depth Y_k.

In fact, only one such experiment has been performed. Thus to make progress, some additional assumptions are required. One possible approach is to consider the different boreholes, which penetrated to the bottom and were completely recovered, as distinct but identical experiments. This would be a reasonable approach in that the sources of the noise could be expected to act equivalently in all of these boreholes. However, there are only seven such boreholes, which is an inadequate sample for application of the above formulae. An additional step can be taken by assuming that the processes which

produce the random noise are independent of depth in the boreholes. Although, as will be discussed in the second section of this chapter, there is reason to think that this assumption may not be precisely true, it can be expected to be approximately valid. Specifically, it is assumed that σ_η^2 and ρ_η are independent of depth or

$$\sigma_\eta^2(Y_k) = \sigma_\eta^2 \tag{10a}$$

$$\rho_\eta(Y_k, Y_{k+n}) = \rho_\eta(n\Delta Y) \tag{10b}$$

If η (which equals ζ or ξ) is the deviation away from the actually chosen smoothing curve appropriate to the variable for which η stands, then $\mu_{\eta*}(Y_k)$ is not zero at all depths, because in choosing the smoothing curves, systematic effects caused by the behavior of the compass unit in the inclinometer have been eliminated, as discussed in Chapter IV-D. This results in a displacement of the chosen smoothing curves away from a curve defined as a running average. This displacement is assumed to be independent of depth. This again can be expected to be only approximately valid. Since the actual displacement involved is in all cases small compared to the amplitude of the scatter (less than 10%), no significant effect on the outcome of the analysis would occur even if the displacement were assumed to be zero. The weaker assumption

$$\mu_\eta(Y_k) = \mu_\eta \tag{10c}$$

is, however, sufficient to reduce the complexity of the formulae. The above assumptions and equation (4) imply that

$$R_\eta(Y_k, Y_{k+n}) = R_\eta(n\Delta Y) \tag{10d}$$

Under these assumptions, formulae (6), (7), and (8) reduce to

$$\mu_{\eta*} = \mu_\eta \tag{11a}$$

$$\sigma^2_{\eta*} = \frac{\sigma^2_\eta}{N^*+1}\left\{1 + 2\sum_{n=1}^{N^*}\left(1 - \frac{n}{N^*+1}\right)\rho_\eta(n\Delta Y)\right\} \tag{11b}$$

$$\mu_{S*} = 0 \tag{12a}$$

$$\sigma^2_{S*} = \frac{2\sigma^2_\eta}{(N^*\Delta Y)^2}\left\{1 - \rho_\eta(N^*\Delta Y)\right\} \tag{12b}$$

$$\mu_{I*}(Y_k) = (k-1)\Delta Y\mu_\eta \tag{13a}$$

$$\sigma^2_{I*}(Y_k) = (k-1)\Delta Y^2\sigma^2_\eta\left\{1 + \frac{2}{N^*+1}\sum_{n=1}^{N^*}\left(1 - \frac{n}{N^*+1}\right)\rho_\eta(n\Delta Y)\right. \tag{13b}$$

$$\left. + \frac{2}{(N^*+1)^2}\sum_{\ell=1}^{k-1}\sum_{n=\frac{-N}{2}}^{\frac{N}{2}}\sum_{n'=\frac{-N}{2}}^{\frac{N}{2}}\left(1 - \frac{\ell}{k-1}\right)\rho_\eta([n-n'+\ell]\Delta Y)\right\}$$

$$n - n' + \ell \neq 0$$

Since all of the statistical functions of interest are independent of depth under the above assumptions, it is natural to suppose that μ_η and $R_\eta(n\Delta Y)$ can be estimated by considering the scatter along the length of the borehole as well as by the outcomes at given Y of different experiments. Thus in analogy to equations (9)

$$\mu_\eta = \frac{1}{N} \sum_{\alpha=1}^{N} \eta(Y_\alpha) \tag{14a}$$

$$R_\eta(n\Delta Y) = \frac{1}{M} \sum_{\alpha=1}^{M} \eta(Y_\alpha)\eta(Y_\alpha + n\Delta Y) \tag{14b}$$

where N is the number of tilt measurements made in the borehole and M = N - n. Estimators of σ_η and $\rho_\eta(n\Delta Y)$ can be computed from equations (3) and (4). μ_η, σ_η, R_η, and ρ_η with $\eta = \zeta$ and $\eta = \xi$ can be used in equations (11b) and (12b) to estimate a standard deviation for the location and slope of the smoothed tilt profiles. Equation (13b) estimates the accuracy with which borehole coordinates are determined.

If the above formulae are applied to each borehole separately, the following results are obtained. The standard deviation σ_ζ ranges from 0.31° to 0.57°, and σ_ξ from 0.29° to 0.98°. The larger scatter in Γ_Z is interpreted to be a result of the relatively large error in azimuth (± 20°). The autocorrelation functions for the separate boreholes $\rho_\zeta(n\Delta Y)$ and $\rho_\xi(n\Delta Y)$ were calculated for n up to 10, corresponding to a maximum interval of 20 m. The normalized correlation coefficients estimated for tilt measurements spaced at these intervals were always small (less than 0.2 for ζ and ξ), except in the case of borehole 2B where ρ_ζ and ρ_ξ attained values up to 0.35 and 0.55, respectively. If the random variables ζ_k and ξ_k are normally distributed, then it can be shown that for ρ_ζ and ρ_ξ much less than one, ρ_ζ and ρ_ξ would be approximately normally distributed with variance 1/(M-3) (Mood, 1950, p. 314). Although ζ and ξ do not seem to obey normal distribution laws as is shown in figure 40, the actual

distributions are not drastically different from normal form, and thus it can be expected that the above estimate of the variance for ρ will be of use in testing the significance of calculated values of ρ_ζ and ρ_ξ. For all of the boreholes except 2B, the calculated values of ρ_ζ and ρ_ξ for $n \geq 1$ are not significantly greater than the standard deviations, which for a typical borehole 300 m deep with 150 tilt measurements would be approximately 0.08. This, along with the fact that the distribution of ρ_ζ and ρ_ξ with increasing separation of the compared points apparently lacks any systematic features, suggests that there is no significant correlation. However, one significant systematic pattern of the distributions for the various boreholes considered separately (not illustrated here) is that the correlation coefficients ρ_ζ and ρ_ξ for a 2 m interval ($n = 1$) are always negative, and for a 4 m interval ($n = 2$) tend to be positive. This suggests that significant correlation exists between the deviations of tilt measurements separated by 2 and 4 m. To test this, all boreholes were considered together, by using equations (14) with the sums including data from all of the boreholes. (N equals the total number of tilt determinations, and $M = N - 9n$.) The resulting normalized autocorrelation functions are illustrated in figure 41. The horizontal dashes are placed one standard deviation (± 0.03) above and below $\rho = 0$. In the case of $\rho_\zeta(n\Delta Y)$, the values for $\rho_\zeta(n\Delta Y)$ with $n \geq 3$ are compatible with the interpretation that $\rho_\zeta(n\Delta Y) = 0$. $\rho_\zeta(1\Delta Y) = -0.12$ and $\rho_\zeta(2\Delta Y) = +0.09$, which are several times the estimated standard deviation (0.03); this must indicate real though weak correlation between adjacent and next-adjacent tilt measurements. A similar distribution for $\rho_\xi(n\Delta Y)$ was

calculated. The values of $\rho_\xi(n\Delta Y)$ seem, however, to be significant out to n = 6. This longer range of significant correlation is due to a large contribution from hole 2B, caused by a strong disturbance in the transverse tilt measurements where large deviations alternating in sign occurred over a considerable depth (fig. 14e). The meaning of such correlations will be of interest in the second section of this chapter. For the present purpose, it is sufficient to note that the correlation $\rho(n\Delta Y)$ is small for $n > 0$, and that significant correlation ceases to exist over intervals short compared with the length over which the running average was made. In this case, the sums involving $\rho(n\Delta Y)$ with $n \geq 1$ in equations (11b), (12b), and (13b), make only a small contribution to the value of the variance calculated for each of the quantities of interest. In view of the many approximations already inherent in this analysis, it is justifiable to neglect those contributions for $n \geq 1$ and to evaluate the variances as if all of the tilt determinations were strictly independent.

Application of formulae (11b), (12b), and (13b) to the borehole data after one year's deformation (figs. 13 and 14) gives standard deviations

$$\sigma_{\eta *} \cong \frac{\sigma_\eta}{7}, \qquad \sigma_{S*} \cong \frac{\sigma_\eta}{71}\, m^{-1}, \qquad \sigma_{I*}(Y) \cong 1.41\sqrt{Y}\ \sigma_\eta\, m$$

where ΔY and N^* were taken to be 2 m and 50. The values of σ_ζ (0.47°) and σ_ξ (0.63°), calculated from all of the boreholes considered together, give standard deviations 0.07° and 0.09° for smoothed tilt, $0.007°\ m^{-1}$ and $0.009°\ m^{-1}$ for the slope of the smoothed tilt profiles, and 20 cm and 27 cm for the integrated tilts at a depth of 300 m. Application of the same formulae to the initial tilt data (fig. 10), gives

standard deviations

$$\sigma_{\eta *} \cong \frac{\sigma_\eta}{4.5}, \qquad \sigma_{S*} \cong \frac{\sigma_\eta}{71}\ \mathrm{m}^{-1}, \qquad \sigma_{I*}(Y) \cong 3.9\sqrt{Y}\ \sigma_\eta\ \mathrm{m}$$

where ΔY and N^* were taken to be 15 m and 20, respectively. For the initial tilt data, σ_ζ and σ_ξ are estimated to be 0.25°. These give standard deviations 0.06° for the smoothed tilt, 0.004° m^{-1} for the slope of the tilt profiles, and 30 cm for the integrated tilts at a depth of 300 m.

Combination of the quantities for initial and deformed boreholes gives standard deviations 0.0015 yr^{-1} and 0.0019 yr^{-1} for the tilting rate $\partial\gamma_x/\partial t$ and $\partial\gamma_z/\partial t$, 0.00014 m^{-1} yr^{-1} and 0.00017 m^{-1} yr^{-1} for the change in slope of the tilt profiles γ_x and γ_z, and 36 cm and 41 cm for differential displacement ΔX and ΔZ.

B. Sources of Noise

The possible sources of noise can be divided into two categories: real noise introduced by the flow, and experimental noise introduced by the method of boring, marking, and recovering the boreholes. The following sources of experimental noise in deformed boreholes can be enumerated:

i) instrumental error in the inclinometer,

ii) non-parallelism of inclinometer and borehole, made possible by the difference in borehole and instrument diameters,

iii) wandering of the boring hotpoint in the initial emplacement of the borehole,

iv) non-centering of the aircraft cable in the initial borehole

v) fluctuations in the diameter of the borehole resulting from changes in hotpoint efficiency, as caused , for example, by accumulation of debris at the bottom of the borehole during boring,

vi) spiraling of the cable-following hotpoint around the aircraft cable during borehole recovery,

vii) modification of the sides of the borehole in the interval between boring and the inclinometry survey as a result of flow and freezing processes caused by the presence of the borehole.

Sources iv) and vi) would, of course, not contribute to scatter in the initial borehole tilt data, as is also the case for real noise.

For some of these sources, a maximum possible contribution can be determined. For source i), instrumental error, the error is estimated on the basis of calibration experiments (Appendix I) to be less than ± 0.1° in tilt magnitude and ± 20° in azimuth of tilt for the electrical inclinometer; a similar accuracy, but with greater reliability in the azimuth, is expected for the optical inclinometer used in the survey of the initial boreholes. Consideration of the difference in diameter between the borehole and inclinometer case, and the length of the case, indicates a maximum possible contribution from source ii) of 1.4° for the electrical inclinometer and 2.0° for the optical inclinometer. Similarly geometrical constraints on the curvature of the recovered borehole implied by the passage of the cable-following hotpoint indicate a maximum of 1.6° for source vi) and 2.5° for source iv). The drilling logs indicate that short term

fluctuations in the rate of hotpoint penetration did not exceed 5% of the average drilling rate. If this reflects a real difference in power input at various depths rather than just fluctuations in ice density, source v) could contribute 0.1°. Similar limits cannot be placed a priori on sources iii) and vii). The fact that the inclinometer could be lowered suggests, however, that no great modification of the borehole could have occurred in the interval between boring and inclinometry, and thus that source vii) probably only contributes weakly to the errors.

The problem is to discover ways in which these various sources of noise can be distinguished, if possible. The depth dependence of the scatter amplitude, the autocorrelation between consecutive measurements of Γ_X and Γ_Z, the cross correlation between measurements of Γ_X and Γ_Z at the same point, and the time development of the scatter amplitude are considered to this end.

If sources ii), iv), and vi) were the main contributors to the scatter in deformed boreholes, then one could expect that the scatter amplitude would be less where the borehole is significantly inclined than where the borehole is nearly vertical. There is little tendency for this to be the case, which suggests that other sources of errors must also enter significantly.

In the first section of this chapter, the autocorrelation functions $\rho_\zeta(n\Delta Y)$ and $\rho_\xi(n\Delta Y)$ were defined. Estimates of the autocorrelation functions indicate the presence of a disturbance in the data of approximately four-meter wavelength (fig. 41). All of the sources, except sources i) and ii), could conceivably exhibit such a periodicity. One might suspect source vi), in which the cable-following hotpoint

spirals around the marker cable as it penetrates the ice, as a likely origin for this feature of the noise in the data. This possibility can be tested by recognizing that if spiraling were the main source of noise, a large deviation in Γ_X would be accompanied by a small deviation in Γ_Z and visa versa. If a two-dimensional histogram were to be constructed with intervals of the deviation of Γ_X along one axis and of Γ_Z along the other axis, then the condition of spiraling would result in a ring of maximum density surrounding the origin, where there would be a region of low density. Such a two-dimensional diagram can be illustrated in one dimension simply by plotting the number of points per unit area in a centered anulus of given thickness on the above histogram versus the radius. This is done in figure 42. Tilt measurements in all of the boreholes are included together. If the main component of the scatter came from spiraling of wavelengths on the order of 4 m, then a distinct minimum could be expected in the density at r = 0. This is not observed. An additional indication that spiraling at four-meter wavelength cannot be the main source of the scatter is given by the fact that geometrical constraints would require the resulting scatter amplitude to be three to four times the observed amplitude.

Comparison of the amplitude of scatter in the initial boreholes and in boreholes after one and two year's deformation is complicated by the fact that in each case a different instrument was used. Since all three instruments (the optical inclinometer, the electrical inclinometer, and the electrical inclinometer with improved compass mechanism) are equivalent in accuracy of measurement of tilt

magnitude, this problem can be circumvented. The standard deviation in the initial tilt magnitudes (fig. 10) was 0.25. In deformed boreholes, a measure of the scatter amplitude that is independent of the azimuth measurement is obtained by considering the scatter in the tilt magnitudes in portions of the holes which have remained planar during the deformation. Thus, the bottom 150 m of boreholes 2A and 3B after one and two year's deformation are considered. After one year's deformation, the amplitudes of scatter (standard deviation) were 0.41° and 0.45°, respectively. This is almost twice the amplitude of scatter in the initial tilt data. After two years, these quantities were 0.50 and 0.47, which are only slightly greater than the corresponding quantities after one year's deformation.

The fact that considerably greater scatter was observed in deformed boreholes indicates that source iii) is not the sole source of noise in deformed boreholes. If the additional noise in the tilt data for deformed holes were real noise caused by actual local fluctuations in flow parameters tied to structural inhomogeneities in the ice, then it could be expected that the amplitude in scatter would increase linearly in time; that is, the increase between the second and third year's data should be approximately the same as that between the first and second year's data. This effect was not observed. However, it cannot be ruled out on this basis alone, since source iv) (non-centering of the aircraft marker cable) is also capable of erasing noise. This would tend to be the case if the aircraft cable were on initial emplacement pulled tight, as was done. It would remain tight because of the extension of the borehole resulting from ice deformation. The

taut aircraft cable would tend to cut corners and thus smooth out irregularities.

If there were real noise in the flow which was not tied to structural inhomogeneity in the ice, but which fluctuated randomly in time at a given element of ice, then one could expect the noise amplitude to increase roughly as the square root of time. The observed time development of the scatter amplitude is not incompatible with this interpretation. Such a process is, however, difficult to imagine.

From the above discussions of the possible maximum contributions of the experimental sources of noise, and the expected effect of these sources on the available statistical quantities, it is clear that no single one of the possible experimental sources of noise can explain the observed characteristics. It is quite possible, however, that all of the experimental sources acting together could produce the observed characteristics. The weak correlation exhibited by tilt measurements spaced two and four meters apart in deformed holes could be something inherited from the initial holes as a result of the action of source iii), or could result from occasional events of spiraling. The latter is suggested by the large contribution which borehole 2B makes to the correlation functions of figure 41. The tilt data for borehole 2B show strong evidence for spiraling between 140 and 210 m. The large amplitude accompanying this event distinguishes it from the typical noise pattern (figs. 13e and 14e). In considering the cross correlation of the Γ_X and Γ_Z deviations, the result expected of spiraling would not be observed because of the rarity of occurrence and the large amplitude of scatter associated

with the events. The increase in scatter amplitude from initial to deformed boreholes could be a result of the additional effect of experimental source vi).

Since the observed properties of the scatter can apparently be produced by the enumerated experimental sources of noise, there is no compelling reason to attribute any of the noise to real features of the flow field. On the other hand, the possibility that such features exist and contribute to the scatter cannot be discounted on purely statistical grounds.

APPENDIX III

FORM OF VELOCITY FIELD FOR A LONGITUDINALLY INDEPENDENT STRAIN-RATE FIELD

For the purpose of discussing the observed velocity and strain-rate fields, a brief derivation of the general form of the velocity field of an x-independent strain-rate field is given below. The question of longitudinal independence of the strain-rate field of a glacier flowing in a cylindrical channel is of considerable importance, because assumption of such independence has been made in all theoretical treatments dealing with the detailed distribution of velocity in valley glaciers (Nye, 1951; 1957, 1965). In addition, an extension of Nye's (1965) treatment of rectilinear flow in cylindrical channels to a more complicated case, with ablation at the surface involving non-zero longitudinal strain rate and motion perpendicular to the direction of main transport, will probably also require such an assumption because of the practical limitations of present computers.

First, the general form of the velocity field is derived and described. A basic incompatibility between x-independent flow in a cylindrical channel and the typical pattern of flow in the ablation region of a valley glacier is discussed.

A. Form of the Velocity Field

Let the x-axis be aligned with the direction of assumed independence of the strain-rate field. Differentiation of the strain-rate

components with respect to x gives

$$\frac{\partial^2 u}{\partial x^2} = 0 \tag{1a}$$

$$\frac{\partial^2 v}{\partial x \partial y} = 0 \tag{1b}$$

$$\frac{\partial^2 w}{\partial x \partial z} = 0 \tag{1c}$$

$$\frac{\partial^2 u}{\partial x \partial y} + \frac{\partial^2 v}{\partial x^2} = 0 \tag{1d}$$

$$\frac{\partial^2 u}{\partial x \partial z} + \frac{\partial^2 w}{\partial x^2} = 0 \tag{1e}$$

$$\frac{\partial^2 v}{\partial x \partial z} + \frac{\partial^2 w}{\partial x \partial y} = 0 \tag{1f}$$

Equations (1a, 1d, 1e) give

$$u = R(y, z)x + h(y, z)$$

$$v = \frac{\partial R}{\partial y}\frac{x^2}{2} + G(y, z)x + g(y, z)$$

$$w = \frac{\partial R}{\partial z}\frac{x^2}{2} + F(y, z)x + f(y, z)$$

Equation (1b) becomes

$$\frac{\partial^2 R}{\partial y^2}x + \frac{\partial G}{\partial y} = 0$$

which requires

$$\frac{\partial^2 R}{\partial y^2} = \frac{\partial G}{\partial y} = 0$$

Similarly, equation (1c) requires

$$\frac{\partial^2 R}{\partial z^2} = \frac{\partial F}{\partial z} = 0$$

and equation (1f) requires

$$\frac{\partial^2 R}{\partial y \partial z} = \frac{\partial G}{\partial z} + \frac{\partial F}{\partial y} = 0$$

These additional conditions give

$$R(y, z) = ay + bz + r$$

$$G(y, z) = -cz + e$$

$$F(y, z) = cy + d$$

where a, b, c, d, and r are constants. Thus

$$u = (ay + bz + r)x + h(y, z) \tag{2a}$$

$$v = -a\frac{x^2}{2} + (e - cz)x + g(y, z) \tag{2b}$$

$$w = -b\frac{x^2}{2} + (d + cy)x + f(y, z) \tag{2c}$$

The x-dependent part of the velocity field associated with the constants a, b, c, d, e, and r can be simply interpreted in terms of simple x-independent deformations. The contribution from the constant r represents uniform longitudinal extension. The motions associated with the remaining constants are best illuminated by

considering the rotation-rate $\omega_{ij} = \frac{1}{2}(u_{i,j} - u_{j,i})$:

$$\omega_{xy} = ax - \frac{1}{2}(e - cz) + \frac{1}{2}\frac{\partial h}{\partial y}$$

$$\omega_{xz} = bx - \frac{1}{2}(d + cy) + \frac{1}{2}\frac{\partial h}{\partial z}$$

$$\omega_{yz} = -cx + \frac{1}{2}\left(\frac{\partial g}{\partial z} - \frac{\partial f}{\partial y}\right)$$

These quantities can be interpreted in terms of a rotation-rate vector $\bar{\omega} = \frac{1}{2}\bar{\nabla} x \bar{u}$ with $\omega_x = \omega_{yz}$, $\omega_y = -\omega_{xz}$, and $\omega_z = \omega_{xy}$. Thus constants d and e represent rotation rates about the y and z axes which are independent of x. The constants a, b, and c represent relative rotation rates of cross sections at different longitudinal position x and correspond to a uniform bending rate about the z axis, a uniform bending rate about the y axis, and torsion along the x axis, respectively. The most general velocity field compatible with an x-independent strain-rate field as represented by equations (2) can be described as a velocity field depending only on y and z (given by h, g, and f) with superposed homogeneous longitudinal extension, uniform bending about the y and z axis, torsion about the x axis, and rigid rotation about the y and z axes. The longitudinal strain rate must be a linear function of y and z.

The motions corresponding to non-zero values of the constants a, b, c, d, and e can be related to real problems in glacier flow. Down glacier curvature of the channel would tend to produce the motions represented by the constants d and e. A gradient in the curvature

of the channel would tend to produce the bending represented by a and b. The torsion associated with c does not have any general application, although it could conceivably be of interest in specialized cases of distribution of ablation rate or longitudinal variation in channel shape.

B. X-Independent Flow in Cylindrical Channels

In a glacier of cylindrical geometry, the requirement that the velocity normal to the bed be zero demands that all constants except r be zero. Thus longitudinal strain rate must be constant. In the ablation region (or accumulation region) of such a glacier, where longitudinal strain rate cannot be zero, the sliding velocity varies linearly along the glacier bed, but the shear stress which drives the sliding is independent of x. This would require a rather special distribution of the parameters influencing sliding, such as bed roughness and basal water pressure. If the parameters which determine sliding response to applied basal shear stress were longitudinally constant, as would seem to be more generally applicable, then either non-cylindrical geometry or longitudinal variation of the strain rates and the stresses must exist.

APPENDIX IV

EQUILIBRIUM OF A VISCOUS SLAB WITH SINUSOIDAL DISTRIBUTION OF NORMAL STRESS APPLIED ON ONE SURFACE

Consider an infinite slab of viscous material, viscosity η, bounded by the surfaces y = 0 and y = H at which the following boundary conditions hold. The shear stress is zero (i.e. $\tau_{xy} = \tau_{yz} = 0$) at the boundaries y = 0 and y = H. A normal stress $\tau_{xy} = -N \cos hz$ is applied at the surface y = 0. We wish to solve for the motions and stresses within the slab for two types of boundary condition at y = H:

(1) normal velocity v vanishes

(2) normal stress τ_{yy} vanishes

For either boundary condition at y = H, the velocity solution must be independent of x and must be periodic in z. Standard methods for analysis of plane-strain problems show that the condition of incompressibility and the equations of equilibrium are satisfied by a velocity field of the form

$$\begin{aligned} v(y, z) &= \Phi(hy) h \cos hz \\ w(yz) &= -\frac{d\Phi}{dy} \sin hz \end{aligned} \tag{1}$$

and a pressure distribution

$$p = -\eta h^2 \left(\frac{1}{h} \frac{d\Phi}{dy} - \frac{1}{h^3} \frac{d^3\Phi}{dy^3} \right)$$

where

$$-\frac{d^4\Phi}{dy^4} + 2h^2 \frac{d^2\Phi}{dy^2} - h^4\Phi = 0 \tag{2}$$

In terms of the function Φ, the stress components of interest can be written as

$$\tau_{yz} = \eta\left(\frac{\partial v}{\partial z} + \frac{\partial w}{\partial y}\right) = \eta h^2 \left\{ - \frac{1}{h^2} \frac{d^2\Phi}{dy^2} - \Phi \right\} \sin hz$$

$$\tau_{yy} = 2\eta \frac{\partial v}{\partial y} - p = \eta h^2 \left\{ \frac{3}{h} \frac{d\Phi}{dy} - \frac{1}{h^3} \frac{d^3\Phi}{dy^3} \right\} \cos hz \qquad (3)$$

Without consideration of the specific form of the function Φ, it can be noted that $w = 0$ and $\tau_{yz} = 0$ at $z = \pm\frac{\pi}{h}$. Thus, the problem is equivalent to that of an infinite strip of thickness H and width $W = \frac{2\pi}{h}$ for which the shear stress and the normal velocity on the sides are required to be zero.

The general solution of equation (2) can be written

$$\Phi(hy) = c \left\{ (1 + \beta hy)e^{-hy} + (\gamma + \delta hy)e^{hy} \right\} \qquad (4)$$

The four constants c, β, γ, δ are to be determined by the normal and tangential boundary conditions at $y = 0$ and $y = H$. Let $\ell = hH$. The normal velocity boundary condition at the surface requires

$$N = 2\eta h^2 c(1 - \gamma) \qquad (5a)$$

The shear stress boundary conditions at $y = 0$ and $y = H$ give

$$1 - \beta + \gamma + \delta = 0 \qquad (5b)$$

$$[1 - (1-\ell)\beta]e^{-\ell} + [\gamma + (1+\ell)\delta]e^{\ell} = 0 \qquad (5c)$$

The normal boundary condition at $y = H$ for cases (1) and (2) can be written as

$$[1 + \beta\ell]e^{-\ell} \pm [\gamma + \delta\ell]e^{\ell} = 0 \qquad (5d)$$

where the plus sign represents the zero normal velocity condition, and the minus sign represents the zero normal stress condition.

Solution of the linear equations (5b, 5c, 5d) for β, γ, and δ gives

$$\beta = \frac{1}{K}\left\{e^{4\ell} + e^{2\ell}(\pm 1 + \ell \mp \ell)\right\}$$

$$\gamma = \frac{1}{K}\left\{e^{2\ell}(\ell^2 \mp \ell^2 \mp 2\ell \mp 1) \pm 1\right\} \qquad (6)$$

$$\delta = \frac{1}{K}\left\{-e^{2\ell}(\mp 1 \mp \ell + \ell) \mp 1\right\}$$

where

$$K = e^{4\ell} - e^{2\ell}(+\ell^2 \mp \ell^2 - 2\ell + 1).$$

c is trivially determined from equation (5a), thus giving the complete solution for the velocity and stress fields.

For case (1), a result of particular interest is the relationship between the applied normal stress amplitude N and the resulting normal velocity amplitude at y = 0. Noting that

$$\Phi(o) = c(1 + \gamma)$$

equations (5a) and (6) with the upper sign give

$$N = 2\eta h^2 \Phi(o) Q(\ell) \qquad (7)$$

where

$$Q(\ell) = \frac{1-\gamma}{1+\gamma} = \frac{e^{2\ell} + 4\ell - \ell^{-2\ell}}{e^{2\ell} - 2(1-2\ell) + \ell^{2\ell}}$$

For case (2) the comparison of the normal velocity amplitude at y = H (the free surface) to the normal velocity amplitude at y = 0 (where

the driving stress is applied) is of interest. From equation (4)

$$R(\ell) = \frac{\Phi(\ell)}{\Phi(o)} = \frac{(1+\beta\ell)e^{-\ell} + (\gamma+\delta\ell)e^{\ell}}{(1+\gamma)}$$

from equations (6)

$$R(\ell) = \frac{2(\ell+1)e^{\ell} + 2\ell e^{-\ell}}{e^{2\ell} + 4\ell + e^{-2\ell}} \tag{8}$$

REFERENCES

Butkovich, T. R., and Landauer, J. K. (1958). "The Flow Law for Ice," Int. Assoc. Sci. Hydrol., Publ. 47, pp. 318-325.

Davenport, W. G., and Root, W. L. (1958). An Introduction to the Theory of Random Signals and Noise. McGraw-Hill Book Company, Inc.

Demorest, M. (1943). "Ice Sheets," Bull. Geol. Soc. Amer., vol. 54, pp. 363-400.

Elliston, G. R. (1963). Bull. Int. Assoc. Sci. Hydrol., vol. 8, no. 2, p. 65.

Gerrard, J. A. F., Perutz, M. F., and Roch, A. (1952). "Measurement of the Velocity Distribution Along a Vertical Line Through a Glacier," Proc. Roy. Soc. London, ser. A, vol. 213, pp. 546-558.

Glen, J. W. (1955). "The Creep of Polycrystalline Ice," Proc. Roy. Soc. London, ser. A., vol. 228, pp. 519-538.

Glen, J. W. (1958). "The Flow Law of Ice," Int. Assoc. Sci. Hydrol.,Publ. 47, pp. 171-183.

Glen, J. W., Lewis, W. V. (1961). "Measurement of Side-Slip at Austerdalsbreen, 1959," Jour. Glaciol., vol. 30, pp. 1109-1122.

Hill, R. (1950). The Mathematical Theory of Plasticity, Oxford Clarendon Press, 350 pp.

Kamb, W. B. (1959). "Ice Petrofabric Observations from Blu Glacier, Washington, in Relation to Theory and Experiment," Jour. Geophys. Res., vol. 64, no. 11, pp. 1891-1909.

Kamb, W. B. (1964). "Glacier Geophysics," Science, vol. 146, no. 3642, pp. 353-365.

Kamb, W. B. and Shreve, R. L. (1966). "Results of a New Method for Measuring Internal Deformation in Glaciers," Trans. Amer. Geophys. Union, vol. 47, p. 190.

Kamb, W. B. and Shreve, R. L. (unpublished).

Kanesewich, E. R. (1963). "Gravity Measurements on the Athabasca Glacier, Alberta, Canada," Jour. Glaciol., vol. 4, pp. 617-630.

Keller, G. V. and Frischknect, F. C. (1961). "Induction and Galvanic Resistivity Studies on the Athabasca Glacier, Alberta, Canada," Geology of the Arctic, vol. 2, pp. 809-832.

Lliboutry, L. (1968). General Theory of Sub-glacial Cavitation and Sliding of Temperate Glaciers," Jour. Glaciol., vol. 7, no. 49, pp. 21-58.

Mathews, W. H. (1959). "Vertical Distribution of Velocity in Salmon Glacier, B. C.," Jour. Glaciol., vol. 3, no. 26, pp. 448-454.

Mathews, W. H. (1964). "Water Pressure Under a Glacier," Jour. Glaciol., vol. 5, no. 38, pp. 235-240.

Meier, M. F. (1960). Mode of Flow of Aaskatchewan Glacier, Alberta, Canada, U.S. Geol. Surv. Profess., paper 351.

Meier, M. F., Allen, C. R., Kamb, W. B., and Sharp, R. P. (unpublished). Surface Velocity and Surface Strain Data from Lower Blue Glacier, Washington.

Mercanton, P. L. (1916). "Vermessungen am Rhone Gletcher 1874-1915," Neue Denkschriften der Schweizerishen Naturforschenden Gesellschaft, vol. III.

Mood, A. M. (1950). Introduction to the Theory of Statistics. McGraw-Hill Book Company, Inc.

Nakaya, U. (1958). Mechanical Properties of Single Crystals of Ice. Part 1. Geometry of Deformation, SIPRE Research Report 28.

Nielsen, L. E. (1955). "Regimen and Flow in Equilibrium Glaciers," Bull. Geol. Soc. Amer., vol. 66, pp. 1-8.

Nye, J. F. (1951). "The Flow of Glaciers and Ice Sheets as a Problem in Plasticity," Proc. Roy. Soc. London, ser. A, vol. 207, pp. 554-572.

Nye, J. F. (1952). "The Mechanics of Glacier Flow," Jour. Glaciol., vol. 2, pp. 82-93.

Nye, J. F. (1953). "The Flow Law of Ice from Measurements in Glacier Tunnels, Laboratory Experiments and the Jungfraufirm Borehole Experiments," Proc. Roy. Soc. London, ser. A, vol. 219, no. 1139, pp. 477-489.

Nye, J. F. (1957). "The Distribution of Stress and Velocity in Glaciers and Ice Sheets," Proc. Roy. Soc. London, ser. A, vol. 239, pp. 113-133.

Nye, J. F. (1959). "A Method of Determining the Strain-Rate Tensor at the Surface of a Glacier," Jour. Glaciol., vol. 3, pp. 409-419.

Nye, J. F. (1960). "The Response of Glaciers and Ice Sheets to Seasonal and Climatic Changes," Proc. Roy. Soc. London, ser. A., vol. 256, no. 1287, pp. 559-584.

Nye, J. F. (1965). "The Flow of a Glacier in a Channel of Rectangular, Elliptic, or Parabolic Cross Section," Jour. Glaciol., vol. 5, pp. 661-690.

Paterson, W. S. B. (1962). Observations on Athabasca Glacier and their Relationship to Theory of Glacier Flow, Ph.D. Thesis, Univ. of B.C., Canada, 158 pp.

Paterson, W. S. B. and Savage, J. C. (1963a). "Geometry and Movement of the Athabasca Glacier," Jour. Geophys. Res., vol. 68, no. 15, pp. 4513-4520.

Paterson, W. S. B., and Savage, J. C. (1963b). "Measurements on Athabasca Glacier Relating to the Flow Law of Ice," Jour. Geophy. Res., vol. 68, no. 15, pp. 4537-4543.

Paterson, W. S. B. (1964). "Variations in Velocity of Athabasca Glacier with Time," Jour. Glaciol., vol. 3, pp. 277-285.

Reid, I. A. (1961). Triangulation Survey of the Athabasca Glacier July 1959. Water Resources Branch, Department of Northern Affairs and National Resources, Ottawa.

Rigsby, G. P. (1953). Studies of Crystal Fabrics and Structures in Glaciers, Ph.D. Thesis, Calif. Inst. of Tech., Pasadena.

Rigsby, G. P. (1957). Effect of Hydrostatic Pressure on Velocity of Shear Deformation of Single Ice Crystals, SIPRE Research Report 32.

Robin, G. de Q. (1967). "Surface Topography of Ice Sheets," Nature, vol. 215, no. 5105, pp. 1039-1032.

Savage, J. C. and Paterson, W. S. B. (1963). "Borehole Measurements in the Athabasca Glacier," Jour. Geophys. Res., vol. 68, no. 15, pp. 4521-4536.

Sharp, R. P. (1953). "Deformation of a Borehole in the Malispina Glacier, Alaska," Bull. Geol. Soc. Amer., vol. 64, pp. 97-100.

Sharp, R. P. (1960). Glaciers, Univ. of Oregon Press, Eugene.

Shreve, R. L. (1961). "The Borehole Experiment on the Blue Glacier, Washington," Int. Assoc. Sci. Hydrol., Publ. 54, pp. 530-531.

Shreve, R. L. and Sharp, R. P. (unpublished). "Internal Deformation and Thermal Anomalies in Lower Blue Glacier, Mount Olympus, Washington, U.S.A."

Topographical Survey (1962). Athabasca Glacier, Dept. of Mines and Technical Surveys, Ottawa.

Weertman, J. (1964). "The Theory of Glacier Sliding," Jour. Glaciol., vol. 5, no. 39, pp. 287-303.

TABLE 1

CHRONOLOGY OF BOREHOLE OPERATIONS

	1966		1967		1968	
Borehole	Initial Boring	Inclino-metry	First Recovery	Inclino-metry	Second Recovery	Inclino-metry
1A	7/13-7/22	7/24	7/22-7/28	7/29		
1B	7/26-8/2	8/2	8/4 -8/10	8/11		
1C	8/17-8/22	8/23	7/11-7/19	7/21		
2A	8/20-8/25	8/25	8/15-8/23	8/24	7/28-7/30	7/30
2B	7/27-8/3	8/3	8/8 -8/21	8/22		
3A	8/9-8/15	8/16	7/1 -7/14	7/15		
3B	8/9-8/16	8/17	7/31-8/4	8/5	7/13-7/19	7/20
4A	8/28-8/29		8/24-8/25	8/25		
5A	8/31-9/4	9/4	6/29-7/6	7/9		

TABLE 2

INITIAL STAKE AND BOREHOLE LOCATIONS

a. Locations of surface markers 8 September 1966
Unit co-ordinate equals 1 m

	W	S	U	x	y	z
7C	3441.03	5955.81	414.43	-166.10	7.03	-390.41
3C	3655.77	5831.11	416.26	-154.99	4.44	-143.21
2C	3916.34	5681.52	420.21	-144.16	-0.26	157.90
6C	4181.89	5534.21	412.10			
7A	3364.18	5827.88	402.73	-16.67	8.57	-399.12
5A	3449.91	5777.26	406.59	-11.89	4.38	-299.69
3A	3579.74	5702.06	407.84	-5.63	2.70	-149.79
1A	3709.73	5627.41	410.15	0.	0.	0.
2A	3839.97	5553.17	409.39	5.36	0.40	149.82
4A	3970.44	5479.75	405.68	10.09	3.79	299.46
6A	4101.80	5408.25	405.69	12.46	3.62	499.00
8A	4190.58	5363.39	409.53			
5B	3373.96	5648.53	399.73	137.50	1.07	-307.22
1B	3632.85	5500.42	399.71	148.53	0.34	-9.17
4B	3895.00	5350.05	396.57	160.26	2.69	292.82

b. Locations of boreholes 8 September 1966
Unit co-ordinate equals 1 m

	W	S	U	x	y	z
1C	3785.52	5753.13	419.10	-146.80	1.04	8.79
5A	3449.58	5783.22	406.59	-17.01	4.73	-302.75
3A	3578.33	5699.73	406.84	-2.92	2.51	-149.95
1A	3709.73	5627.41	410.15	0.	0.	0.
2A	3839.51	5557.38	409.70	1.83	0.33	147.46
4A	3960.58	5467.85	405.36	25.19	3.08	296.25
3B	3508.65	5580.11	401.43	135.49	-0.50	-156.16
1B	3639.99	5505.74	400.15	138.77	0.56	-8.48
2B	3765.63	5434.66	399.33	145.20	0.95	138.96

TABLE 3

SURFACE VELOCITIES

Units: velocity, m yr^{-1}; azimuth, degrees east of north; plunge, degrees above horizontal

Stakes 66 - 67	V	Azimuth	Plunge	u†	v‡	w†	Interval
7C	34.47	39.1	2.6	34.23	-3.90	-1.30	9/8/66 - 7/13/67
3C	50.39	37.6	1.7	50.15	-4.90	-0.57	9/8/66 - 7/13/67
2C	52.61	35.6	-0.5	52.50	-3.12	1.22	9/8/66 - 7/13/67
6C	32.42	36.5	1.7	32.26	-3.15	0.28	9/8/66 - 7/13/67
7A	31.25	37.2	6.3	30.76	-5.53	-0.13	9/8/66 - 7/13/67
5A	40.39	37.7	3.7	40.03	-5.37	-0.49	9/8/66 - 7/13/67
3A	46.85	37.1	2.5	46.56	-5.23	-0.15	9/8/66 - 7/13/67
1A	49.92	36.3	-0.1	49.80	-3.33	0.53	9/8/66 - 7/13/67
2A	51.10	36.3	-1.0	51.02	-2.63	0.63	9/8/66 - 7/28/67
4A	47.56	36.4	-0.3	47.46	-2.96	0.48	9/8/66 - 7/28/67
6A	34.79	36.9	1.2	34.66	-3.08	0.06	9/8/66 - 7/28/67
5B	38.52	37.3	3.7	38.11	-5.58	-0.26	9/8/66 - 7/13/67
1B	47.04	37.1	0.8	46.88	-3.89	-0.14	9/8/66 - 7/13/67
4B	43.73	37.6	1.4	43.54	-4.01	-0.48	9/8/66 - 7/13/67
Boreholes 66 - 67							
1C	54.05	36.2	1.0	53.84	-4.64	0.66	9/8/66 - 7/28/67
5A	41.28	37.5		41.25		-0.43	9/8/66 - 7/28/67
3A	47.84	37.0	1.7	47.62	-4.63	-0.02	9/8/66 - 7/28/67
1A	49.92	36.3	-0.1	49.80	-3.33	0.53	9/8/66 - 7/13/67
2A	51.04	36.0	-1.0	50.97	-2.61	0.84	9/8/66 - 7/28/67
4A	47.31	36.6	0.1	47.19	-3.28	0.33	9/8/66 - 7/28/67
3B	45.18	36.8	2.1	44.94	-4.70	0.12	9/8/66 - 7/28/67
1B	48.17	37.1	-0.2	48.07	-3.08	-0.14	9/8/66 - 7/28/67
2B	47.94	37.2		47.87		-0.21	9/8/66 - 7/28/67
Boreholes 67 - 68							
5A	37.01	37.6		36.95		-0.44	7/28/67 - 7/28/68
3A	43.15	36.8		43.12		0.08	7/28/67 - 7/28/68
1A	47.21	36.6		47.20		0.27	7/13/67 - 7/28/68
2A	46.11	36.4		46.10		0.46	7/28/67 - 7/28/68
4A	42.53	36.8		42.53		0.08	7/28/67 - 7/28/68
3B	40.09	37.5		40.06		-0.35	7/28/67 - 7/28/68
1B	43.02	37.0		42.99		-0.04	7/28/67 - 7/28/68
2B	46.11	36.4		42.62		-0.34	7/28/67 - 7/28/68

† standard error 0.20 m yr^{-1} ‡ standard error 0.35 m yr^{-1}

TABLE 4

TIME VARIATION OF SURFACE VELOCITY

u_{67} is average velocity over interval 9/6/66 - 7/28/67.

u_{68} is average velocity over interval 7/28/67 - 7/28/68.

$\delta_e = u_{67} \frac{\partial u_{67}}{\partial x} X$ 1 yr is change expected if velocity field were time-independent.

$\delta_m = u_{68} - u_{67}$ is measured change in velocity.

$\delta = \delta_m - \delta_e$ gives change in velocity resulting from time variation of the velocity field.

Units: m yr^{-1}

Borehole	δ_e	δ_m	$\delta^\dagger$
1A	-1.12	-3.84	-2.72
1B	-1.11	-4.08	-2.97
2A	-1.02	-4.87	-3.85
2B	-1.05	-5.15	-4.10
3A	-1.05	-5.50	-3.45
3B	-0.90	-4.88	-3.98
4A	-0.80	-4.66	-3.86
5A	-0.74	-4.30	-3.56

† standard error 0.35 m yr^{-1}

TABLE 5

SURFACE STRAIN RATE

$e_{x'x'}$
$e_{z'z'}$ are tabulated in units yr^{-1}.
$e_{x'z'}$

Arrangement is geographical; tabulated values apply to the center of the square within which they are listed.

Sections	7	5	3	1	2	4	6	8
E	-0.021 -0.002 0.048	-0.026 0.005 0.026	-0.024 0.007 0.009	-0.021 0.008 -0.003	-0.019 0.001 -0.014		-0.004 0.045 -0.142	
C	-0.019 -0.002 0.051	-0.021 0.005 0.025	-0.022 0.004 0.011	-0.020 0.003 -0.011	-0.019 0.000 -0.015	-0.009 0.002 -0.051	-0.005 0.050 -0.141	
A	-0.010 -0.002 0.049	-0.016 0.003 0.021	-0.020 0.001 0.010	-0.023 -0.001 -0.002	-0.023 -0.002 -0.013	-0.016 0.004 -0.040	-0.012 0.045 -0.123	
B	-0.010 -0.000 0.056	-0.017 0.001 0.014	-0.023 0.000 0.005	-0.025 -0.002 -0.002	-0.022 -0.002 -0.012	-0.016 0.005 -0.037	-0.019 0.043 -0.114	
D	-0.007 0.000 0.051	-0.012 -0.001 0.013	-0.015 0.001 0.001	-0.017 0.000 -0.004	-0.016 -0.005 -0.011	-0.018 0.009 -0.033	-0.028 0.048 -0.111	
F								

Lines

Standard error for $e_{x'x'}$ and $e_{z'z'}$ 0.0007 yr^{-1}.

Standard error for $e_{x'z'}$ 0.0006 yr^{-1}.

TABLE 6

TIME VARIATION OF SURFACE STRAIN RATE

$\frac{\partial u}{\partial x_\beta}$ 67 is average surface strain rate over interval 66-67.

$\frac{\partial u}{\partial x_\beta}$ 68 is average surface strain rate over interval 67-68.

Numbers on horizontal line segments give $\frac{\partial u}{\partial z}$ 68 - $\frac{\partial u}{\partial z}$ 67 half way between the ends of the segment.

Numbers on vertical line segments give $\frac{\partial u}{\partial x}$ 68 - $\frac{\partial u}{\partial x}$ 67 half way between the ends of the segment.

Units: yr^{-1}

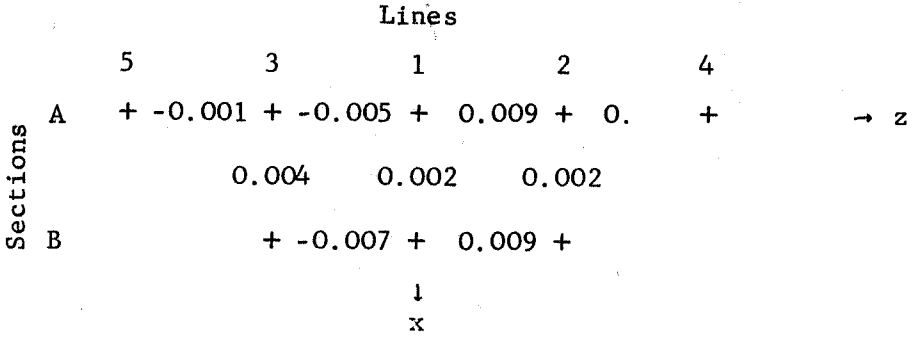

Standard error 0.003

TABLE 7

AZIMUTH OF TILT AT THE SURFACE IN DEFORMED BOREHOLES

A_1 = azimuth of tilt in boreholes.
A_2 = azimuth of local surface slope.
A_3 = azimuth of local surface velocity.
A4 = azimuth of mean surface velocity.

Units: degrees east of north

Borehole	A_1	A_2	A_3	A_4
1A	-52	33	36.3	36.9
1B	-140	24	37.1	36.9
1C	-46	40	36.2	36.9
2A		23	36.0	36.9
2B		30	37.2	36.9
3A	-52	51	37.0	36.9
3B	-40	40	36.8	36.9
4A	+133	27	36.6	36.9
5A	-37	58	37.5	36.9

TABLE 8

TIME RATE-OF-CHANGE OF $\frac{\partial u}{\partial y}$ IN BOREHOLES

$\frac{\partial}{\partial t}\frac{\partial u}{\partial y}$ is calculated from equation (2b) of Chapter IV.

Borehole 2A		Borehole 3B	
depth y(m)	$\frac{\partial}{\partial t}\frac{\partial u}{\partial y}(yr^{-2})$	depth y(m)	$\frac{\partial}{\partial t}\frac{\partial u}{\partial y}(yr^{-2})$
0	+0.002	0	-0.004
50	-0.004	50	-0.006
100	-0.008	100	-0.002
150	-0.006	150	-0.007
200	-0.003	200	-0.002
250	+0.002	250	0.000
300	0.000	285	+0.031

TABLE 9

COMPARISON OF VALUES OF v AT THE SURFACE AND BED

v_s = surface velocity given by triangulation

$v_b = \alpha_x^b u_b + \alpha_z^b w_b$

where α_x^{b*} is the longitudinal slope of the bed with respect to the x axis and α_z^{b*} is the transverse slope of the bed with respect to the z axis.

$$v_p = v(y_s) - \int_{y_s}^{y_b} \left(\frac{\partial u}{\partial x} + \frac{\partial w}{\partial z} \right) dy$$

where y_s and y_b give the location on the y-axis of the surface and bed.

units: m yr^{-1}

Borehole	v_s †	v_b ‡	v_p	$v_b - v_p$	$v_b - v_s$
1A	-3.3	+0.7	-0.5	+1.2	+4.0
1B	-3.5	+0.8	-0.9	+1.7	+4.3
2A	-2.6	+1.0	+0.3	+0.7	+3.6
2B	-3.6§	+0.5	+1.5	-0.5	+4.1
3A	-4.9	-0.9	-1.4	+0.5	+4.0
3B	-4.7	-0.9	-1.8	+0.9	+3.8
5A	-5.4	-2.1§	-1.1	-1.0	+3.3

* Slopes of the bed with respect to the surface were determined by differencing of borehole depths. Where the comparison can be made the slopes thus calculated agree well with the seismic results of Paterson and Savage (1963a).

† Standard error 0.35 m yr^{-1} (except as noted).

‡ Standard error 0.5 m yr^{-1} (except as noted).

§ Standard error 0.8 m yr^{-1}.

TABLE 10

SUMMARY OF STANDARD ERRORS FOR FLOW QUANTITIES AT BOREHOLES

	u, w (m yr^{-1})	v (m yr^{-1})	e_{xy}, e_{yz} (yr^{-1})	e_{xx}, e_{zz} (yr^{-1})	e_{xz} (yr^{-1})
Surface	0.22	0.35	0	0.001	0.001
Depth of 300 m	0.46	0.5	0.003	0.004	0.003

TABLE 11

WIDTH RATIOS OF LONGITUDINAL VELOCITY CONTOURS

Section A

u contour (m yr^{-1})	50	48	46	44
width ratio	0.89	0.97	1.00	1.04

Section B

u contour (m yr^{-1})	48	46	44	42
width ratio	0.61	0.83	0.90	0.95

TABLE 12

ROTATION AT THE SURFACE

Rotation rates acting at the glacier surface as estimated from borehole tilt data giving $\frac{\partial u'}{\partial y'}$ and $\frac{\partial w'}{\partial y'}$ (r), triangulation data giving $\frac{\partial v'}{\partial x'}$ and $\frac{\partial v'}{\partial z'}$ (t), and surface slope data (s) are compared.

	$\omega_{y'x'}$ (yr^{-1})			$\omega_{y'z'}$ (yr^{-1})		
Borehole	r	t	s	r	t	s
1A	-0.001	+0.004	-0.002	+0.012	+0.008	+0.004
1B	-0.003		-0.005	+0.002		+0.002
1C	-0.001		+0.002	+0.008	+0.006	+0.002
2A	-0.003		+0.001	-0.002	+0.001	0.
2B	-0.004		-0.003	-0.003	-0.002	0.
3A	-0.002	+0.001	0.	+0.010	+0.007	+0.002
3B	-0.002		0.	+0.017	+0.007	+0.001
4A	-0.003		0.	-0.013	-0.002	-0.002
5A	-0.002		0.	+0.010	+0.002	+0.001
Standard error	0.003	0.003		0.004	0.003	

TABLE 13

EFFECTS OF BENDING

The observed difference in longitudinal strain rate $\Delta\frac{\partial u}{\partial y}$ (between the ice surface and the bed) is compared with value produced by bending as estimated from borehole tilt data (r), triangulation data (t), surface curvature gradient (s), and bed curvature gradient (b).

	$\frac{\partial u}{\partial x}$ (yr^{-1})	$-H\frac{\partial \omega_{x'y'}}{\partial x'}$ (yr^{-1})			
Flow line		r	t	s	b
1	+0.022	+0.004	+0.020	+0.004	+0.020
2	+0.016	+0.002		+0.006	
3	+0.012	+0.	-0.003	-0.003	
Standard error	0.002	0.008	0.006		

TABLE 14

LATERAL FLUX

$\langle w \rangle_{H(z)}$ as observed, and predicted by equation (5) of Chapter VI are compared.

Line	Observed	Predicted
1	-0.68	-0.29
2	+0.54	+0.63
3	-0.89	-1.17
4		+1.58
5	-1.76	-2.04

TABLE 15

DEPTHS OF SIGNIFICANT POINTS IN LOG η VS. LOG $\dot{\epsilon}$ PLOTS

d_1 = depth above which curvature of the smoothed longitudinal tilt profile is not determined.

d_2 = depth at which $\dot{\epsilon}$ reaches a minimum value.

d_3 = depth below which the log η vs. log $\dot{\epsilon}$ plot is approximately linear.

Depths are given in meters.

Borehole	d_1	d_2	d_3
1A	40	100	240
1B	150	165	235
1C	150	70	170
2A	100	105	215
2B	50	140	275
3A	75	95	185
3B	75	95	200
4A	50	75	
5A	100	75	155

TABLE 16

POWER LAW PARAMETERS AS DETERMINED FROM LINEAR DEPTH DEPENDENCE OF SHEAR STRESS

Borehole	α	B bar $yr^{1+\alpha}$
1A	0.82	0.78
1B	0.67	1.32
2A	0.56	1.82
2B	0.88	0.68
3A	0.86	0.69
3B	0.98	0.50
5A	0.69	1.17
all holes	0.81	0.85

TABLE 17

POWER LAW PARAMETERS AS DETERMINED BY
LEAST SQUARE MINIMIZATION OF RESIDUAL BODY FORCES

Borehole and depth range	α	B (bar $yr^{1+\alpha}$)	rms residual body force (units of ρg_x)
1A (0 - 300)	0.57	1.79	0.310
1A (240 - 300)	0.73	1.39	0.083
1B (0 - 300)	0.53	1.91	0.310
1B (235 - 300)	0.62	1.61	0.287
2B (0 - 295)	1.04	0.51	0.265
2B (275 - 290)	1.09	0.50	0.022
2A (0 - 290)	0.57	2.21	0.138
2A (95 - 250)	0.66	1.63	0.080
3B (0 - 285)	1.07	0.26	0.402
3B (200 - 280)	0.83	0.59	0.166
3A (0 - 280)	0.71	1.79	0.362
3A (75 - 275)	0.70	1.87	0.331
5A (0 - 250)	0.81	0.66	0.372
5A (155 - 240)	0.61	0.96	0.065
all holes with complete depth range, including 4A and 1C	0.72	1.03	0.398
all holes with depth ranges as given in second entry for each hole above	0.68	1.23	0.425

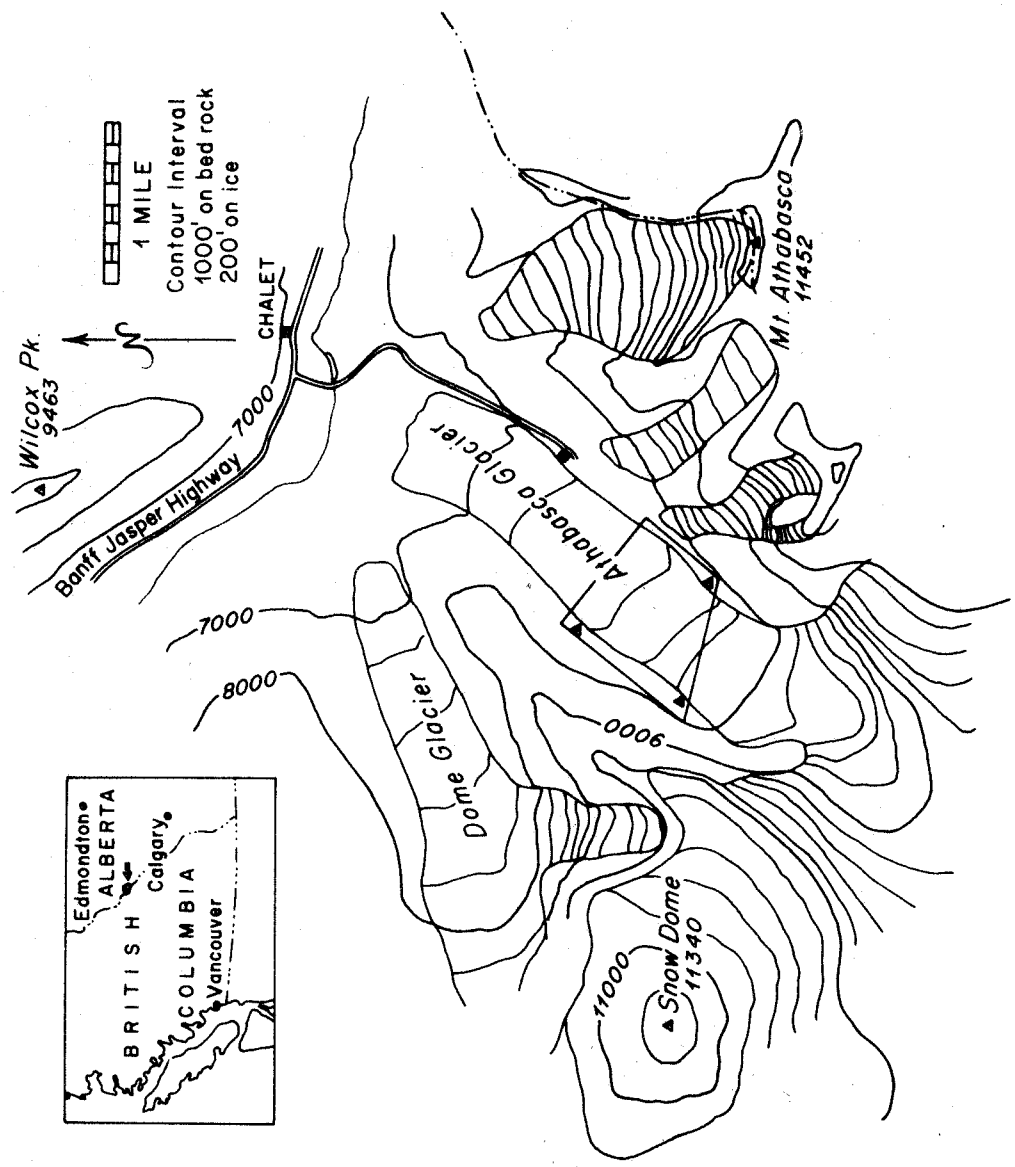

FIGURE 1. MAP OF ATHABASCA GLACIER AND VICINITY

Map modified from Jasper National Park Map (1:190,080) and aerial photographs (1962). Outline shows field area and locations of triangulation stations.

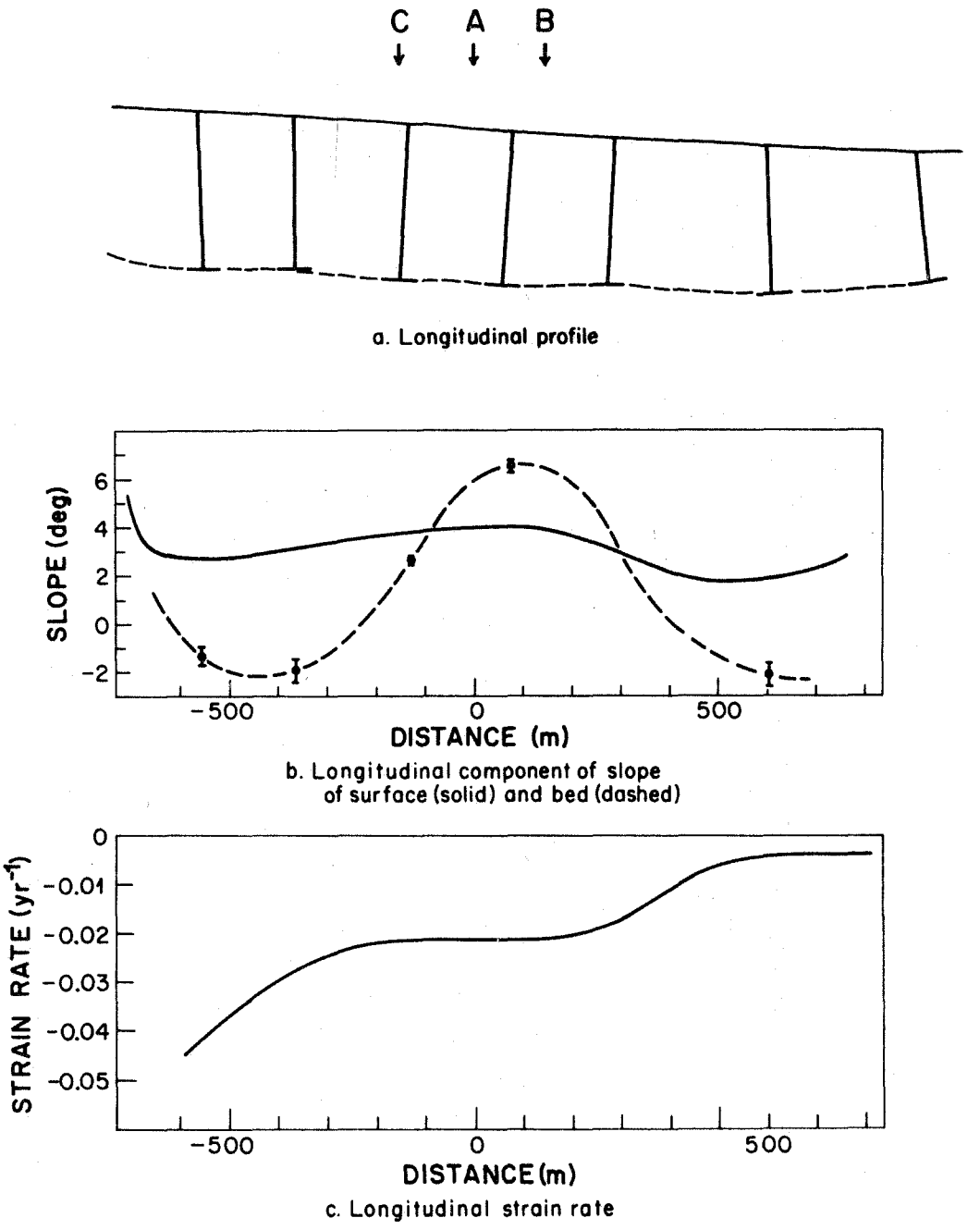

FIGURE 2. CENTER LINE GEOMETRY AND SURFACE STRAIN RATE

Data are from Paterson (1962). Heavy line segments in longitudinal profile represent reflecting surfaces observed in a seismic survey. Errors in bed slope are as given by Paterson (1962). Arrows C, A, and B give locations of cross sections in which boreholes were placed during this field experiment.

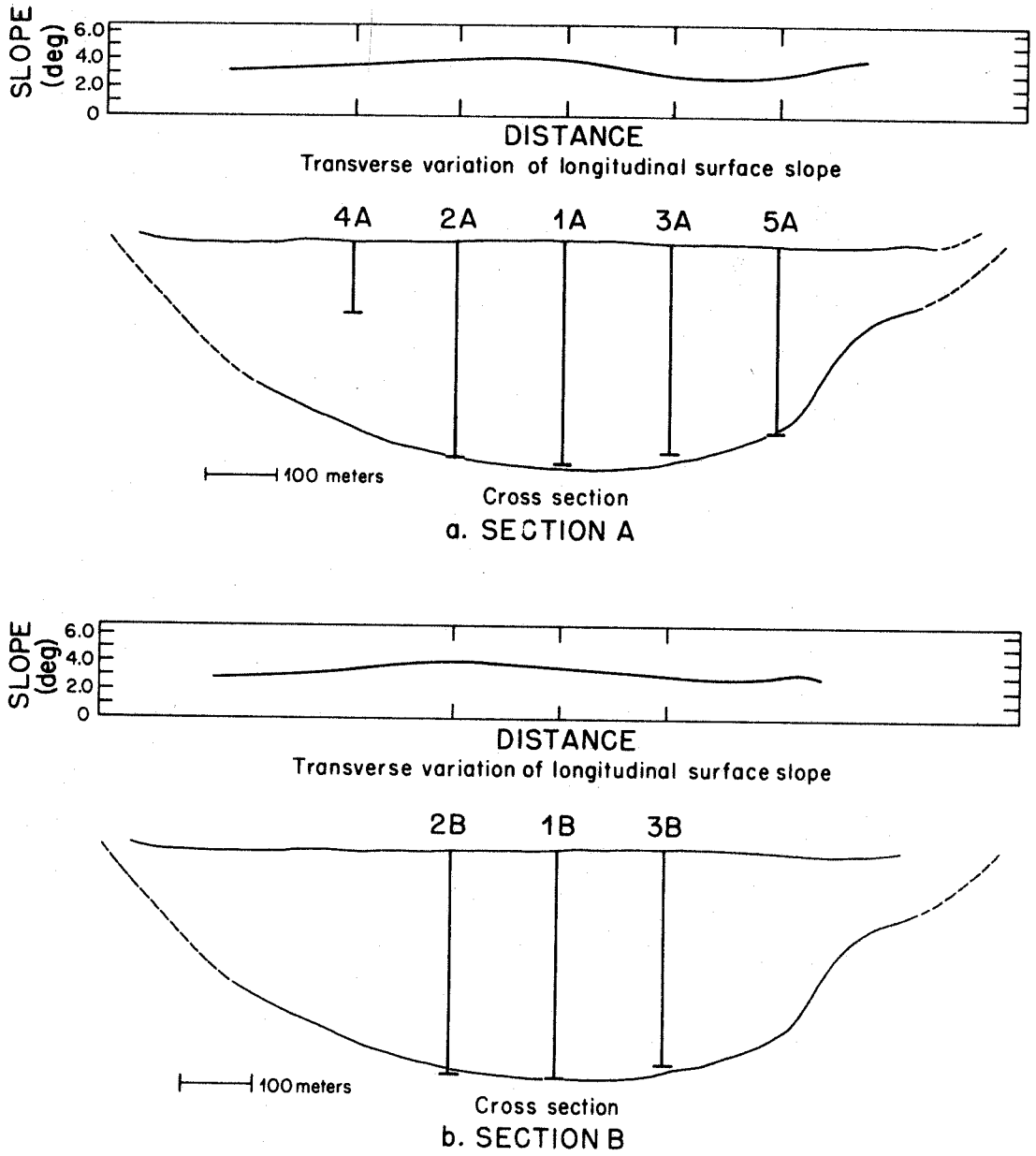

FIGURE 3. CROSS SECTION GEOMETRY

The transverse profile shown is the C-section of Paterson (1962). Surface slopes were measured from the topographic map (Topographic survey, 1962). Vertical lines represent boreholes of the present study.

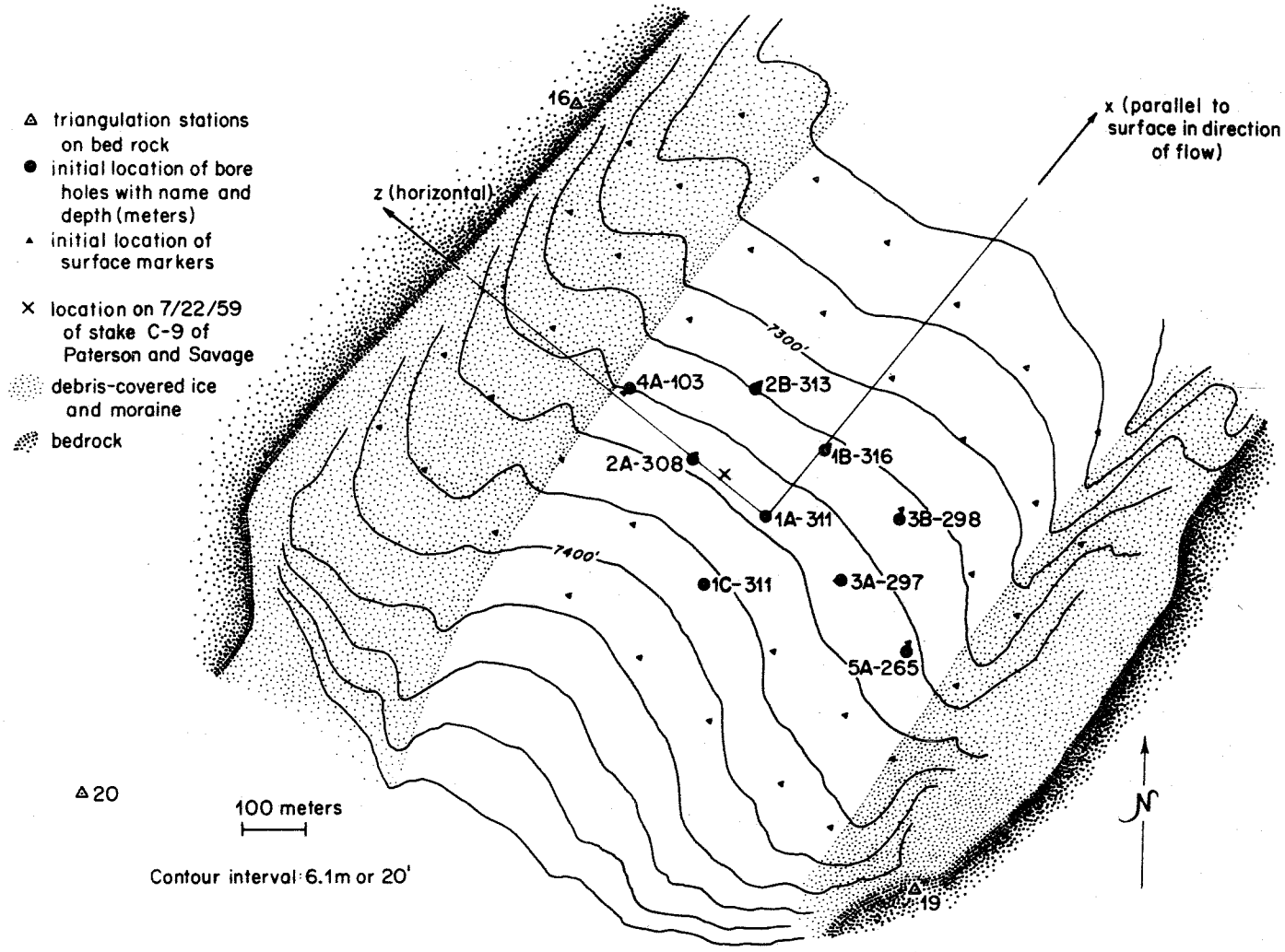

FIGURE 4. TOPOGRAPHIC MAP OF THE FIELD AREA

Topography is from the Athabasca Glacier Map (Topographical Survey, 1962). Elevations on 9/8/66 were approximately 3 meters lower than as shown. Bedrock stations are numbered after Reid (1961).

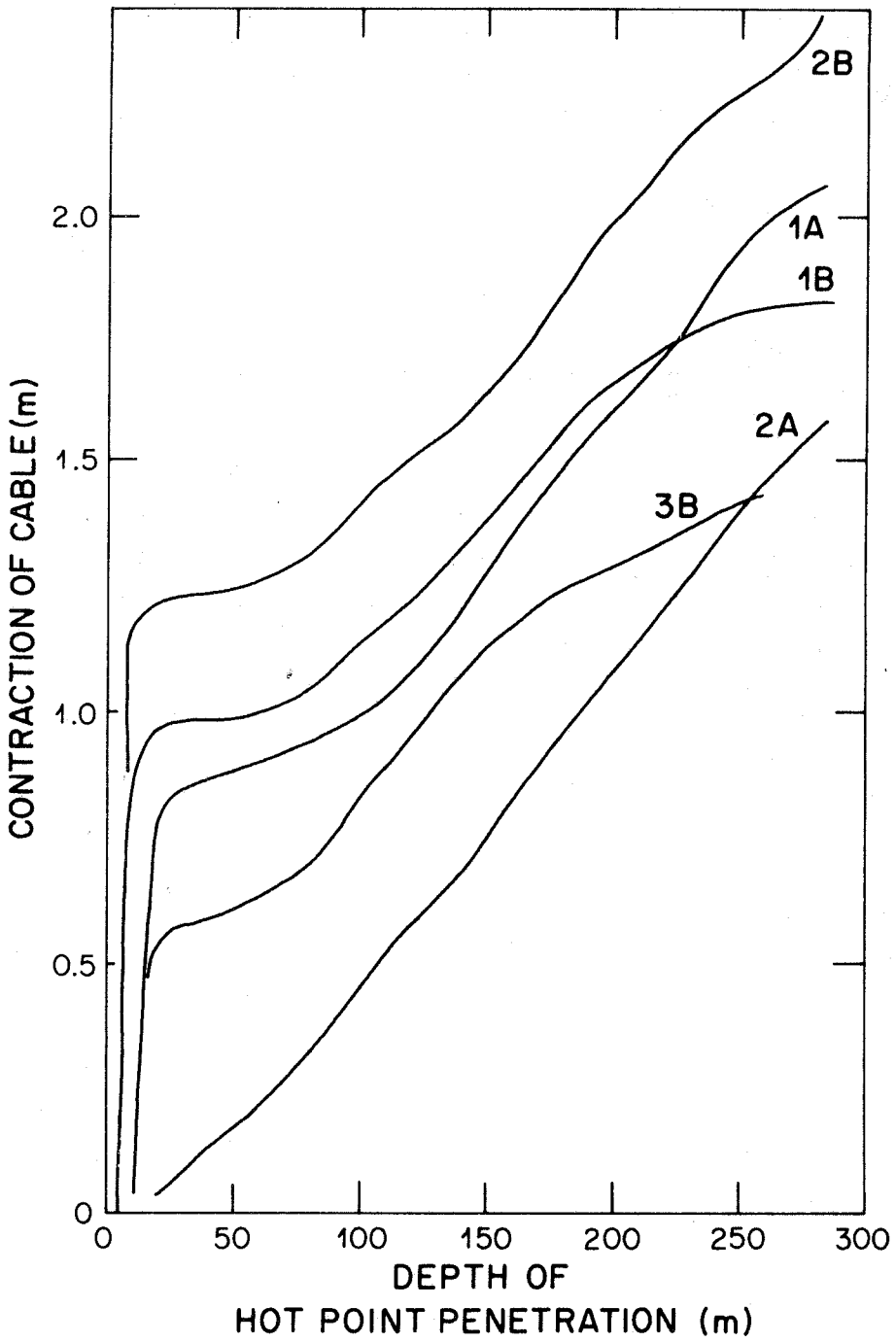

FIGURE 5. RELEASE OF STRAIN IN AIRCRAFT CABLES

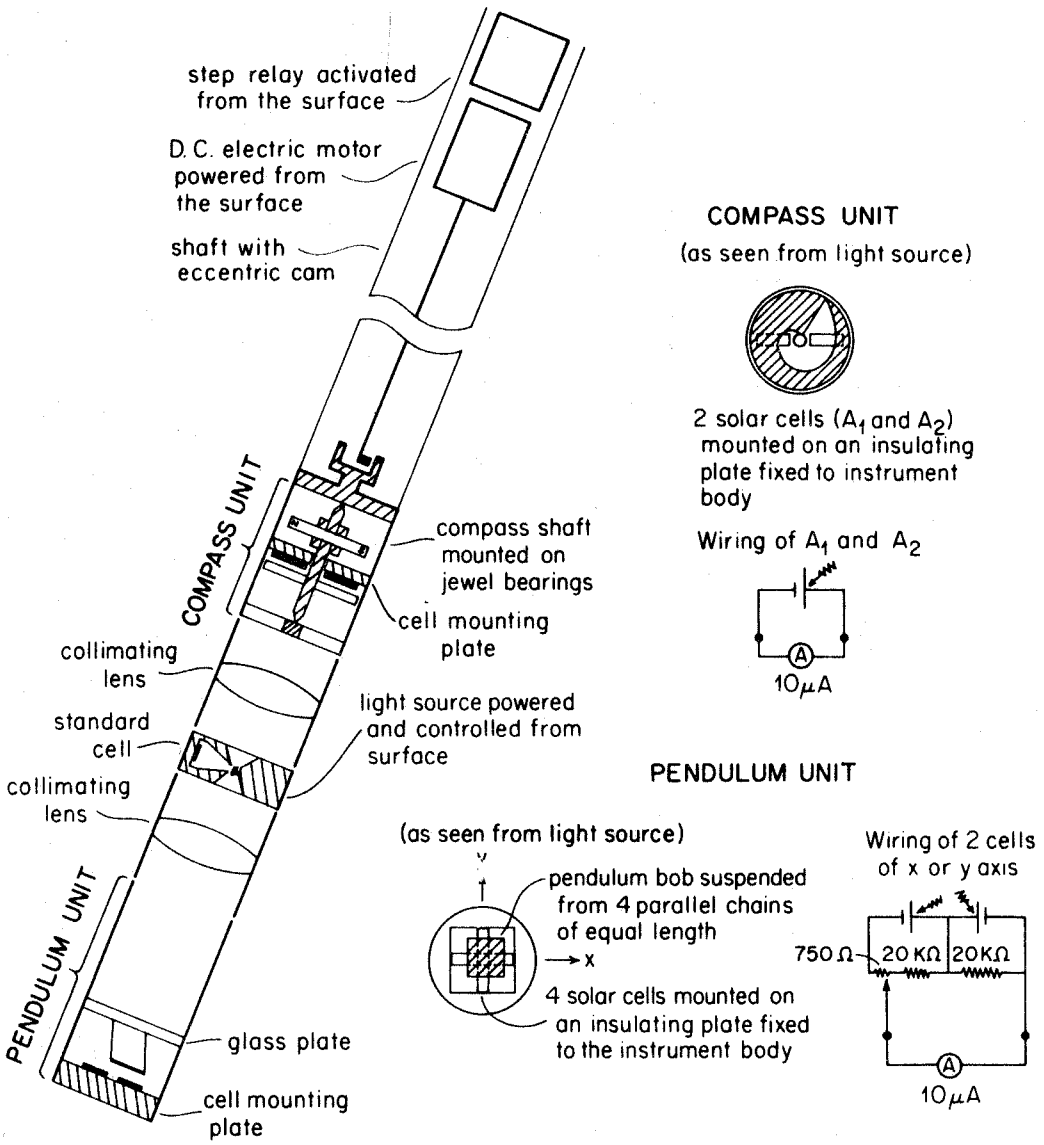

FIGURE 6. ELECTRICAL INCLINOMETER

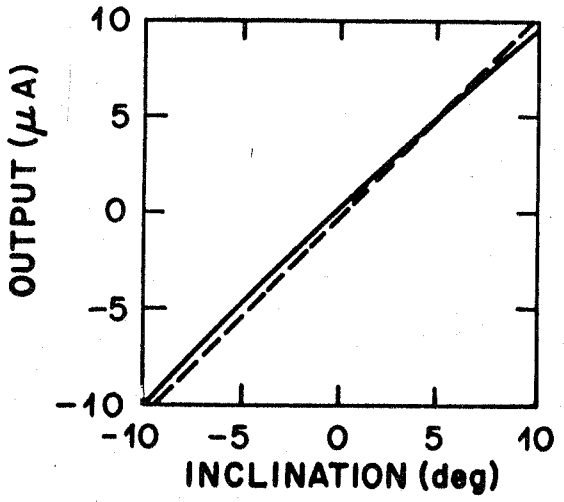

a) Pendulum output

——— y axis

----- x axis

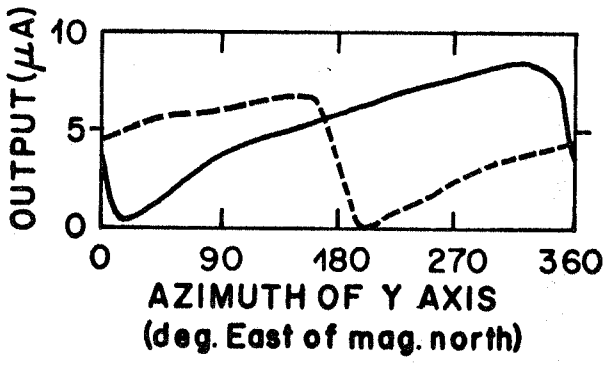

b) Compass output

——— A_1

----- A_2

FIGURE 7. CALIBRATION CURVES FOR ELECTRICAL INCLINOMETER

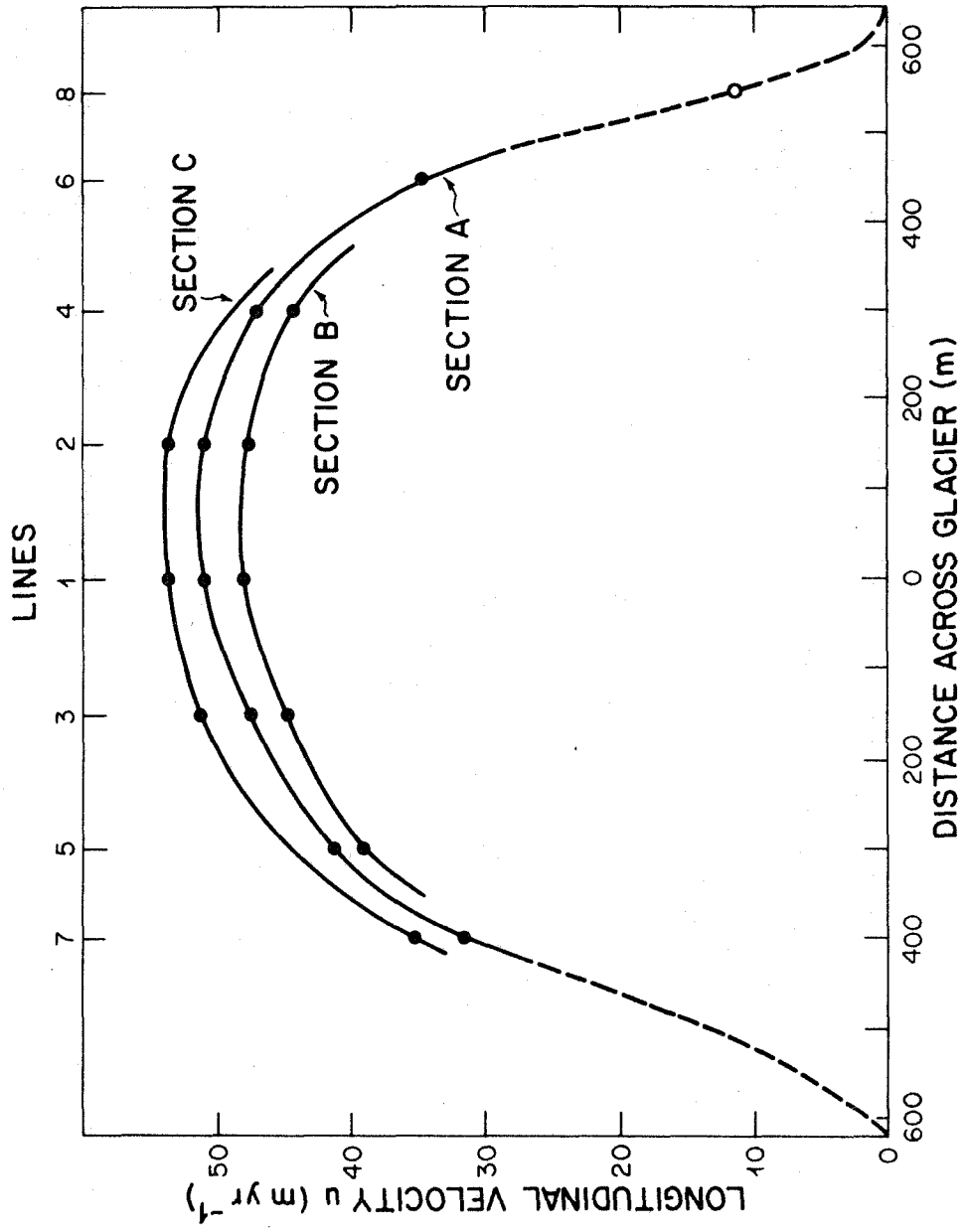

FIGURE 8. LATERAL VARIATION OF SURFACE VELOCITY

Solid circles give velocity of markers determined directly by triangulation. The open circle gives velocity as estimated from measured velocities at adjacent stakes and tape measurements.

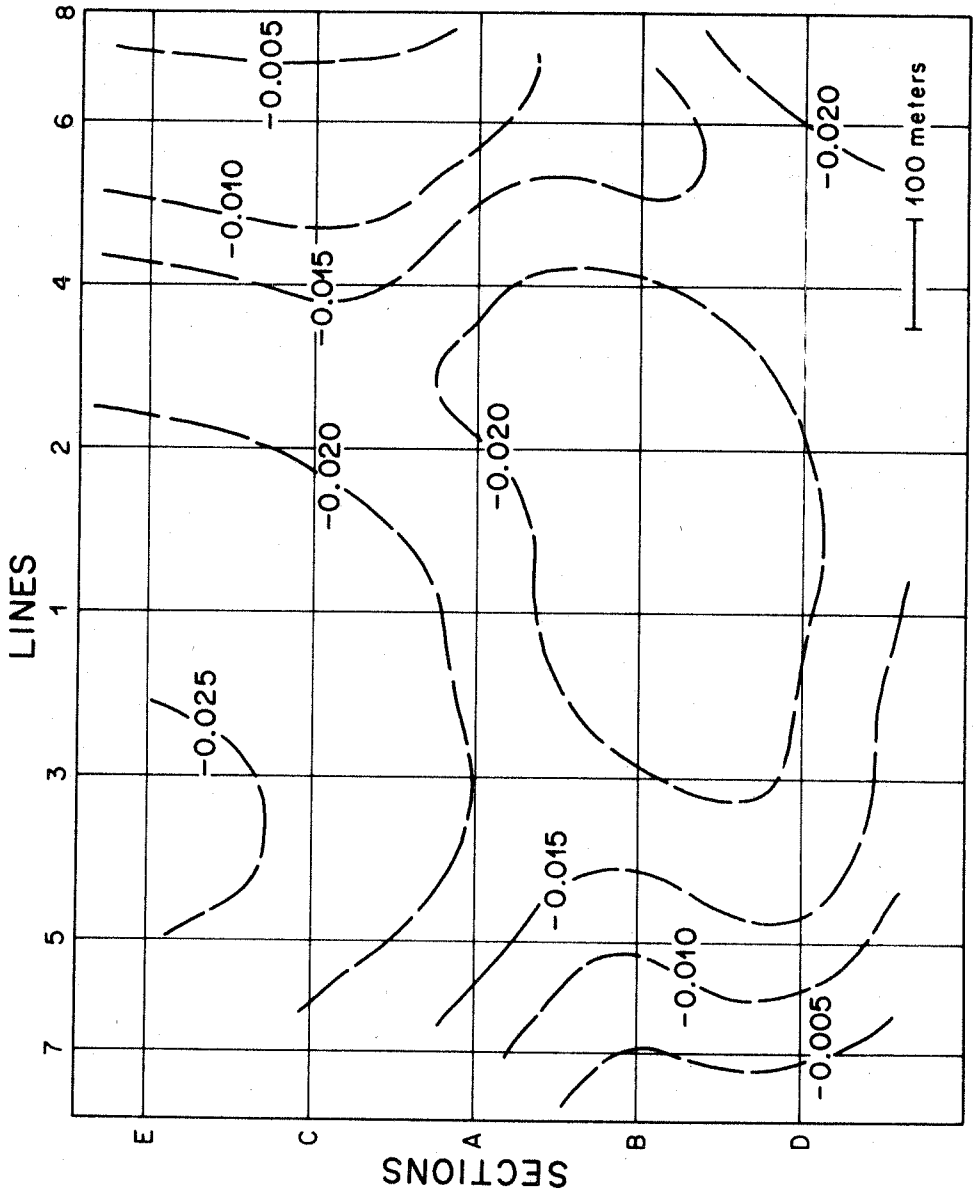

FIGURE 9a. SURFACE STRAIN RATE

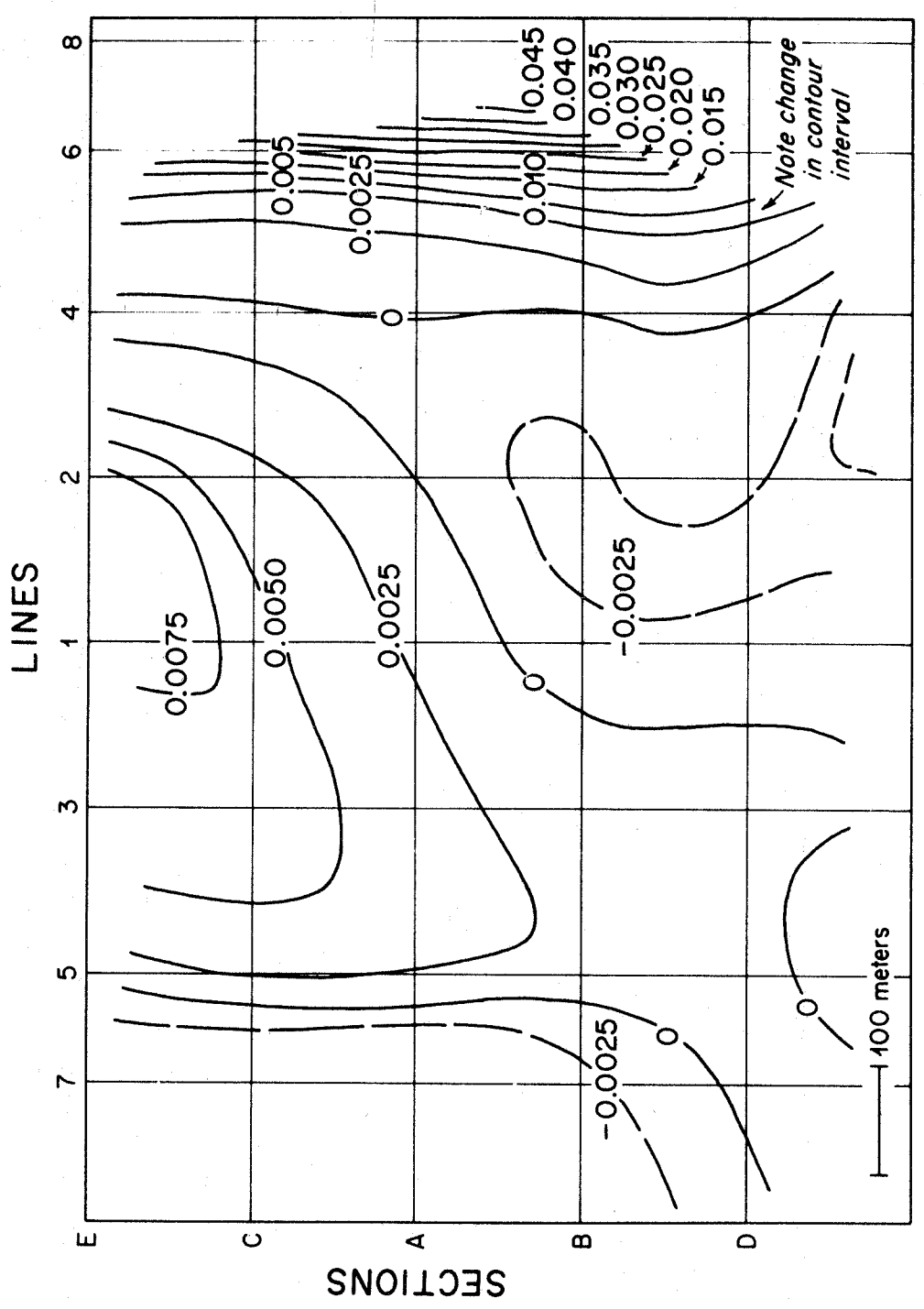

FIGURE 9b. SURFACE STRAIN RATE

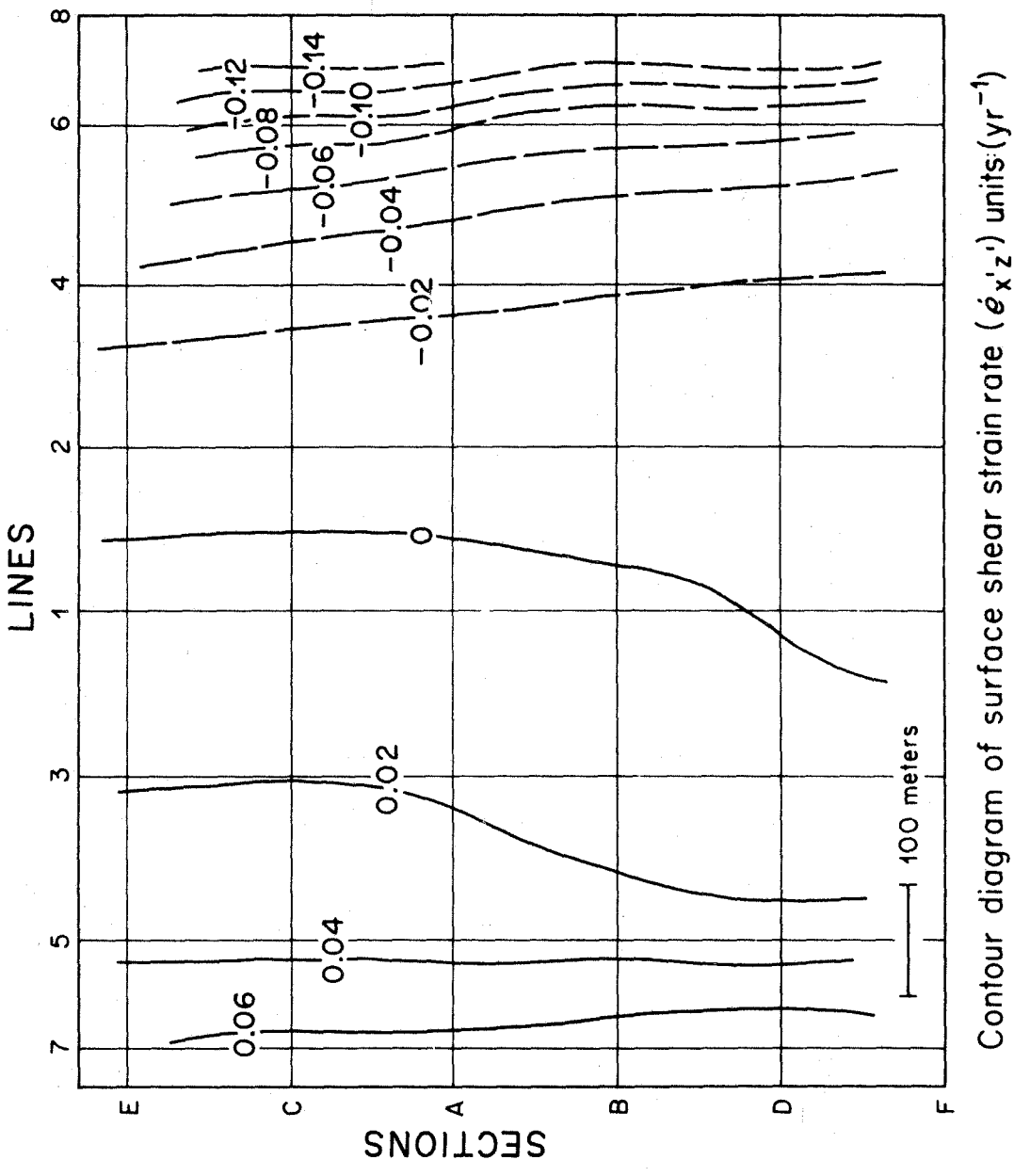

FIGURE 9c. SURFACE STRAIN RATE

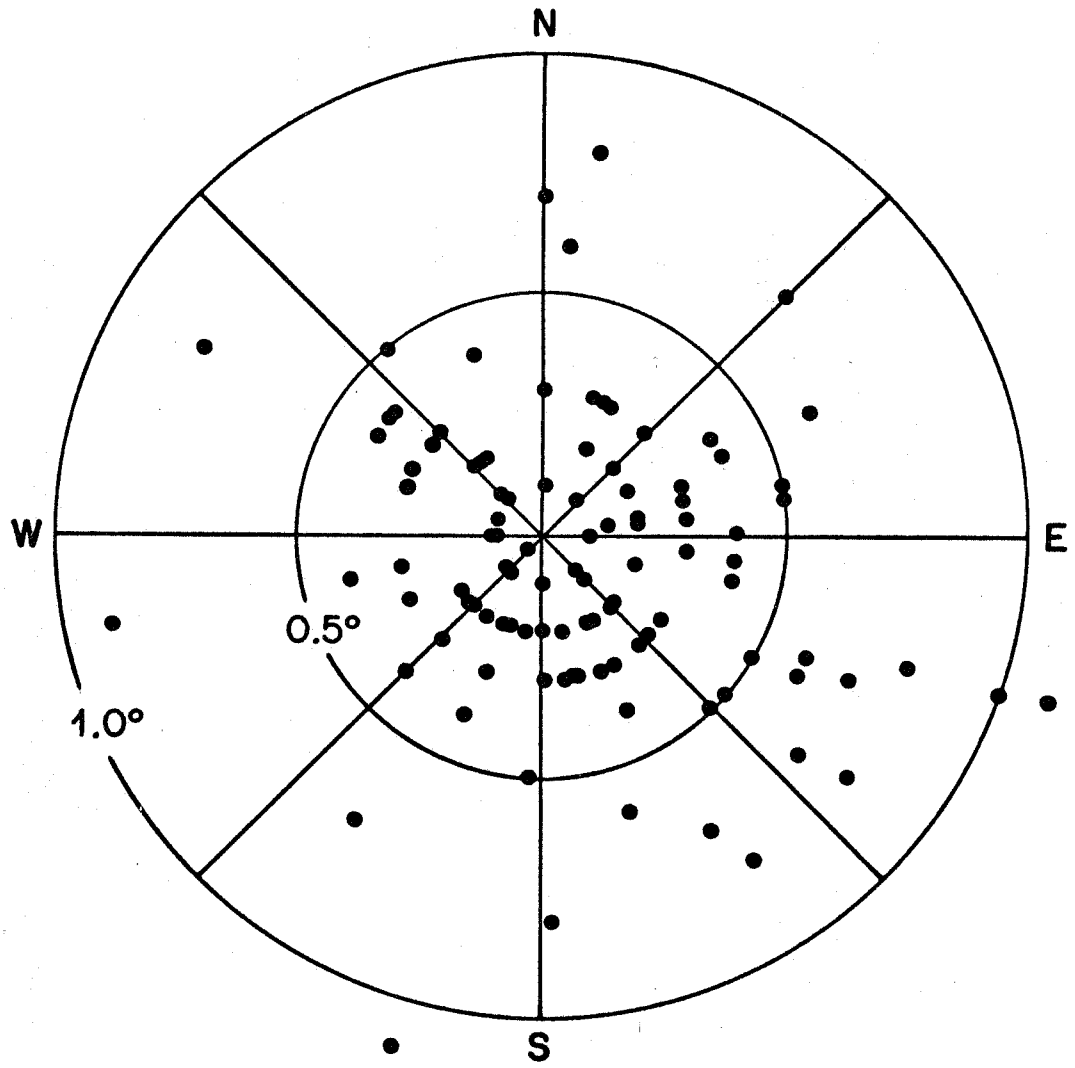

FIGURE 10. TILT MEASUREMENTS IN UNDEFORMED BOREHOLES

FIGURE 11. MAGNITUDE OF TILT IN DEFORMED BOREHOLES

Date gives time of tilt measurement. (See following pages.)

a. Borehole 1A 7/29/67
b. Borehole 1B 8/11/67
c. Borehole 1C 7/21/67
d. Borehole 2A 8/24/67
e. Borehole 2B 8/22/67
f. Borehole 3A 7/15/67
g. Borehole 3B 8/5/67
h. Borehole 4A 8/25/67
i. Borehole 5A 7/9/67
j. Borehole 2A 7/30/68
k. Borehole 3B 7/20/68

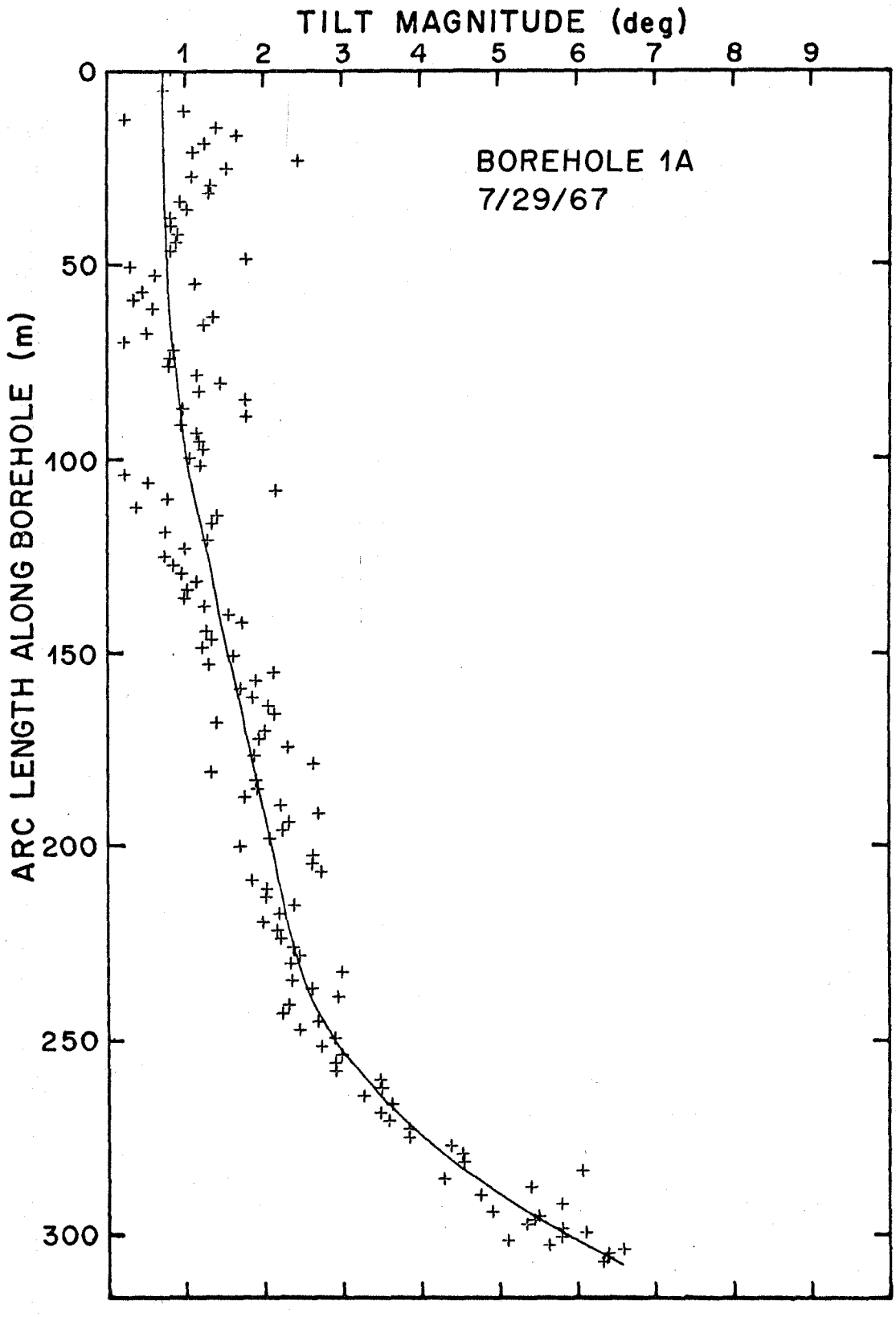
TILT MAGNITUDE (deg)
1
2
3
4
5
6
7
8
9
0
50
100
150
200
250
300
ARC LENGTH ALONG BOREHOLE (m)
BOREHOLE 1A
7/29/67

FIGURE 11a

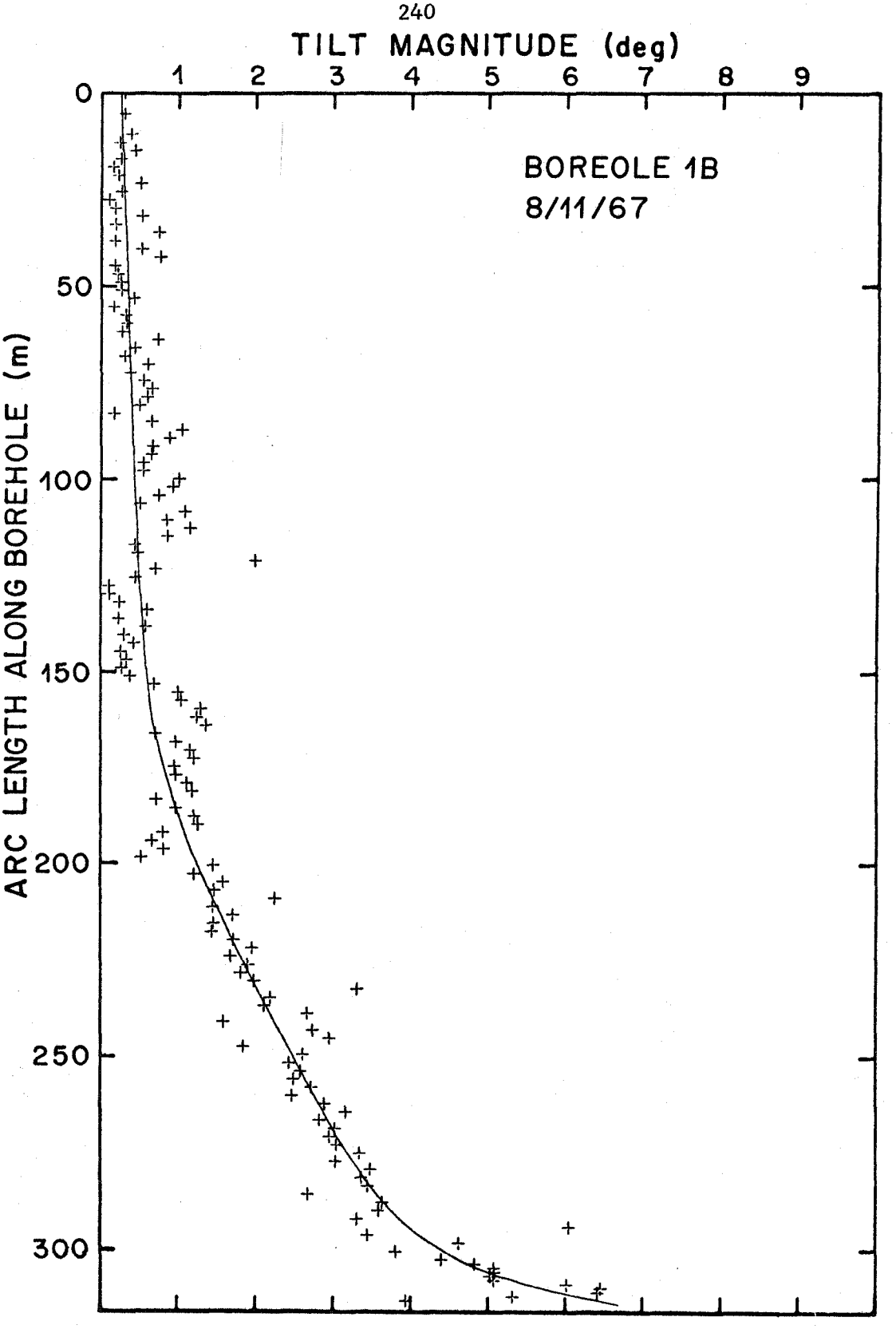
TILT MAGNITUDE (deg)
1
2
3
4
5
6
7
8
9
0
50
100
150
200
250
300
ARC LENGTH ALONG BOREHOLE (m)
BOREOLE 1B
8/11/67

FIGURE 11b.

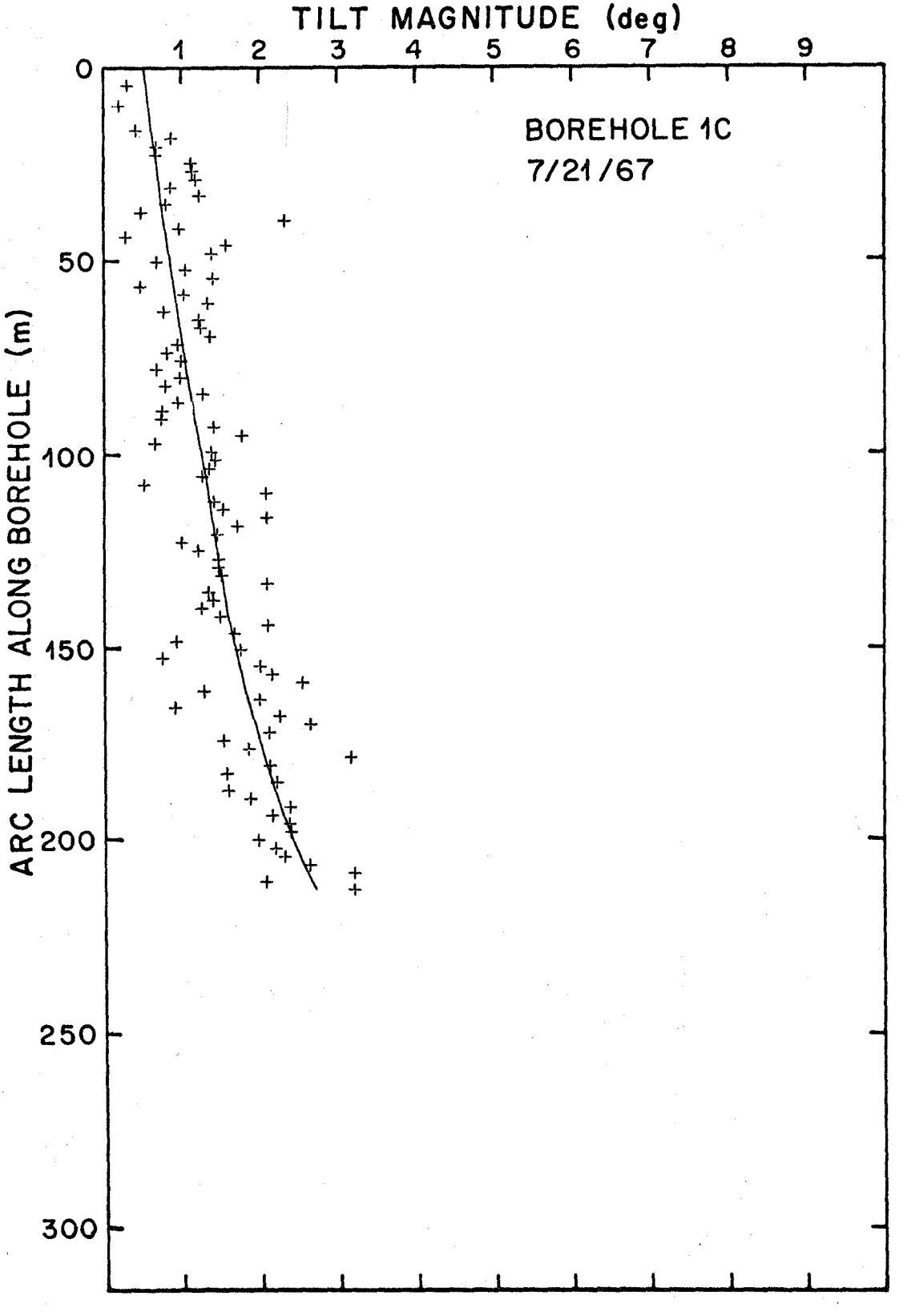
TILT MAGNITUDE (deg)
1
2
3
4
5
6
7
8
9
BOREHOLE 1C
7/21/67
ARC LENGTH ALONG BOREHOLE (m)
0
50
100
150
200
250
300

FIGURE 11c.

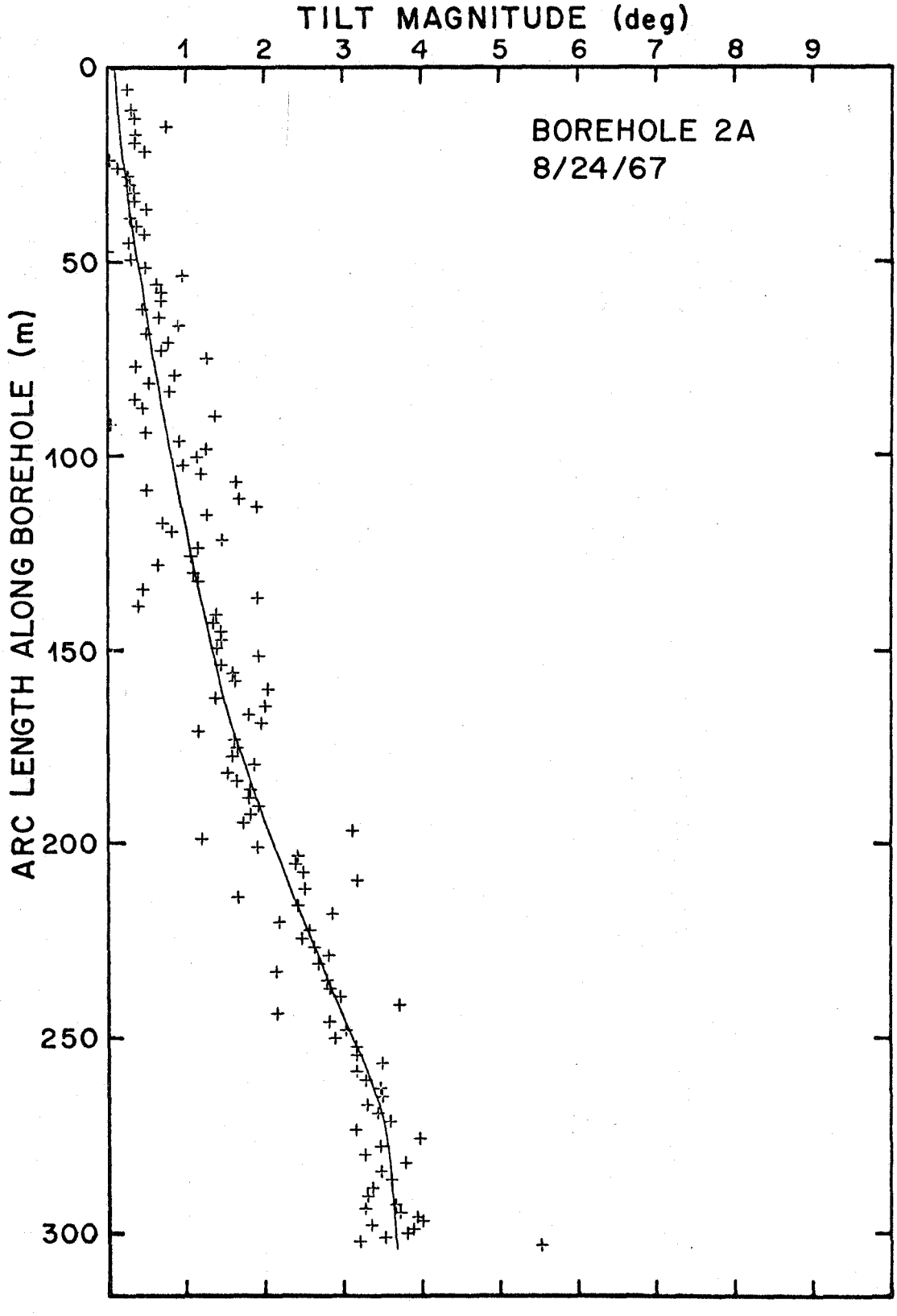
TILT MAGNITUDE (deg)
1
2
3
4
5
6
7
8
9
0
50
100
150
200
250
300
ARC LENGTH ALONG BOREHOLE (m)
BOREHOLE 2A
8/24/67

FIGURE 11d.

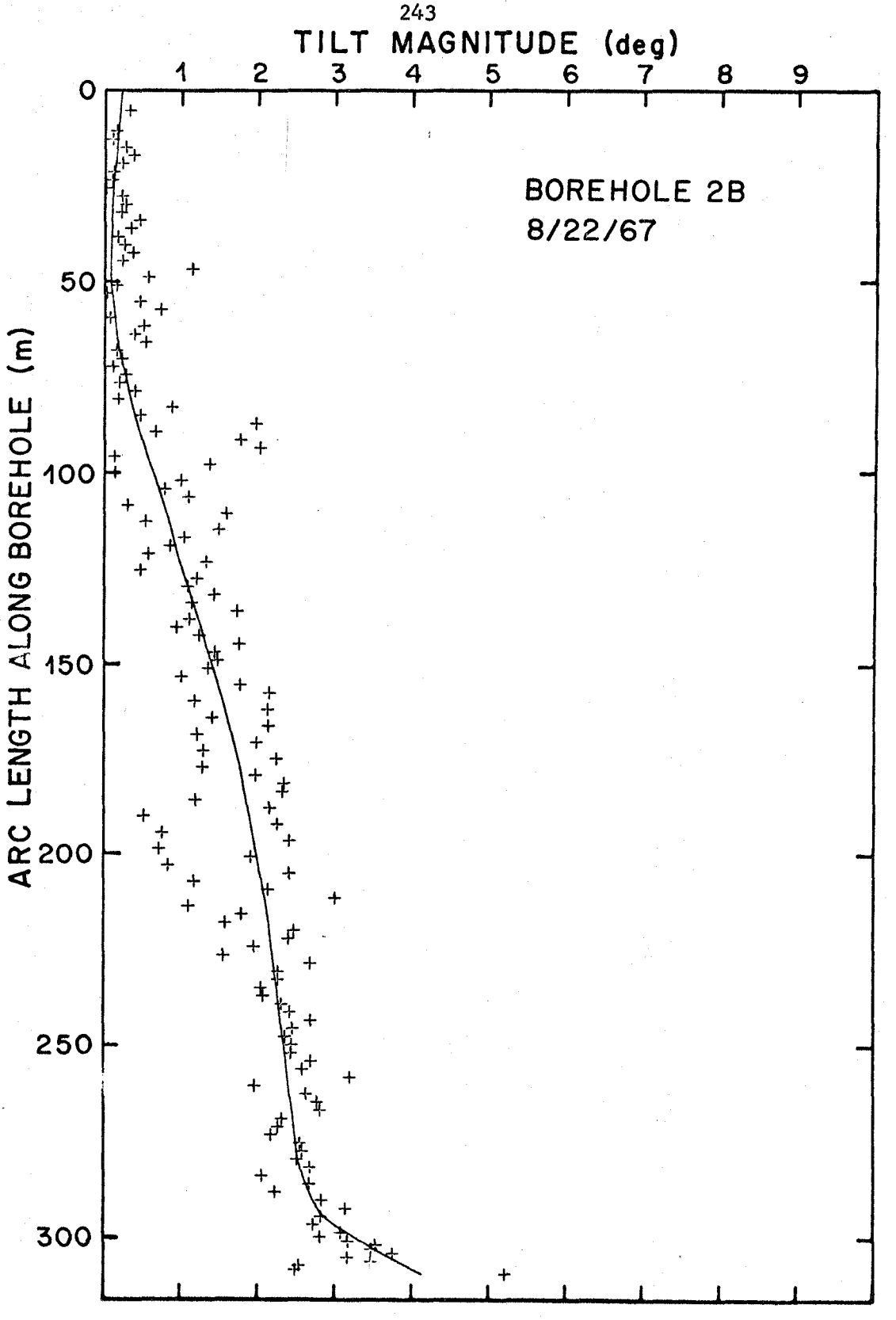
TILT MAGNITUDE (deg)
1
2
3
4
5
6
7
8
9
0
50
100
150
200
250
300
ARC LENGTH ALONG BOREHOLE (m)
BOREHOLE 2B
8/22/67

FIGURE 11e.

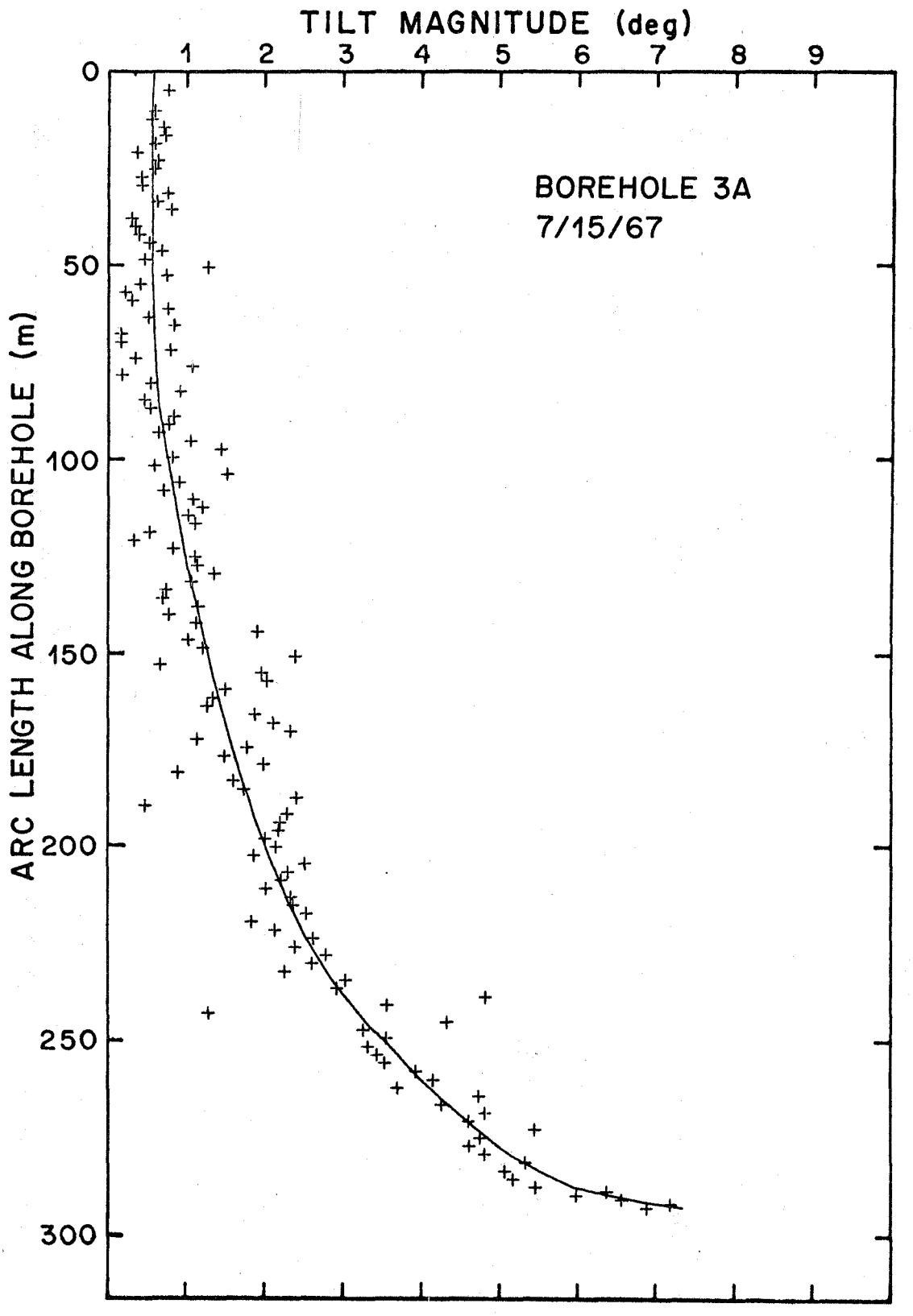
TILT MAGNITUDE (deg)
1
2
3
4
5
6
7
8
9
0
50
100
150
200
250
300
ARC LENGTH ALONG BOREHOLE (m)
BOREHOLE 3A
7/15/67

FIGURE 11f.

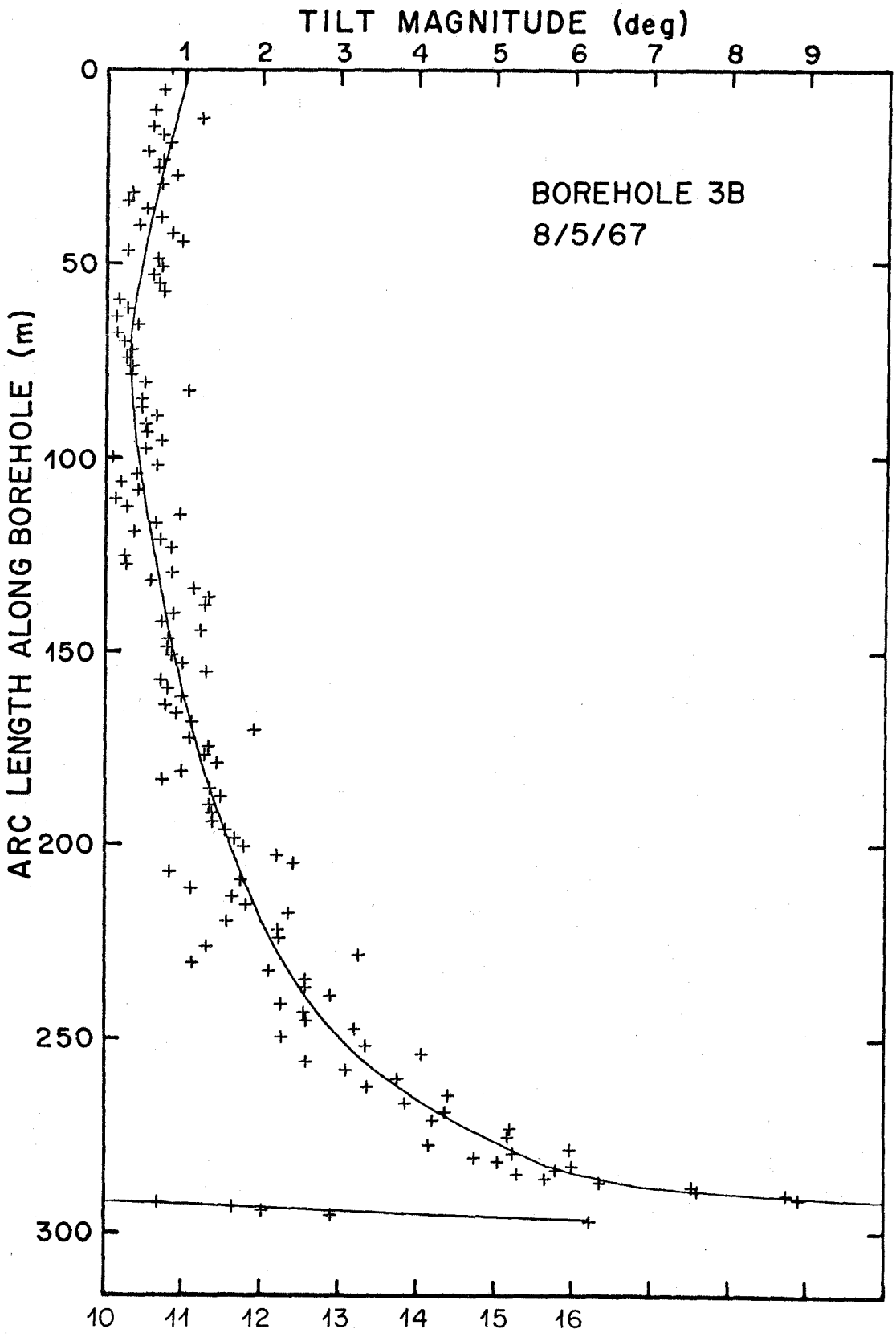
TILT MAGNITUDE (deg)
1
2
3
4
5
6
7
8
9
BOREHOLE 3B
8/5/67
ARC LENGTH ALONG BOREHOLE (m)
0
50
100
150
200
250
300
10
11
12
13
14
15
16

FIGURE 11g.

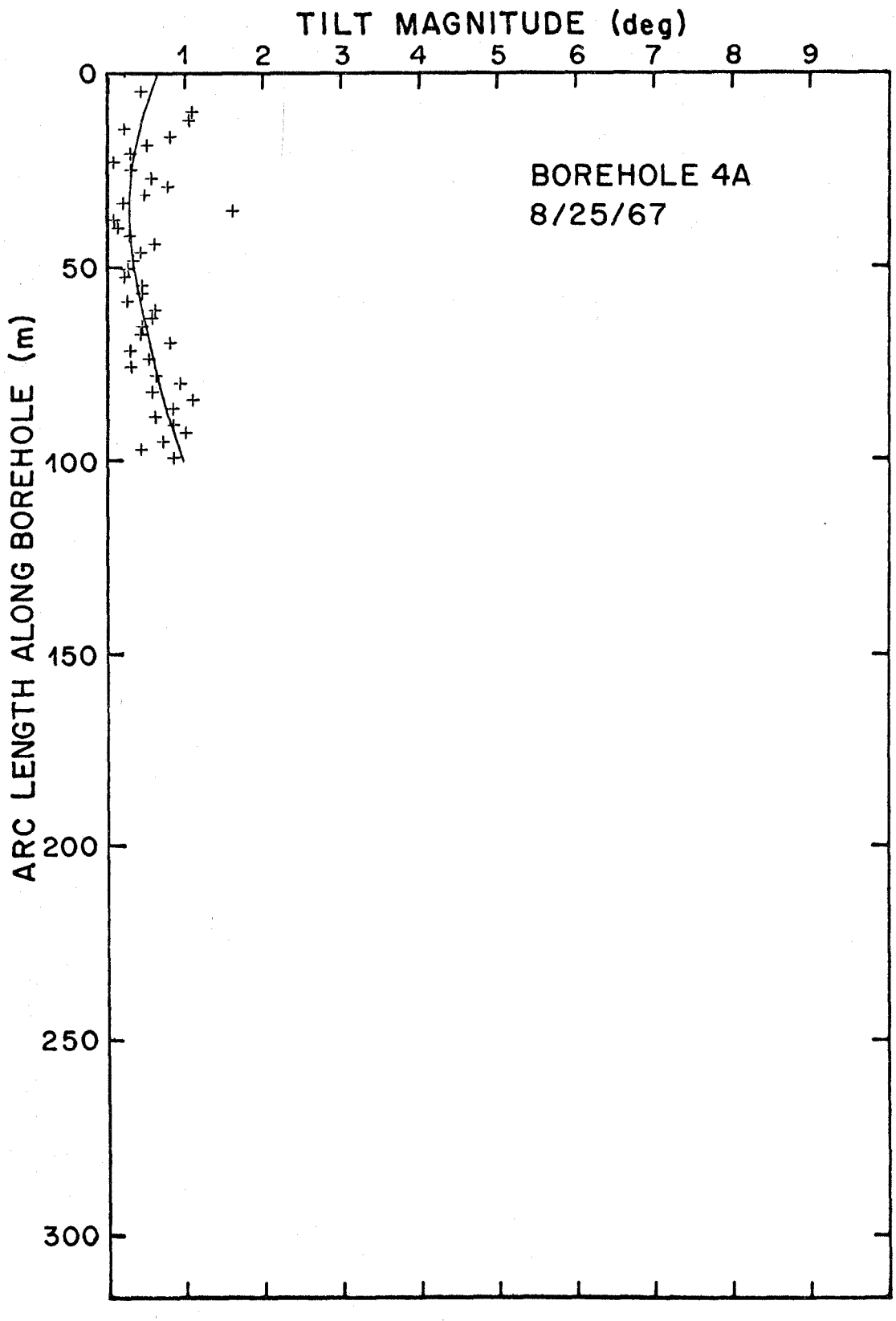
TILT MAGNITUDE (deg)
1
2
3
4
5
6
7
8
9
0
50
100
150
200
250
300
ARC LENGTH ALONG BOREHOLE (m)
BOREHOLE 4A
8/25/67

FIGURE 11h.

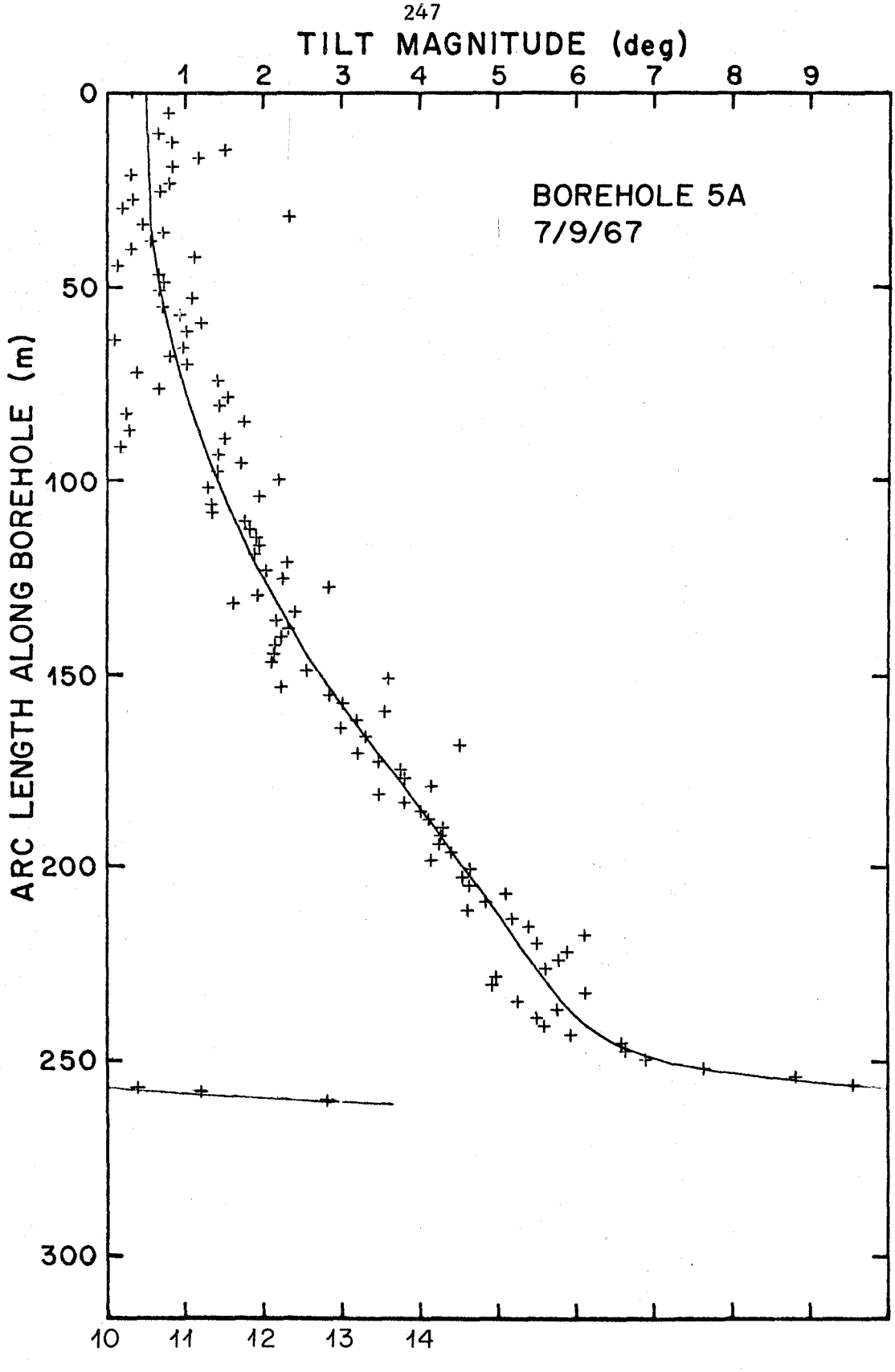
TILT MAGNITUDE (deg)
1
2
3
4
5
6
7
8
9
BOREHOLE 5A
7/9/67
ARC LENGTH ALONG BOREHOLE (m)
0
50
100
150
200
250
300
10
11
12
13
14

FIGURE 11i.

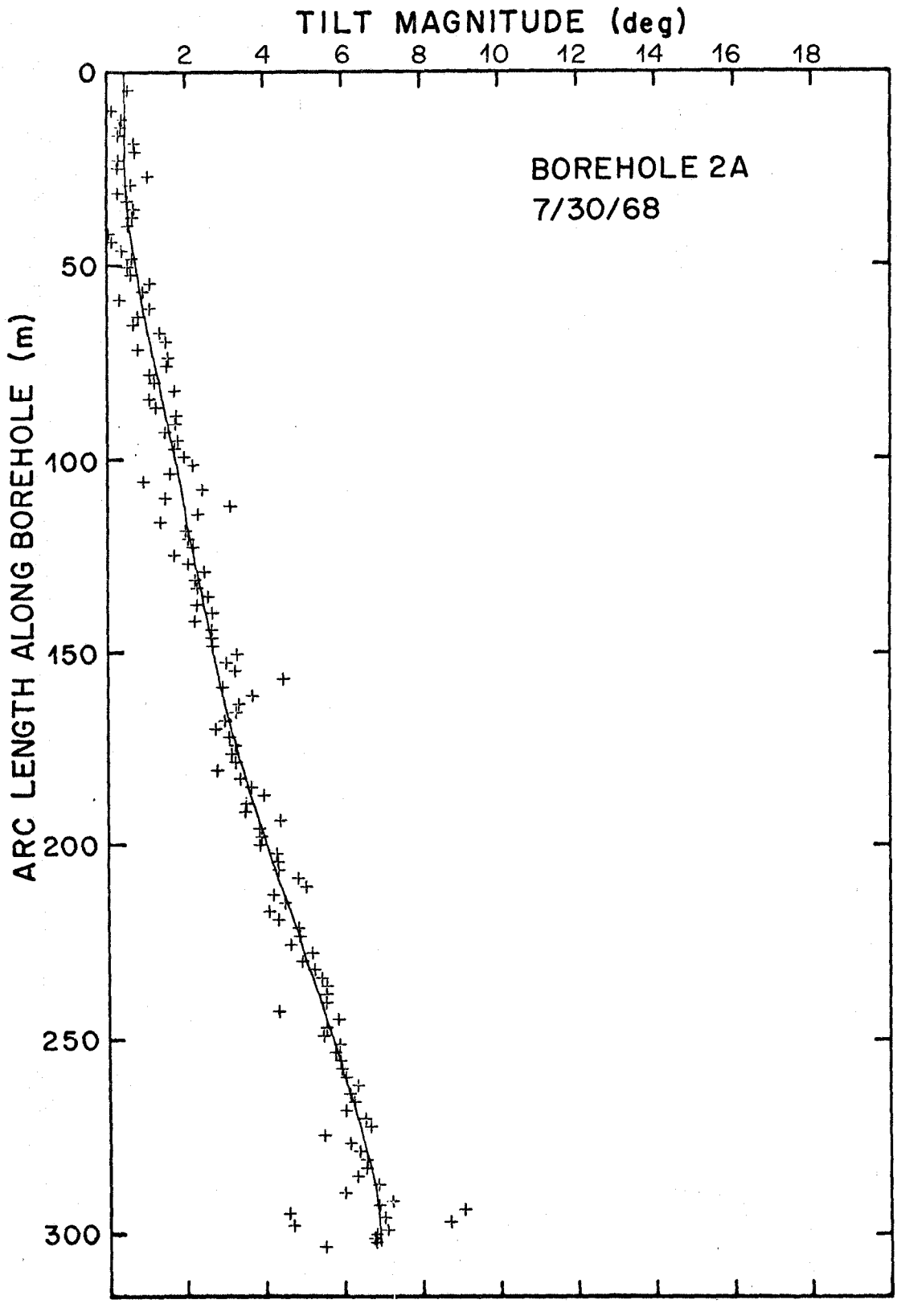
TILT MAGNITUDE (deg)
2
4
6
8
10
12
14
16
18
0
50
100
150
200
250
300
ARC LENGTH ALONG BOREHOLE (m)
BOREHOLE 2A
7/30/68

FIGURE 11j.

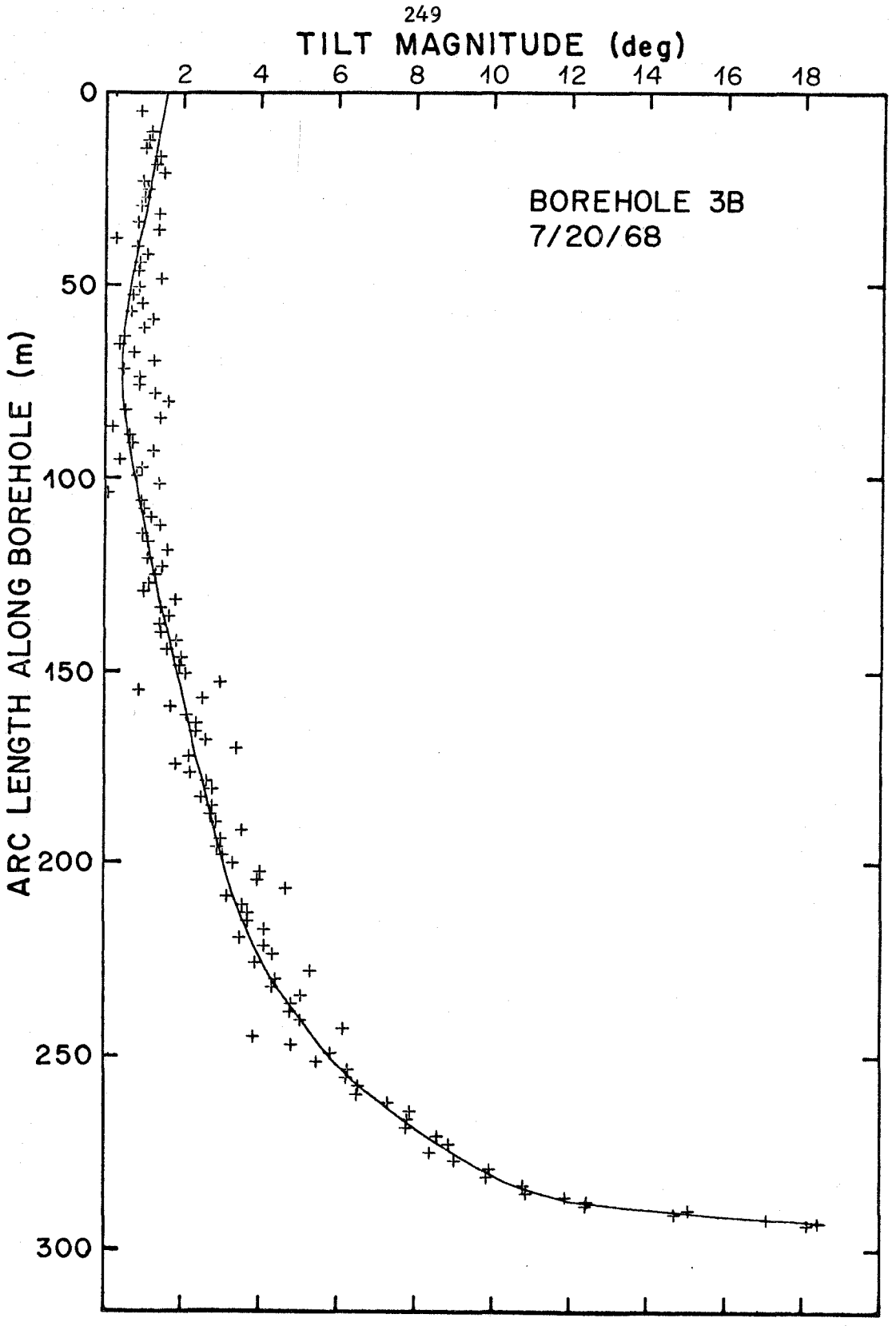
TILT MAGNITUDE (deg)
2
4
6
8
10
12
14
16
18
0
50
100
150
200
250
300
ARC LENGTH ALONG BOREHOLE (m)
BOREHOLE 3B
7/20/68

FIGURE 11k.

FIGURE 12. AZIMUTH OF TILT IN DEFORMED BOREHOLES

Date gives time of tilt measurement. Arrow indicates azimuth of average surface velocity. (See following pages.)

a. Borehole 1A 7/29/67
b. Borehole 1B 8/11/67
c. Borehole 1C 7/21/67
d. Borehole 2A 8/24/67
e. Borehole 2B 8/22/67
f. Borehole 3A 7/15/67
g. Borehole 3B 8/5/67
h. Borehole 4A 8/25/67
i. Borehole 5A 7/9/67
j. Borehole 2A 7/30/68
k. Borehole 3B 7/20/68

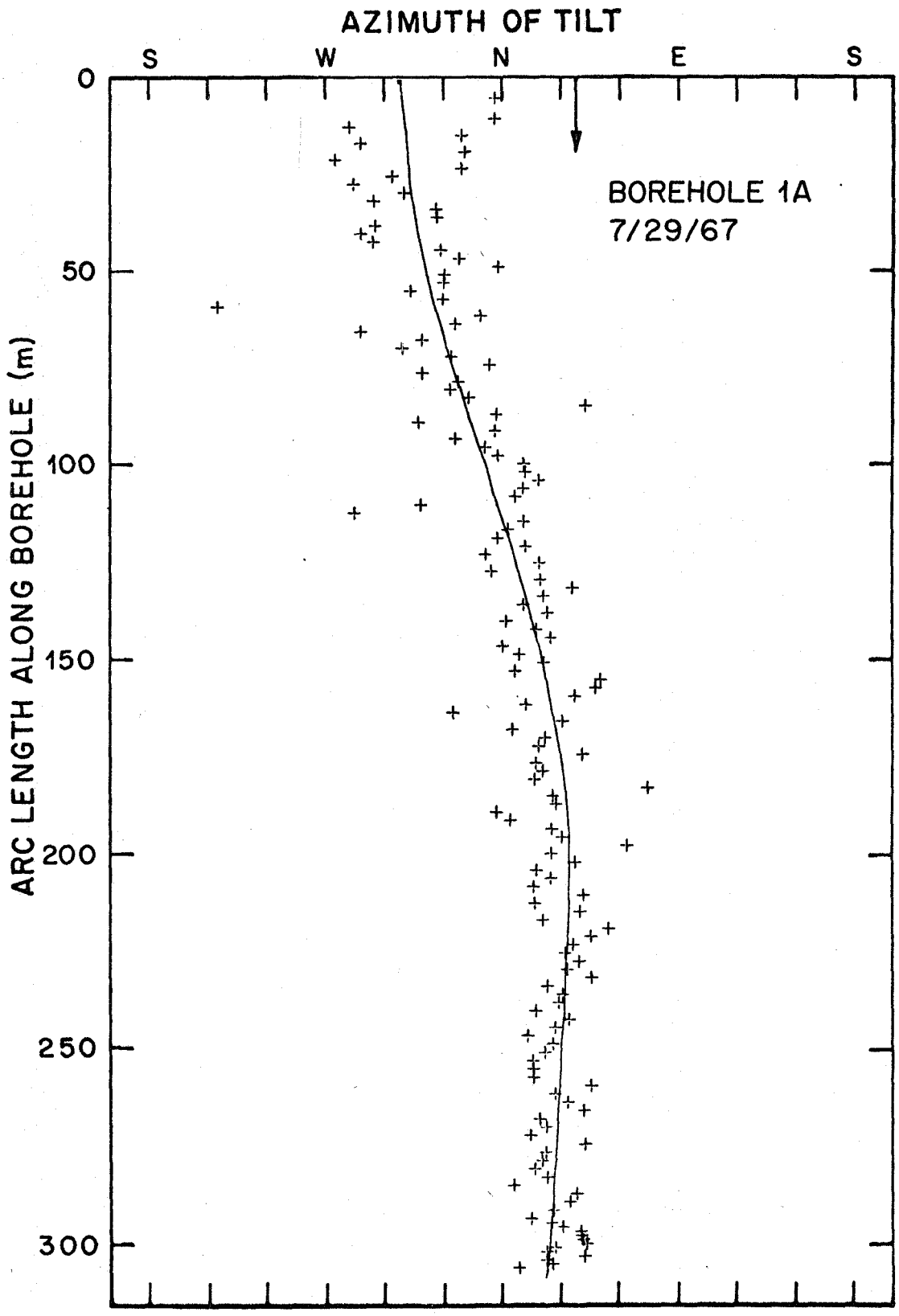
AZIMUTH OF TILT
S
W
N
E
S
0
50
100
150
200
250
300
ARC LENGTH ALONG BOREHOLE (m)
BOREHOLE 1A
7/29/67

FIGURE 12a.

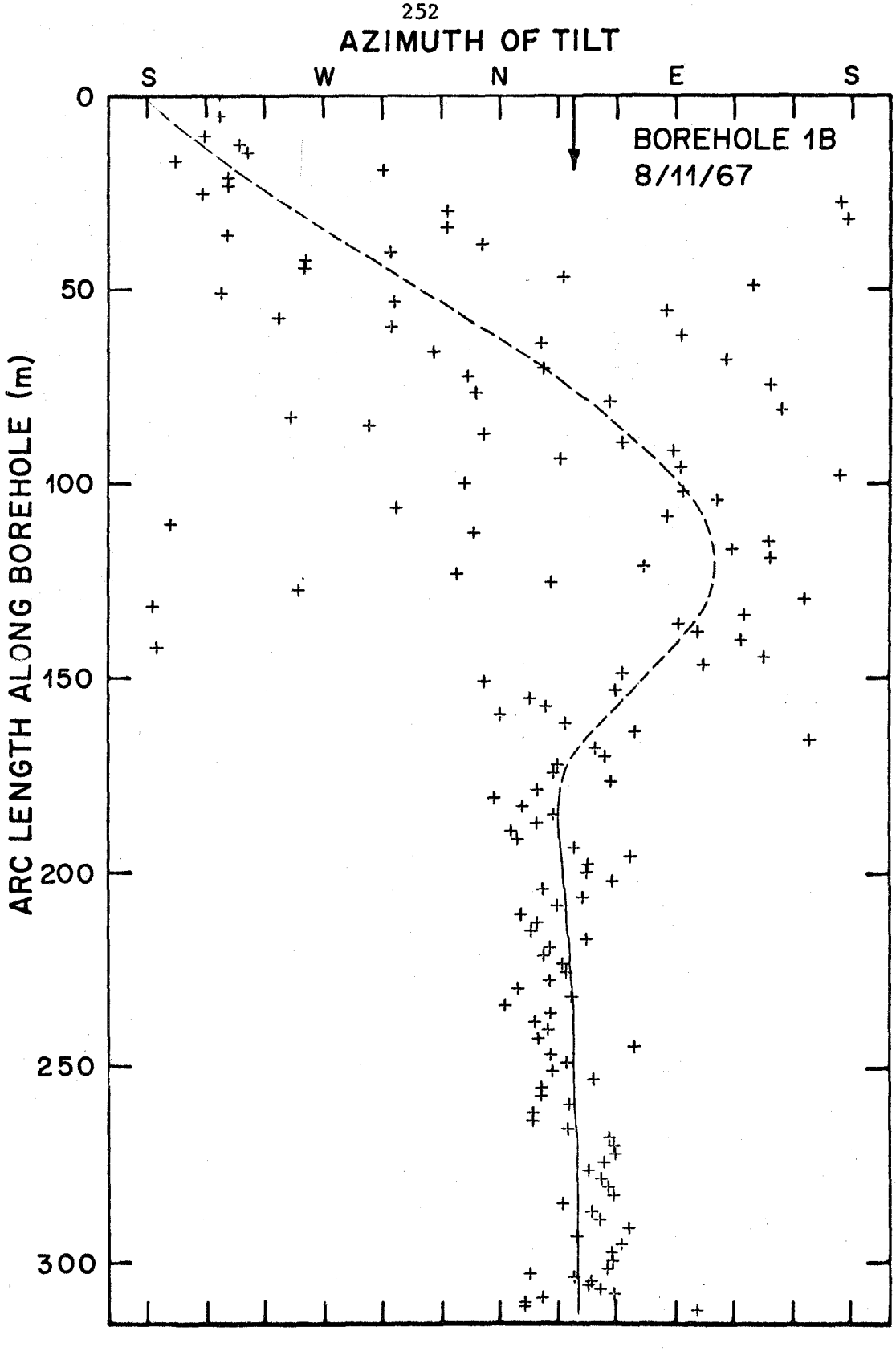
AZIMUTH OF TILT
S
W
N
E
S
0
50
100
150
200
250
300
ARC LENGTH ALONG BOREHOLE (m)
BOREHOLE 1B
8/11/67

FIGURE 12b.

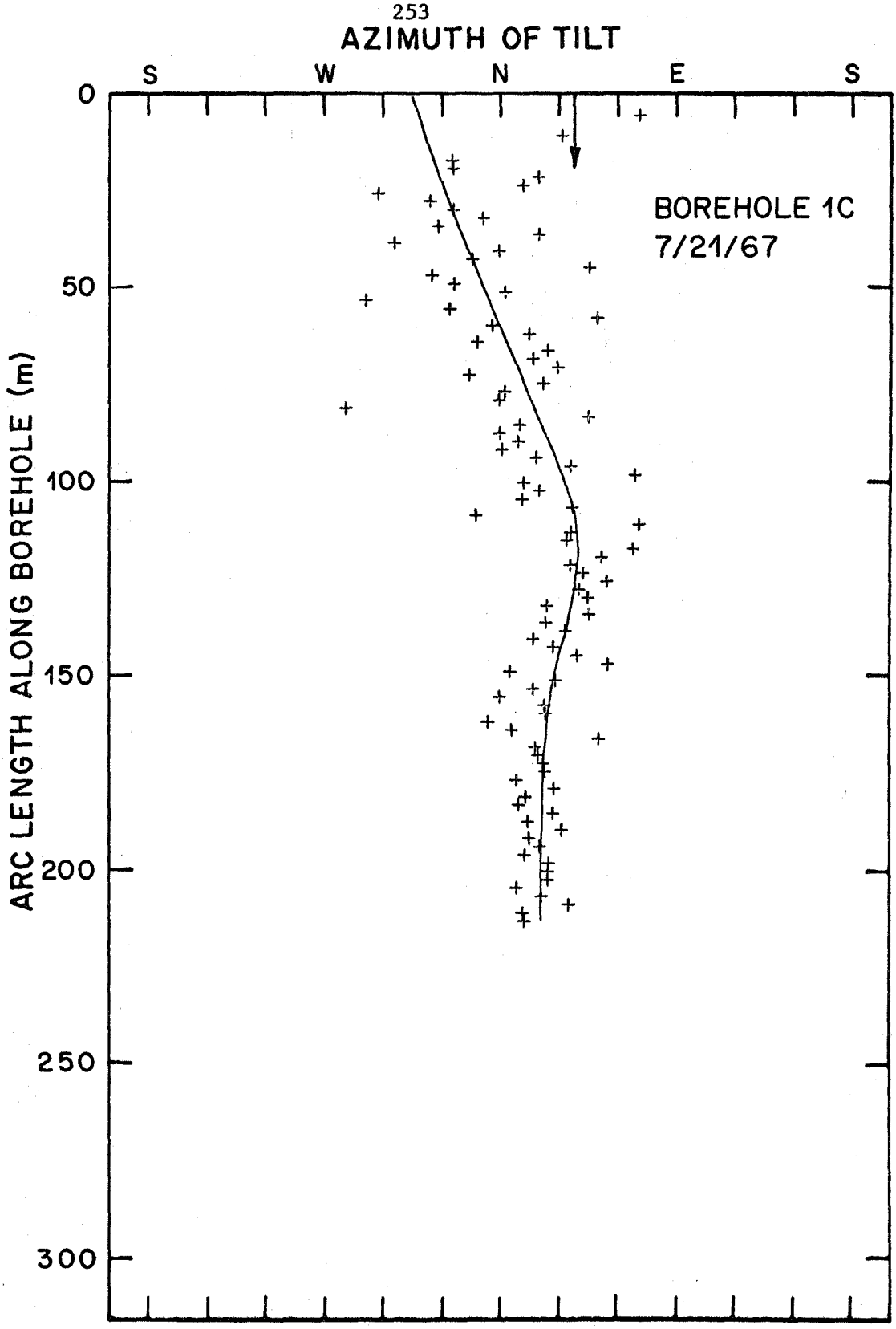
AZIMUTH OF TILT
S
W
N
E
S
0
50
100
150
200
250
300
ARC LENGTH ALONG BOREHOLE (m)
BOREHOLE 1C
7/21/67

FIGURE 12c.

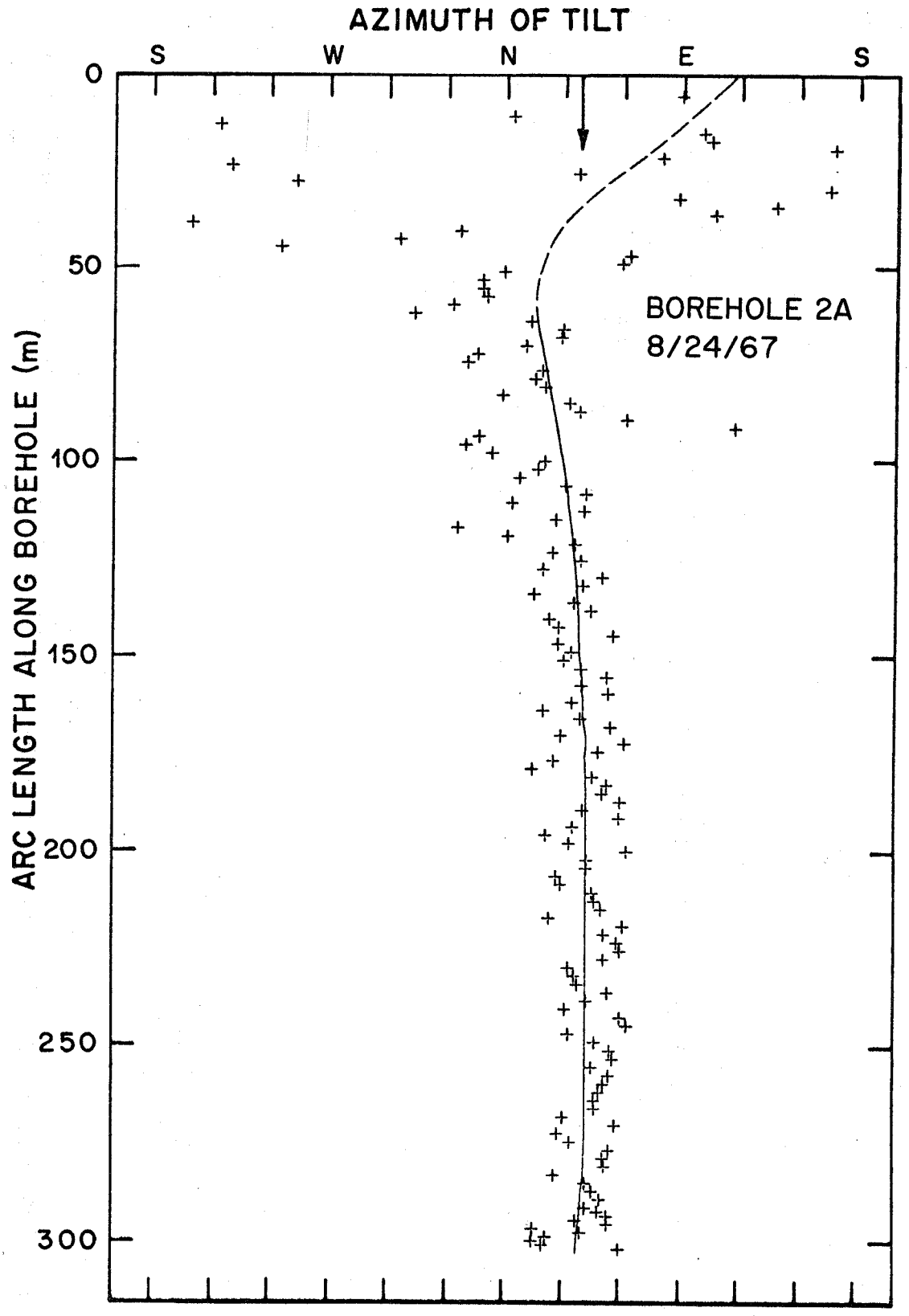
AZIMUTH OF TILT
S
W
N
E
S
0
50
100
150
200
250
300
ARC LENGTH ALONG BOREHOLE (m)
BOREHOLE 2A
8/24/67

FIGURE 12d.

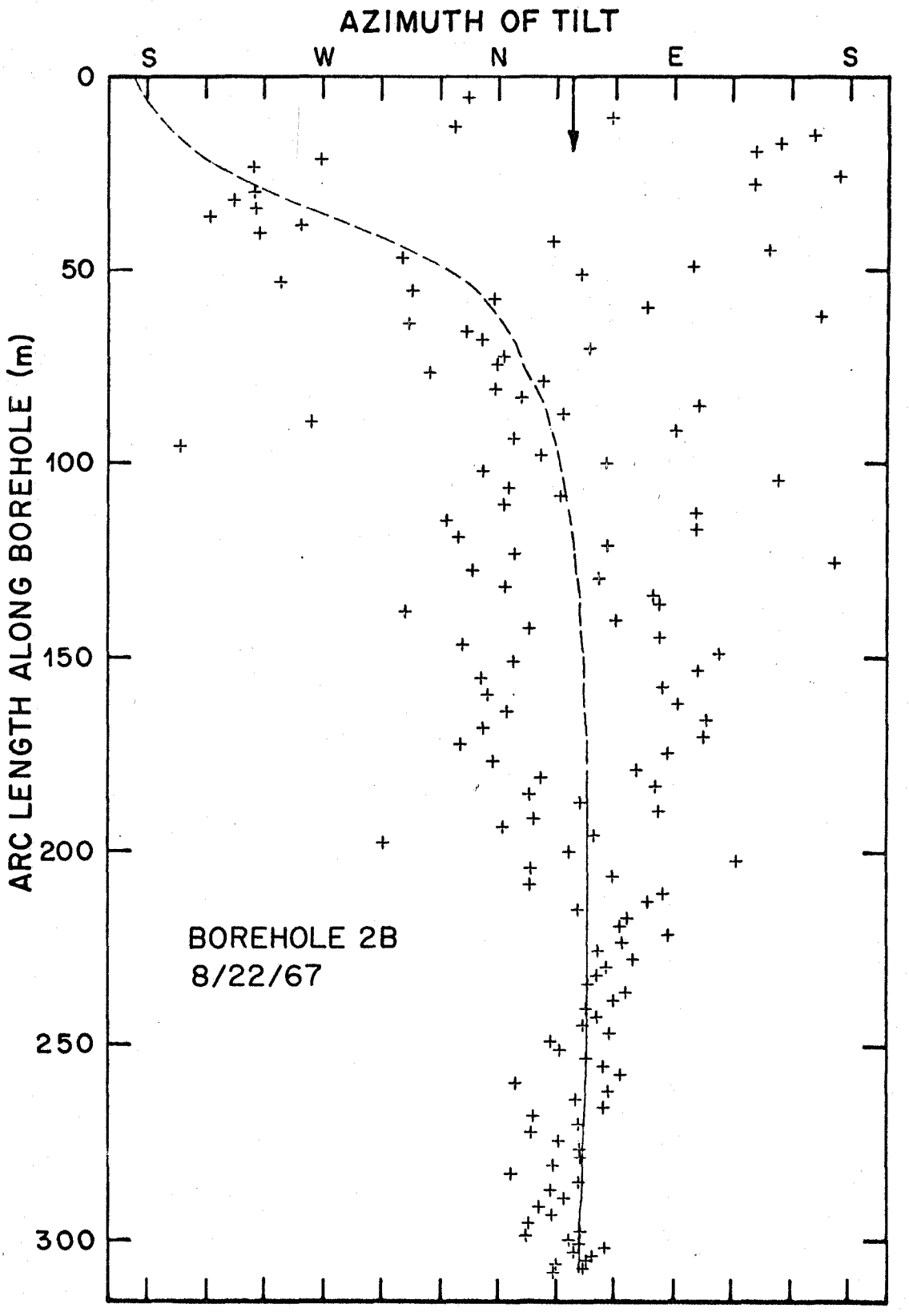
AZIMUTH OF TILT
S
W
N
E
S
0
50
100
150
200
250
300
ARC LENGTH ALONG BOREHOLE (m)
BOREHOLE 2B
8/22/67

FIGURE 12e.

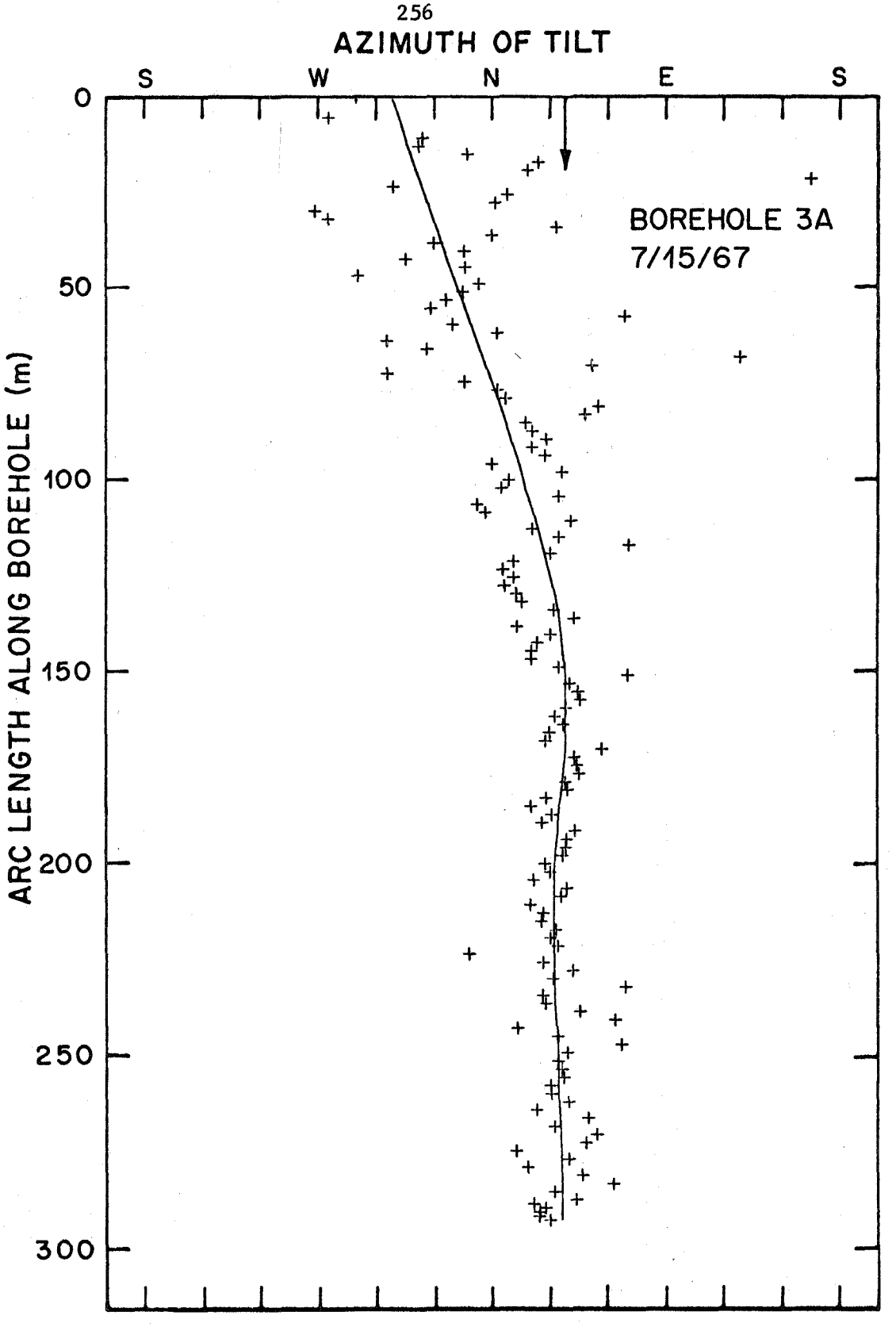
AZIMUTH OF TILT
S
W
N
E
S
0
50
100
150
200
250
300
ARC LENGTH ALONG BOREHOLE (m)
BOREHOLE 3A
7/15/67

FIGURE 12f.

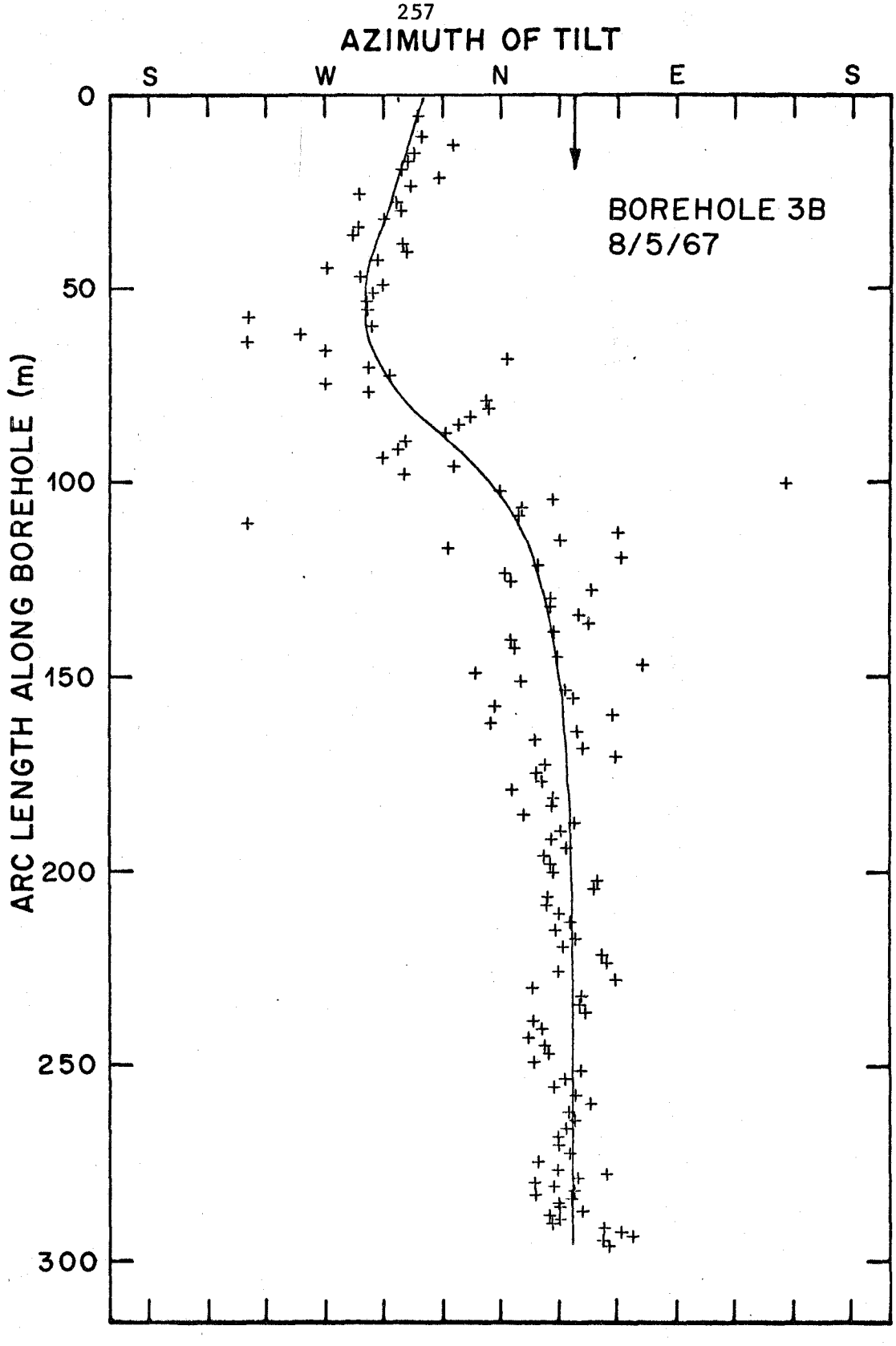
AZIMUTH OF TILT
S
W
N
E
S
0
50
100
150
200
250
300
ARC LENGTH ALONG BOREHOLE (m)
BOREHOLE 3B
8/5/67

FIGURE 12g.

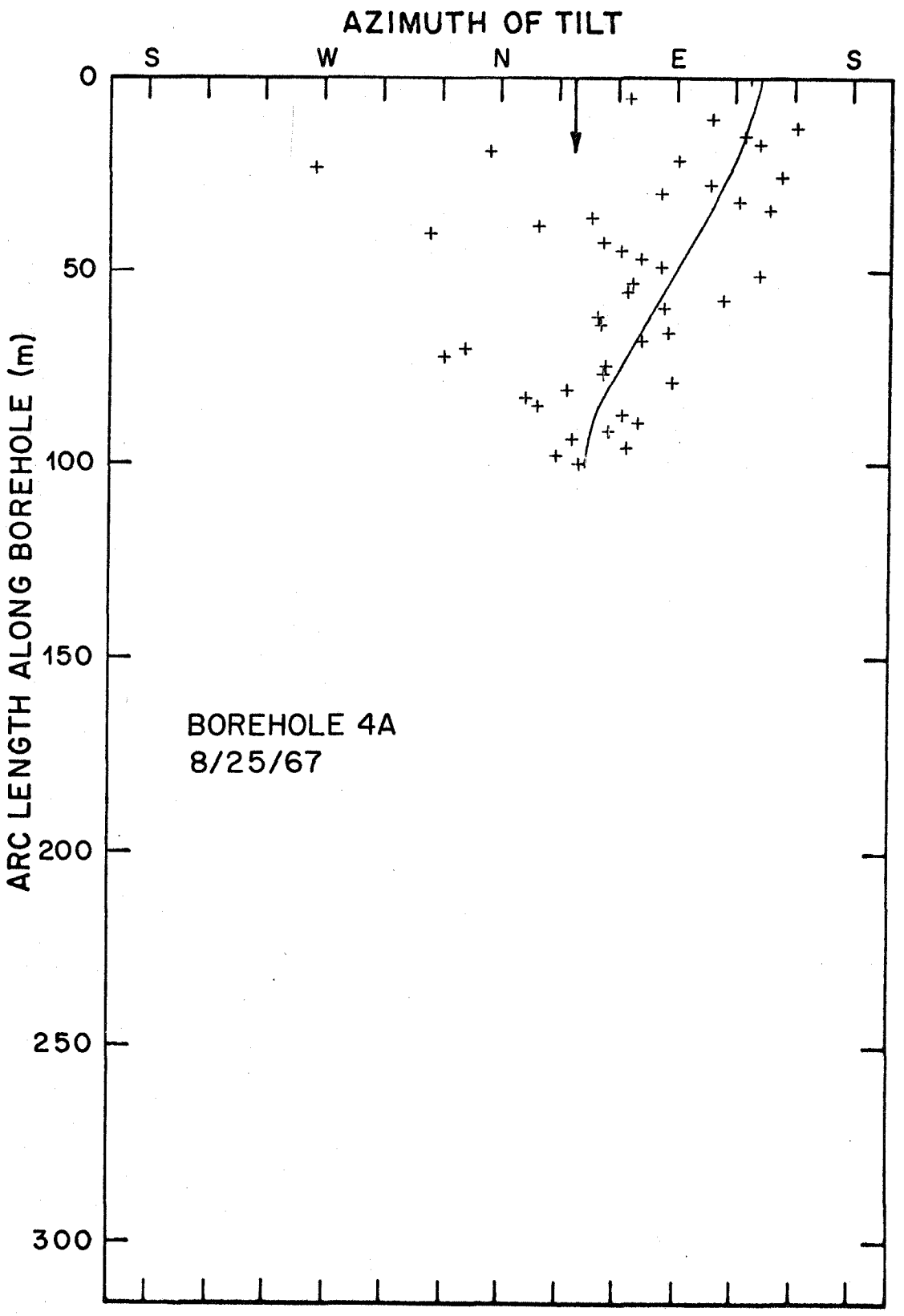
AZIMUTH OF TILT
S
W
N
E
S
0
50
100
150
200
250
300
ARC LENGTH ALONG BOREHOLE (m)
BOREHOLE 4A
8/25/67

FIGURE 12h.

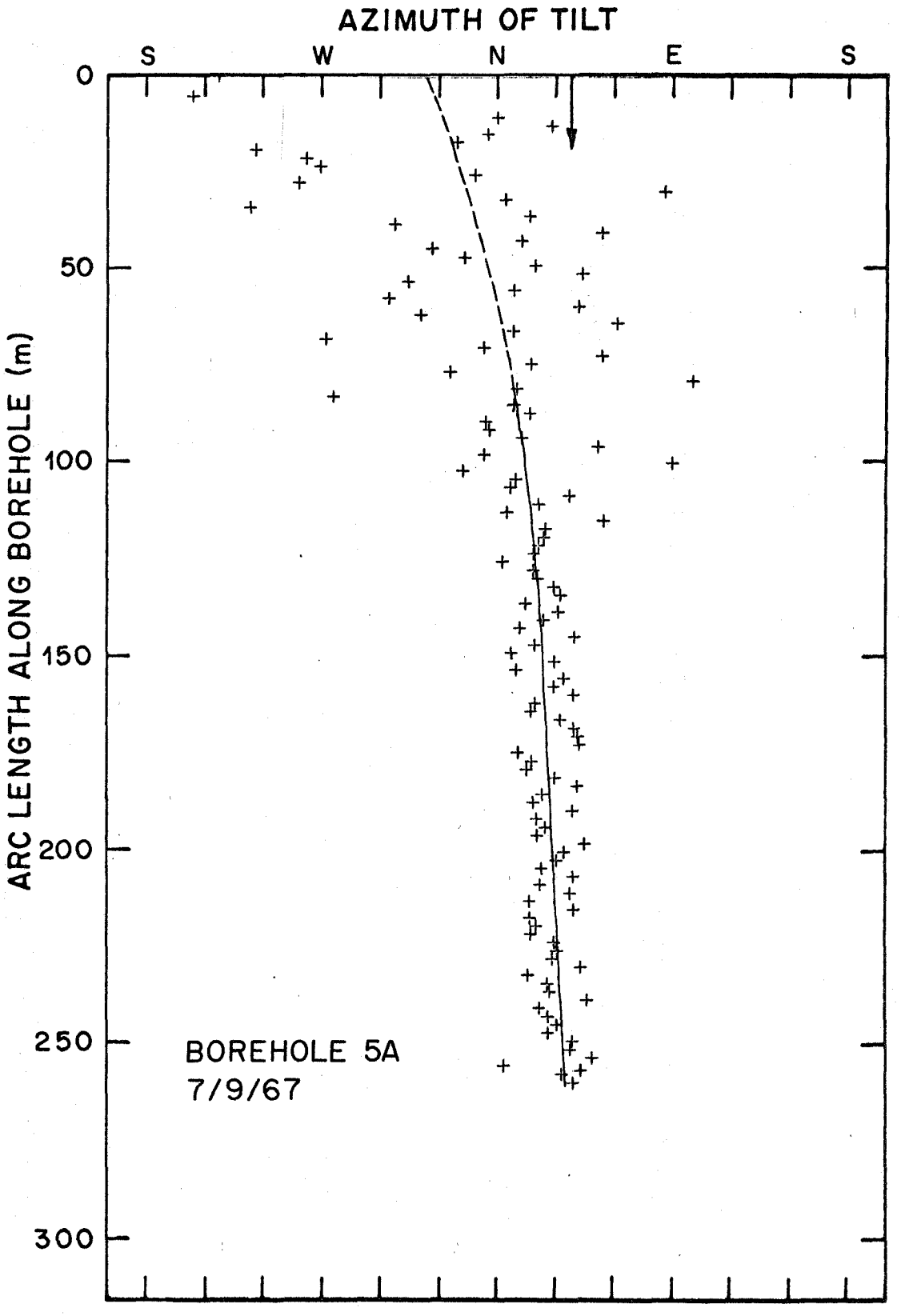
AZIMUTH OF TILT
S
W
N
E
S
0
50
100
150
200
250
300
ARC LENGTH ALONG BOREHOLE (m)
BOREHOLE 5A
7/9/67

FIGURE 12i.

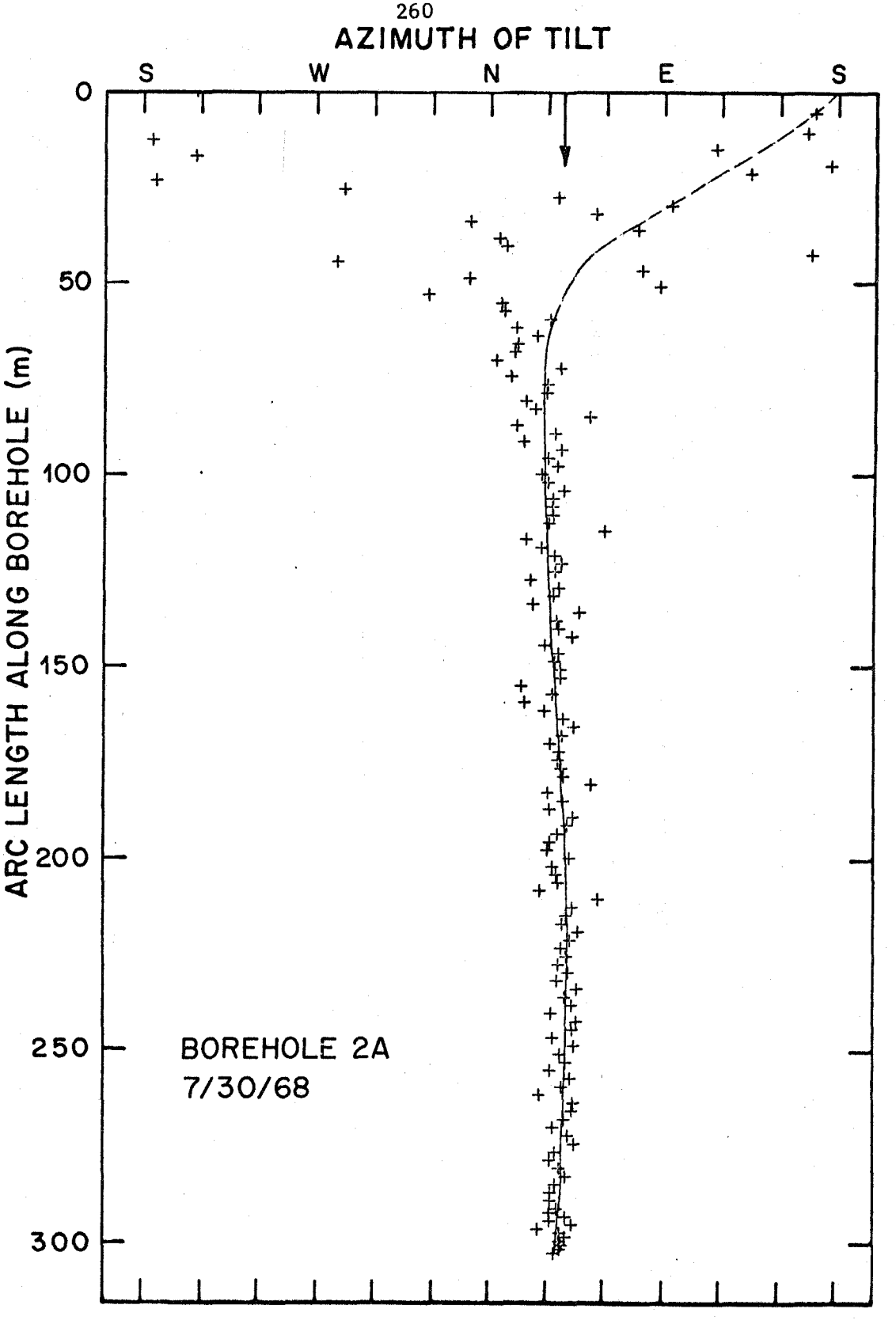
AZIMUTH OF TILT
S
W
N
E
S
0
50
100
150
200
250
300
ARC LENGTH ALONG BOREHOLE (m)
BOREHOLE 2A
7/30/68

FIGURE 12j.

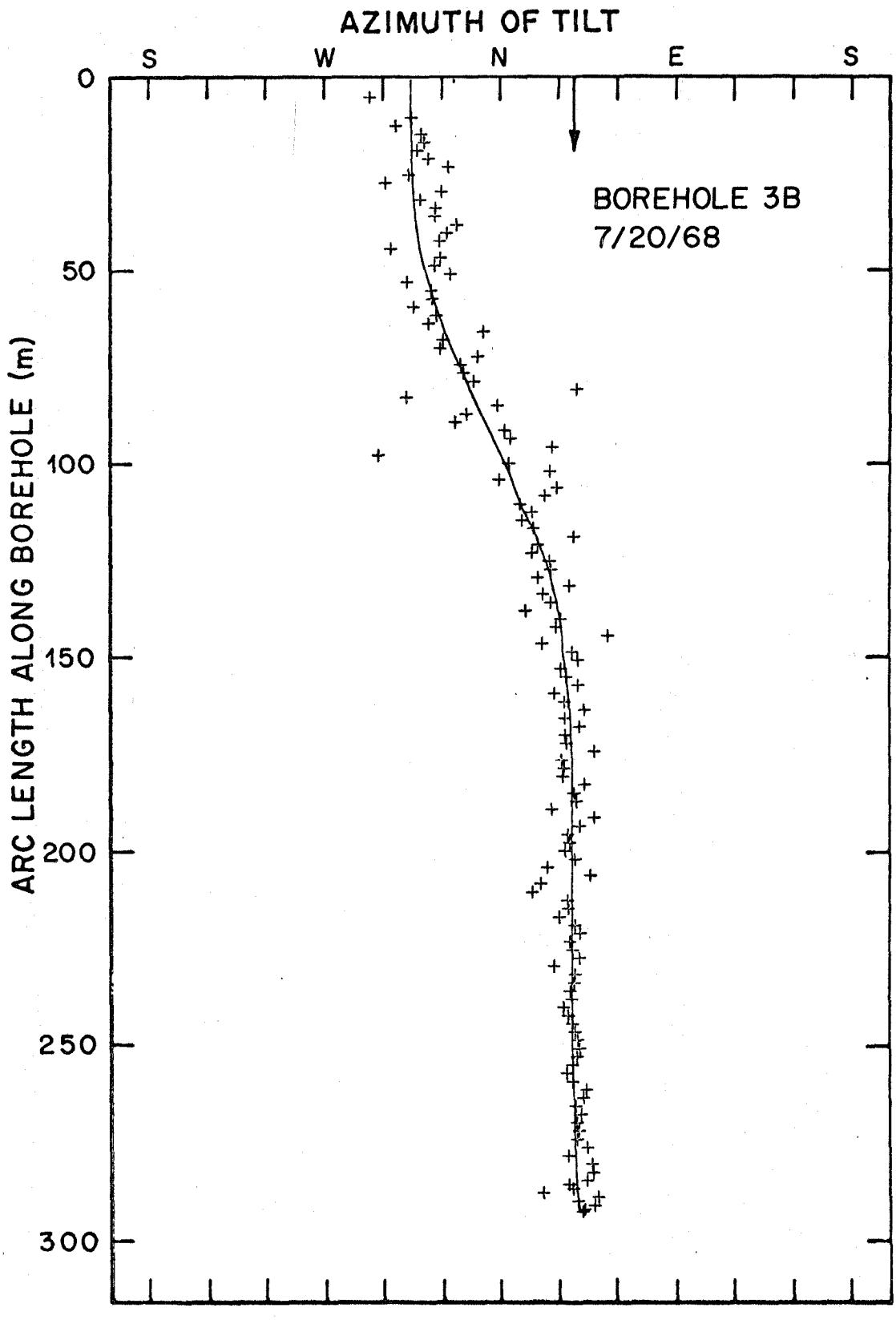
AZIMUTH OF TILT
S
W
N
E
S
0
50
100
150
200
250
300
ARC LENGTH ALONG BOREHOLE (m)
BOREHOLE 3B
7/20/68

FIGURE 12k.

FIGURE 13. LONGITUDINAL COMPONENT OF TILT IN DEFORMED BOREHOLES

Plotted values are normalized to a one year interval by dividing the values measured at the time of inclinometry by the interval of time in years between completion of the original borehole and inclinometry of the deformed borehole. (See following pages.)

a. Borehole 1A 66-67
b. Borehole 1B 66-67
c. Borehole 1C 66-67
d. Borehole 2A 66-67
e. Borehole 2B 66-67
f. Borehole 3A 66-67
g. Borehole 3B 66-67
h. Borehole 4A 66-67
i. Borehole 5A 66-67
j. Borehole 2A 66-68
k. Borehole 3B 66-68

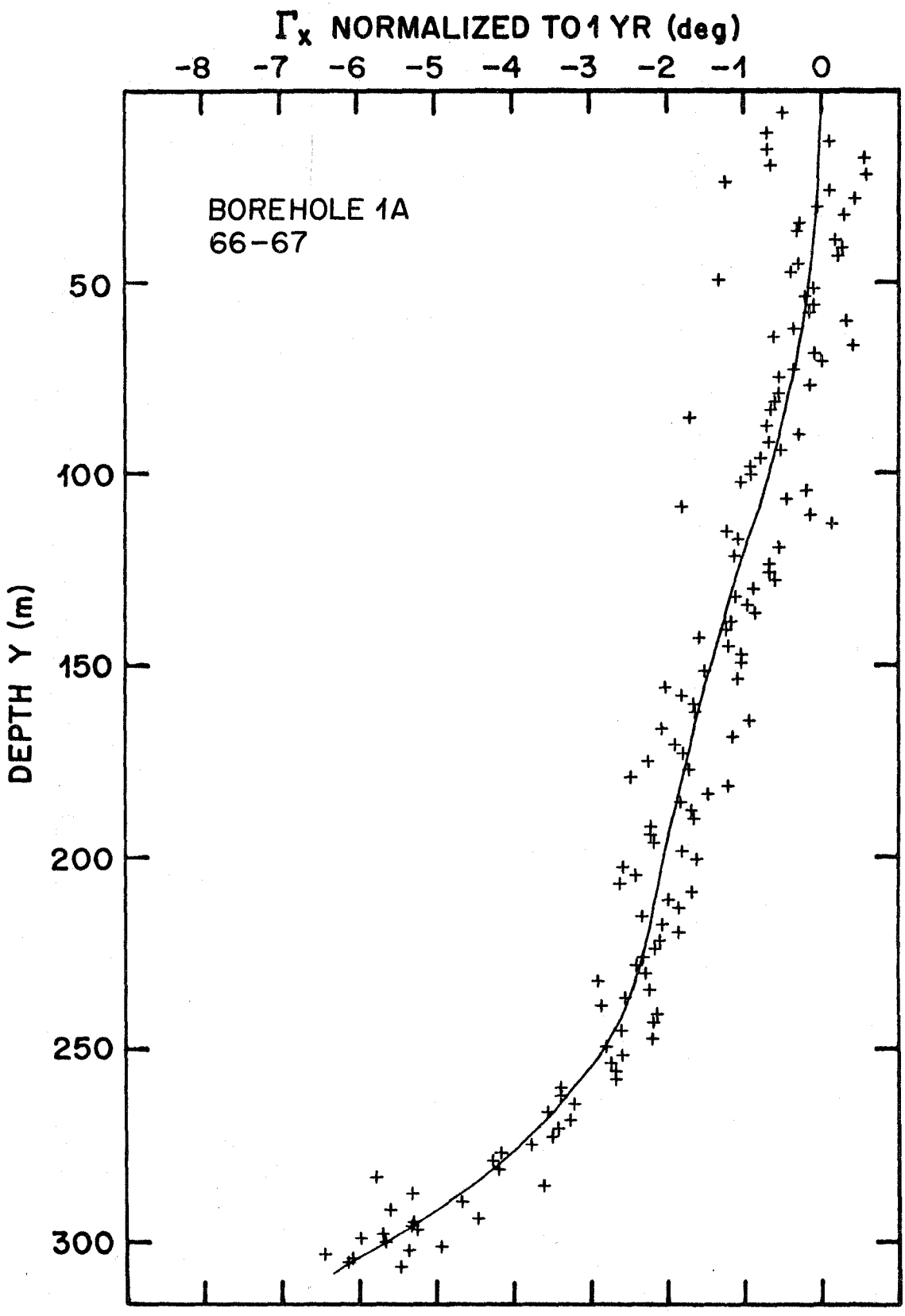
Γ_x NORMALIZED TO 1 YR (deg)
-8
-7
-6
-5
-4
-3
-2
-1
0
BOREHOLE 1A
66-67
DEPTH Y (m)
50
100
150
200
250
300

FIGURE 13a.

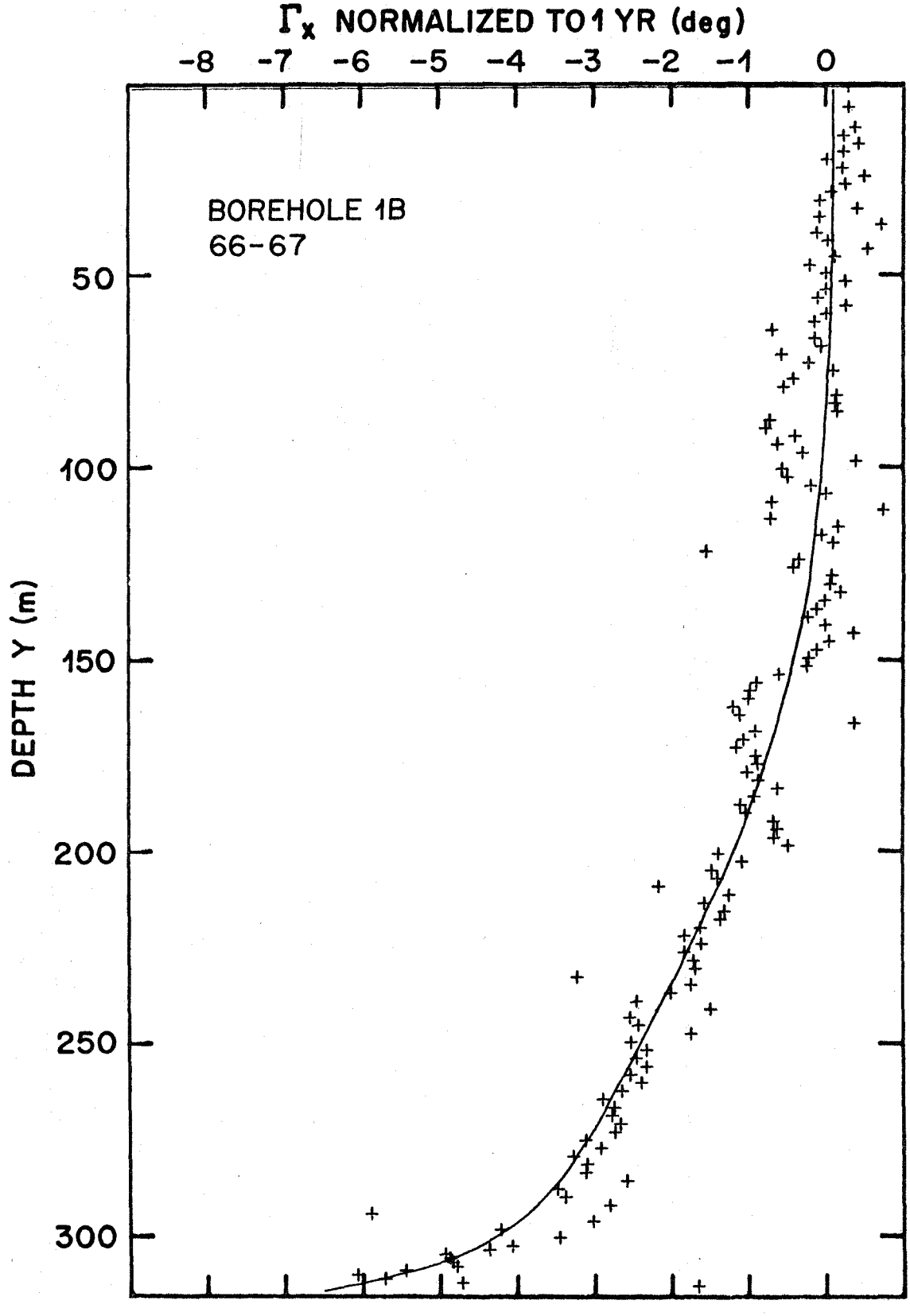
Γ_x NORMALIZED TO 1 YR (deg)
-8
-7
-6
-5
-4
-3
-2
-1
0
BOREHOLE 1B
66-67
DEPTH Y (m)
50
100
150
200
250
300

FIGURE 13b.

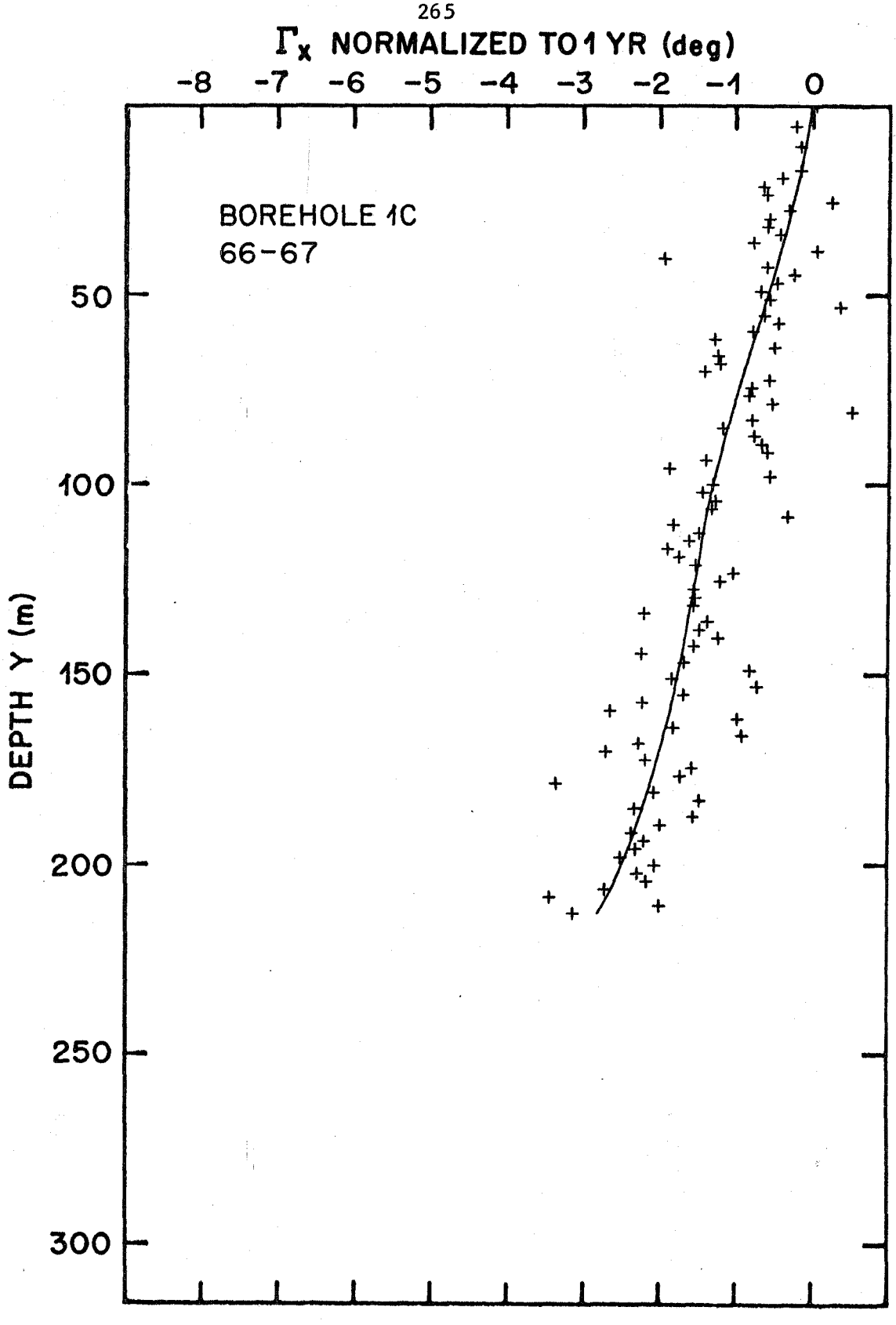
Γ_x NORMALIZED TO 1 YR (deg)
-8
-7
-6
-5
-4
-3
-2
-1
0
BOREHOLE 1C
66-67
DEPTH Y (m)
50
100
150
200
250
300

FIGURE 13c.

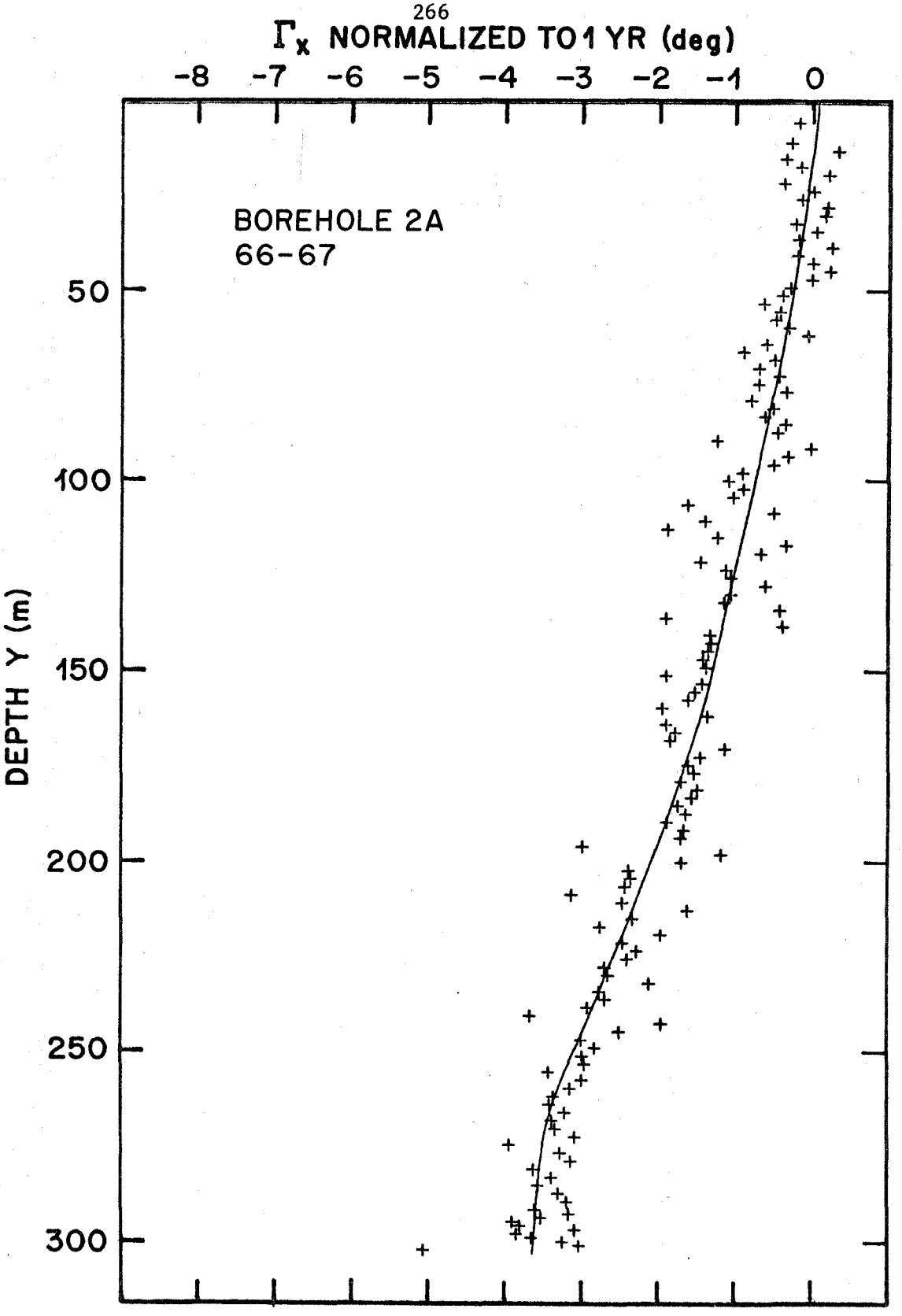
Γx NORMALIZED TO 1 YR (deg)
-8
-7
-6
-5
-4
-3
-2
-1
0
BOREHOLE 2A
66-67
DEPTH Y (m)
50
100
150
200
250
300

FIGURE 13d.

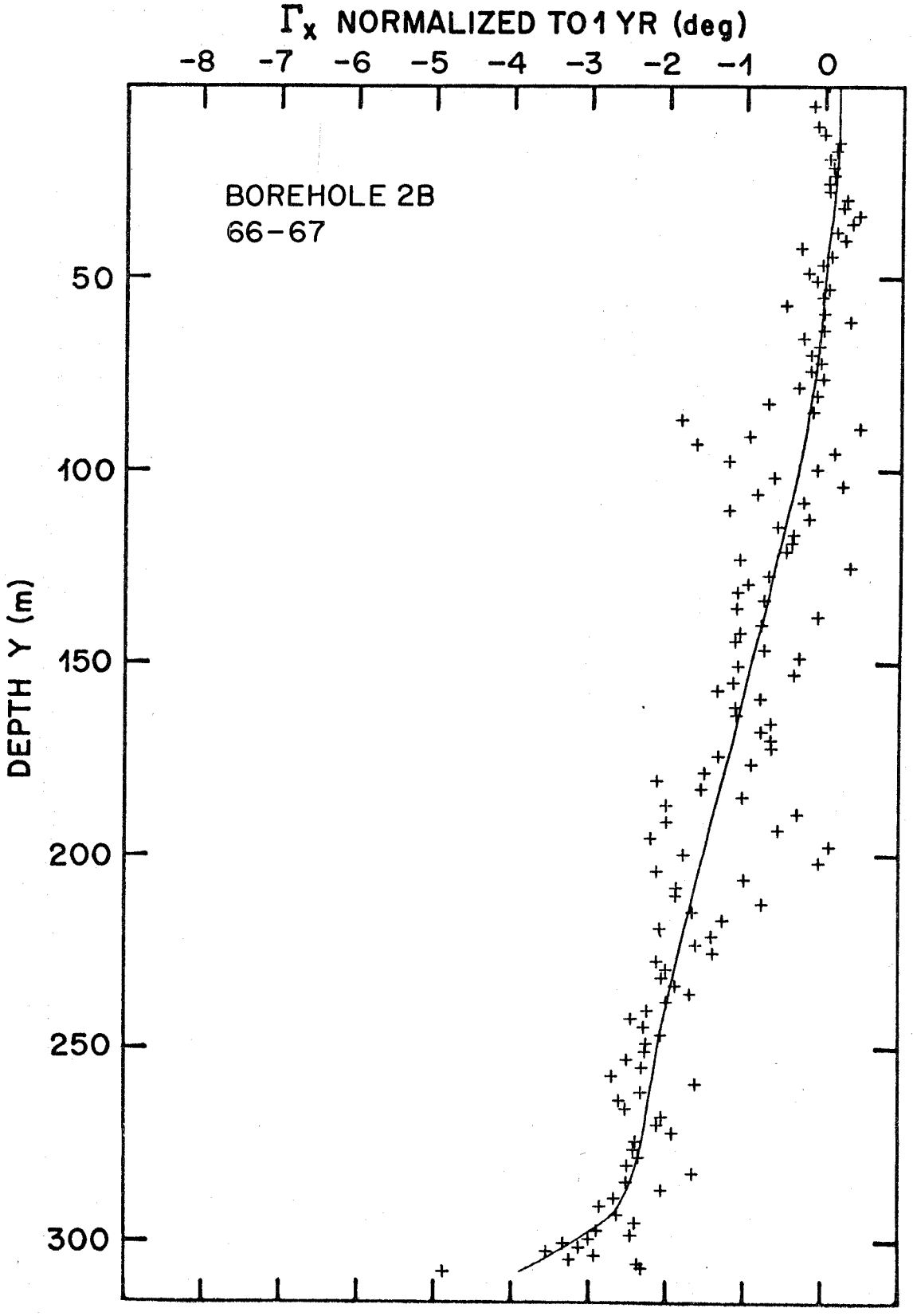
Γ_x NORMALIZED TO 1 YR (deg)
-8
-7
-6
-5
-4
-3
-2
-1
0
BOREHOLE 2B
66-67
DEPTH Y (m)
50
100
150
200
250
300

FIGURE 13e.

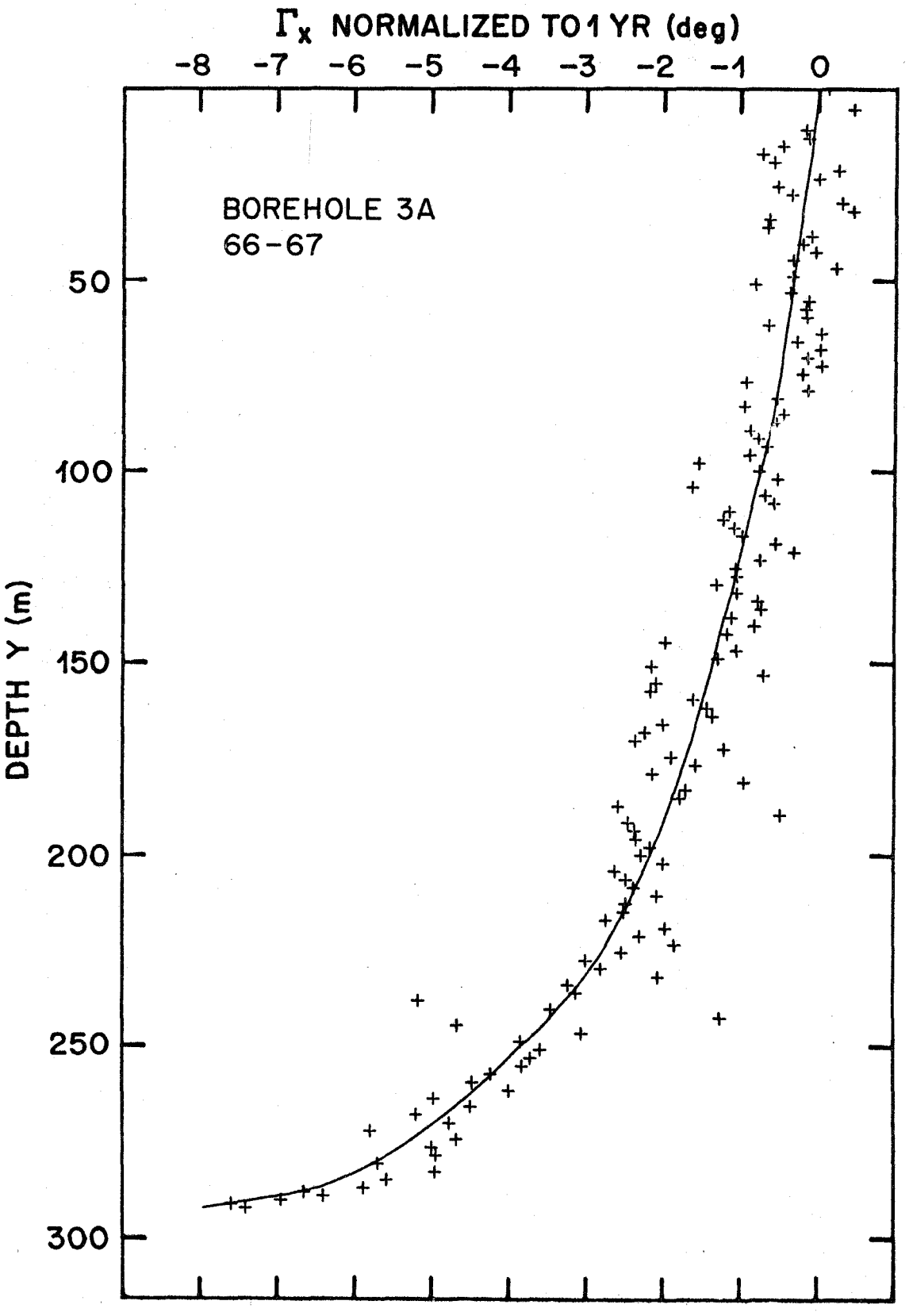
Γ_x NORMALIZED TO 1 YR (deg)
-8
-7
-6
-5
-4
-3
-2
-1
0
BOREHOLE 3A
66-67
DEPTH Y (m)
50
100
150
200
250
300

FIGURE 13f.

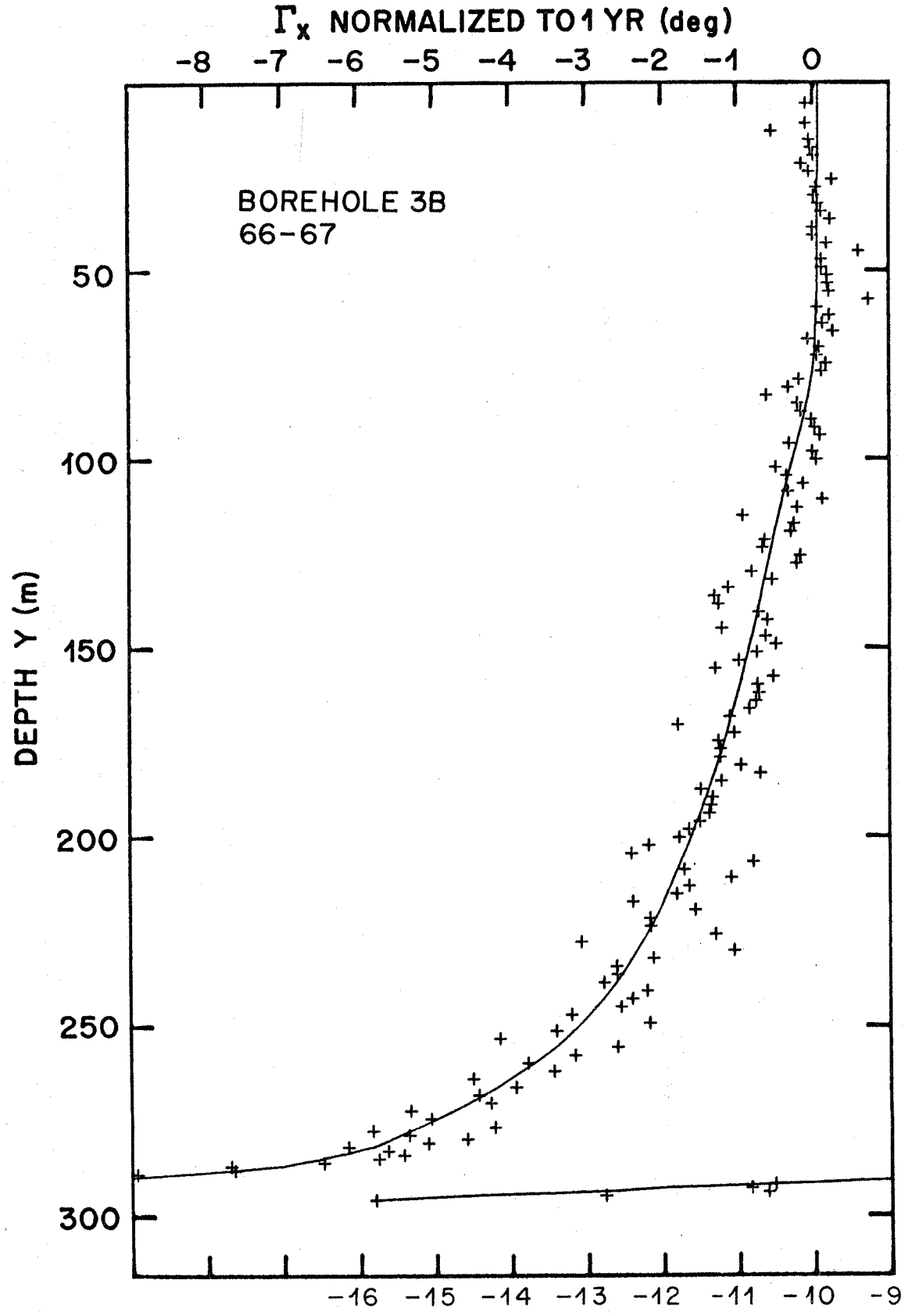
Γ_x NORMALIZED TO 1 YR (deg)
-8 -7 -6 -5 -4 -3 -2 -1 0
BOREHOLE 3B
66-67
DEPTH Y (m)
50
100
150
200
250
300
-16 -15 -14 -13 -12 -11 -10 -9

FIGURE 13g.

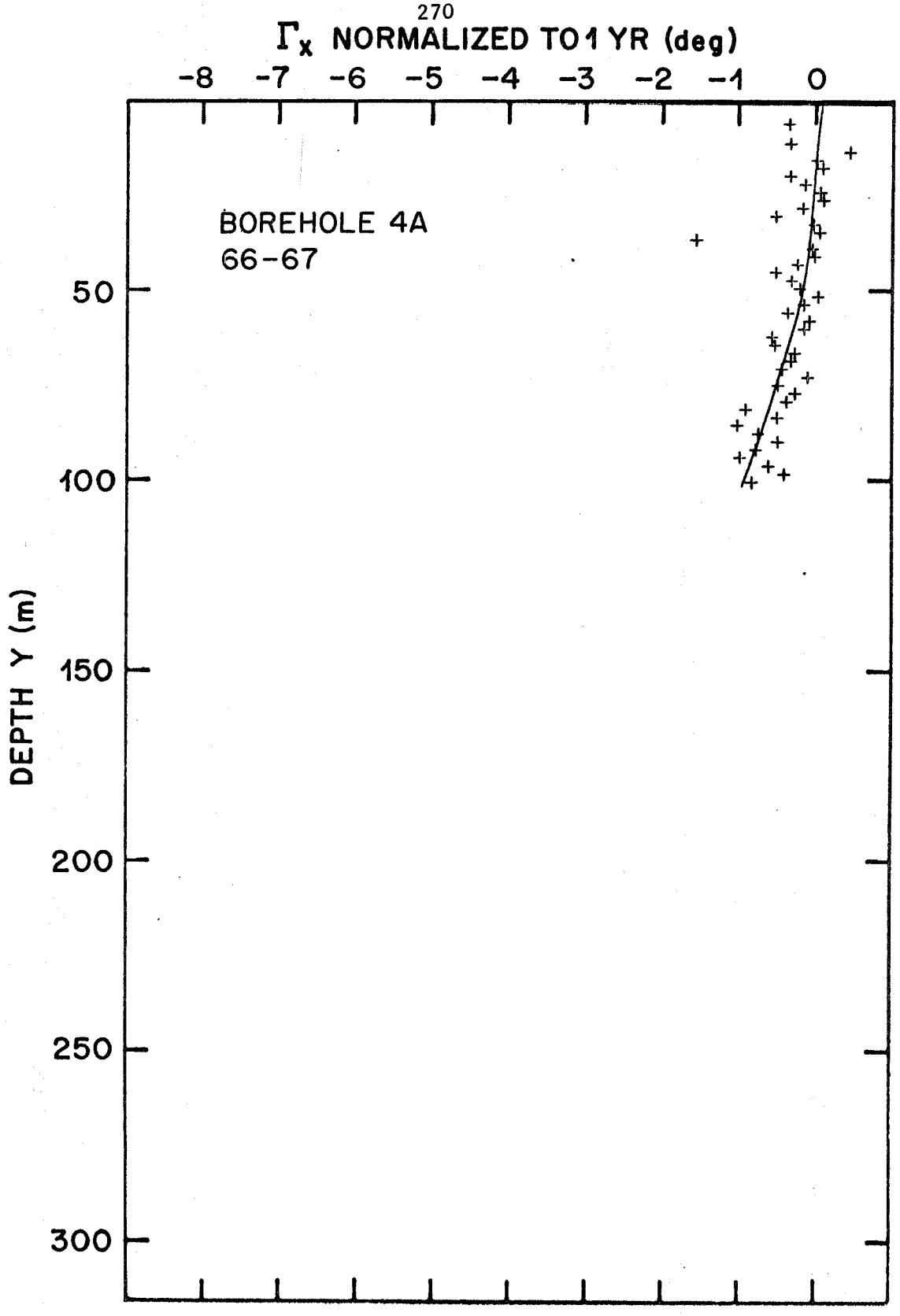
Γ_x NORMALIZED TO 1 YR (deg)
-8
-7
-6
-5
-4
-3
-2
-1
0
BOREHOLE 4A
66-67
DEPTH Y (m)
50
100
150
200
250
300

FIGURE 13h.

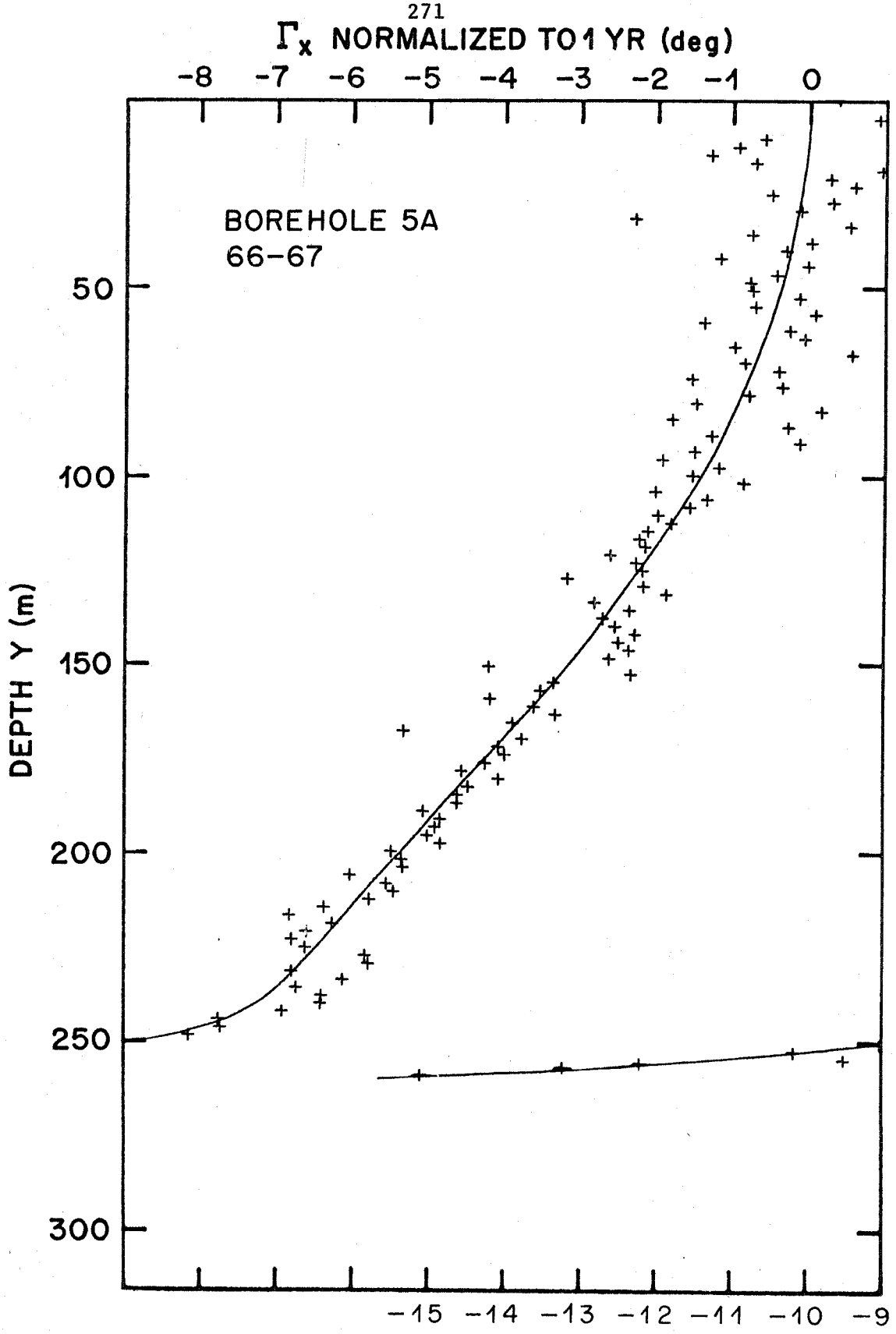
Γ_x NORMALIZED TO 1 YR (deg)
-8 -7 -6 -5 -4 -3 -2 -1 0
BOREHOLE 5A
66-67
DEPTH Y (m)
50
100
150
200
250
300
-15 -14 -13 -12 -11 -10 -9

FIGURE 13i.

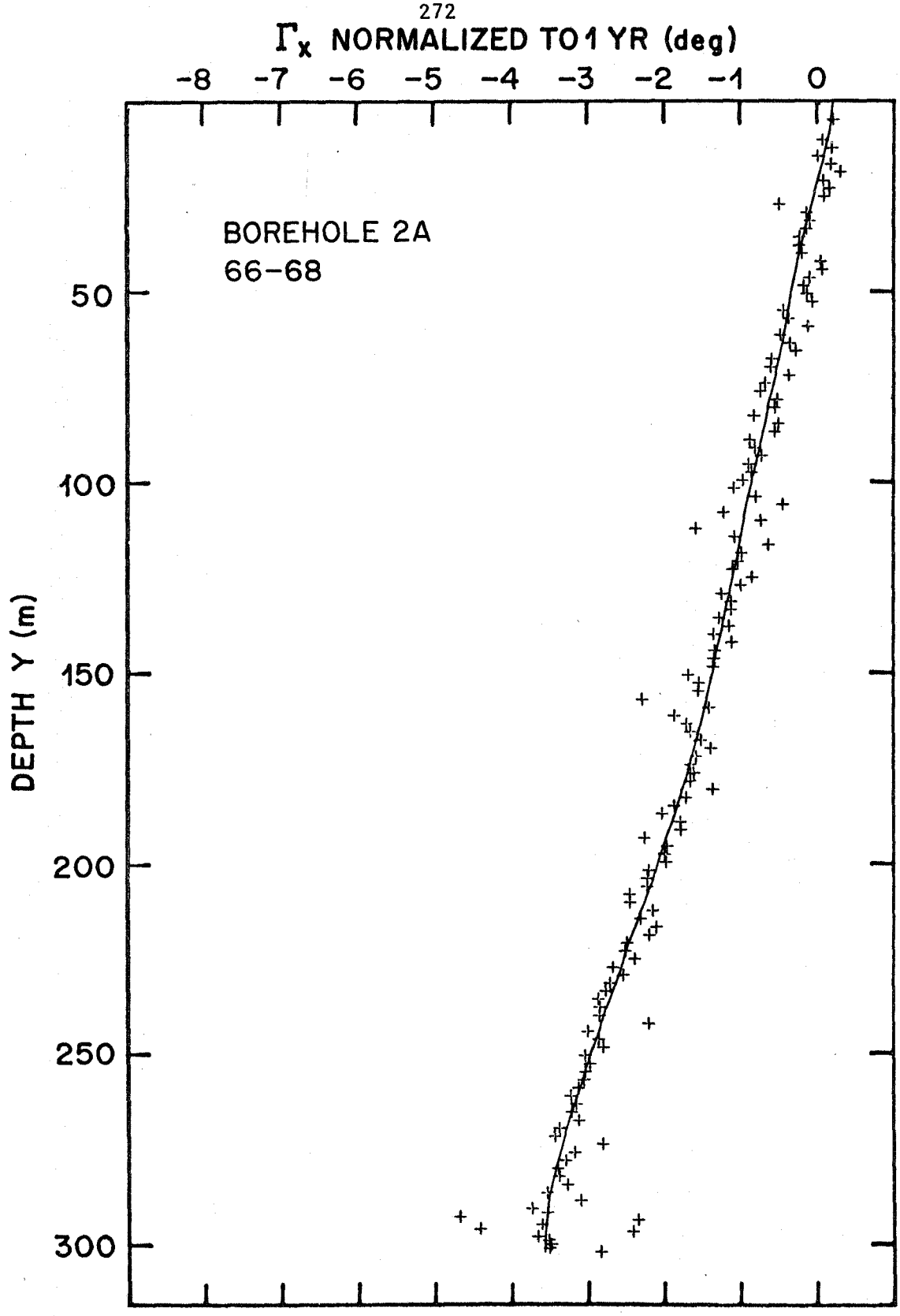
Γ_x NORMALIZED TO 1 YR (deg)
-8
-7
-6
-5
-4
-3
-2
-1
0
BOREHOLE 2A
66-68
DEPTH Y (m)
50
100
150
200
250
300

FIGURE 13j.

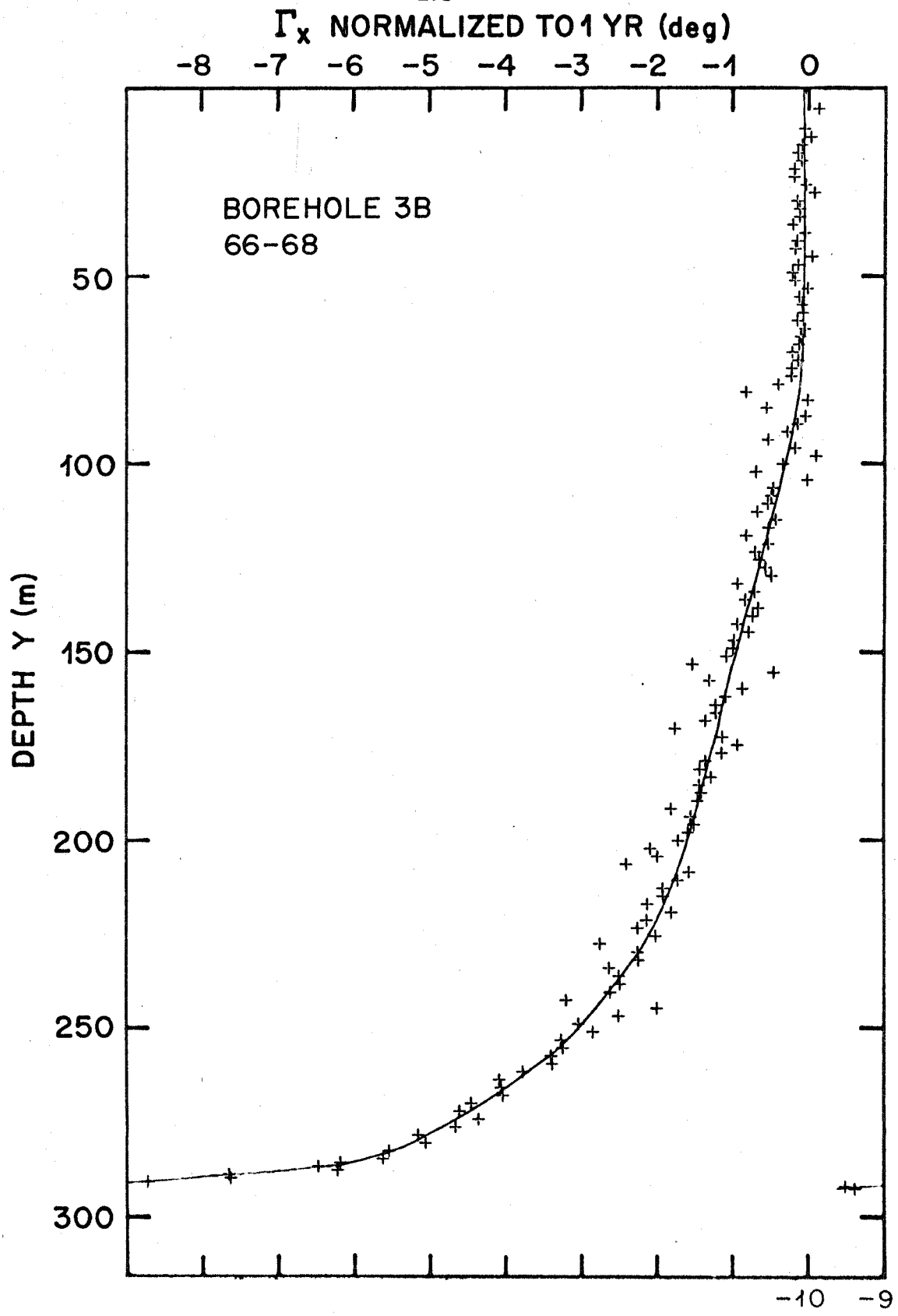
Γ_x NORMALIZED TO 1 YR (deg)
-8
-7
-6
-5
-4
-3
-2
-1
0
BOREHOLE 3B
66-68
DEPTH Y (m)
50
100
150
200
250
300
-10
-9

FIGURE 13k.

FIGURE 14. TRANSVERSE COMPONENT OF TILT IN DEFORMED BOREHOLES

Plotted values are normalized to a one year interval by dividing the values measured at the time of inclinometry by the interval of time in years between completion of the original borehole and inclinometry of the deformed borehole. (See following pages.)

a. Borehole 1A 66-67
b. Borehole 1B 66-67
c. Borehole 1C 66-67
d. Borehole 2A 66-67
e. Borehole 2B 66-67
f. Borehole 3A 66-67
g. Borehole 3B 66-67
h. Borehole 4A 66-67
i. Borehole 5A 66-67
j. Borehole 2A 66-68
k. Borehole 3B 66-68

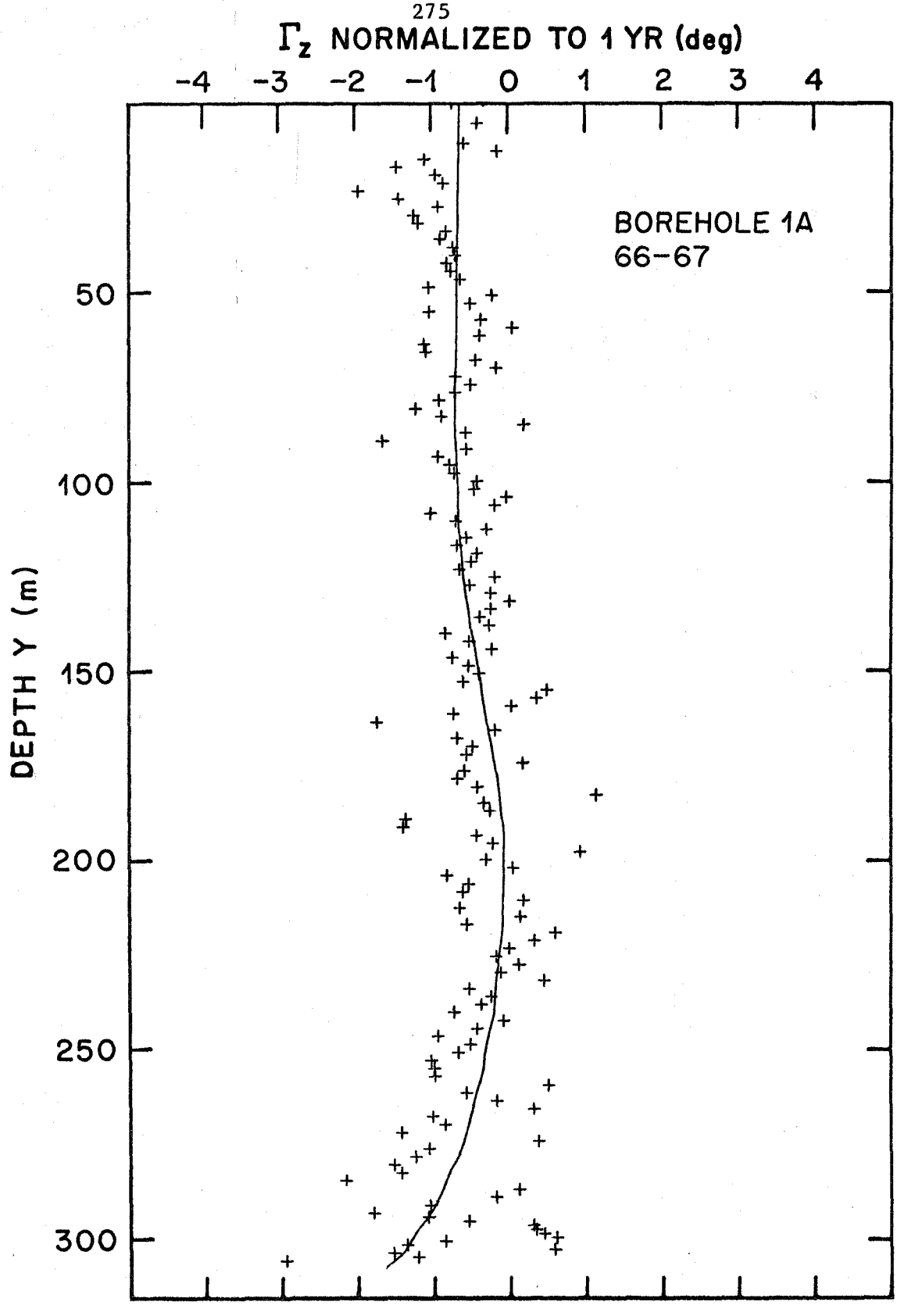
Γ_z NORMALIZED TO 1 YR (deg)
-4
-3
-2
-1
0
1
2
3
4
BOREHOLE 1A
66-67
DEPTH Y (m)
50
100
150
200
250
300

FIGURE 14a.

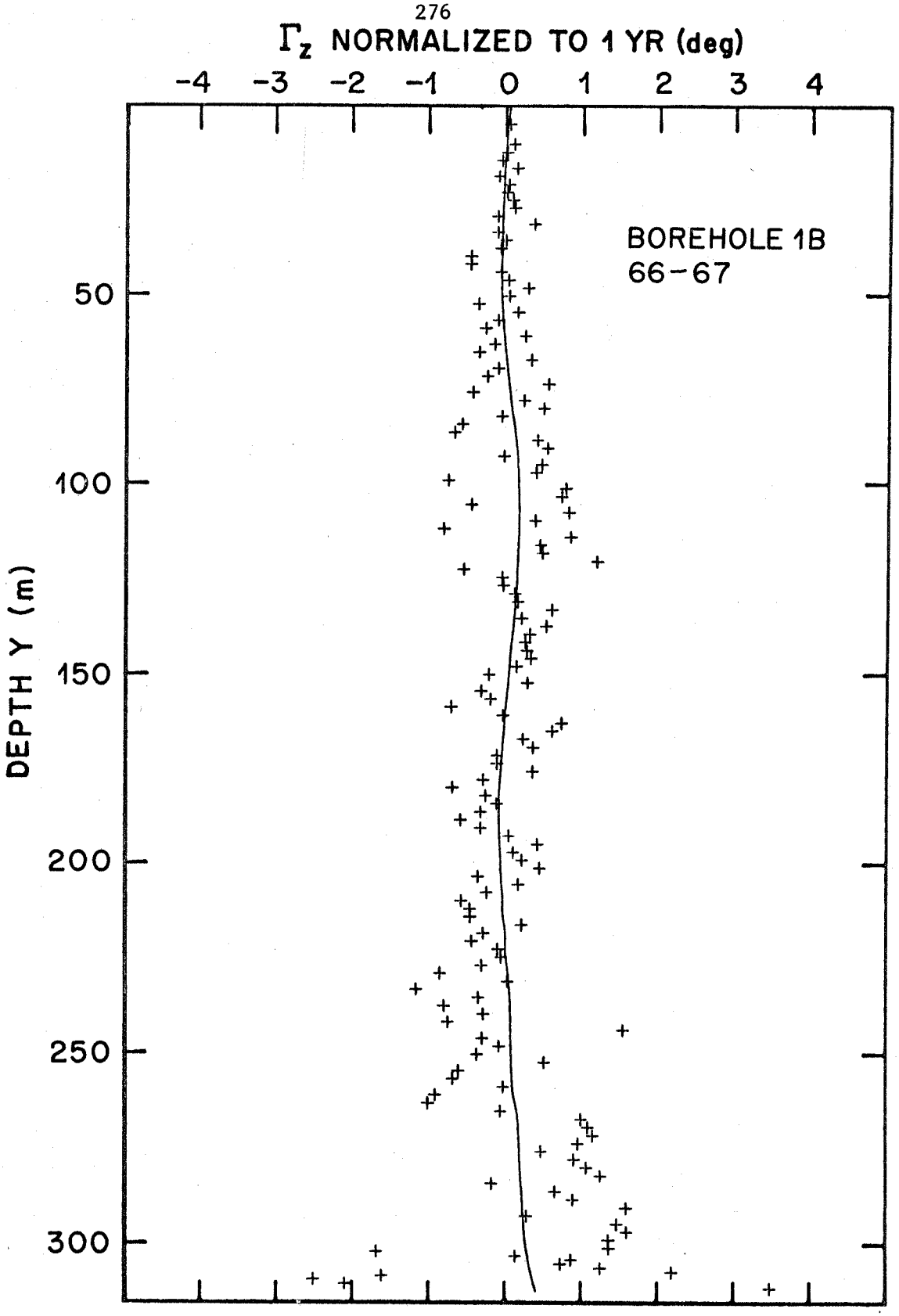
Γ_z NORMALIZED TO 1 YR (deg)
-4
-3
-2
-1
0
1
2
3
4
BOREHOLE 1B
66-67
DEPTH Y (m)
50
100
150
200
250
300

FIGURE 14b.

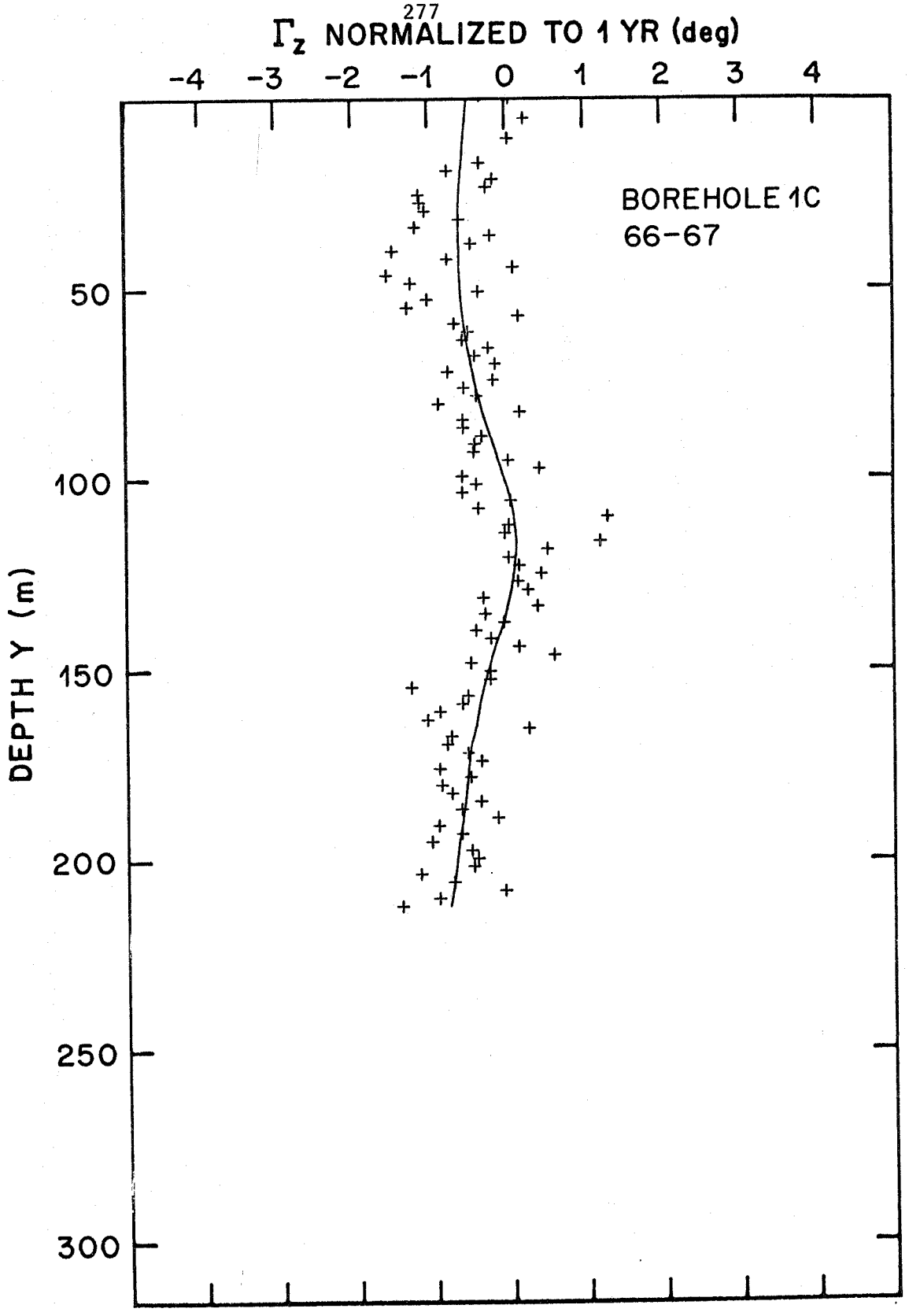
Γ_z NORMALIZED TO 1 YR (deg)
-4
-3
-2
-1
0
1
2
3
4
BOREHOLE 1C
66-67
DEPTH Y (m)
50
100
150
200
250
300

FIGURE 14c.

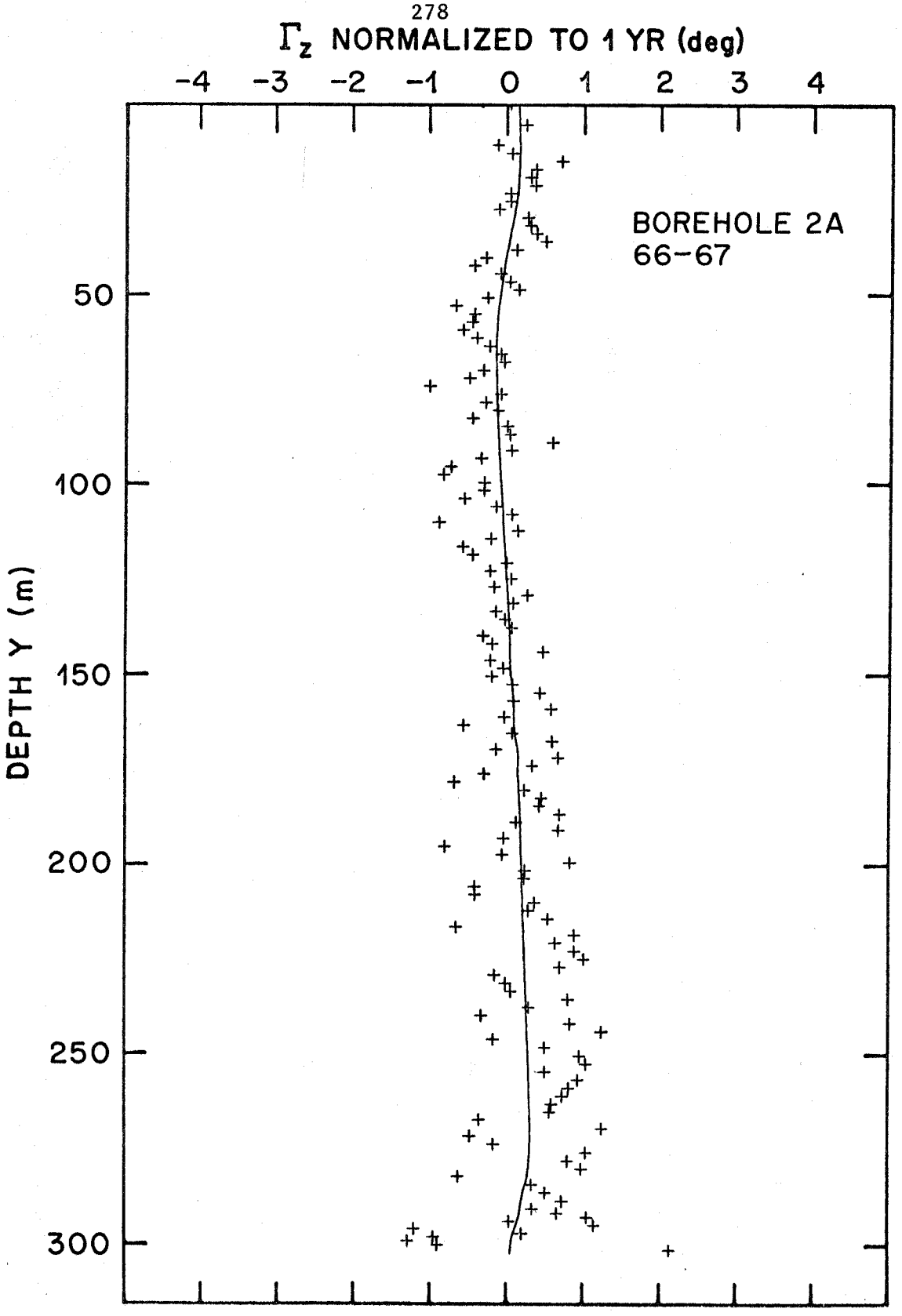
Γ_z NORMALIZED TO 1 YR (deg)
-4
-3
-2
-1
0
1
2
3
4
BOREHOLE 2A
66-67
DEPTH Y (m)
50
100
150
200
250
300

FIGURE 14d.

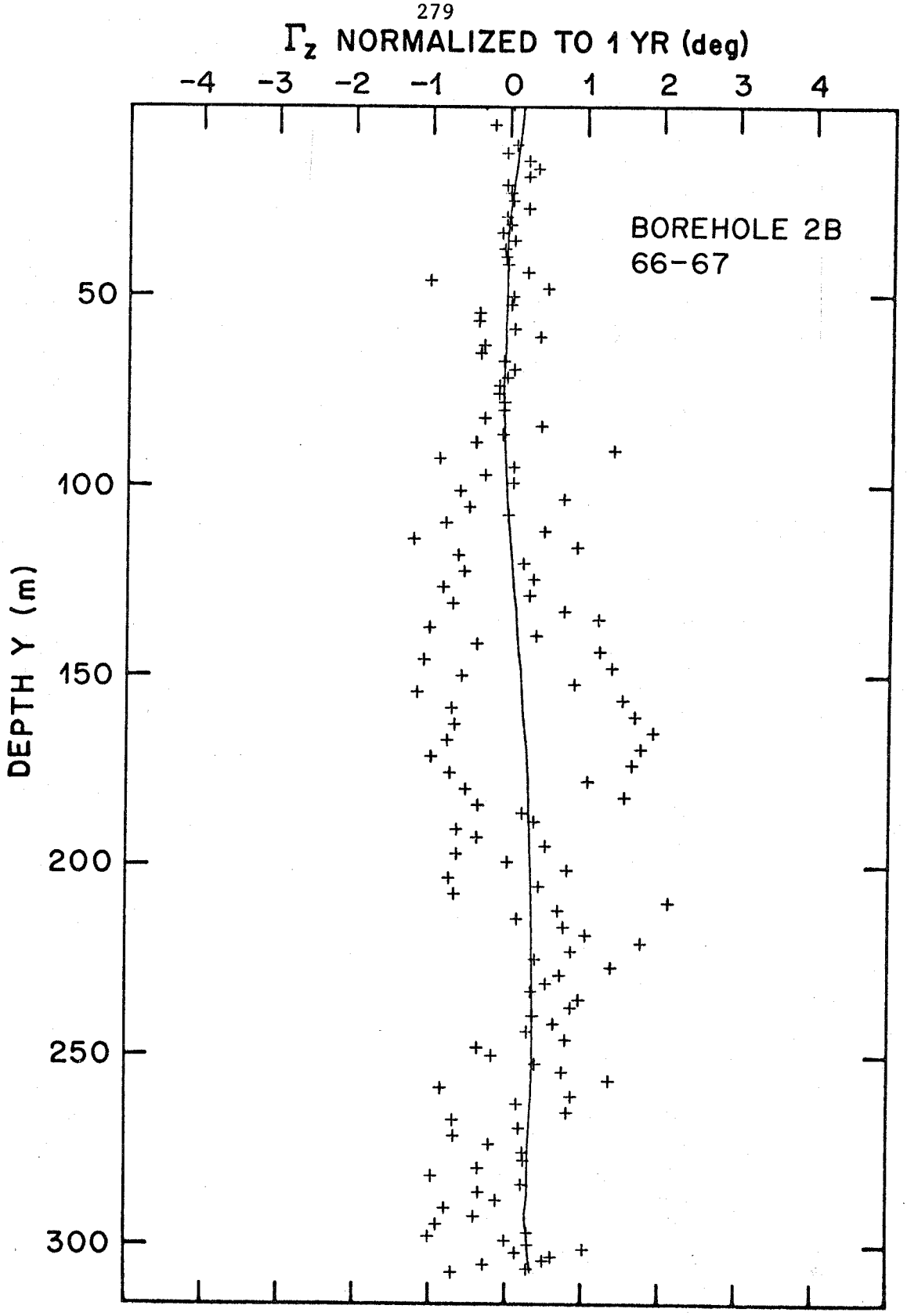
Γ_z NORMALIZED TO 1 YR (deg)
-4
-3
-2
-1
0
1
2
3
4
BOREHOLE 2B
66-67
DEPTH Y (m)
50
100
150
200
250
300

FIGURE 14e.

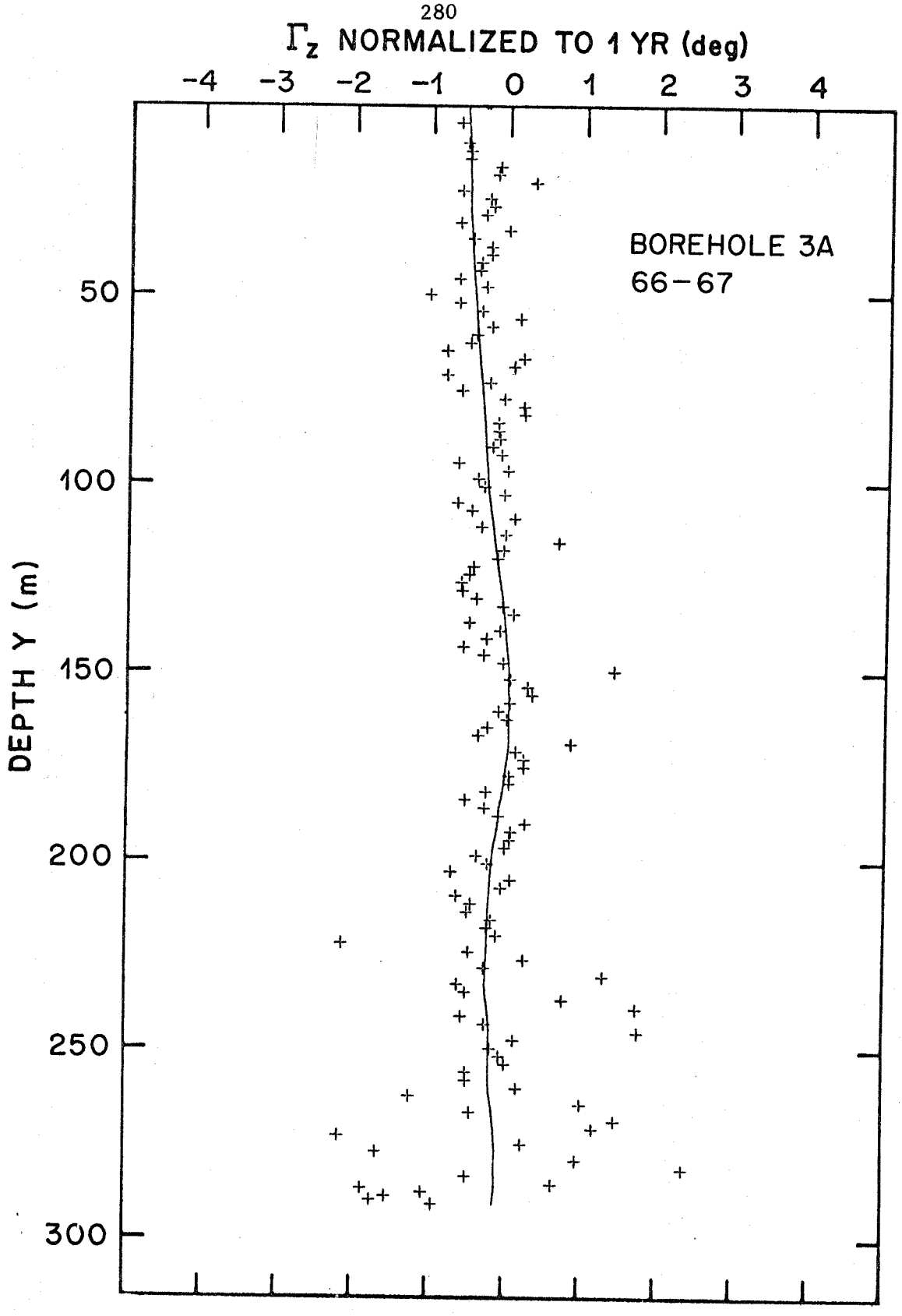
Γ_z NORMALIZED TO 1 YR (deg)
-4
-3
-2
-1
0
1
2
3
4
BOREHOLE 3A
66-67
DEPTH Y (m)
50
100
150
200
250
300

FIGURE 14f.

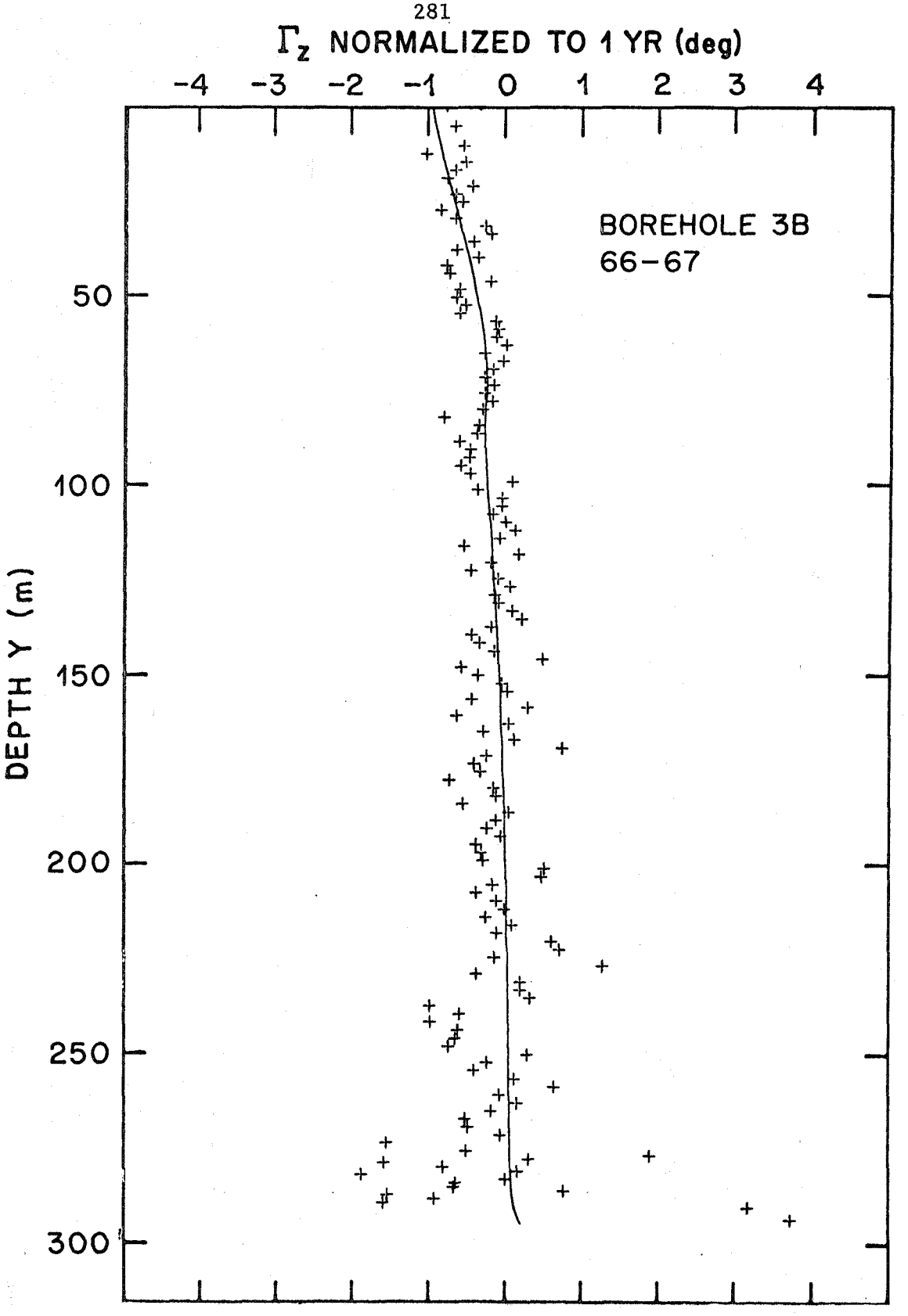
Γ_z NORMALIZED TO 1 YR (deg)
-4
-3
-2
-1
0
1
2
3
4
BOREHOLE 3B
66-67
DEPTH Y (m)
50
100
150
200
250
300

FIGURE 14g.

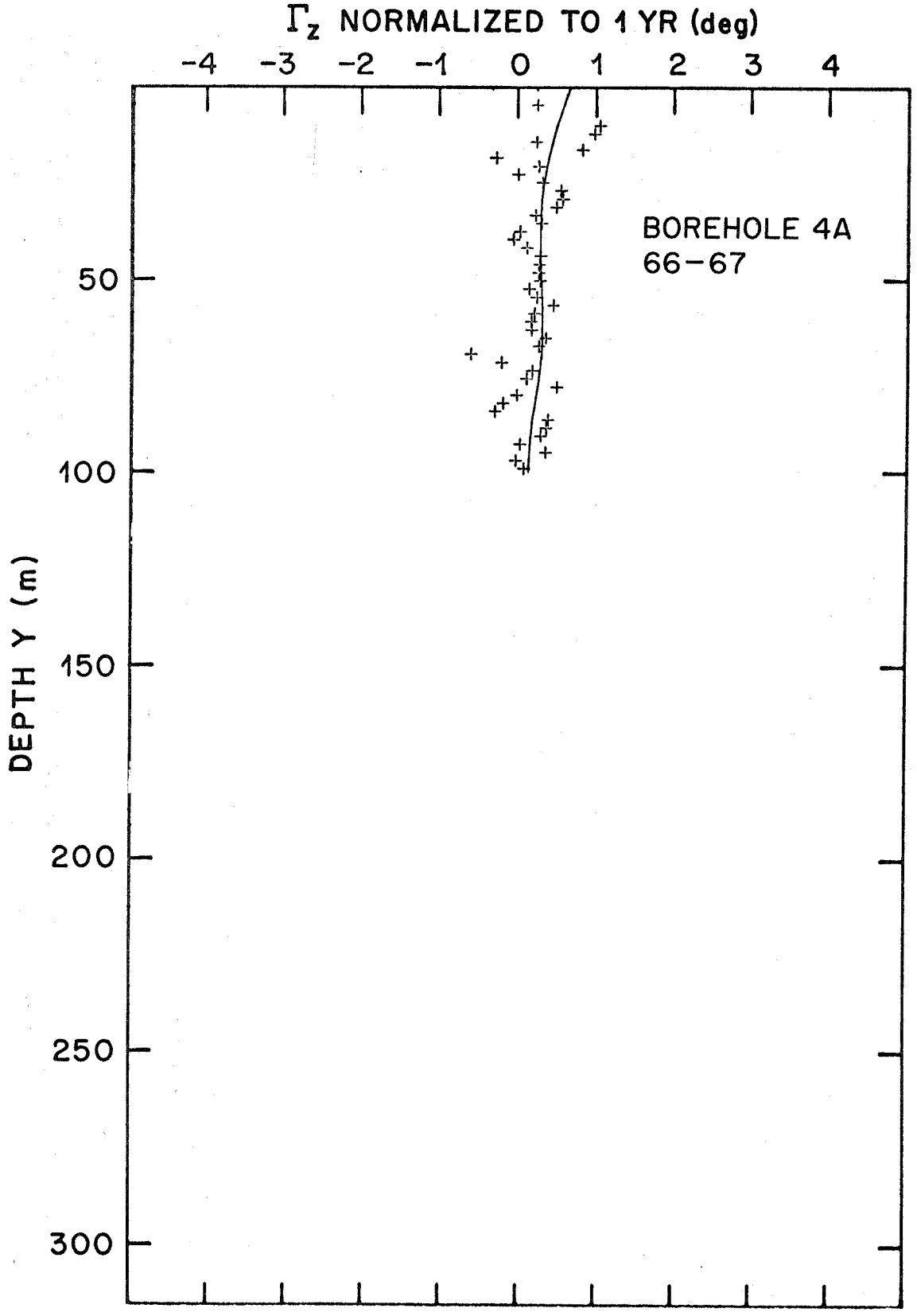
Γ_z NORMALIZED TO 1 YR (deg)
-4
-3
-2
-1
0
1
2
3
4
BOREHOLE 4A
66-67
DEPTH Y (m)
50
100
150
200
250
300

FIGURE 14h.

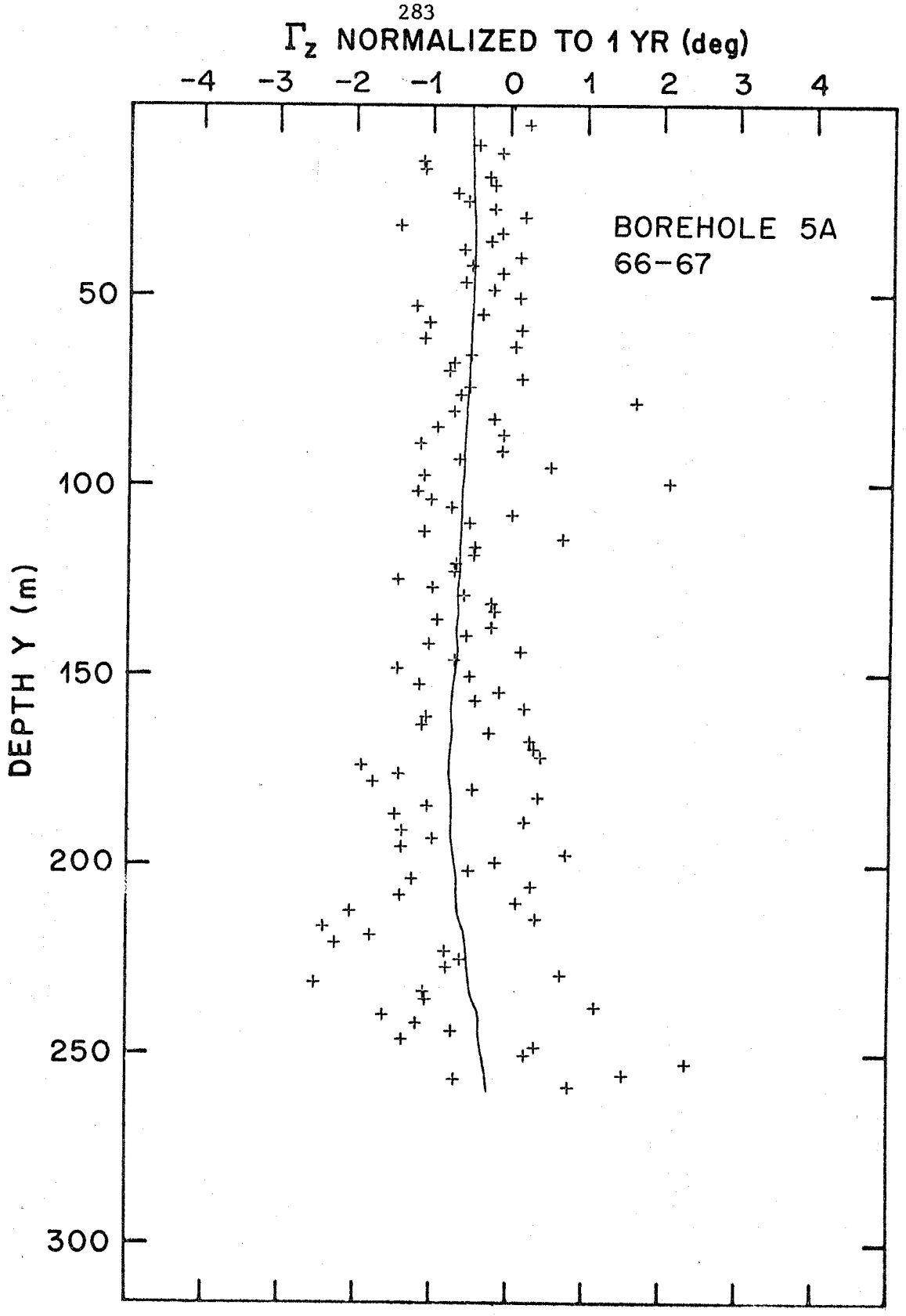
Γ_z NORMALIZED TO 1 YR (deg)
-4
-3
-2
-1
0
1
2
3
4
BOREHOLE 5A
66-67
DEPTH Y (m)
50
100
150
200
250
300

FIGURE 14i.

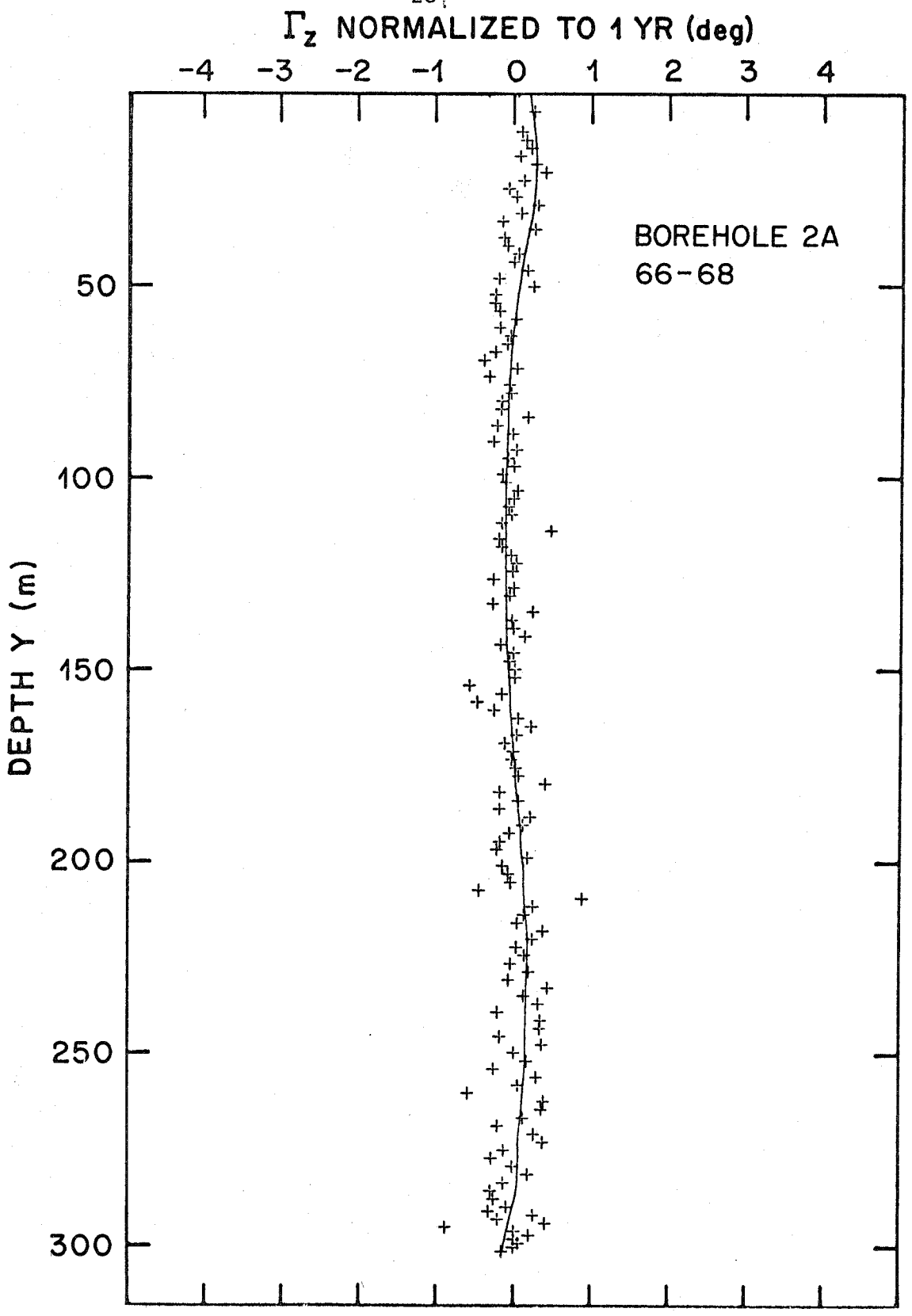
Γ_z NORMALIZED TO 1 YR (deg)
-4
-3
-2
-1
0
1
2
3
4
BOREHOLE 2A
66-68
DEPTH Y (m)
50
100
150
200
250
300

FIGURE 14j.

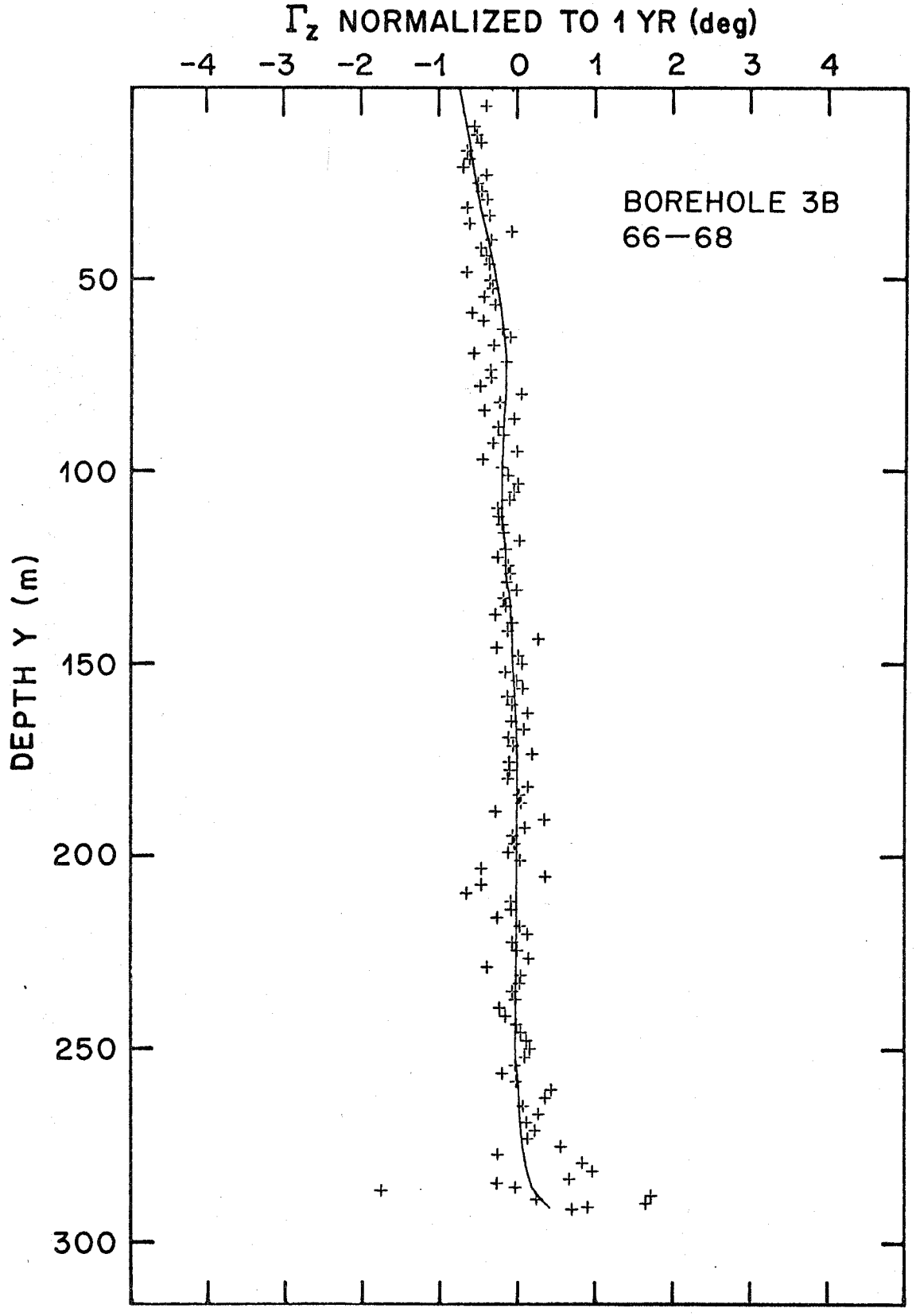
Γ_z NORMALIZED TO 1 YR (deg)
-4
-3
-2
-1
0
1
2
3
4
BOREHOLE 3B
66—68
DEPTH Y (m)
50
100
150
200
250
300

FIGURE 14k.

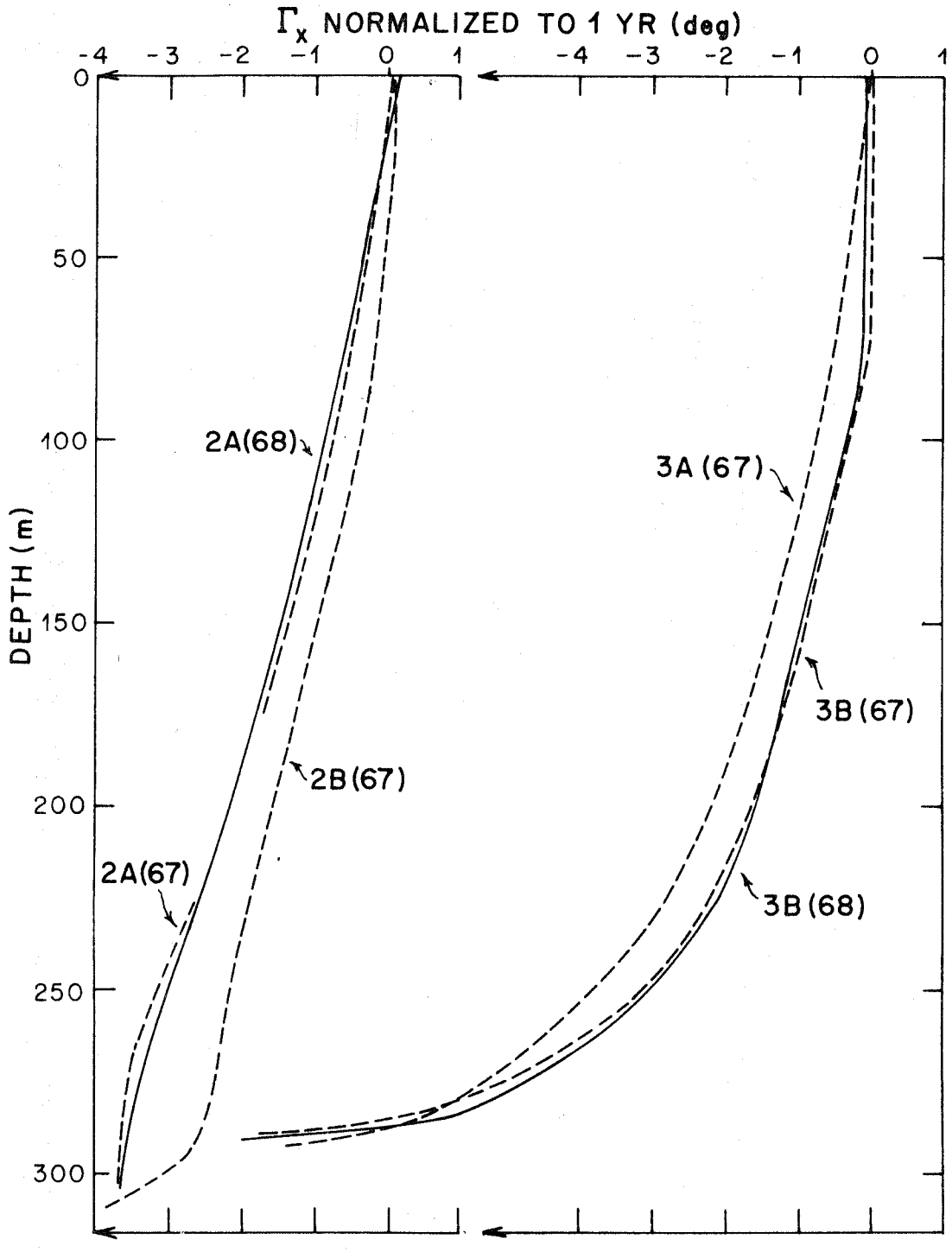

FIGURE 15. COMPARISON OF TILT PROFILES FOR 66-67 AND 66-68 INTERVALS

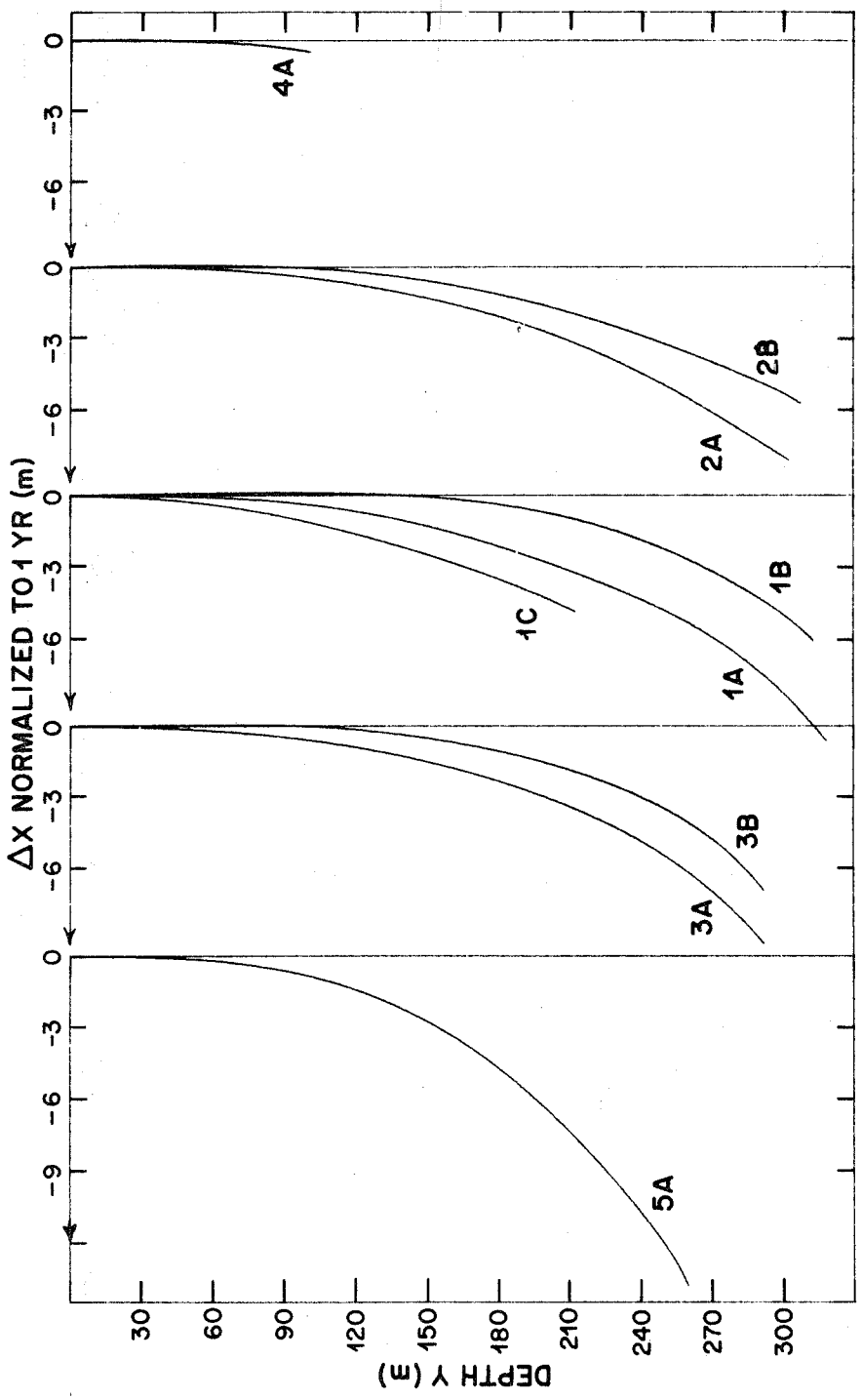

FIGURE 16. LONGITUDINAL DIFFERENTIAL DISPLACEMENT IN BOREHOLES

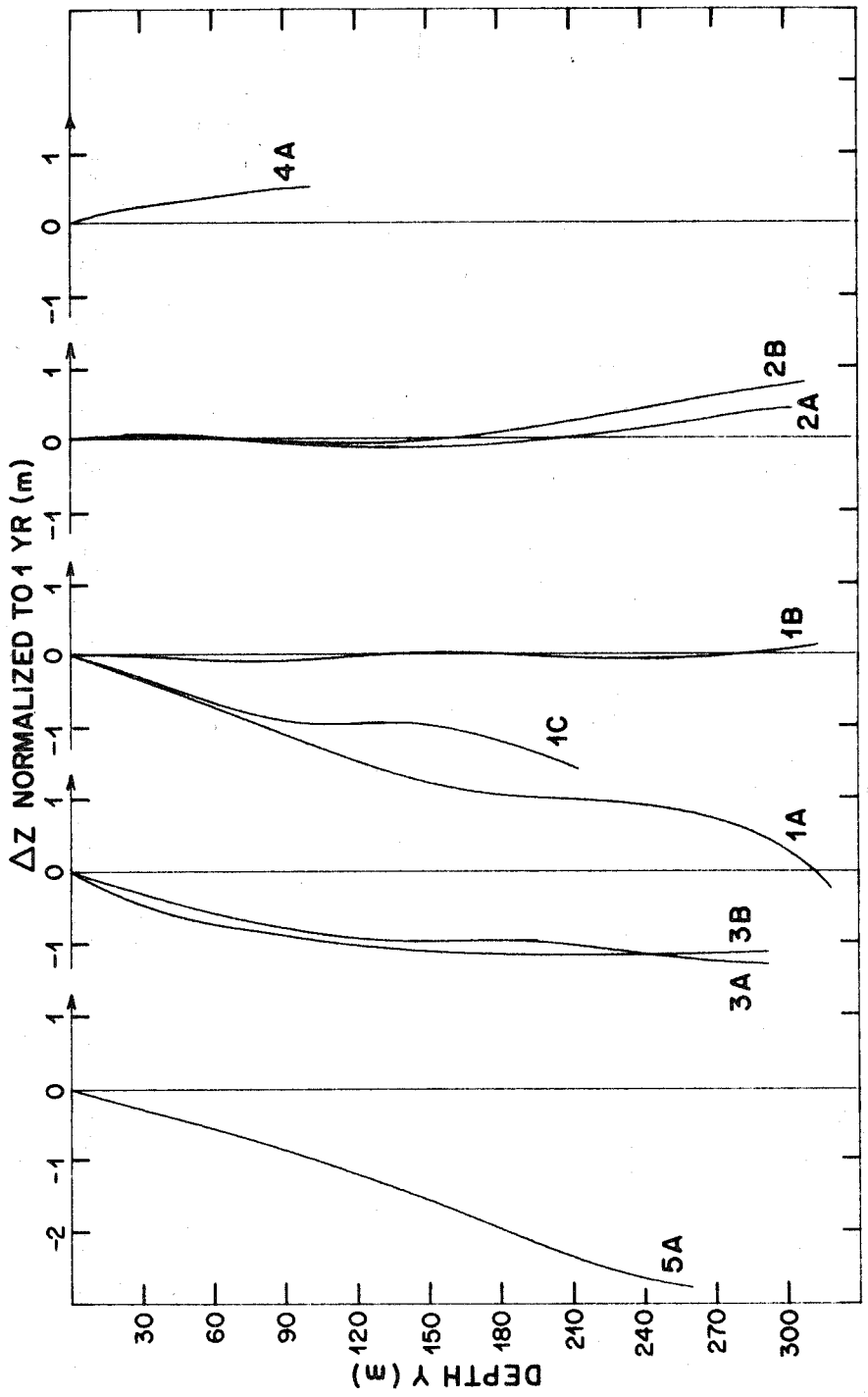

FIGURE 17. TRANSVERSE DIFFERENTIAL DISPLACEMENT IN BOREHOLES

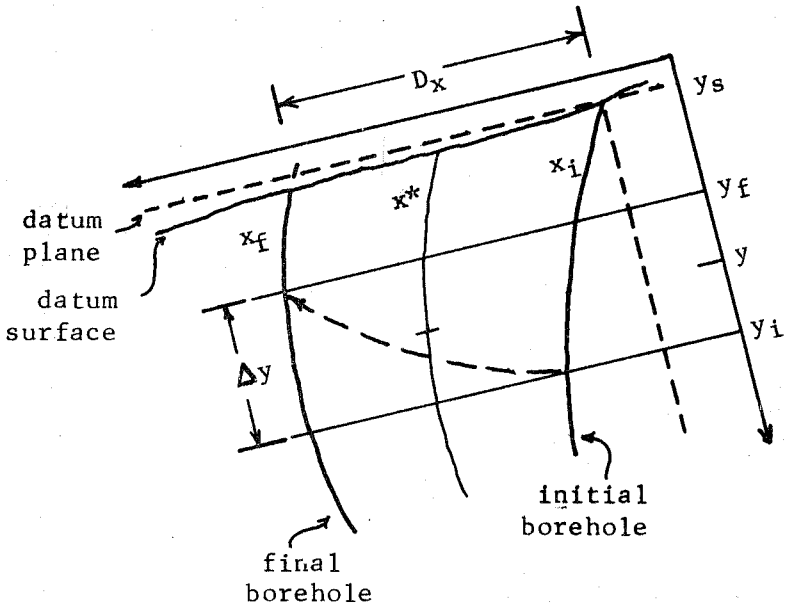

FIGURE 18. CALCULATION OF VELOCITY FROM BOREHOLE COORDINATES

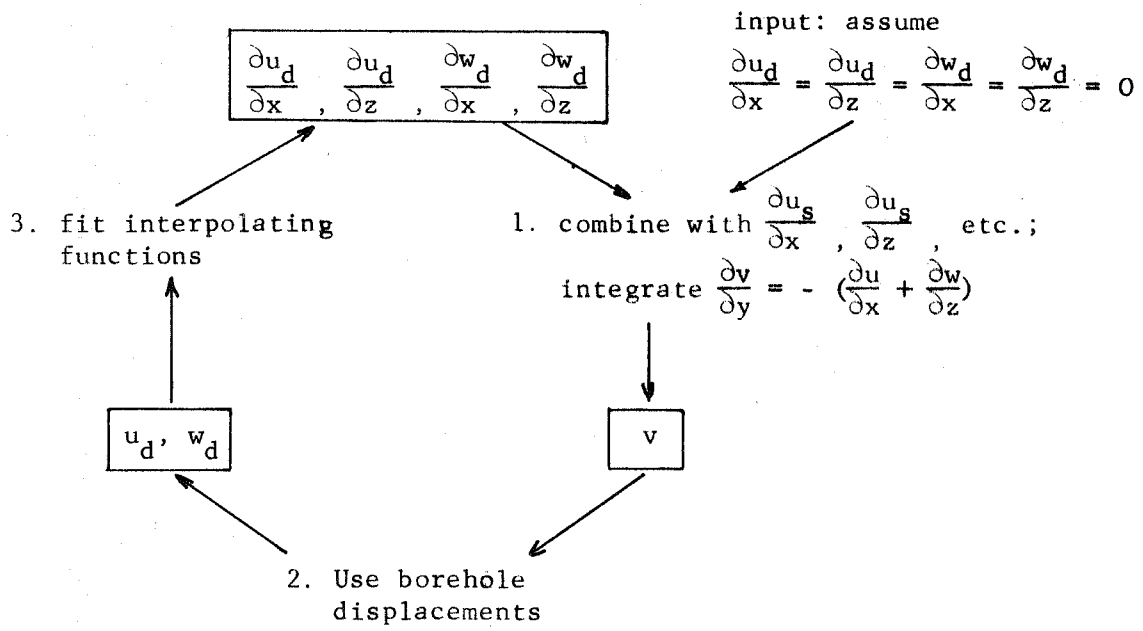

FIGURE 19. ITERATIVE CYCLE FOR CALCULATION OF VELOCITY AND STRAIN RATE

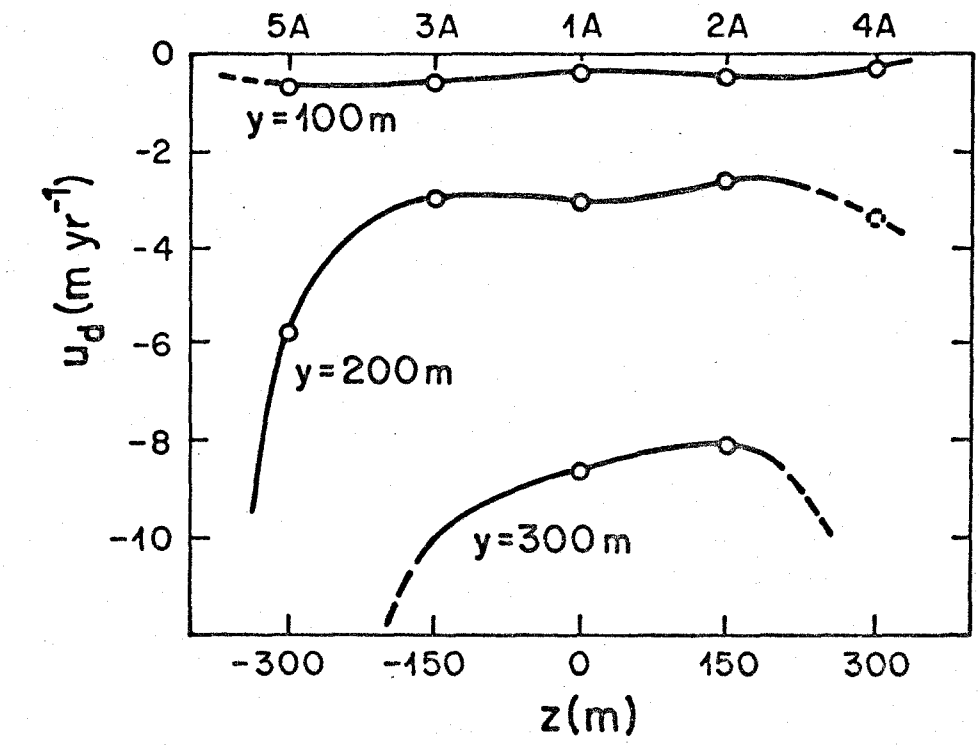

a) u_d vs. z for selected depths at section A

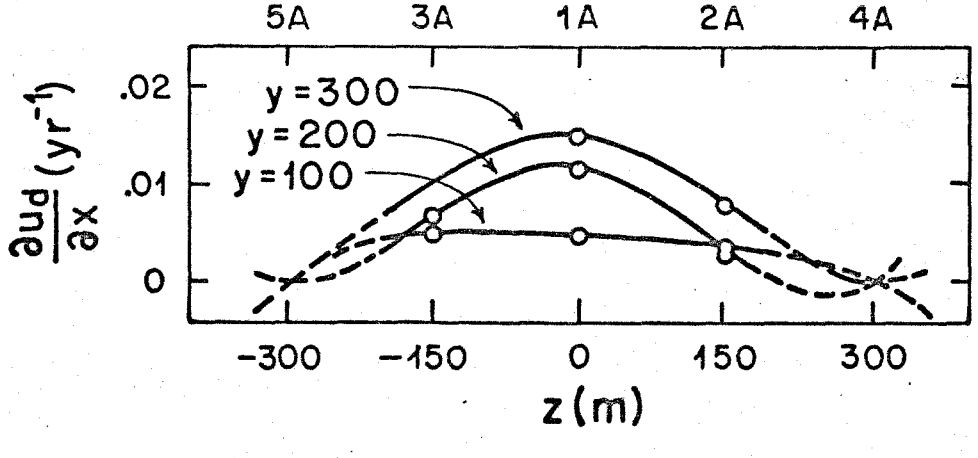

b) $\frac{\partial u_d}{\partial x}$ vs. z for selected depths at section A

FIGURE 20. INTERPOLATION OF LONGITUDINAL DIFFERENTIAL VELOCITY

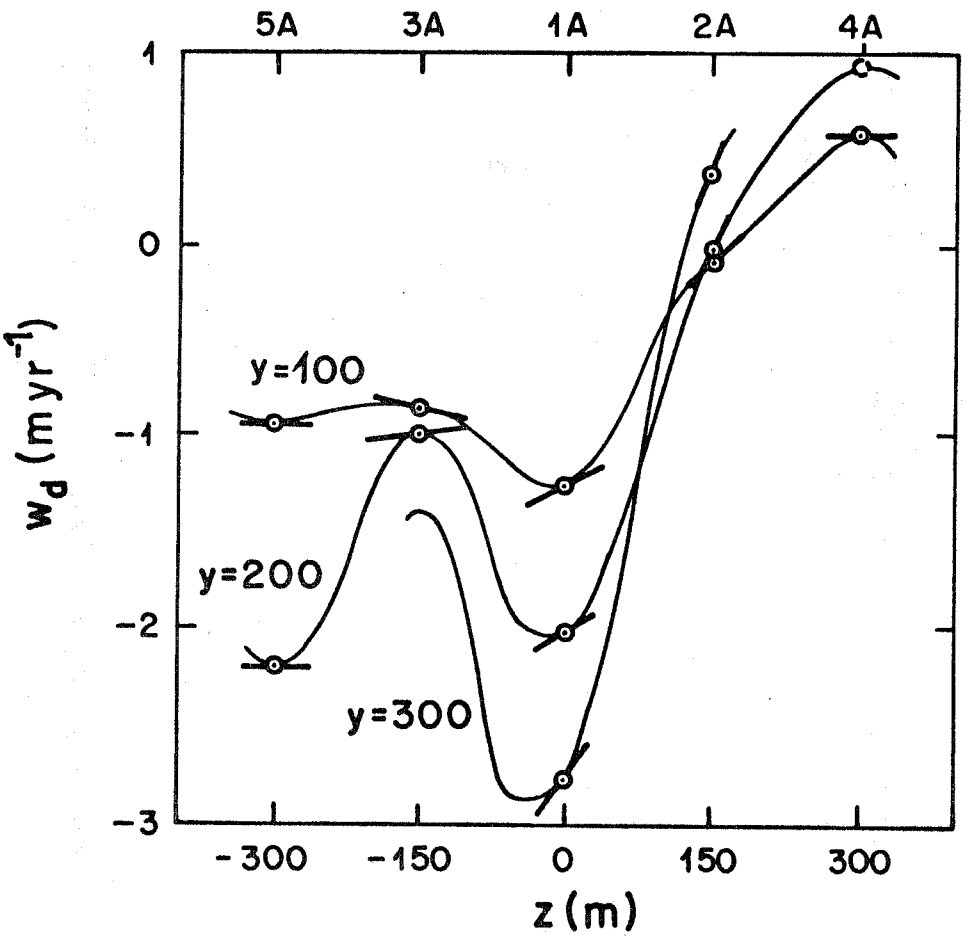

FIGURE 21. INTERPOLATION OF TRANSVERSE DIFFERENTIAL VELOCITY
Computed derivatives $\frac{\partial w_d}{\partial z}$ are represented by line segments; curves represent interpolating functions which are compatible with the computed slopes.

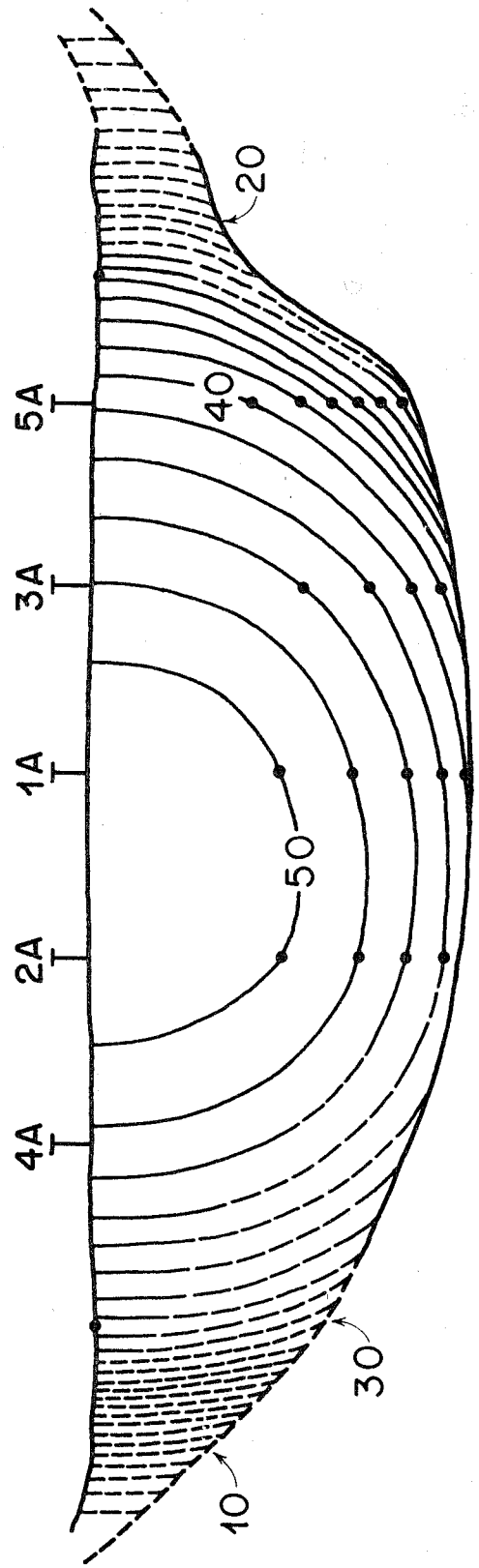

FIGURE 22a. CONTOUR DIAGRAM OF LONGITUDINAL VELOCITY AT SECTION A
Contour interval is 2 m yr^{-1}.

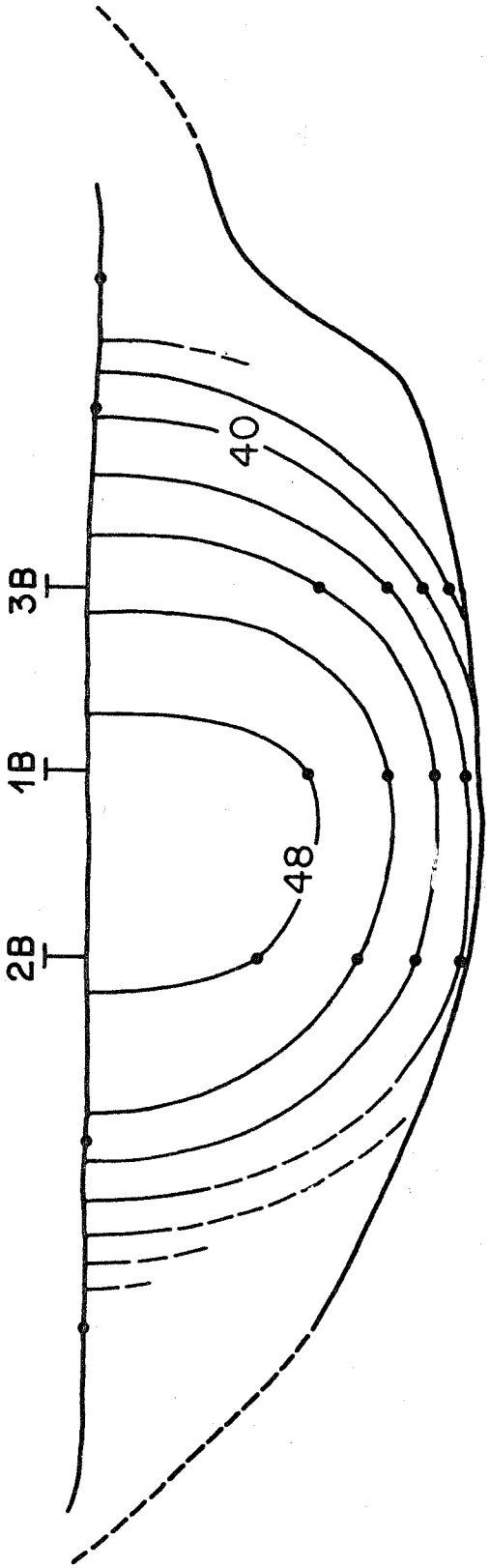

FIGURE 22b. CONTOUR DIAGRAM OF LONGITUDINAL VELOCITY AT SECTION B
Contour interval is 2 m yr^{-1}.

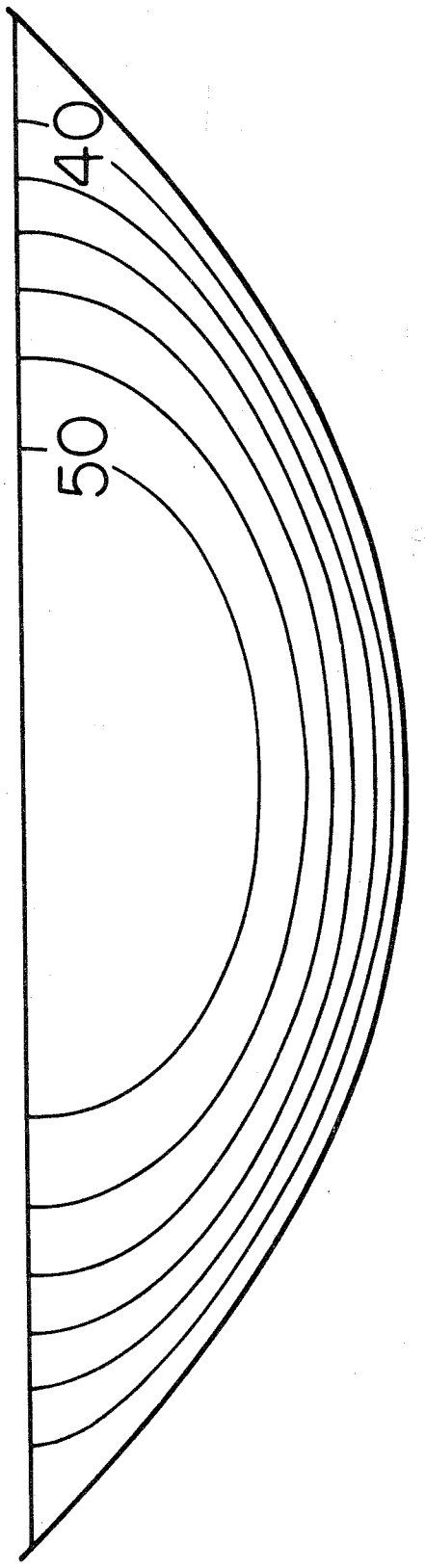

FIGURE 23. THEORETICAL DISTRIBUTION OF LONGITUDINAL VELOCITY (NYE, 1965)

The distribution of velocity for rectilinear flow in a cylindrical, parabolic channel (width ratio 2) of a homogeneous material obeying a power-type flow law (n = 3) as calculated by Nye has been scaled to cover approximately the observed range of velocity.

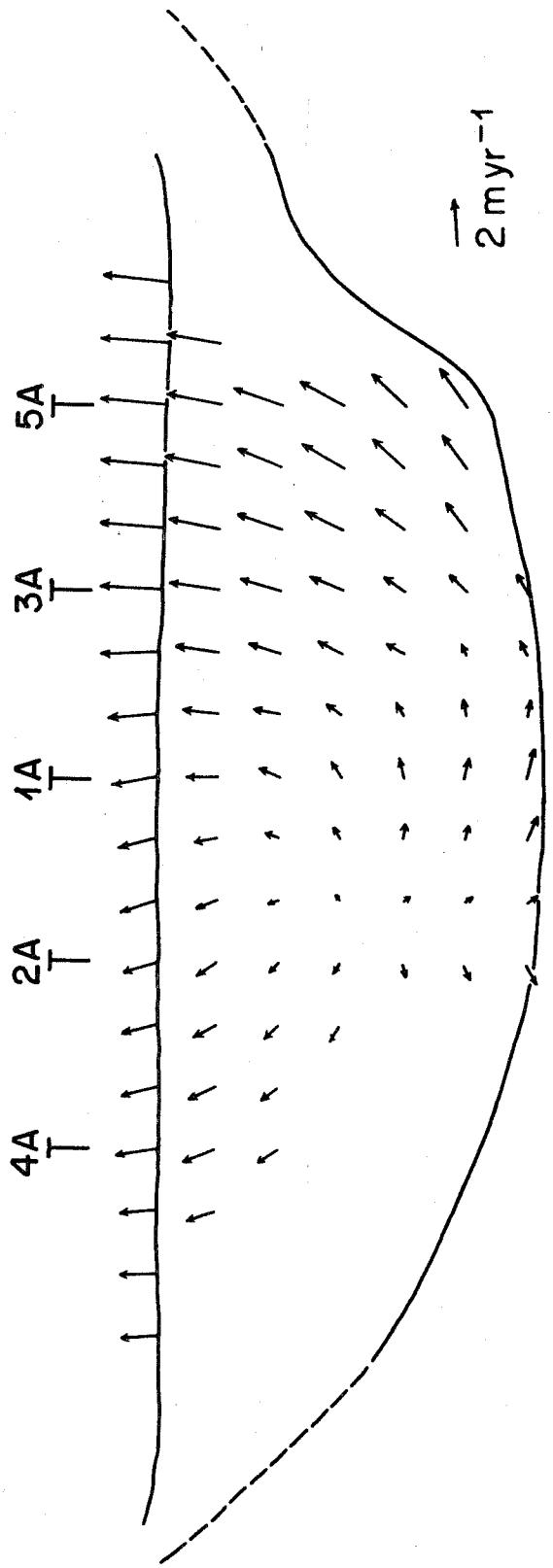

FIGURE 24a. VECTOR DIAGRAM OF TRANSVERSE VELOCITY AT SECTION A

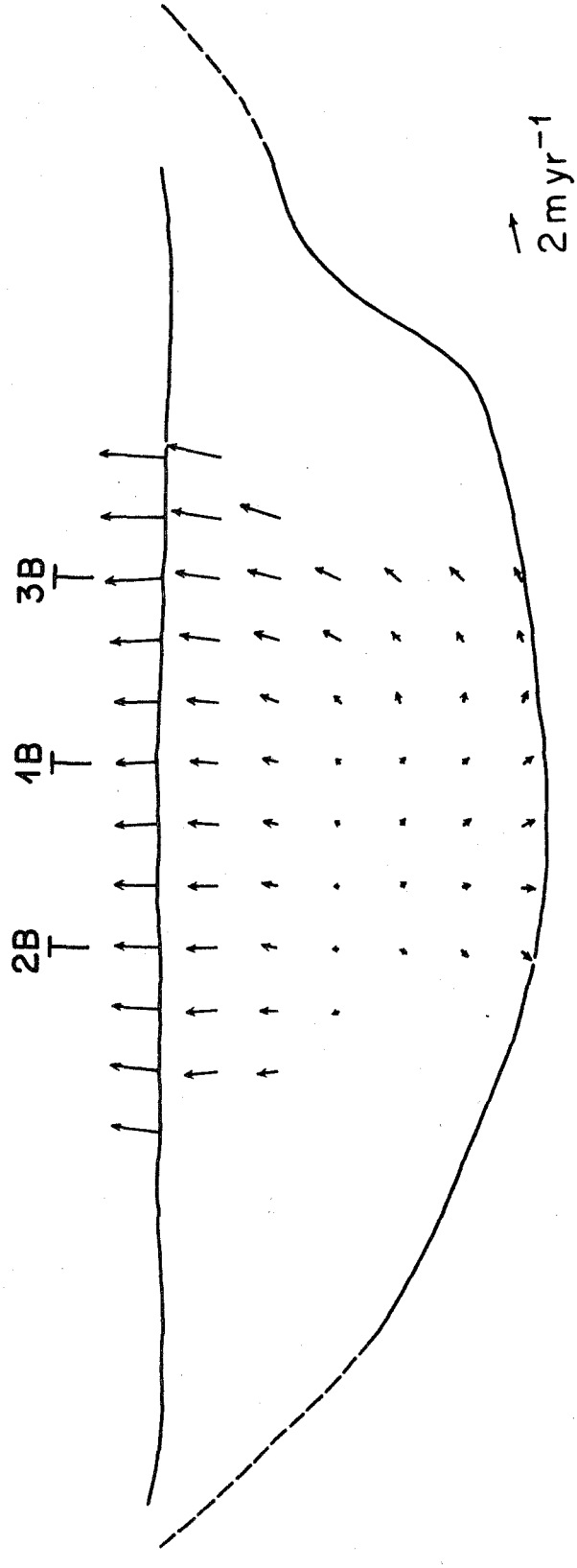

FIGURE 24b. VECTOR DIAGRAM OF TRANSVERSE VELOCITY AT SECTION B

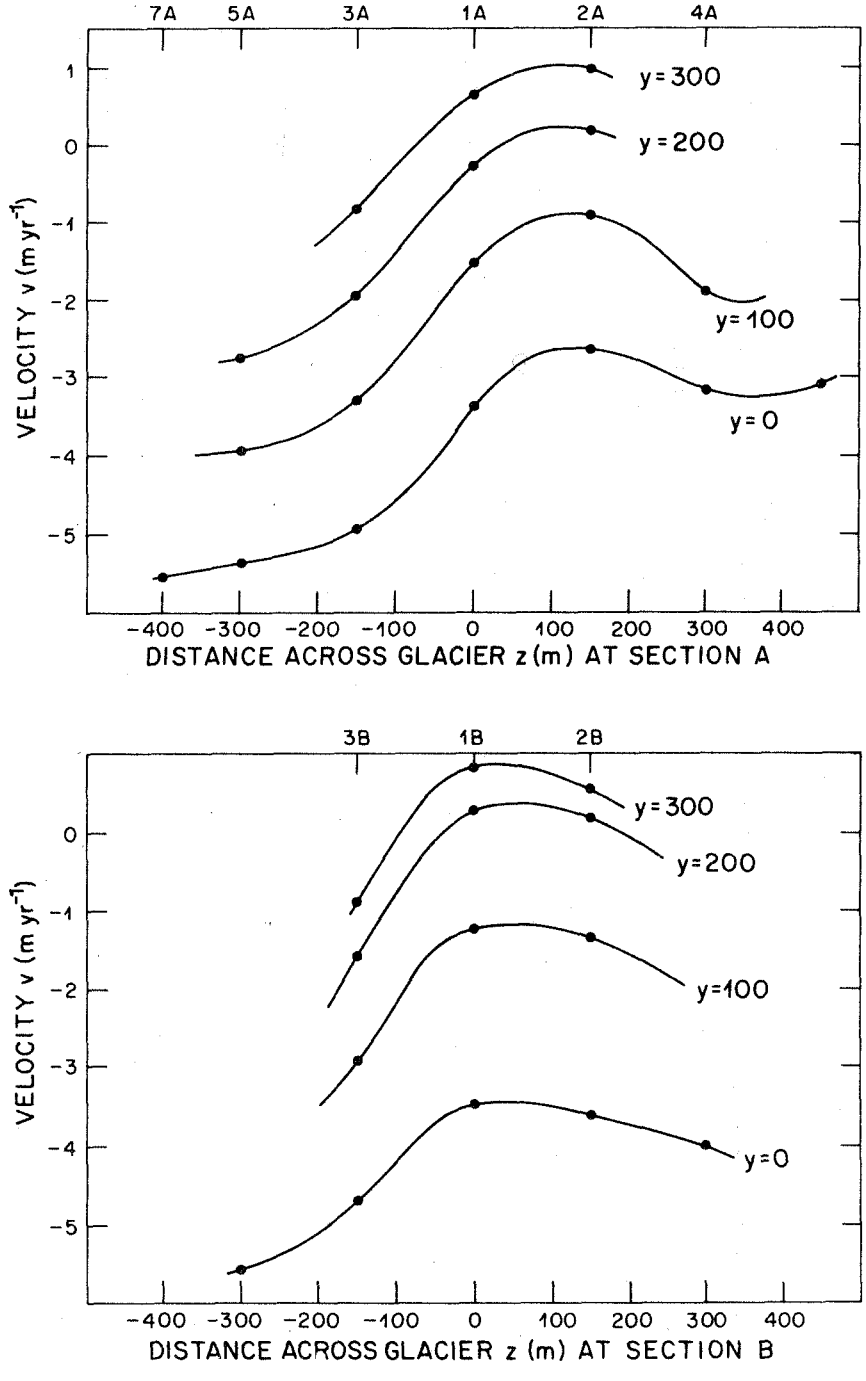

FIGURE 25. TRANSVERSE VARIATION OF y COMPONENT OF VELOCITY

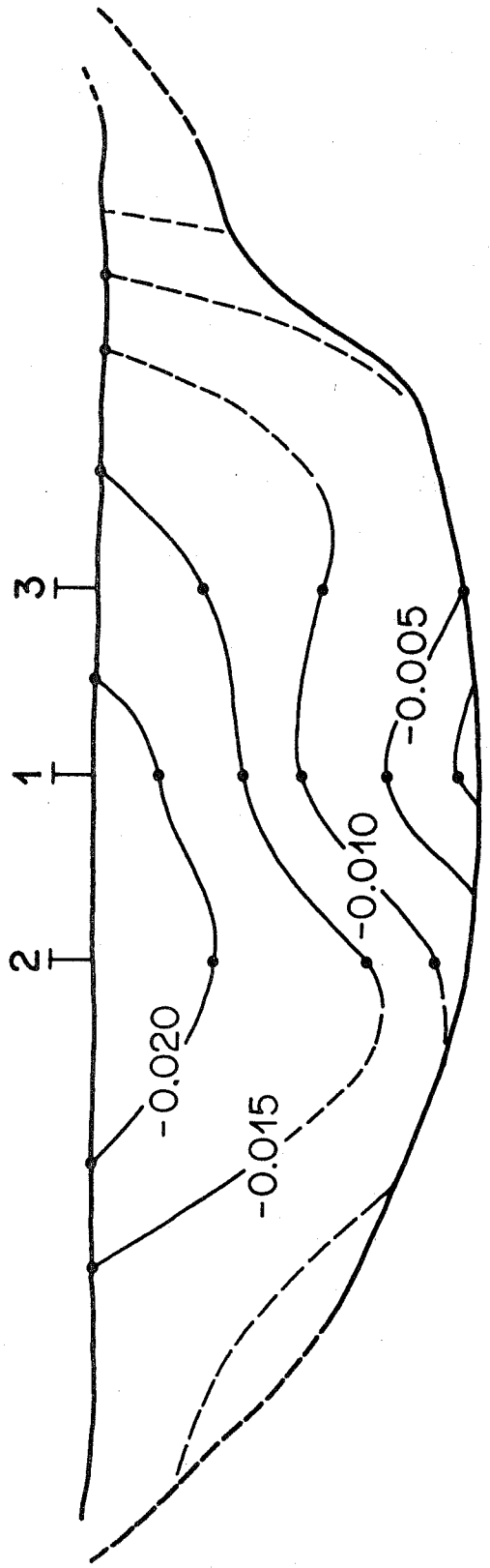

FIGURE 26. CONTOUR DIAGRAM OF LONGITUDINAL STRAIN RATE

Gives $\frac{\partial u}{\partial x}$ midway between sections A and B.

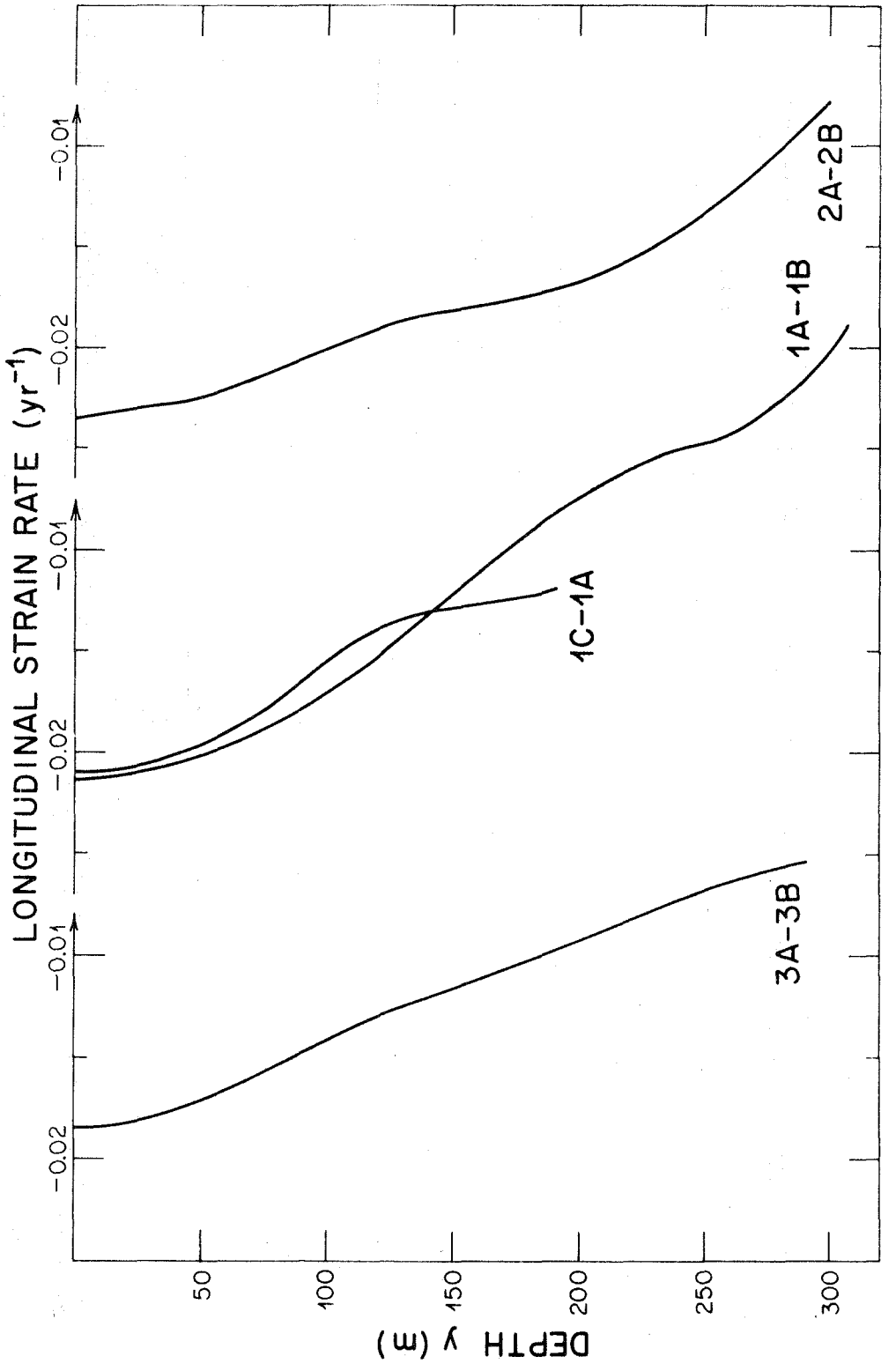

FIGURE 27. DEPTH DEPENDENCE OF LONGITUDINAL STRAIN RATE

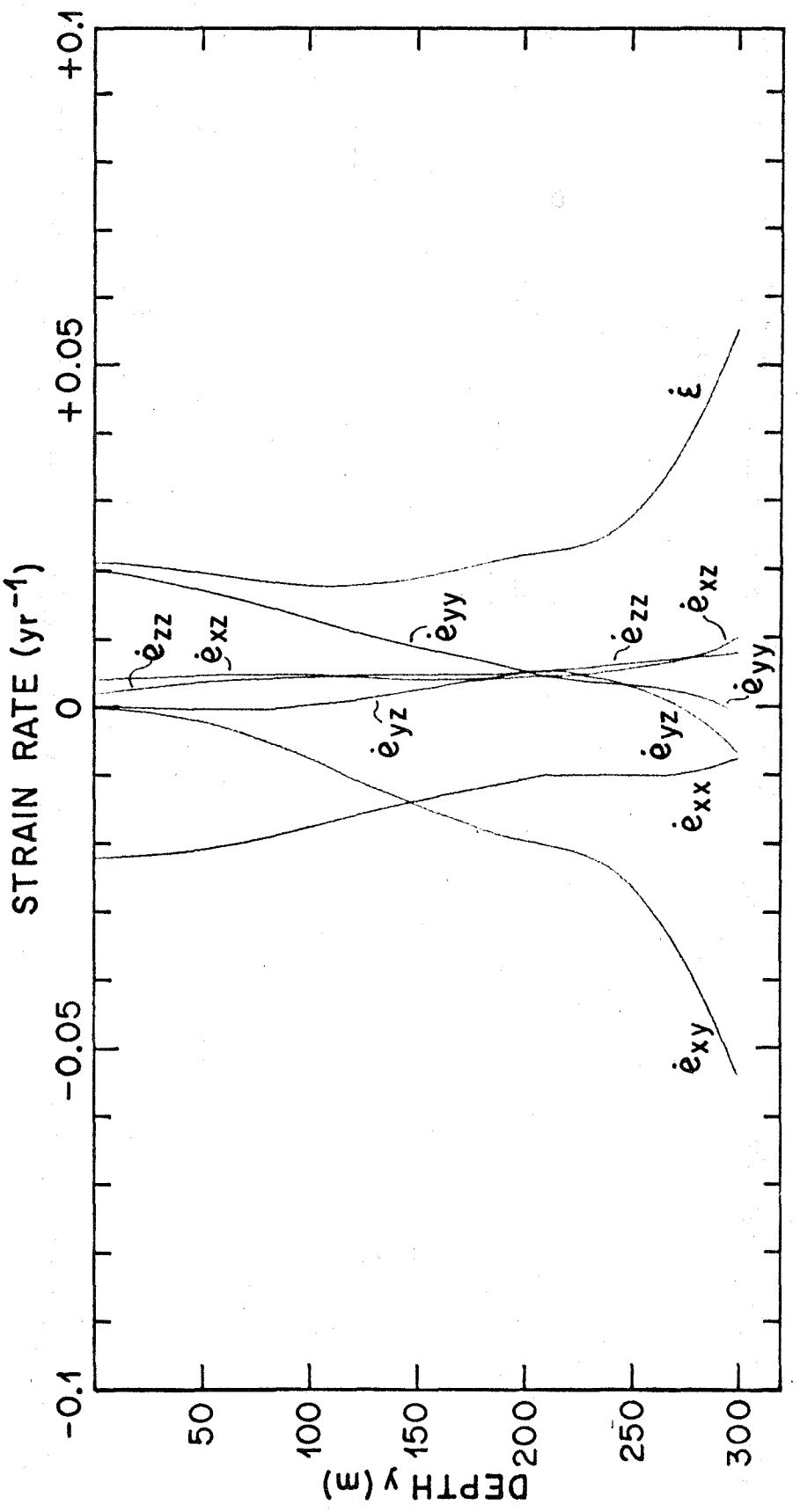

FIGURE 28a. STRAIN RATE AT BOREHOLE 1A

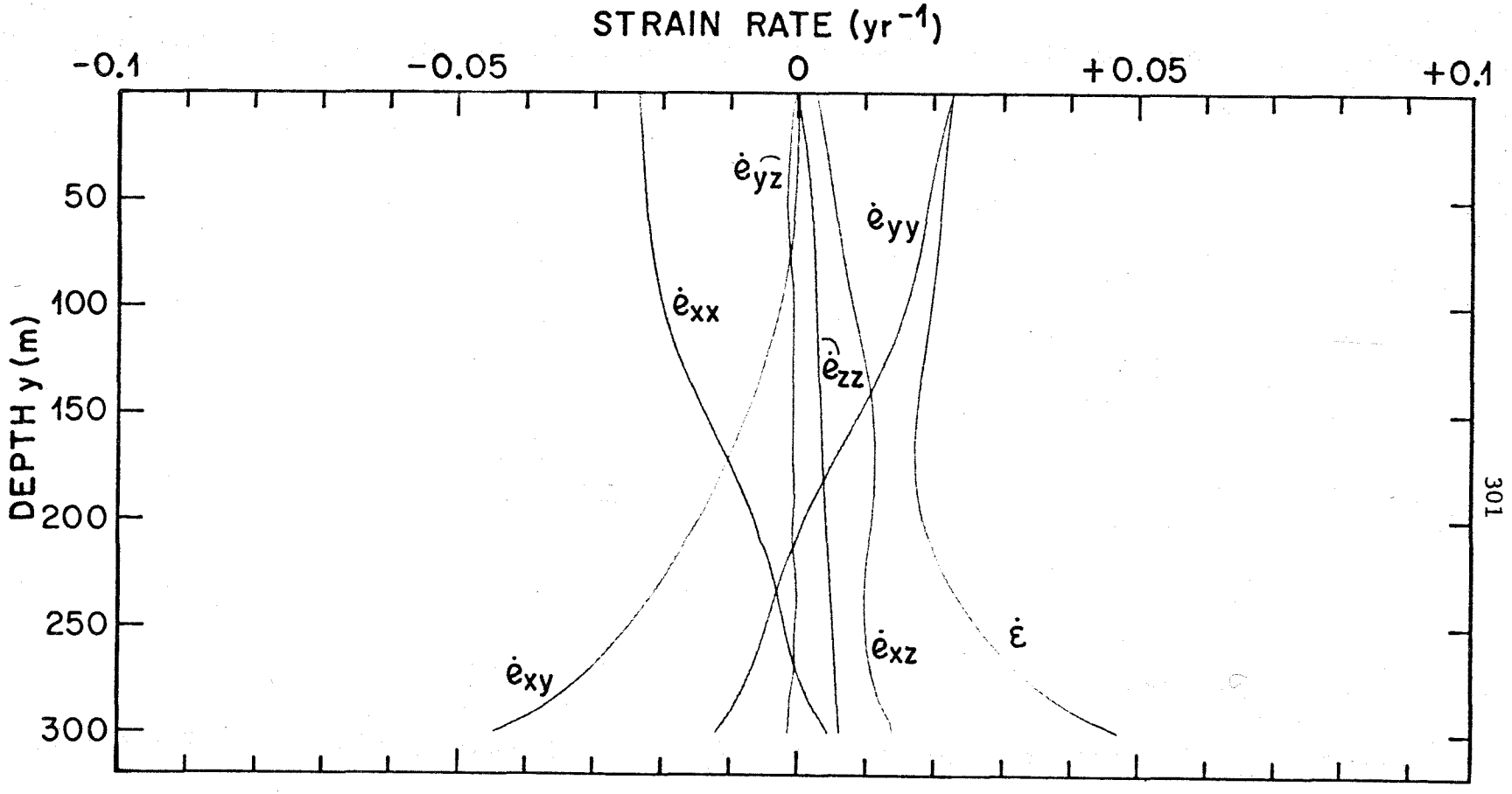

FIGURE 28b. STRAIN RATE AT BOREHOLE 1B

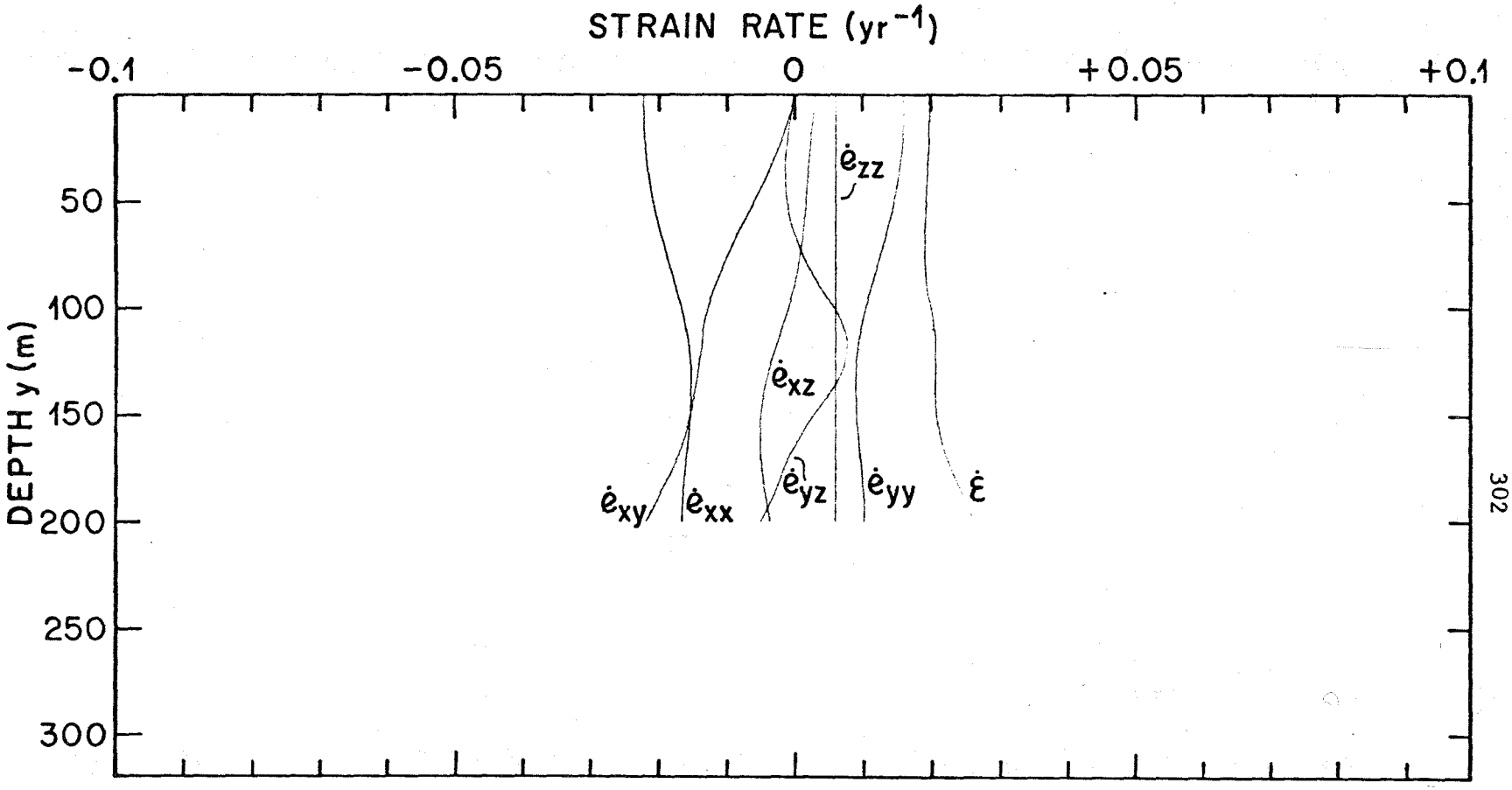

FIGURE 28c. STRAIN RATE AT BOREHOLE 1C

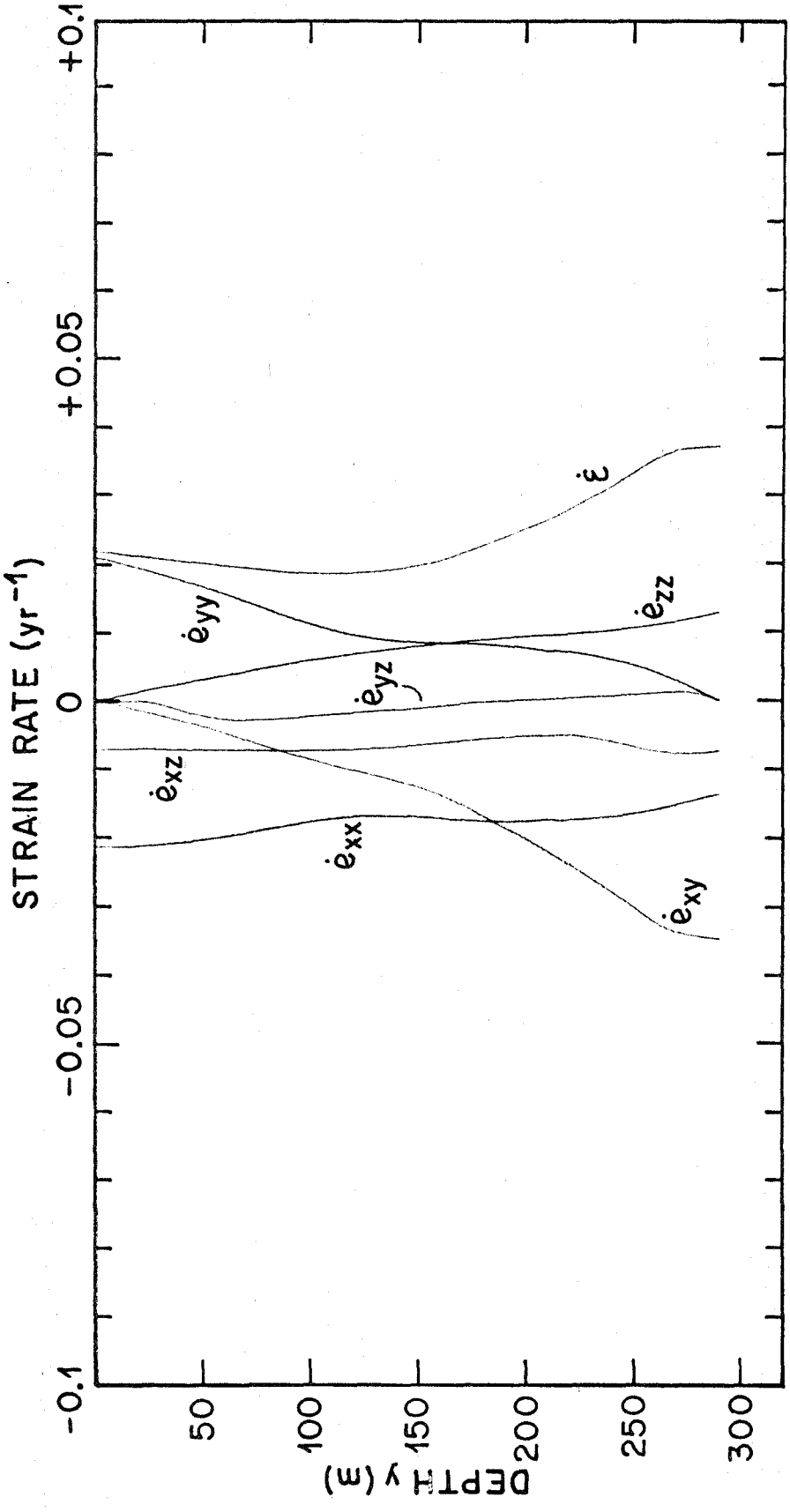

FIGURE 28d. STRAIN RATE AT BOREHOLE 2A

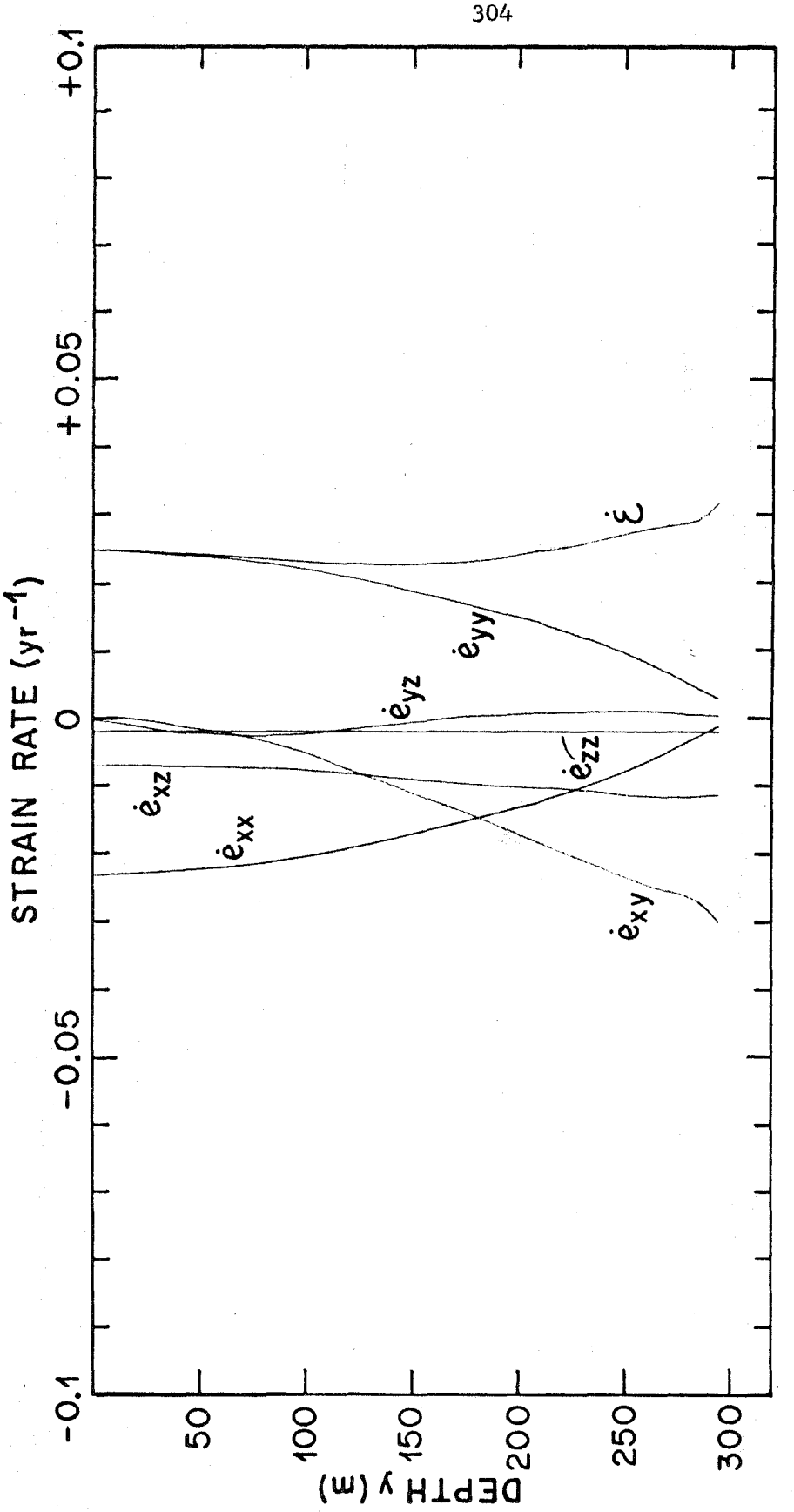

FIGURE 28e. STRAIN RATE AT BOREHOLE 2B

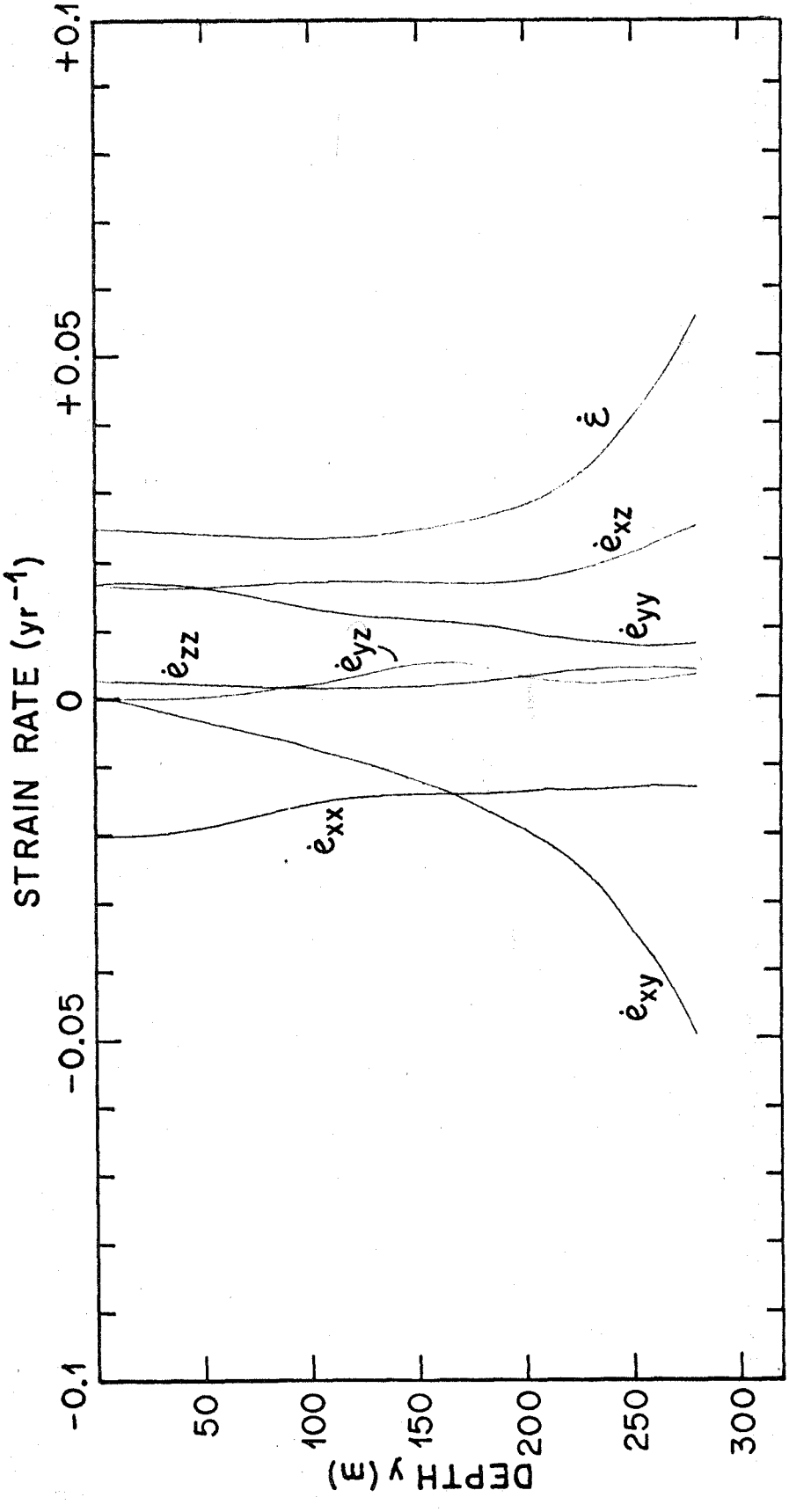

FIGURE 28f. STRAIN RATE AT BOREHOLE 3A

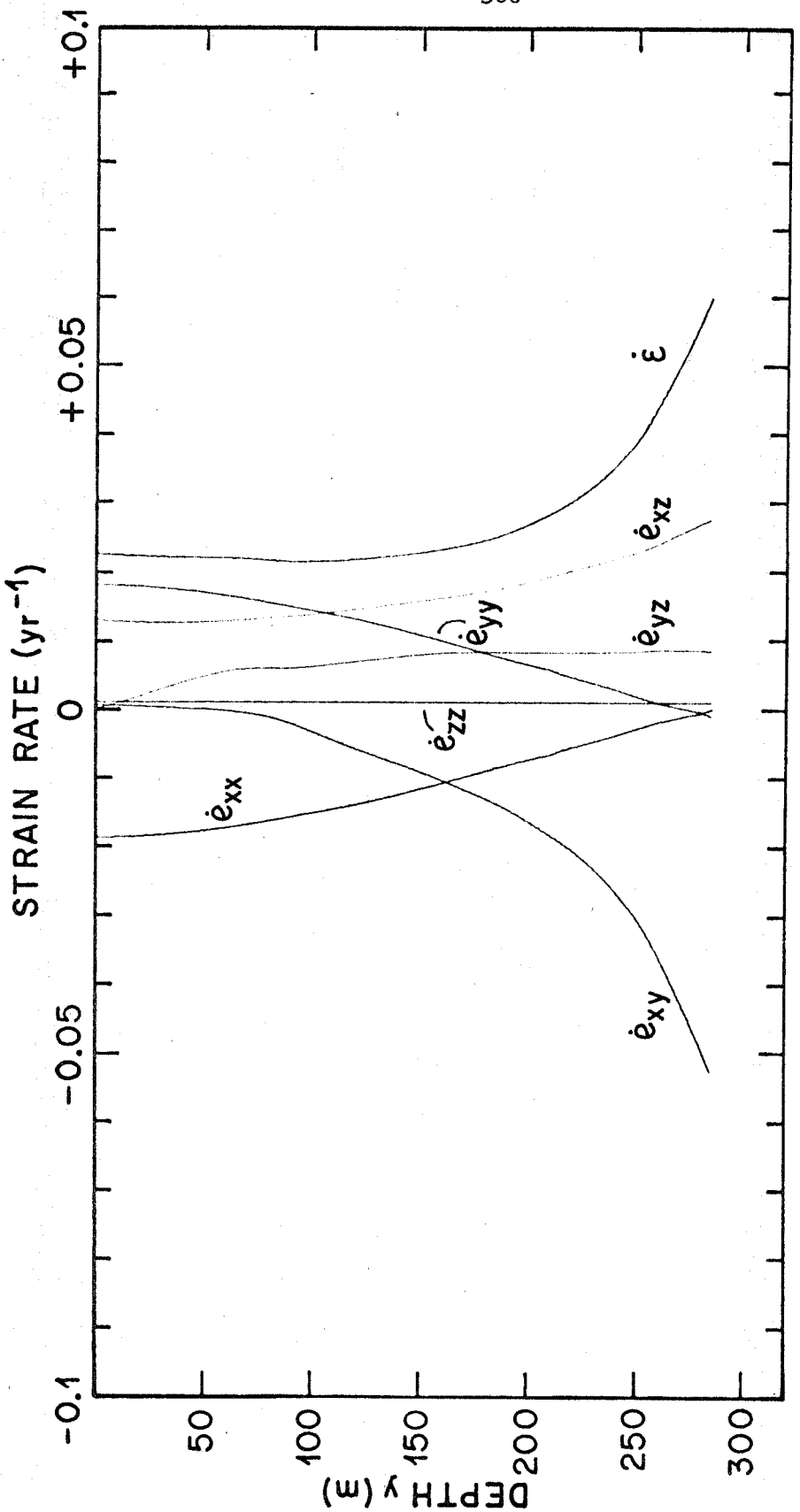

FIGURE 28g. STRAIN RATE AT BOREHOLE 3B

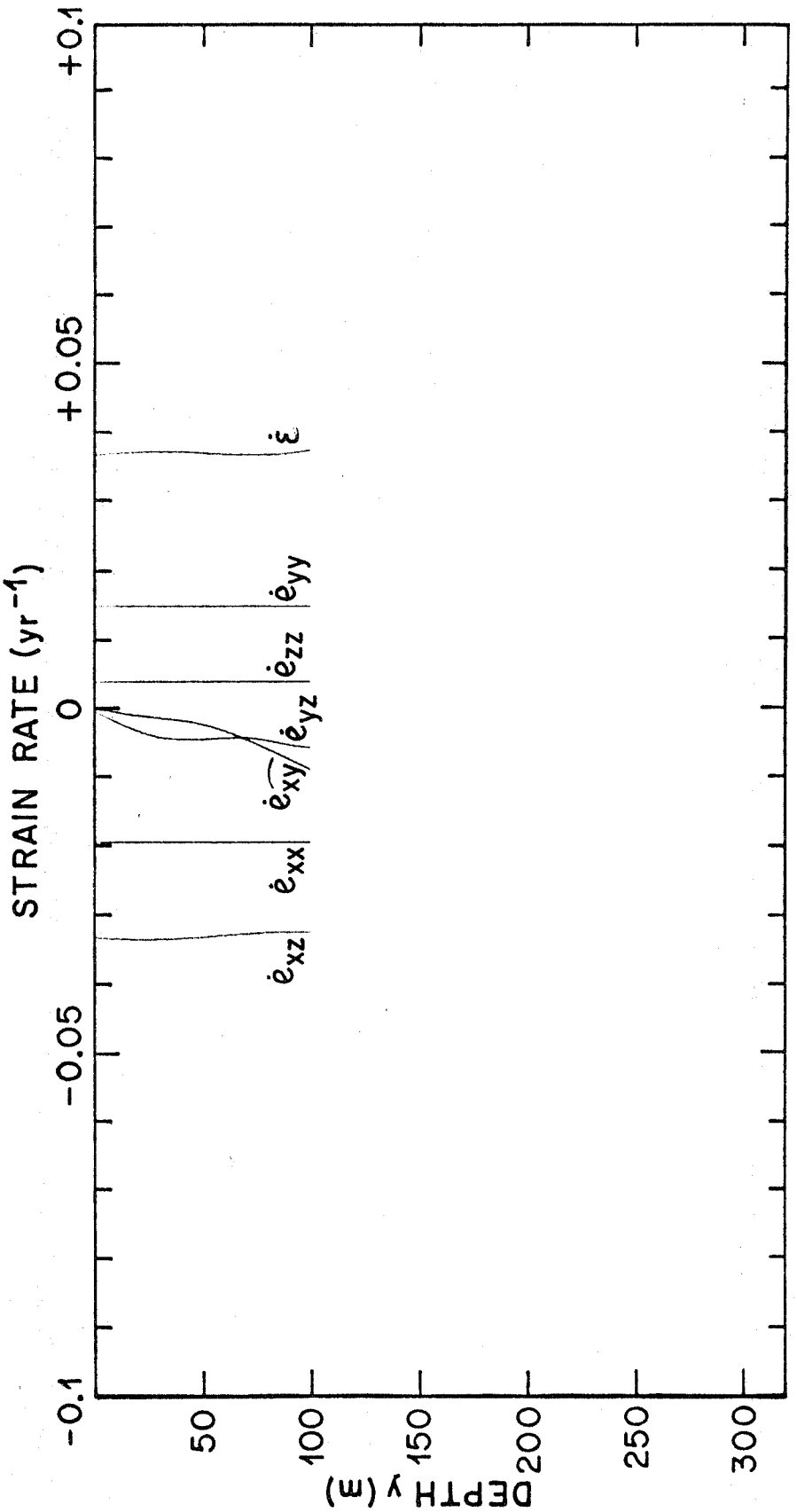

FIGURE 28h. STRAIN RATE AT BOREHOLE 4A

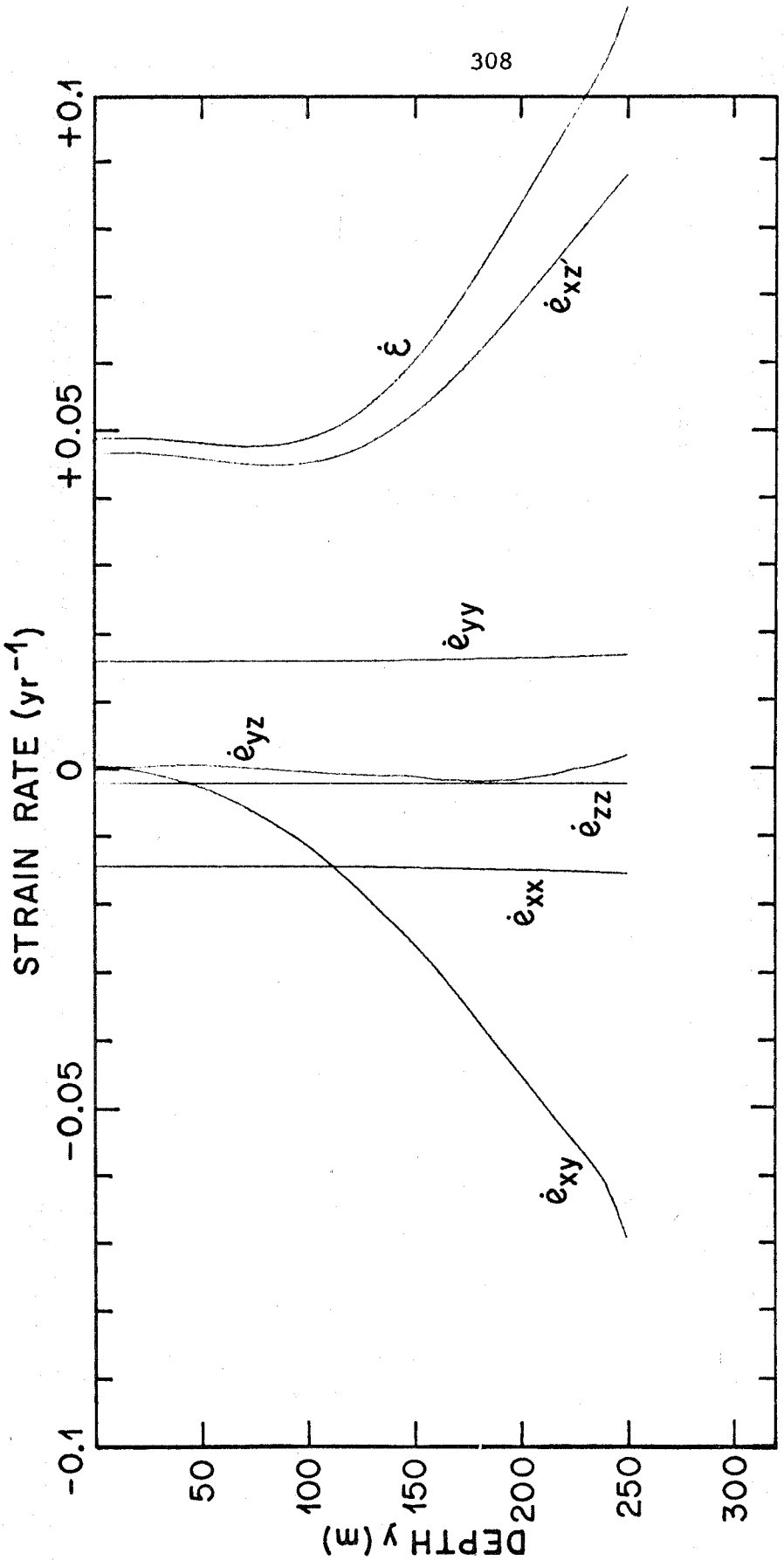

FIGURE 28i. STRAIN RATE AT BOREHOLE 5A

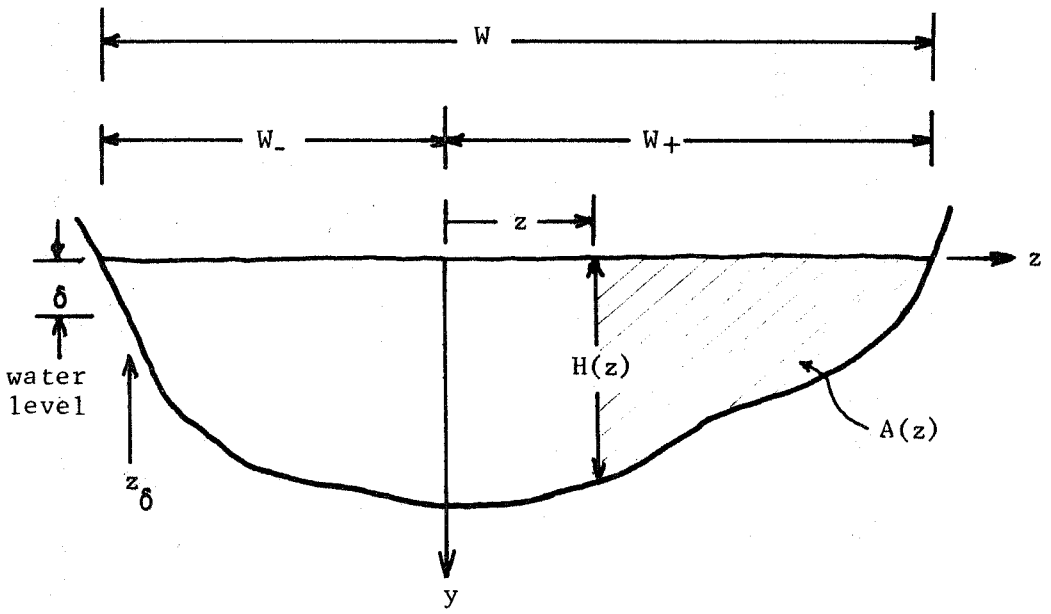

FIGURE 29. DEFINITION OF GEOMETRICAL QUANTITIES IN A CROSS SECTION

The following additional quantities are also defined:

H = H(0) is the maximum depth of the cross section;
A = A(W_) is the area of the cross section;
P is the length of the ice rock contact.

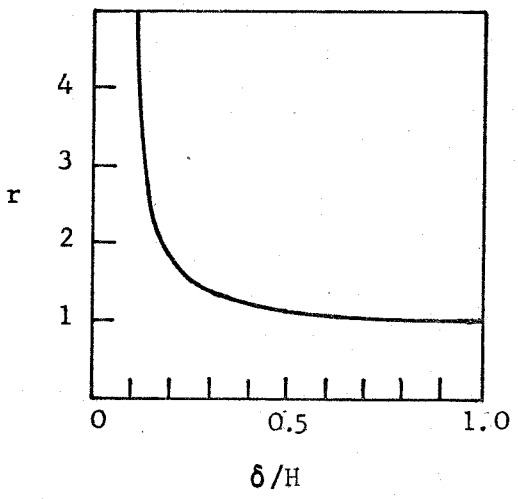

FIGURE 30. DEPENDENCE OF PRESSURE RATIO ON WATER LEVEL

$r(\delta)$ gives the ratio of the difference in hydrostatic overburden and water pressure at the top of the water column (depth δ), to the same difference at the deepest part of the channel (depth H).

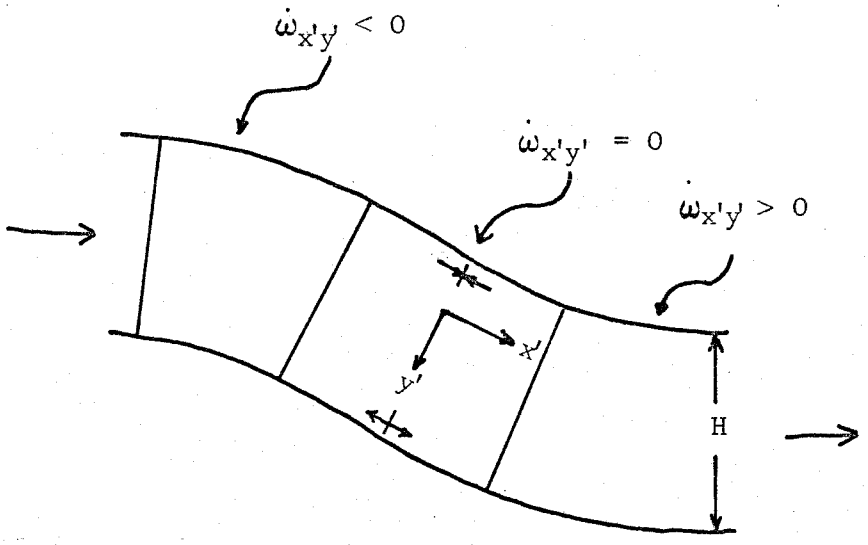

FIGURE 31. BENDING AS A RESULT OF A LONGITUDINAL GRADIENT IN BED CURVATURE

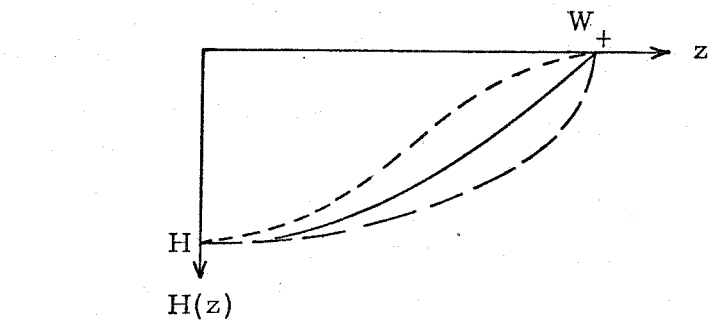

cross section geometry

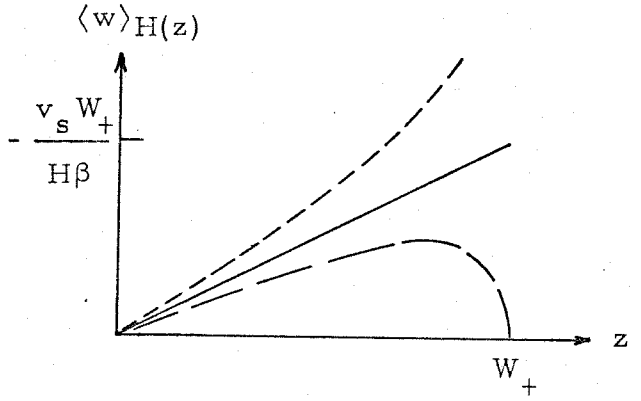

distribution of average lateral velocity

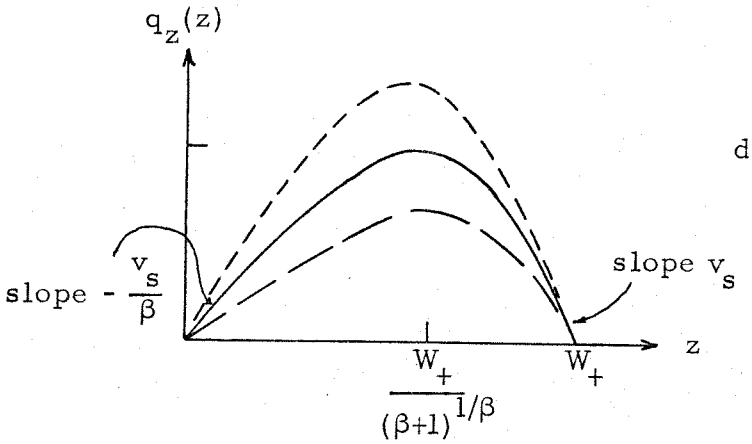

distribution of lateral flux

FIGURE 32. LATERAL FLOW IN CYLINDRICAL CHANNELS

Form of cross section geometry, average lateral velocity, and lateral flux are shown schematically for channel shapes given by $H(z) = H(1-(|z|/W_+)^{\beta})^{1/\alpha}$. Solid line is for $\alpha = 1$, $\beta > 1$; long dashes are for $\alpha < 1$, $\beta > 1$; short dashes are for $\alpha > 1$, $\beta > 1$.

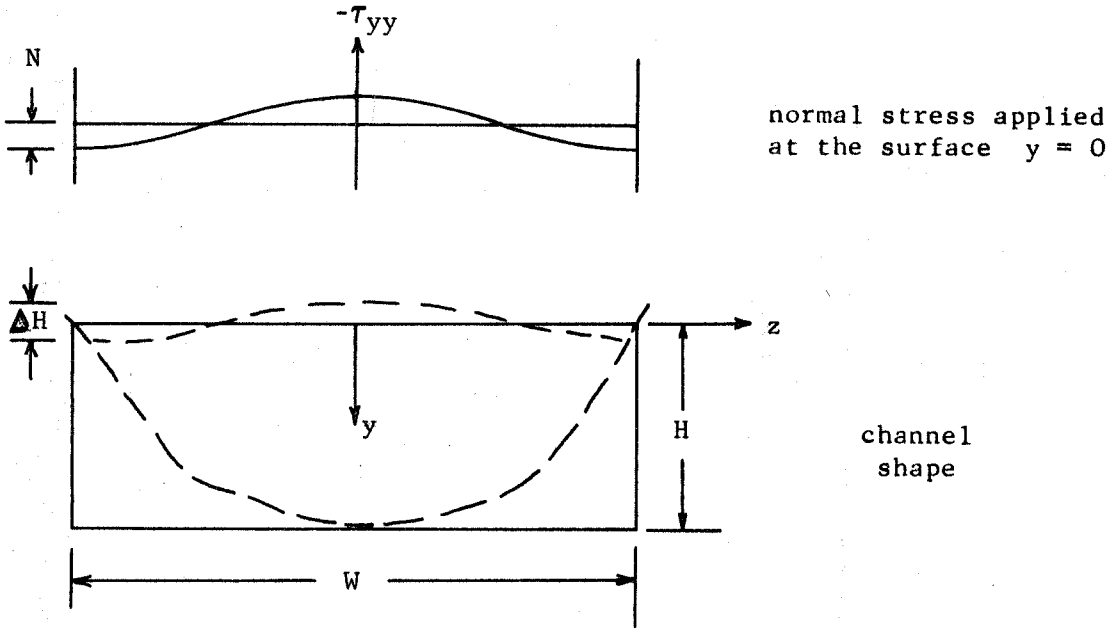

FIGURE 33. VISCOUS SLAB WITH NORMAL LOADING ON UPPER SURFACE

Dashed line indicates a hypothetical glacier cross section and its relation to the assumed geometry and distribution of normal loading.

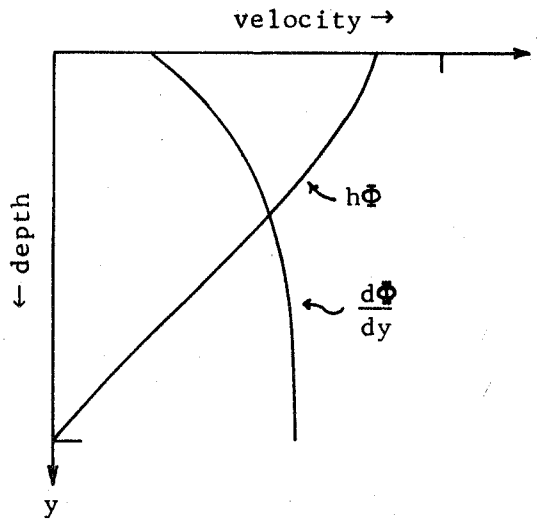

FIGURE 34. FLOW IN A VISCOUS SLAB WITH NORMAL LOADING ON UPPER SURFACE

Curves give forms of depth distribution of $v = \Phi(hy)\ h \cos hz$ and $w = -\frac{d\Phi}{dy} \sin hz$.

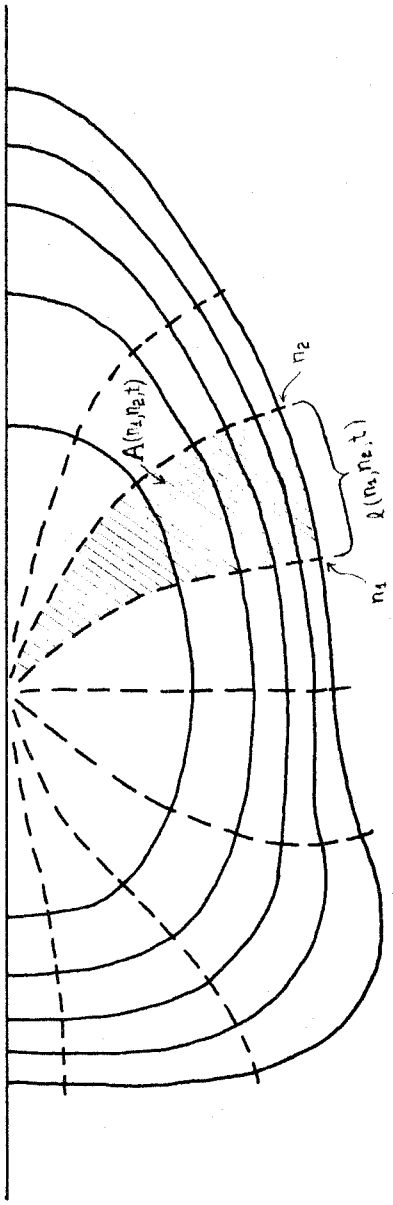

FIGURE 35. VELOCITY CONTOURS AND CHARACTERISTICS

——— Velocity contours
----- Characteristics normal to velocity contours

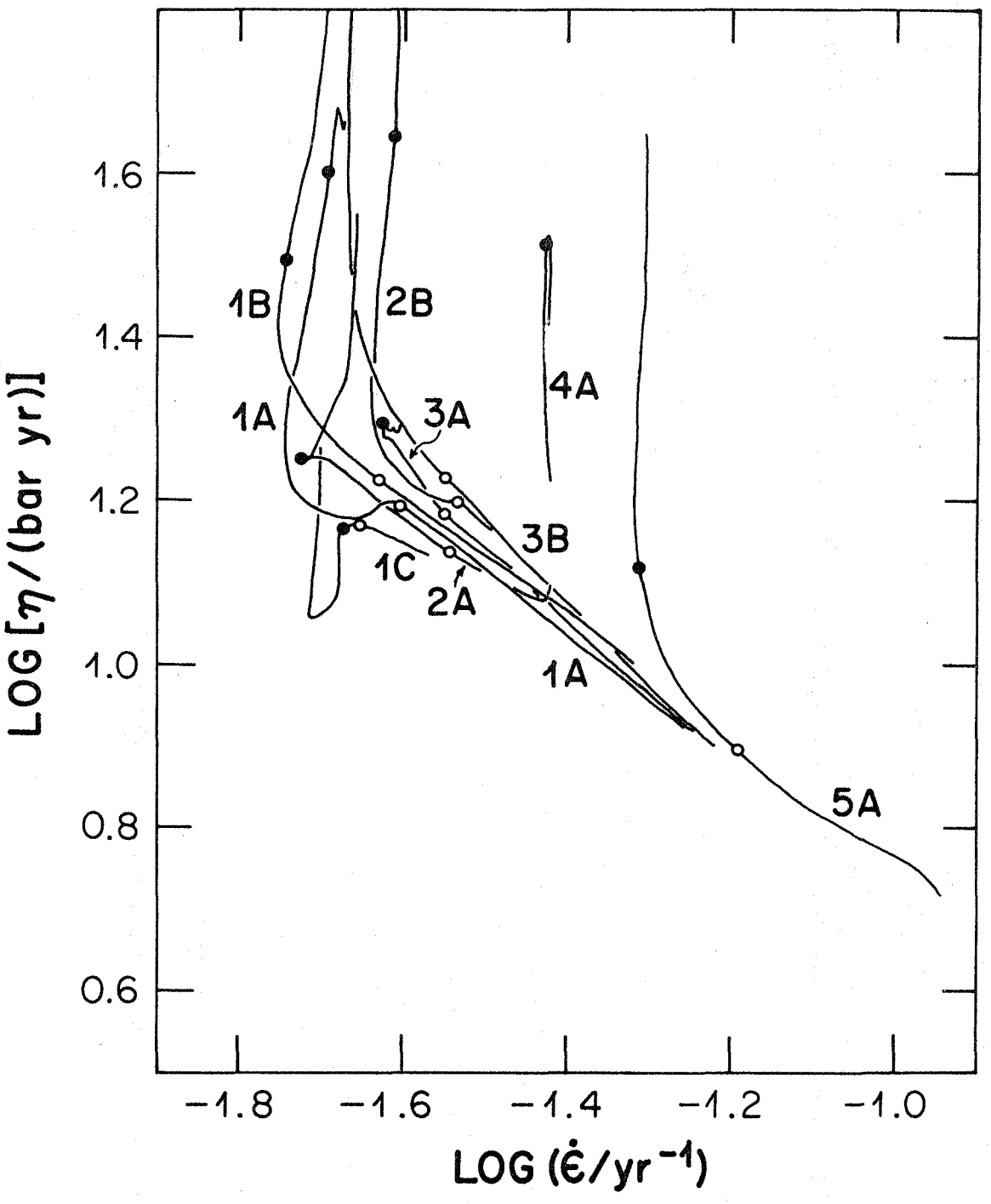

FIGURE 36. LOG (η) VS: LOG (ϵ)

η is calculated from an assumed linear depth distribution of shear stress by equation (15) of Chapter VII, with $\bar{x}$ parallel to the local surface at the top of each borehole.

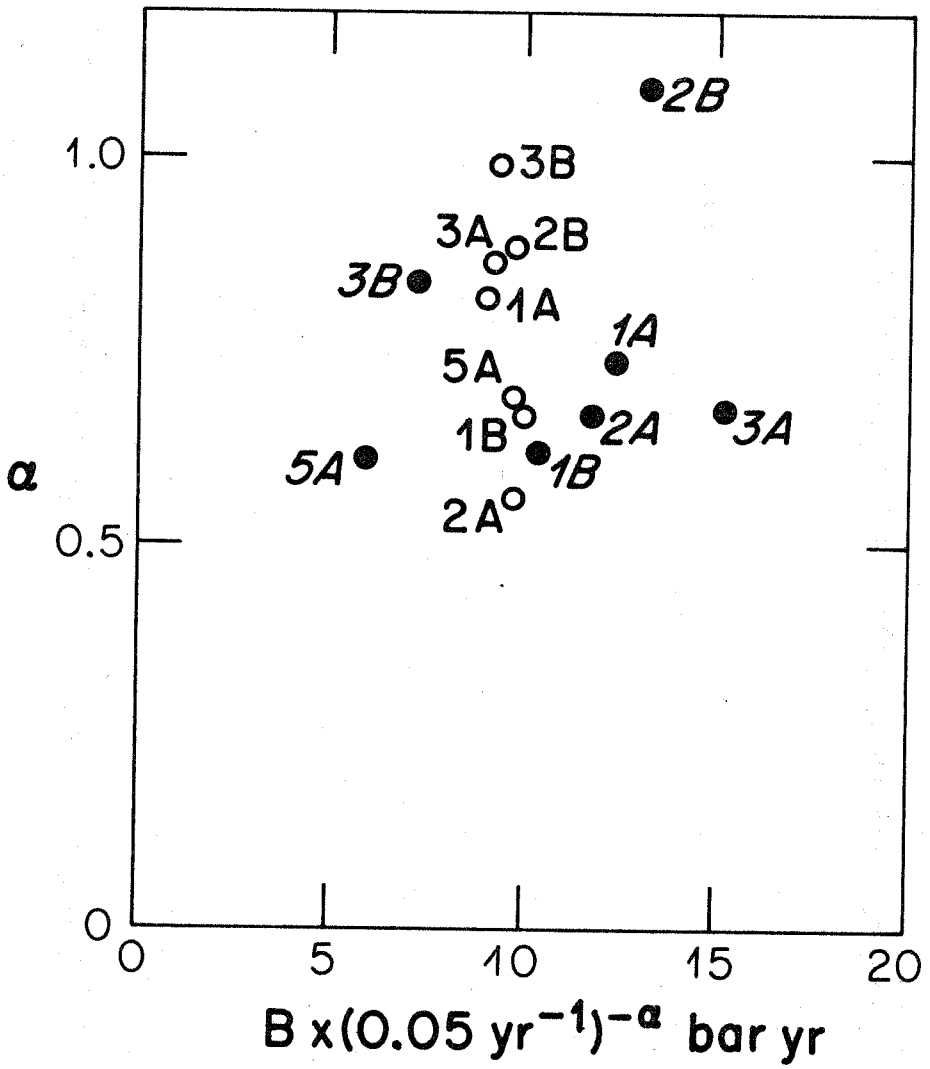

FIGURE 37. FLOW-LAW PARAMETERS FOR LOWER PORTIONS OF SINGLE BOREHOLES

○ Parameters calculated from an assumed linear depth distribution of shear stress

● Parameters calculated by least squares minimization of residual body forces

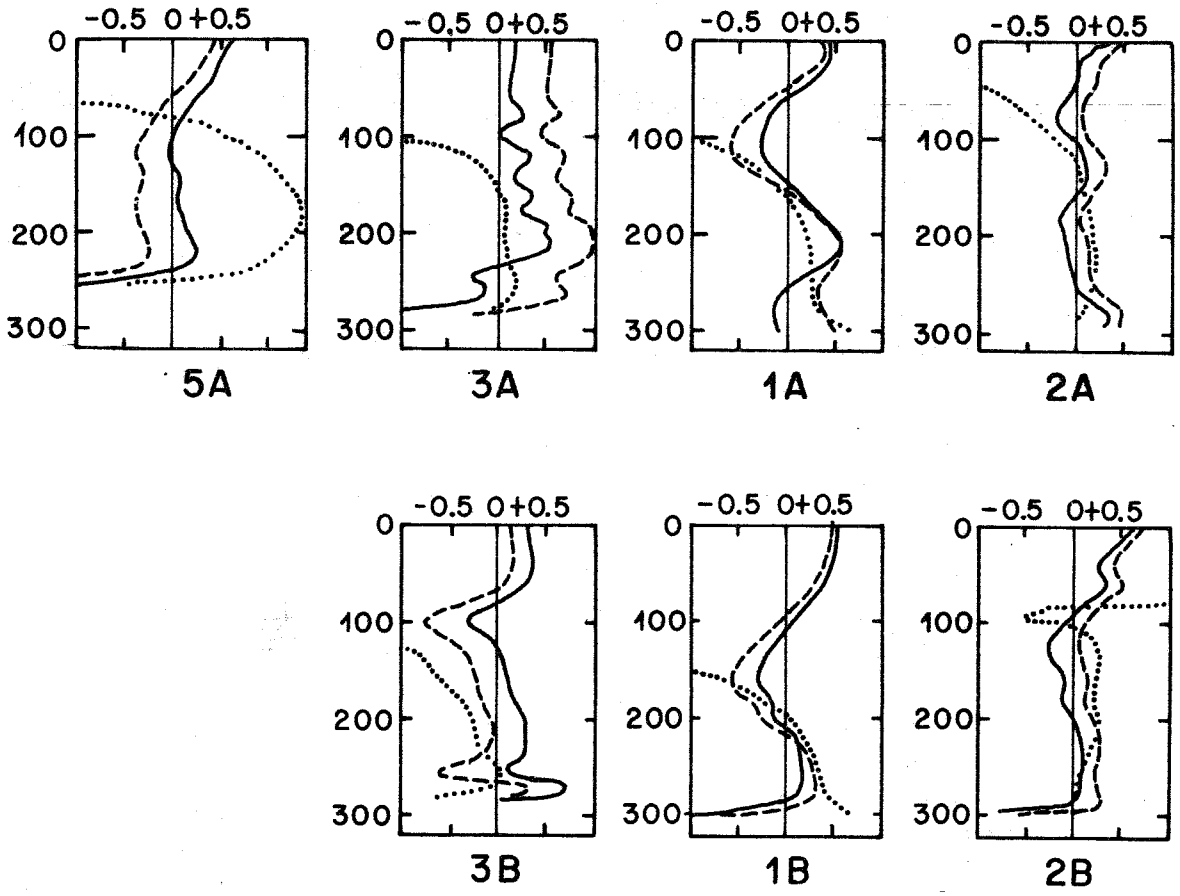

FIGURE 38. DISTRIBUTION OF RESIDUAL FORCES

Dotted line gives residual forces for viscosity distribution computed from a linear depth dependence of shear stress. Dashed line gives residual forces for power law derived from a linear depth dependence of shear stress. Solid line gives residual forces for least squares power law.

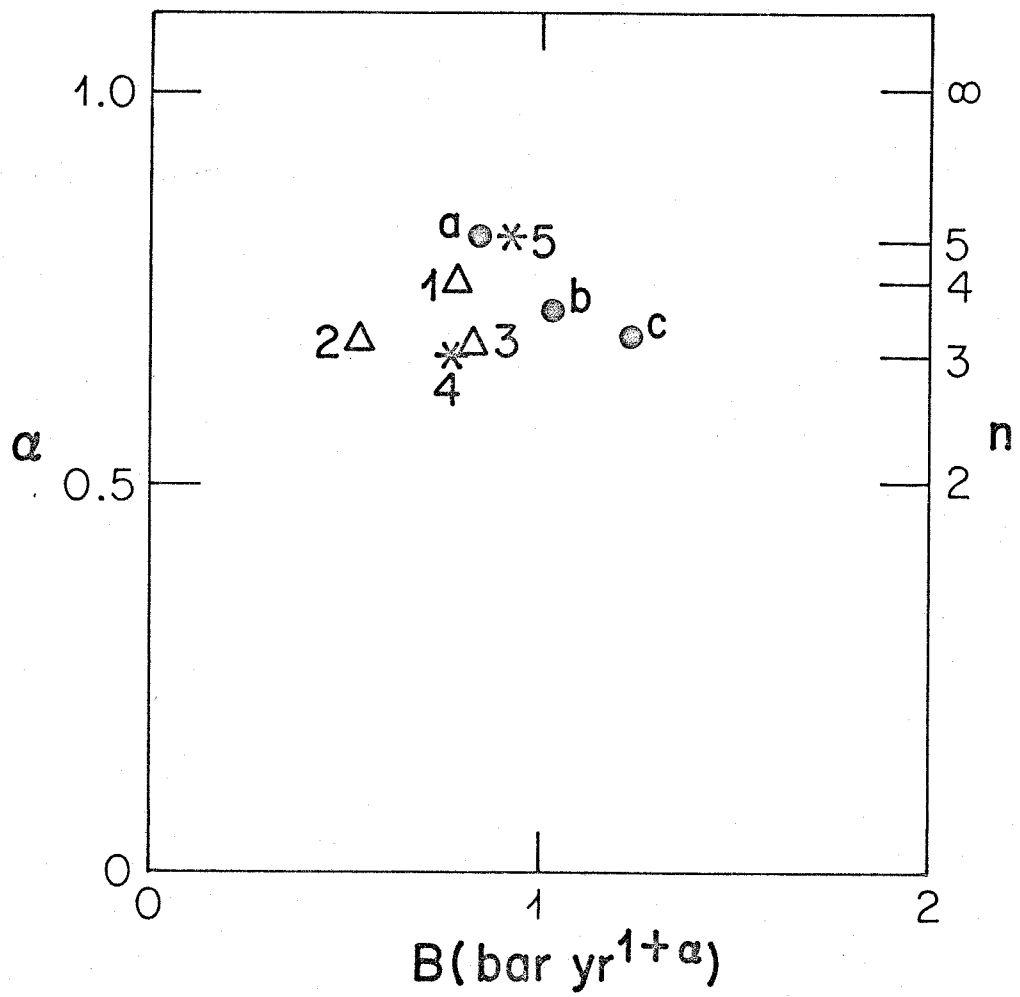

FIGURE 39. RESULTS FOR POWER-LAW PARAMETERS

Flow law parameters as determined from a combined analysis of all boreholes with a linear distribution of shear stress (a) and as determined by least squares minimization of residual forces for complete depth ranges (b) and lower portions (c) of all boreholes are compared to experimental parameters as given by Glen (1955) (1) and (2) and Butkovich and Landauer (3) and to parameters determined by field measurements as reported by Nye (1953) (4) and Kamb and Shreve (5).

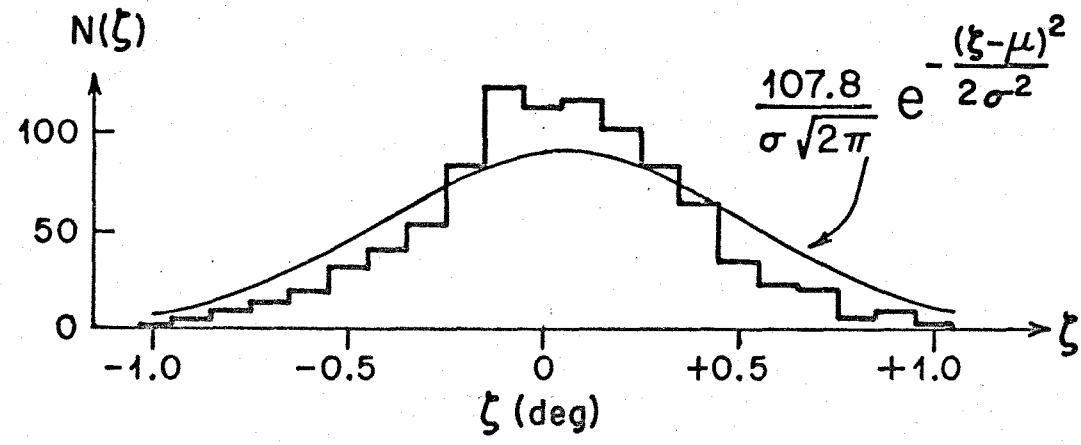

a. Deviations ζ of longitudinal tilts Γ_X from the smoothing curve

$\mu = 0.048$ $\sigma = 0.47$

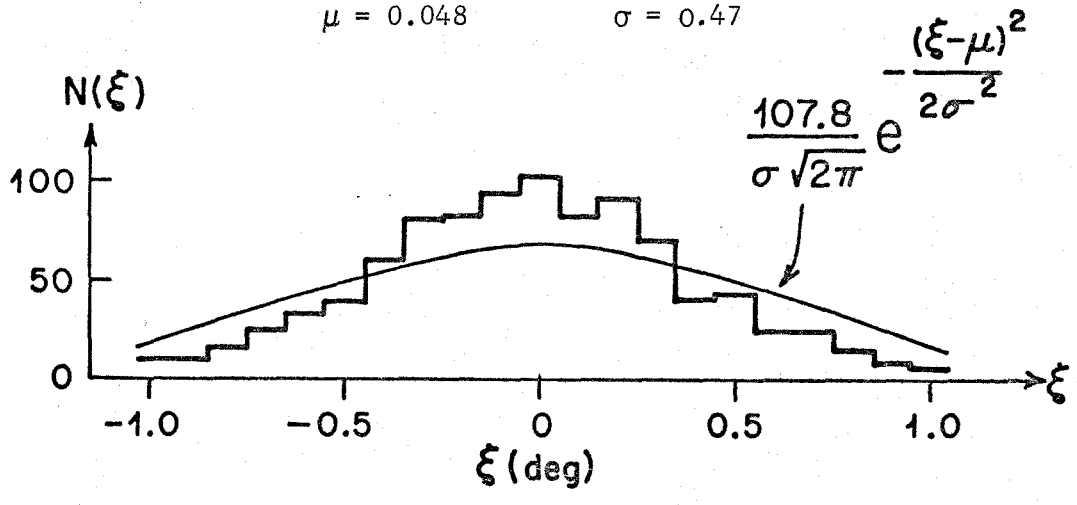

b. Deviations ξ of transversd tilts Γ_Z from the smoothing curve

$\mu = 0.010$ $\sigma = 0.63$

FIGURE 40. DEVIATIONS OF MEASURED TILT FROM SMOOTHING CURVE

Histogram plots of deviations are compared with Gaussian curves of identical mean μ and standard deviation σ The Gaussian curves are normalized to include the same area as the histograms.

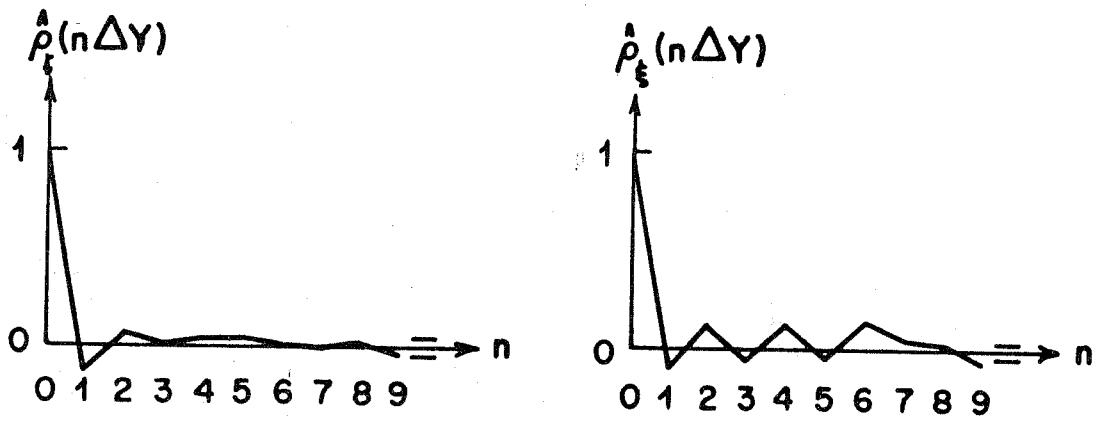

FIGURE 41. AUTO CORRELATION FUNCTIONS FOR TILT COMPONENTS

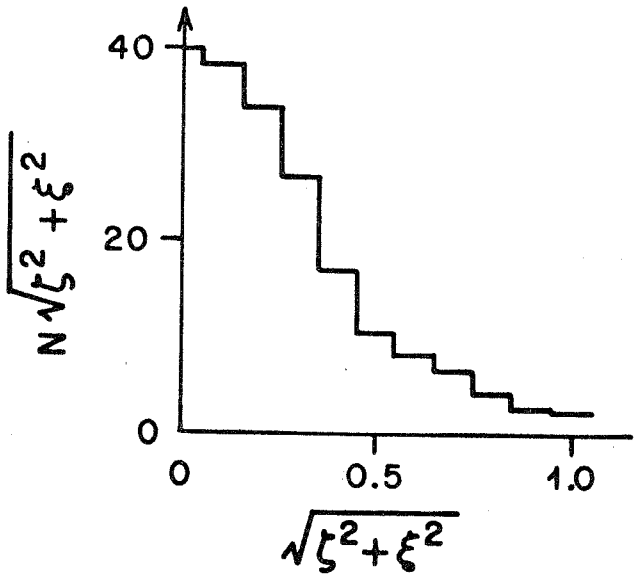

FIGURE 42. RADIAL DISTRIBUTION OF TILT DEVIATIONS